TO STUDY THE EFFECT STATIC LOADING ON CRACK PROPAGATION BY USING SIMULATION AND VIBRATION SIGNAL

Thesis Submitted For the Award of the Degree of

DOCTOR OF PHILOSOPHY
in

Mechanical Engineering

By

Sumit

41700071

Supervised By

Dr. Manpreet Singh

LOVELY PROFESSIONAL UNIVERSITY
PUNJAB
2022

Declaration

I hereby **certify** that the work which is being presented in the dissertation entitled, **"To study the effect static loading on crack propagation by using Simulation and Vibration Signal",** by Sumit Registration Number (4700071) in partial fulfillment of requirement for the award of the degree of Ph.D. (Mechanical Engineering) submitted in Lovely Professional University, Phagwara, Punjab (India) is an authentic record of my own work carried out during a period from July 2017 to April 2022 under the supervision of Dr. Manpreet Singh, Professor, Mechanical Engineering Department. The matter presented in this thesis has not been submitted by me to any other University / Institute in India or abroad for the award of any degree or diploma.

Signature of the Student

This is to certify that the above statement made by the candidate is correct to the best of my/our knowledge.

Signature of the Supervisor

Certificate

University. **Reg. Number**: 41700071

Name: Sumit

Title of Dissertation: **To study the effect static loading on crack propagation by using Simulation and Vibration Signal**. We the below signed, after checking the dissertation mentioned above and the official record book (s) of the student, hereby state our approval of the dissertation submitted in partial fulfillment of the requirement of the degree of Doctor of Philosophy in Mechanical Engineering at Lovely Professional University, Phagwara, Punjab (India). We are satisfied with the volume, quality, correctness, and originality of the work.

Signature of the Supervisor

Abstract

Bearing plays crucial role in supporting the rotating shaft and to withstand different kind of loading. Thus failure in the bearing not only halts shaft operation but it effect machine functioning as a whole. The most prominent cause of bearing failure is crack on any of its mating surfaces. The crack when initiated still the bearing can be used for sometimes but this time duration is depending majorly on loading conditions. In this work, effect of static loading was studied meticulously on the crack propagation and this may help in effective prediction of remaining useful life (RUL). To analyze the effect of loading on crack propagation axial groove defect was seeded on outer race of taper roller bearing and bearing was made to run under five different static loading conditions (without load, 5Kg, 10 Kg, 15 Kg, 20 Kg) on the outer race. The axial groove defect size was selected to help the propagation smoothly as it was difficult to initiate the crack with the normal working conditions. Taper roller bearing was made to run continuously under static loading condition for the purpose of crack propagation analysis. The vibration signals were recorded at intermediate intervals of time and stored in the computer for further processing. Generally, when the roller was coming in contact with the outer race defect the impulses in the vibration signal were started appearing and with the propagation of defect the nature of impulse started changing. This change was observed by signal processing technique. CWT based analysis was carried out to calculate width of crack using Bio-orthogonal wavelet and results were compared using image processing software image J. Bi-orthogonal wavelet was having capability of magnifying low and high frequency spikes in the scalogram graph, which makes it easier to spot the entry and exit points of crack in the time domain. Furthermore, statistical analysis such as crest factor, SNR, RMS, skewness, kurtosis, shannon entropy were calculated. Statistical analysis which was also carried out for the recorded signals at different intervals of times and observed that the Shannon entropy value was showing sudden rise with almost 5 times increase with the edge breakage (visually verified) while crack was propagating.

However, in the statistical analysis none of the parameter has shown correlation with the crack propagation. To develop the correlation of crack propagation Shannon entropy of high, medium and low frequency band of continuous wavelet based (CWT) was carried out using different available mother wavelets. Shannon entropy for high frequency band of CWT using Daubechies 10 as mother wavelet has responded well to the crack propagation as the value showed sudden rise and overall increase for edge breakage and for crack propagation respectively. High frequency band of CWT using Daubechies 10 was found suitable for detecting edge breakage and crack growth at the same time because of its capability to respond transient characteristics for large duration of time. In addition to that the simulation was also carried out using FEM on the similarly constructed model and contact stress analysis was carried out. The contact stress analysis was able to detect three edge breakages instead of five in the experimental case and with the minor variation in the time frame. Finite element not only provides the value of stress but also gives information about location where maximum stress concentration occurs.

The effect of loading condition was also observed from the experimentation that in case of maximum static load of 20 kg the crack propagates quickly in terms of area and width and bearing was stopped for running at 116.5 hours because propagation was increased rapidly after 109 hours of continuous running. Whereas, the propagation grows rapidly after 136 hours of running, 169 hours of running, 239 hours of running and 267.5 hours of running for 15 kg, 10 Kg, 5 Kg and no load conditions respectively. Subsequently, the bearing was finally stopped at 166 hours, 178.5 hours, 245.5 hours and 285 hours for 15 kg, 10 Kg, 5 Kg and no load conditions respectively Hence from experiments it was observed that the loading conditions affect on the crack propagation is significant.

Key words: *vibration analysis, condition monitoring, wavelet, crack propagation, effect of loading, Crack propagation, Statistical Analysis, , FEM based analysis, Taper roller bearing, CWT*

Structure of thesis

Chapter 1: Provides an introduction to the condition monitoring techniques used for feature extraction in rolling element bearing, as well as the significance of work and its objectives.

Chapter 2: Kinematics of rolling element bearing along with its characteristic frequencies was explained. From the literature survey different conventional techniques used for analyzing the crack propagation and different feature extraction using vibration based techniques was discussed along with research gap.

Chapter 3: In this chapter experimental set up along with its specification and arrangement was discussed which was used to obtain vibration signals from the defective rolling element bearing. In addition to this basic concept of FEM and simulation procedure was also discussed.

Chapter 4: Provides information related to experimental work which was carried out for studying the interim changes occurred during crack propagation and different vibration based signal processing techniques used was presented and discussed in detail.

Chapter 5: Deals with the simulation results such as contact analysis, transient analysis which was carried out using ANSYS APDL. Validation of simulation result with the experimental results was also discussed and presented in detail in this chapter.

Chapter 6: Provides the conclusion and proposes further work which can be done for condition monitoring of rolling element bearing or other rotating parts such as gears.

Graphical Abstract

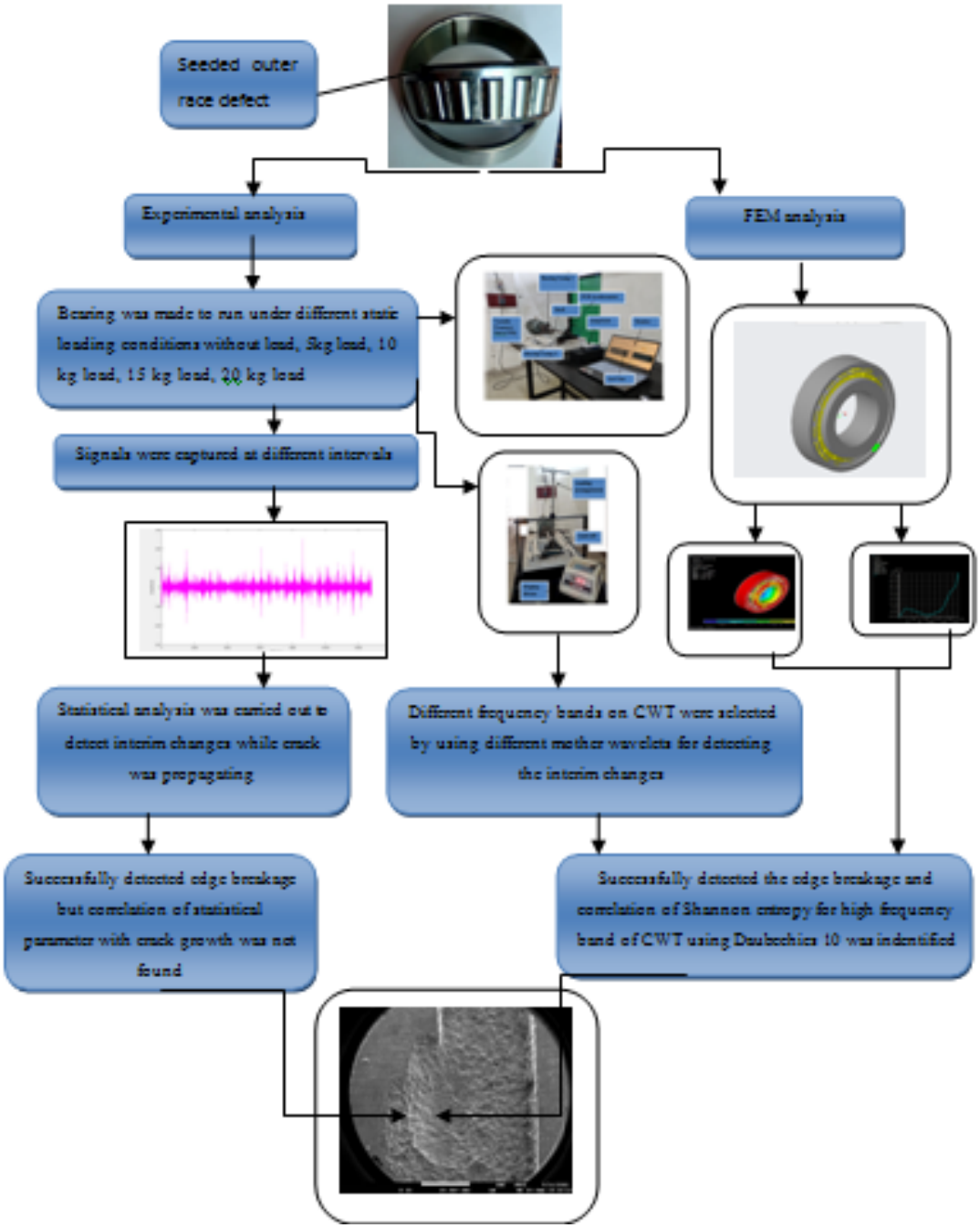

Acknowledgements

First and Foremost, I would like to express my sincere gratitude with pride and pleasure to my supervisor **Prof. Dr. Manpreet singh,** for introducing me to the research topic (**To study the effect static loading on crack propagation by using Simulation and Vibration Signal)** and enlightening me about research. His engagement in my learning process with patience and motivation throughout the course of this research work is thankfully acknowledged. His thoughtful guidance helped me in all the time of research and writing of this thesis. I am very grateful to Dr. Vijay Kumar, Head of the School, Mechanical Engineering, Lovely Professional University for extending the facilities which needed at various stages of this work. Also special thanks to all my colleagues of Mechanical Engineering Department for their extensive discussions around my work and moral support.

Besides my major advisor, I would like to thank the Dr. Gurpreet singh Phull, Rajeev Dhiman for helping me for preparation of experimental set up from design to fabrication. I also would like to thank the rest of my research advisory committee for insightful comments and valuable advice during my progress evaluations. I am extremely grateful to my parents and family for their love, prayers, caring and sacrifices for educating and preparing me for my future.

I express our sincere thanks and gratitude to university authority for allowing me to undergoing my research work.

Sumit

Lovely Professional University

Contents

Declaration ..... **II**

Certificate ..... **III**

Abstract ..... **IV**

List of Figures ..... **XII**

List of Tables ..... **XVI**

List of Abbreviations ..... **XVII**

Chapter 1 Introduction **1**

1.1 Introduction: 1

1.2 Classification of rolling element bearing 1

1.2.1 Ball Bearings 2

1.2.2 Tapered Roller Bearing 2

1.2.3 Cylindrical Roller Bearing 2

1.3 Bearing parts 2

1.4 Function of bearing 3

1.5 Bearing failure modes and classification of faults 6

1.6 Techniques for detecting defect 13

1.7 Thermography: 15

1.8 Wear Debris 15

1.9 Acoustic Emission (AE) technology 15

1.10 Vibration based analysis techniques: 16

1.10.1 Time domain techniques 16

1.10.2 Frequency domain techniques 19

1.10.3 Time-Frequency techniques 20

1.11 Signal processing 26

1.12 Motivation 29

1.13 Objectives of the research 29

Chapter 2 Literature Survey 30
2.1 Introduction 30
2.2 Effect of loading on different element of bearing 30
2.3 Kinematics of cylindrical roller bearing 31
2.4 Conventional techniques for analyzing crack propagation: 34
2.5 Significance of vibration analysis in defect identification: 35
2.6 Simulation Techniques: 46
2.7 Scope and research gap 49
Chapter 3 Experimental methodology and modeling 50
3.1 Introduction 50
3.2 Experimental Test Rig: 50
3.3 Instrumentation 53
3.4 Experimental Procedure 56
3.5 Test rig design using CREO 60
3.6 Simulation Procedure: 61
3.7 Taper roller bearing modeling 72
3.8 FEM analysis: 75
3.9 Methods for FEA Solution (h- and p method) 78
3.10 Types of Structural Analysis 79
Chapter 4 Experimental result and discussion 81
4.1 Introduction 81
4.2. Defect identification using FFT 82
4.3 Statistical analysis 84
4.4 Defect width measurement using CWT 100
4.5 High, medium, low frequency band analysis using CWT 109
4.5.1 Frequency band analysis without load 109
4.5.2 Frequency band analysis 5 Kg load 114
4.5.3 Frequency band analysis 10 Kg load: 119

4.5.4 Frequency band analysis 15 Kg load 122
4.6.5 Frequency band analysis 20 Kg load 126
4.6 Absolute energy criterion 130
Chapter 5: Simulation result and validation 137
5.1 Introduction: 137
5.3 Model Validation 138
5.4 Defect identification: 141
5.2 Transient analysis for taper roller bearing using Ansys 147
Chapter 6 Conclusion and Future Scope **153**
References **156**
Annexure 1 ..... **180**
Annexure 2 ..... **185**
Annexure 3 ..... **190**
Annexure 4 ..... **202**
List of publication **207**

List of Figures

Fig 1. 1 Schematic diagram of roller bearing.....3
Fig 1. 2 Loads and Bending Moment on taper roller bearing 5
Fig 1. 3 Represents different load acting on taper roller bearing and line diagram of rolling element bearing supported by shaft is shown in Fig 1.3(b).....5
Fig 1. 4 Bath curve 8
Fig 1. 5 Bearing damage classification.....10
Fig 1. 6 Bearing defects a) Wear marks due to foreign matter. b)Fatigue spall on bearing inner race c)flaking d) Corrosion.....11
Fig 1. 7 Raw signal for outer race defect in bearing 16
Fig 1. 8 FFT for defective bearing.....20
Fig 1. 9 CWT of bearing outer race defect showing burst.....23
Fig 1. 10 Wavelet function Ψ(t) and shifted wavelet function Ψ(t-k).....24
Fig 1. 11 Low scale and high scale wavelet.....24
Fig 1. 12 Haar wavelet and its magnitude spectrum 25
Fig 1. 13 Flow chart Signal Processing 28

Fig 2. 1 Mass, Stiffness and damping model of bearing 36
Fig 2. 2 Kinematics of the roller motion around the edge of the defect area: state 1 is before shock, state 38
Fig 2. 3 Typical Vibration Impact duration and corresponding to roller duration over an outer race defect. 40
Fig 2. 4 Tree structure for wavelet packet transform 42
Fig 2. 5 Hertzian Contact Zone and Indentation of a roller on an elastic surface.....45

Fig 3. 1 Complete set up bearing test rig 51
Fig 3. 2 Load Cell arrangement for measuring load.....52

Fig 3. 3 Schematic drawing of a piezo-electronic accelerometer 55
Fig 3. 4 Time domain waveform and FFT generated by lab view 56
Fig 3. 5 Lab View icons for capturing signal.....57
Fig 3. 6 Load cell used for experimentation 59
Fig 3. 7 Taper roller Bearing with (a) outer race defect (b) enlarge view of outer race defect.....60
Fig 3. 8 Designing of test rig using Creo 61
Fig 3. 9 Taper roller bearing parts inner race, defective outer race, cage and assembled model 64
Fig 3. 10 Meshed model of taper roller bearing with outer race defect.....65
Fig 3. 11 Three dimensional element used in ANSYS.....66
Fig 3. 12 Contact between roller and inner race and roller and outer race 69
Fig 3. 13 : All degree of freedom constrained outer race 70
Fig 3. 14 Bearing parameters 72
Fig 3. 15 Assembled view of taper roller bearing with outer race defect.(NBC 30205)..73

Fig 4. 1(a) Experimental Test Rig (b) Line diagram of test rig 82
Fig 4. 2 Raw Vibration signal without load for outer race defect 83
Fig 4. 3 FFT of raw vibration signal.....84
Fig 4. 4 Experimental result of crest factor, SNR, RMS, skewness, Kurtosis, Shannon entropy without load.....88
Fig 4. 5 Scanning electron microscope (SEM) without load 89
Fig4. 6 RMS and Shannon entropy values from duration 170 hours onward for no load condition. 90
Fig4. 7 Experimental result of crest factor, SNR, RMS, skewness, Kurtosis, Shannon entropy of 5 kg load.....91
Fig 4. 8 RMS and Shannon entropy values from duration 190 hours onward for 5kg load.. 92

Fig4. 9 Scanning electron microscope (SEM) for 5 Kg 93
Fig 4. 10 Experimental result of crest factor, SNR, RMS, skewness, Kurtosis, Shannon entropy 10 kg load 93
Fig 4. 11RMS and Shannon entropy values from duration 114 hours onward for 10kg load. 94
Fig 4. 12 Scanning electron microscope (SEM) for 10 Kg.....95
Fig 4. 13 Experimental result of crest factor, SNR, RMS, skewness, Kurtosis, Shannon entropy 15 kg load 96
Fig 4.14 RMS and Shannon entropy values from duration 110 hours onward for 15kg load 96
Fig 4. 15 Scanning electron microscope (SEM) for 15 Kg.....97
Fig 4. 16 Experimental result of crest factor, SNR, RMS, skewness, Kurtosis, Shannon entropy 20 kg load. 98
Fig 4. 17 RMS and Shannon entropy values from duration 80 hours onward for 20 kg load condition. 99
Fig 4. 18 Scanning electron microscope (SEM) for 20 Kg.....100
Fig 4. 19 crack propagation without load 103
Fig 4. 20 Increase in crack area in (mm^2) for various loading conditions 104
Fig 4. 21 CWT images and experimental images (a)178 Hours (b) 235 hours (c)246 hours 106
Fig 4. 22 Overall defect width in (mm) for various loading conditions 108
Fig4. 23 Shannon entropy values for high frequency band of CWT using Haar, db2, morl and db10 wavelets 113
Fig 4. 24 Shannon entropy values for medium frequency band of CWT using Haar, db2, morl and db10 wavelets 113
Fig4. 25 Shannon entropy values for low frequency band of CWT using Haar, db2, morl and db10 wavelets 114
Fig4. 26 Shannon entropy values for high frequency band of CWT using Haar, db2, morl and db10 wavelets 117

Fig 4. 27 Shannon entropy values for medium and low frequency band of CWT using Haar, db2, morl and db10 wavelets for 5kg load. 118
Fig4. 28 Shannon entropy values for high, medium and low frequency band of CWT using Haar, db2, morl and db10 wavelets for 10 Kg load 122
Fig 4. 29Shannon entropy values for high, medium and low frequency band of CWT using Haar, db2, morl and db10 wavelets for 15 Kg load 125
Fig4. 30 Shannon entropy values for high, medium and low frequency band of CWT using Haar, db2, morl and db10 wavelets for 20 Kg load 128
Fig 4. 31 Shannon entropy values for high frequency band of CWT using db10 wavelet for all the loading conditions 129
Fig4. 32 Absolute energy graph for 0, 5, 10, 15, 20 Kg load 132
Fig 4. 33 Energy Dispersive Spectroscopy(EDS) for No load 134
Fig 4. 34 Effect of loading on hardness value.....136

Fig 5. 1Discretization process showing nodes and elements.....137
Fig 5. 2 Contact penetration using ANSYS and experiment 140
Fig 5. 3 Raw Vibration signal using ANSYS and experiment.....142
Fig 5. 4 FFT of raw signal and simulated signal.....144
Fig 5. 5 FFT of signal after crack propagation.....146
Fig 5. 6 Assembled view of taper roller bearing with enlarged view of outer race defect 146
Fig 5. 7 Transient analysis of displacement.....148
Fig 5. 8 Transient analysis of contact stresses 149
Fig 5. 9 Graph showing maximum amplitude and stresses 150
Fig 5. 10Transient response of contact stresses 151
Fig 5. 11 High Frequency Component (db10) and Stress analysis 152

List of Tables

Table3. 1 Specification of test rig 52
Table3. 2 Data Acquisition 9230 configurations 53
Table3. 3 Specification of load cell 58
Table3. 4 Taper roller Bearing(NBC-30205) Specification 63
Table3. 5 Contact setting for creating contact 68
Table3. 6 Bearing Specification as per catalogue: 73
Table3. 7 Properties of material Taper roller bearing Properties (NBC30205) 74

Table 4. 1 Statistical parameter calculated at various time intervals for without loading condition 85
Table 4. 2 Defect width measured using image J software and CWT graph. 107
Table 4. 3 Shannon entropy values for high, medium and low frequency bands of CWT using Haar, db2, morl and db10 as mother wavelet 110
Table 4. 4 Shannon entropy values for high, medium and low frequency bands of CWT for 5 kg load using Haar, db2, morl and db10 as mother wavelet.....115
Table 4. 5 Shannon entropy values for high, medium and low frequency bands of CWT for 15 kg load using Haar, db2, morl and db10 as mother wavelet.....123
Table 4. 6 Shannon entropy values for high, medium and low frequency bands of CWT for 20 kg load using Haar, db2, morl and db10 as mother wavelet.....126

Table 5. 1Contact penetration in mm experimental and simulation.....140

List of Abbreviations

BSF	Ball spin frequency
BPFO	Ball pass frequency of the outer race
EDM	Electric discharge machining
BPFI	Ball pass frequency of the inner race
FTF	Fundamental train frequency
FFT	Fast Fourier transform
IFFT	Inverse Fast Fourier transform
CWT	Continuous wavelet transform
RMS	Root mean square
FEM	Finite element method
APDL	ANSYS Parametric Design Language
STFT	Short-time Fourier transform
CF	Crest Factor
KU	Kurtosis
SEM	Scanning electron microscope
EDS	Energy-Dispersive X-Ray Spectroscopy
Lab VIEW	Laboratory Virtual Instrument Engineering Workbench

Chapter 1 Introduction

1.1 Introduction: Bearing plays crucial role in rotating components and found applications in construction machinery, automobiles, machines, turbines, motors etc [1-5]. Bearing is mostly used for supporting the rotating shaft, enable the equipment to take extremely high speed and for taking high loads at good efficiency. Main reasons for failure of rotating machinery are shaft, seals, bearings etc and study suggests that maximum number of failures is happening due to failure of bearing. [6-12]. Main reasons for bearing failure includes heavier loading than expected, insufficient or improper lubrication, improper handling, inadequate sealing, or too tight fits resulting in lack of clearance in bearing. In most of the rotating machineries bearing are subjected to fatigue loading which results in fatigue crack growth and causes premature failure of bearing. Failure in the bearing not only halts operation but it affect the machine functioning as a whole. Major reason of failure in bearing is the crack and when it is initiated still the bearing can be used for sometimes but this time duration is depending majorly on loading conditions. Loading conditions can make crack to propagate unpredictably in the bearing. Without indication, a minor crack in the bearing due to loading will easily deteriorate into a dangerous failure mode. Early identification of such defects along with the severity of damage under different loading condition of the bearing may avoid malfunctioning and breakdown of machines.

1.2 Classification of rolling element bearing

1) Ball Bearings
2) Roller Bearings
3) Cylindrical Roller Bearings
4) Tapered Roller Bearings

1.2.1 Ball Bearings

Ball bearings use balls as rolling elements between two rings which are separated by retainers. During operation retainer also make the distance between balls constant. Ball bearings can support both radial loads (perpendicular to the shaft) and axial loads (parallel to the shaft). It is used for low load speed applications where balls offer lower friction than rollers. Major advantage of ball bearings is that it can also operate even when the bearing races are misaligned.

1.2.2 Tapered Roller Bearing

Tapered roller bearings use conical rollers that run on conical races. Most of the roller bearings support only radial loads, but tapered roller bearings support both radial and axial loads. They can generally carry higher loads than ball bearings due to greater area of contact. Main parts of taper roller bearing are inner race, outer race, cage and taper roller. Taper roller bearing found application in mining engines, agriculture, construction etc.

1.2.3 Cylindrical Roller Bearing

Cylindrical roller bearings are similar to ball bearings except that they use a cylinder roller instead of a ball or taper roller. They typically have load capacity higher than the taper roller bearings and mostly used for high speed application such as gear boxes, transmission system, engine rocker arms, pumps, steering system etc.

1.3 Bearing parts

Rolling element bearing is basically assembly of outer race, inner race, ball/ roller and cage. Inner race in general fits on the rotating shaft, outer race fits inside the bearing

housing and balls or rollers are rolling element between the surfaces of two races to provide rolling action. Cage separates the balls or rollers so that they roll between two races. The schematic diagram of roller bearing is shown in the Fig 1.1. Rolling contact area which includes outer race, inner race or ball/roller are the main failure elements in bearing because this part are frequently subjected to fatigue loading.

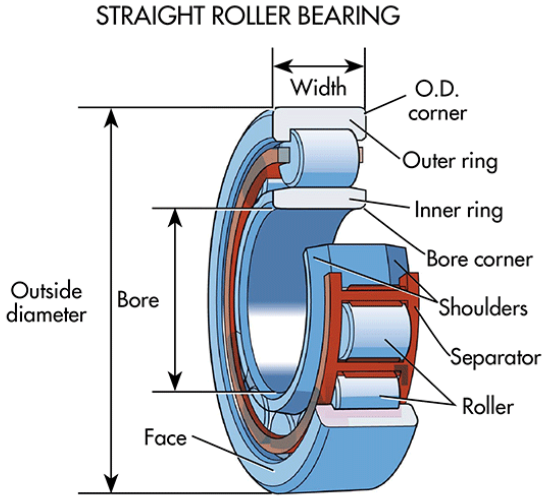

Fig 1. 1 Schematic diagram of roller bearing

1.4 Function of bearing

The main function of bearing is to ensure stability of rotating shaft subjected to fatigue loads during its working operation and which acts from different directions and to constrained motion. In addition to this Equation 1bearing also provide frictionless rotation of shaft without slip. Main functions of bearing are:

1.4.1 Withstand load

Load on the bearing may occur from any of the direction sometimes bearing may bear loads from multiple directions also. Different load bear by the bearing during its working are classified as radial load, thrust load, angular load. The prime objective of the bearing is to bear the load without failure however the type of bearing used is having its own set

of applications and classified with respect to load. The different type of loads incur on bearing are as follows:

1.4.1.1 Radial Load

When the direction of load is across the radius of the bearing it means load is acting perpendicular to the supported shaft is known as radial load. This type of load will try to push the bearing in the downward direction. Most suitable bearing for supporting the radial load is taper roller bearing.

1.4.1.2 Thrust load:

When the direction of load is parallel to the supporting shaft then this type of load is called as thrust load. To prevent failure against the thrust load high strength is required. Most suitable bearing for supporting thrust load is thrust bearing also known as axial bearing.

1.4.1.3 Angular load:

If the load is neither perpendicular to supporting shaft nor parallel to the supporting shaft then the load is known as angular load. Bearing requires withstanding both combined radial and thrust load in angular loading. Taper roller bearing is mostly used to with stand against the angular load.

Further loading are classified as static and dynamic load. The static load includes the magnitude of the horizontal force and vertical force, externally applied force on the rolling elements of a bearing as a function of the relative displacement of the rolling element bearings. The outer and inner race of the bearing in a concentric position, separated by a uniform radial clearance are shown in Fig 1.2 The displacement of the outer ring was a result of the application of radial load on it along the y-axis is shown. Increase in load beyond the specific limit will result in premature failure of bearing. [13-18]. Radial load and axial load along with the moment acting on the bearing is shown in Fig 1.2.

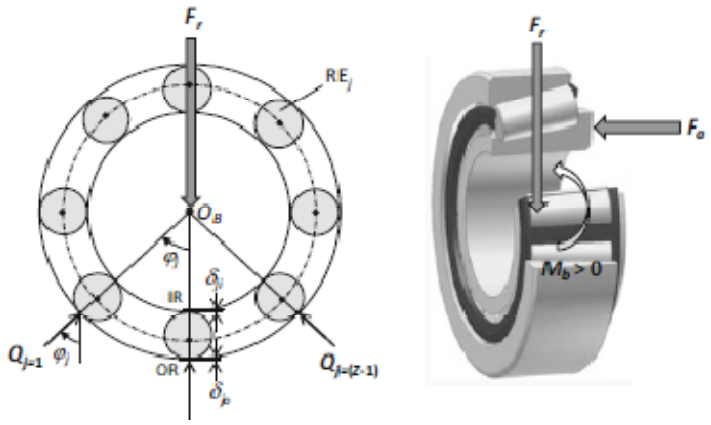

Fig 1. 2 Loads and Bending Moment on taper roller bearing

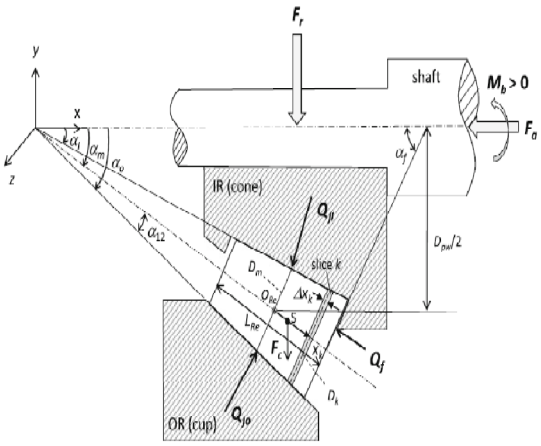

Fig 1. 3 Represents different load acting on taper roller bearing and line diagram of rolling element bearing supported by shaft is shown in Fig 1.3(b)

$$\sum F_X = 0$$

$$F_1 + F_2 - P = 0$$

$$\sum M = 0$$

$$F_1 l - F_2 (l - a) = 0$$

$$F_1 = P(1 - a / l)$$

$$F_2 = P\frac{a}{l}$$

Load during working operation on the shaft are produced by gears, pulleys etc. Bearing which is used to support the shaft produced vertical reactions which may be determined from equilibrium equations. If N number of loads acts on shaft then reaction of bearing can be obtained by principal of superposition and is given by equation 1.1.

$$F_1 = \sum P_k (1 - \frac{a_k}{l})$$

$$F_2 = \sum P_k \frac{a_k}{l}) \qquad (1.1)$$

1.4.2 Reducing friction

Friction generated in mating parts in rolling element bearing produces heat and results in power loss. Another function of bearing is to reduce friction between its mating components during its working operation. Inner race and outer race surface of rolling element bearing is having a smooth surface which also helps to decrease friction.

1.5 Bearing failure modes and classification of faults

In today's competitive world, any industry cannot sustain if its downtime is high due to the failure of any part of equipment. Industries used a variety of repair methods to keep equipment in good working order. The aim of maintenance is to keep machinery and plants running efficiently and safely. Breakdown maintenance and preventive maintenance are the two most common forms of maintenance techniques. Breakdown maintenance drastically effects the production of any company. Maintenance on a fixed schedule or routine maintenance and condition-based maintenance are all forms of preventive maintenance. One of the most useful predictive maintenance strategies is

condition monitoring. Machine condition monitoring provides enough information where fault is produced so that necessary action taken to avoid premature failure. The ability to calculate various parameters in real time and compare the results with established failure mechanisms is essential for successful diagnosis. Machine condition monitoring provides information on the current state, rate of degradation, and efficiency of the equipment [38-45]. To avoid unexpected failures, any deterioration in performance can be detected and preventive action taken at the appropriate time. This is accomplished by analyzing parameters such as wear debris in oil, vibration, acoustic emission, and temperature measurement etc [46-51]. Changes in measuring parameters in system monitoring assist in the identification of fault growth, and helps in failure prediction [52-55]. Corrective maintenance actions may be planned from the features extracted. The use of condition monitoring in bearings results in lower maintenance costs, increased machine availability and increased safety. Offline or online condition monitoring is both used in industries. Bathtub Curve is a graph that is commonly used to graphically show a run-to-failure of any part. There are three major regions where condition monitoring of component can be done and is defined by bath tub curve is shown in Fig 1.4.

1) Stage-1: Infant mortality (initial running-in): Stage-2: Normal life Stage-3: Wear out phase

Infant mortality phase basically shows the premature failure of any component. This is the main phase where the studies the prominently applied. Failures in this section are typically caused by manufacturing defects, improper assembly, wrong design and material defects. Second phase is also known as normal life where rate of failure is very less. Failure in this region occurs due to overloading, misalignment, hidden defects, cracks etc. In last phase normally wear and tear occurs and generally parts fails after spending its normal life. Failures in this region are generally caused by wear, fatigue, progressive deterioration, corrosion etc. This phase represents the end completing the life cycle.

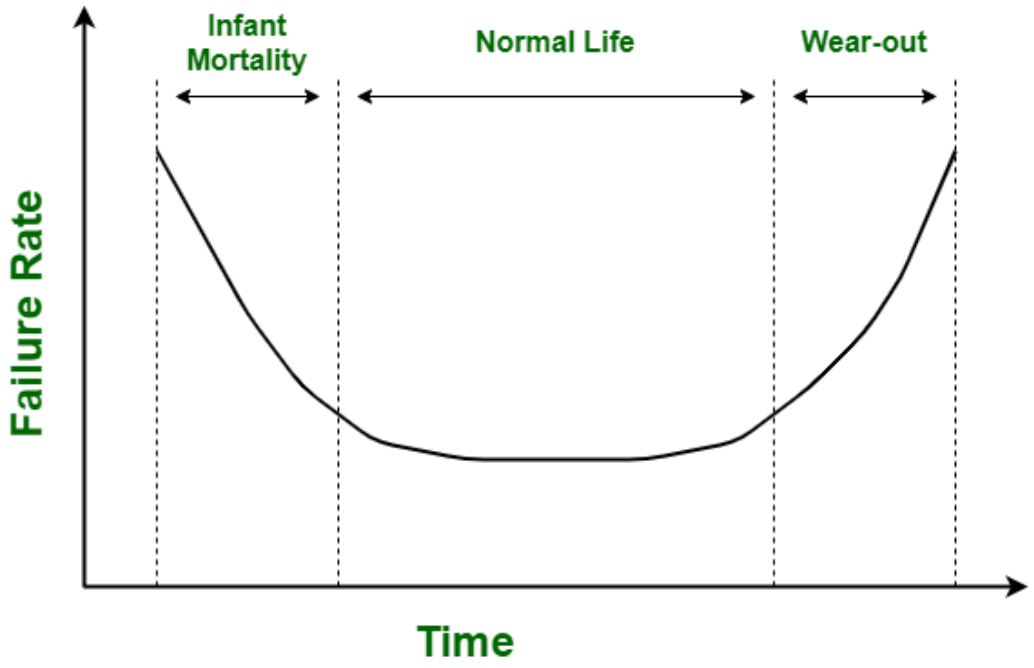

Fig 1. 4 Bath curve

In rolling element bearing external load is distributed and bear equally among all the rolling parts. Uneven load distribution drastically affects the life of bearing life and causes premature failure of bearing. During operation due to fatigue loading bearing are constantly subjected to compressive stresses which produce flaking or crack on surface of bearing. Flaking usually occur due to material fatigue and repeated stresses. One of the main reasons for occurrence of flaking or crack is the abnormal heavy axial load or impact load on bearing. Flaking occurs as material fragments break away when the rolling elements move over the cracks. The flaking grows worse over time, ultimately making the bearing ineffective and not able to perform its function. The number of revolutions a rolling bearing will perform before incipient flaking occurs is known as the life of rolling element. This is not to imply that the bearing cannot be used but flacking will results in increase in noise and vibration level in bearing.[32-34]. Heavy load acting on the bearing also generates more heat on to the bearing and changes the properties of the material and reduces the service life on bearing. [19-24]

Faults classification plays a very important role in vibration based condition monitoring because the number of different faults may give similar or different symptoms even they can occur at the same time. In recent day condition monitoring using vibration analysis and artificial intelligent techniques play significant role for giving solution to the complex problems. Techniques which are mostly used for fault classification includes Artificial Neural Network(ANN), Fuzzy logic, genetic algorithm, and support vector machines are such intelligence techniques popular in bearing fault diagnosis among the researchers. [24-25]

Artificial Neural Network (ANN) is a set of assembly of artificial neurons, which are interconnected to solve specific problem. For information processing, these neurons use a computational/mathematical model. Due to its ability to extract useful information from complex data, ANN is commonly used to solve problems that are difficult or impossible to solve using common computational and statistical techniques such as pattern recognition, fault detection, and classification [26-28]. In rolling element bearings defects are classified in two ways local defects which include defect crack, pits, spells, and defects caused by fatigue, waviness, surface roughness, off sized rolling element, misaligned races, and defect generated during manufacturing and installations are common distributed defects in rolling element bearings. Bearing damage classification are shown in Fig 1.5.

Each of these factors causes different types of damage and leaves a distinct mark on the bearing. As a result, inspecting a faulty bearing helps to establish a judgment on the nature of the damage and take the appropriate steps to prevent it from happening again in the majority of cases. Another major reason for bearing failure is the fatigue loading. The number of revolutions performed by the bearing and the intensity of the load define how long it might take for the first sign of fatigue to appear. Fatigue is due to shear stresses that develop cyclically below the load carrying surface of the bearing. These stresses eventually result in cracks that spread up to the surface. [29-31]

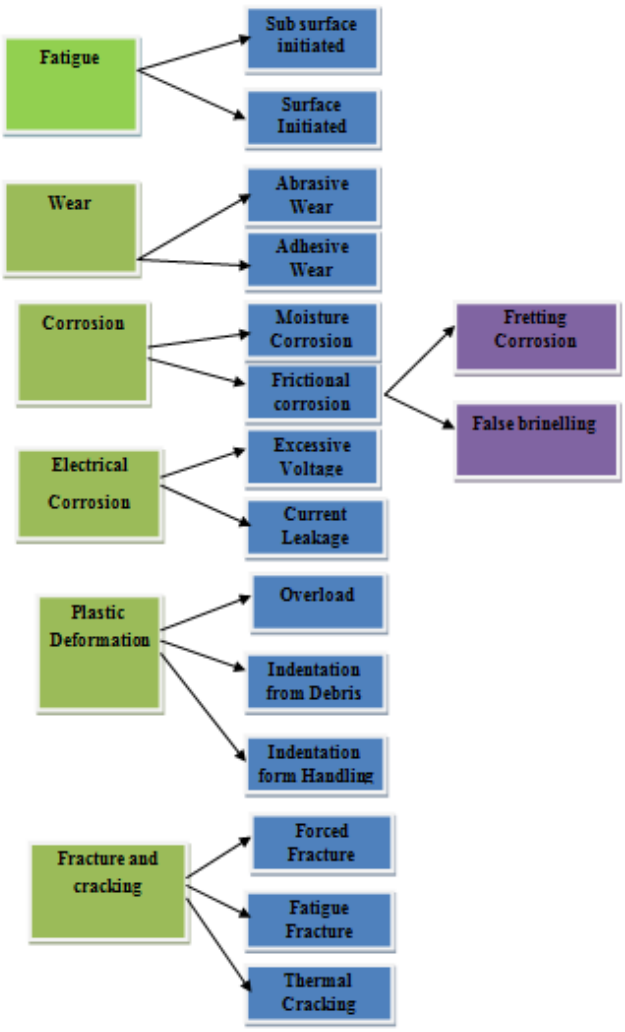

Fig 1. 5 Bearing damage classification

Few main reasons of bearing failure are:

1.5.1 Foreign Matter

Wear and pitting are two of the most common causes of bearing problems. Foreign matter is one of the most common reasons for bearing disorder and produces wear and pitting. This may be due to abrasive material, dirt, dust, steel chips, etc. The number of distinguishing marks such as scratches, indentation, and pits on the affected surface areas

was usually produced due to foreign matter. Periodic noise appears from the bearing during its working may indicate this form of defect. Adhesion with lubrication is among the most common causes of foreign matter in bearings.

a) b)

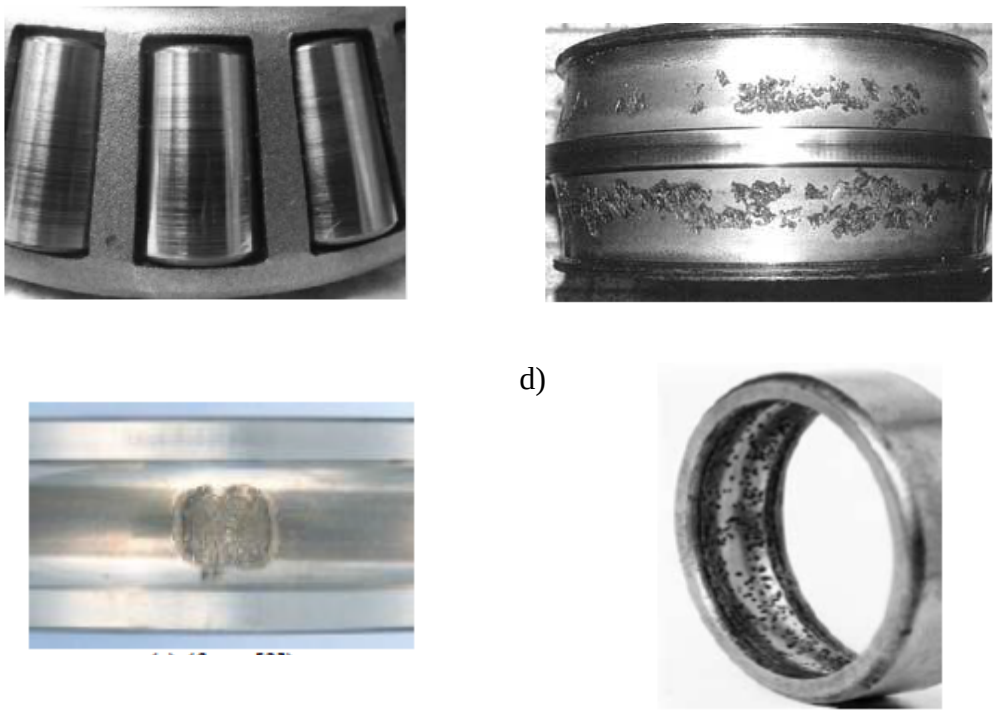

c) d)

Fig 1. 6 Bearing defects a) Wear marks due to foreign matter. b)Fatigue spall on bearing inner race c)flaking d) Corrosion

1.5.2 Bearing Fatigue

During the working operation the bearing rolling element rotates and moves to a new loading region it is subjected to repeated compressive and tensile stress. This results in the removal of metals from the surface of component's of bearing. Spalling or flaking is shown in Fig 1.6, a local defect in bearings produced due to fatigue in bearing. Excessive noise and vibration will be created by the damaged bearing due to such defects and causes premature failure of bearing. [35-36]

1.5.3 Brinelling

Brinelling is due to complicated phenomenon of mechanical and chemical reaction. The contact surfaces of bearings will be distorted or affected in the brinelling. Brinelling is occurred due to overloading and impact caused by dynamic loading. When the elastic limit of the raceway is exceeded, material leaves indentations on various locations of rolling element bearing components known as brinelling. False brinelling is the corrosion of the raceway surface caused by fretting.

1.5.4 Corrosion

Bearings are affected by the presence of water and acids in the working environment, which produces chemical attack on the bearing metal resulting in corrosion. Corrosion is shown by red and brown marks on surfaces. Corrosion causes pitting on surfaces and produces erratic and noisy signals.

1.5.5 High Temperature

Excessive heat generation or inadequate lubrication in the bearing causes the temperature of the bearing to increase results in surface crack in rolling element bearing. High temperatures decrease the hardness of bearing and further changes the properties of material causes early bearing failure. Overheating might occur due to misalignment excessive load or excessive vibrations transmitted to the bearing which changes the material properties and affect its normal working function.

1.5.6 Improper Installation

The inner race of the bearing and the shaft are installed in a press using interference fit. Improper installation often produces axial or radial preloading. Improper installation is distinguished by loose fits, tight fits, misalignment, housing shape, and incorrect bearing selection. During operation improper installation along with misalignment induces unbalanced force on the bearing and generates excessive heat.

1.5.7 Improper lubrication

Overheating is caused by a lack of lubrication or the inappropriate selection of lubricant. Insufficient lubrication between contact surfaces creates a high stress region and causes the contact surfaces being welded together, deep scratches and welding of contact surfaces. Improper lubrication in rolling bearings can cause high friction, high amplitude and vibration levels due to surface to surface contact between the parts.

1.5.8 Plastic deformation

Plastic deformation occurs between the surfaces in contact due to excessive stationary load or impact load applied on rolling element bearing. This results in a localized defect in the bearing. Plastic deformation will cause excessive noise and vibration in bearing during its running operation and drastically affects the life of bearing. [37]

1.6 Techniques for detecting defect

Without indication, a minor fault in the bearing will easily deteriorate into a dangerous failure mode. As a consequence, it is important to focus on it on a regular basis. Vibration-based Condition Monitoring is an important feature of predictive maintenance, which has gained popularity over the decades **[57].** Fault detection, diagnostic, and prognosis are the three primary phases of vibration-based condition monitoring [58-62]. The ability to locate and detect faults as early as possible in critical component such as bearing is important to prevent sudden failure and study suggest crack is the major reason of failure. During operation when a rolling element collides with a defect or crack on a bearing element, the rolling element's vibration energy changes. Change in vibration energy excites the bearing component. This will result in increase in amplitude of vibration at excited frequencies and impulses are produced at regular interval of time corresponds to defect frequency. Time domain, frequency domain and time-frequency domain analyses are the common methods of analyzing vibration signals for extracting useful feature about location and severity of the fault **[63-67].** From the time domain

analysis usually find out statistical parameters such as root mean square value, peak value, crest factor and moments like kurtosis. Time domain contains the information when it happens and graph is plotted between amplitude vs time. In frequency domain analysis various frequencies extracted from vibration signal like natural frequency, characteristic fault frequencies and its harmonics by different transformation methods such as fast Fourier transform and provides information what happens. For getting advantage of what happens and when time-frequency domain analysis techniques happen where used such as wavelet transform, Discrete wavelet transform, Short term Fourier transform. Coinciding local defect and distributed defect in bearing is results so many different frequencies in spectrum, which is quite difficult to identify the informational frequency. Carrying out this analysis manually has its own limitations. In Vibration based condition monitoring vibration signature of the systems was captured using a data acquisition system, and the signals was processed into a format from which important information can be extracted. Since the existence of a fault is determined by the nature of a sensor signal, signal processing is required as a methodology to determine whether the processed signal includes any features which can indicate the presence of a fault.

The signal processing techniques are widely used in defect detection and its measurement because of their powerful ability to react on the minor changes in the vibration signal. In this section these techniques will be discussed in brief with their practical significance in extracting the features of vibration signal

1) Thermography.

2) Wear debris

3) Acoustic Emission (AE) technology

4) Time Domain

5) Frequency Domain

6) Finite element analysis

7) Time Frequency domain Techniques

8) Strain Measurement.

9) Oil Analysis.

1.7 Thermography: Vibration analysis and thermography techniques are both widely used in industries as preventive and predictive maintenance**.** The infrared radiation emitted by the body's surface is used to create a thermal image, which can then be used to locate hot regions on the body. Hot spots are caused due to the component deterioration with passage of time. Themograpghic camera is used to locate the hot spots and acts a valuable tool in condition monitoring. Thermal Energy emitted from target surface is measured in thermography and it found application in many fields such as spectral thermography, material testing, electrical equipments, biomedical applications, vibro-thermography, thermal imaging systems etc.

1.8 Wear Debris: In this technique lubricant is taken at different interval of time and chemical analysis of lubricant was performed. Wear debris analysis is normally used for detecting faults and analyzing abnormal wear pattern. In wear debris analysis SEM/EDX on filtered metal debris samples was analyzed and different spots of silicon, carbon, iron (Fe), oxygen etc were identified and calculated in average weight percentage.

1.9 Acoustic Emission (AE) technology: One of the non-destructive techniques is acoustic emission measurements that have been used to detect defects in components. The generation of transient elastic waves caused by an energy emitted from a localized source within the material is referred to as acoustic emission (AE). When an external load is applied to a system, stress waves are released which propagate to the surface and can be easily detected by using acoustic sensors [94-95]. Acoustic emission technology found

applications in condition monitoring and diagnosis of rotating equipments such as pumps, bearing, gear box etc.[96-98]

1.10 Vibration based analysis techniques: Different vibration based analysis techniques broadly classified as time domain techniques; Frequency based techniques, Time frequency techniques.

1.10.1 Time domain techniques

The signal recorded from any machine component through DAQ device has to be processed for extracting useful information. The general graph of acceleration vs time analysis or any processing done without making any changes in the time domain is known as time domain processing of the signal is shown in Fig 1.7

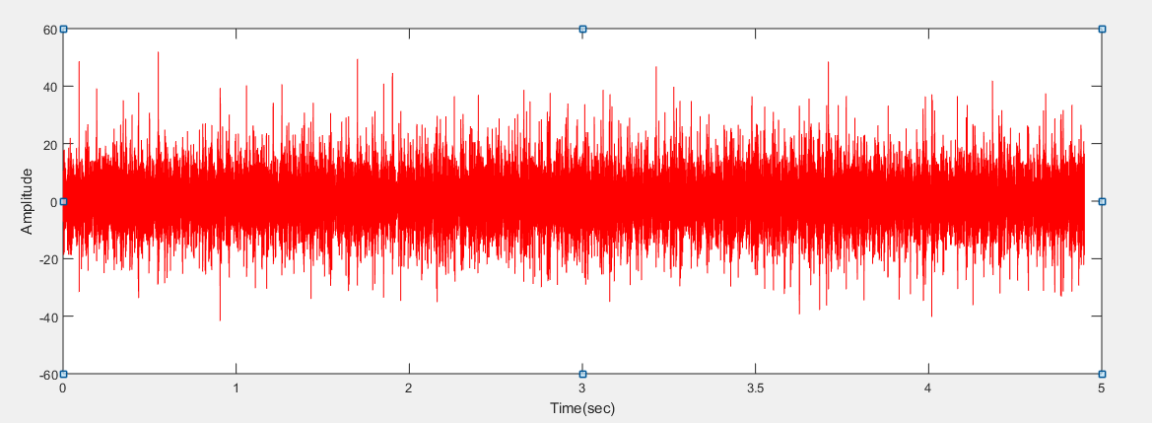

Fig 1. 7 Raw signal for outer race defect in bearing

In condition monitoring, statistical features of vibration signal are powerful tool to detect relevant features. Extracting the statistical values such as standard deviation, RMS, Skewness, Kurtosis, Shannon entropy etc. of the simple acceleration vs time data helps in

estimating the state of system as any abrupt change in statistical value indicates fault or condition of the component [68-73]. Each statistical parameter is having its own characteristic for detecting the minor changes in the vibration signal. Generally, statistical values are used for distributed defects such as wear out surface, misalignment and imbalance because of their capability to extract features in synchronization with the calculated values [74-75]. In such cases statistical parameters can be helpful in analyzing such changes using vibration signal. Nevertheless, the scope of statistical parameter is not limited to detect the defects but for many other cases such as effect of loading conditions, variable rpm and contact characteristics can be analyzed.

1.10.1 .1 Root mean square (RMS):

RMS value is related to power or amplitude of the signal. If the amplitude of the vibration level is increased then appearance of defect can easily be detected by using statistical parameter RMS and it can be used for detection of fault. Result of RMS in case of defective bearing and normal bearing can be compared for detection of fault. Theoretically RMS can be calculated by formula.

$$RMS = \sqrt{\frac{\sum_{k=1}^{n} x_k^2}{n}} \qquad (1.2)$$

x_k is the signal amplitude and n denotes for total data points.

1.10.1 .2 Standard Deviation: It is represented by letter σ is used to measure the data from mean position or value.

$$\sigma = \sqrt{\frac{\sum_{k=1}^{n} (x_k - \bar{x})^2}{n}} \qquad (1.3)$$

$\bar{x}$ reflects the signal's average value of amplitude When there is defect then the peak of amplitude will increase it will cause increase in value of standard deviation and cause more deviation from its mean value. If mean is zero then standard deviation is equal to RMS value of signal

1.10.1.3 Skewness: It indicates symmetry of data and if calculated is negative then curve is shifted to left if it is positive then curve is shifted to right and when it is zero then the curve is perfectly symmetric to the to the normal distribution curve. It generally gives the good indication for the cases having the local defects signatures in the form of sharp impulses.

$$Skewness = \frac{1}{n}\frac{\sum_{k=1}^{n}(x_k - \bar{x})^3}{\sigma^3} \qquad (1.4)$$

1.10.1.4 Kurtosis: Kurtosis is a statistical parameter gives information of impulsiveness in the signal. Higher value of kurtosis gives higher value at mean and longer tail. kurtosis value increases with increase in defect due to impulse created when rolling element pass through the defective region. Hence it can be used for detecting faults in rolling element bearing [76]. It generally gives the good indication for the cases having the local defects signatures in the form of sharp impulses.

$$Kurtosis = \frac{\frac{1}{n}\sum_{k=1}^{n}\left[x_k - \bar{x}\right]^4}{\left[\frac{1}{n}\sum_{k=1}^{n}\left[x_k - \bar{x}\right]^2\right]^2} \qquad (1.5)$$

1.10.1.5 Shannon entropy (SE): Shannon entropy gives information about the randomness of data in signal. Shannon entropy measures the randomness in raw signal by using logarithmic scale. This uses of logarithmic scale to amplify the values of final result even if there is small variation in randomness of the measured signal. This parameter is widely used in many applications such as image processing [77], structural health monitoring [78], motor fault diagnostics [79] and gear fault detection for extracting features [80]. Mathematically for a random signal x with N outcomes x_0, x_1, x_2.....x_{N-1} and with probability of $P(x_i)$ can be expressed by equation (1.6). If there are '*N*' number of total outcomes and '*ri*' as incident rate of each possible outcome then

$$P(xi) = \frac{ri}{N} \tag{1.6}$$

And total number of outcomes is given by equation (1.7):

$$N = \sum_{i=0}^{N=1} n \tag{1.7}$$

Rewriting the expression of SE is given by equation (1.8)

$$S(X) = \log_2 N - \frac{1}{N} \sum_{i=0}^{N=1} n \log_2 n \tag{1.8}$$

1.10.2 Frequency domain techniques

The most prominently used technique for frequency domain is Fast Fourier Transformation (FFT). The FFT of raw signal changes the time domain signal to frequency domain and during this time domain information is completely lost. It generally converts the signal into two parts real and imaginary and in general real part is plotted for the representation. The frequency contents of raw signal are displayed in the

graph and frequency contents strongly present in the signal can be analyzed using FFT is shown in Fig.1.8.

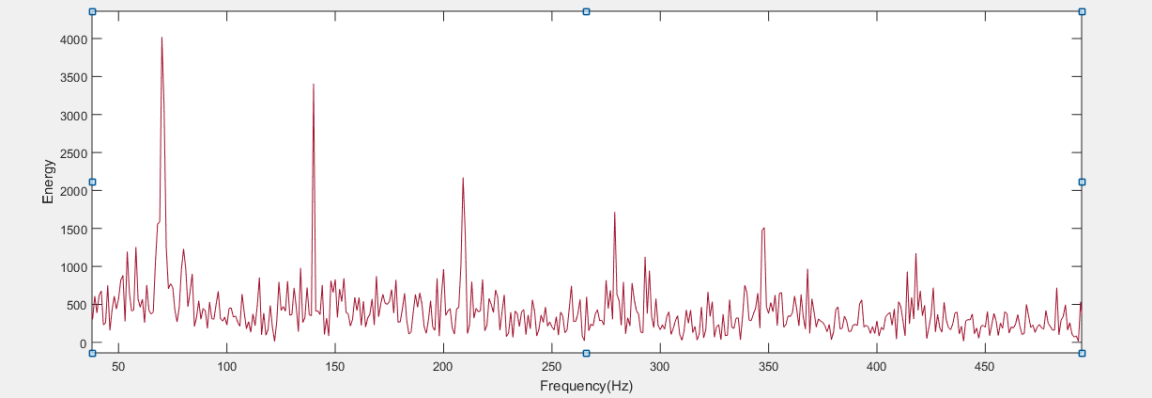

Fig 1. 8 FFT for defective bearing

It is possible to re-construct the raw signal from the FFT graph by using the function inverse fast Fourier transform IFFT. The frequency domain techniques are well suited where particular frequency event need to be detected for instance such as outer race defect frequency, inner race defect frequency, fundamental train frequency etc The equation (1.9) represents the FFT *x(f)* of signal *x(t)* and *t* signifies time.

$$x(f) = \int_{-\infty}^{\infty} x(t) e^{-i2\pi f t} dt \qquad (1.9)$$

1.10.3 Time-Frequency techniques

Both time and frequency domain information are established in time-frequency techniques. There are many transforms used in the time -frequency techniques but most common transform is continuous wavelet transform (CWT). This function is operated by scaling function and translation function through mother wavelet. The scaling function is driving the frequency components for the presentation for example

$$f(x) = \int_{-\infty}^{\infty} x(t).e^{\iota wt} .dx \tag{1.10}$$

$$f(x) = \int_{-\infty}^{\infty} f(x).e^{-\iota wt} .dx \tag{1.11}$$

high frequency components of the signal goes to the low scale and low frequency to the high scale. The equation for CWT is as follows

$$Xb(a,b) = \frac{1}{a^{1/2}} \int_{-\infty}^{\infty} X_{(t)} \mu\{\frac{t-b}{a}\} dt$$
$$X(t) = signal \quad function$$
$$\mu \quad = Mother\ wavelet \quad . \tag{1.12}$$

(a) Short Time Fourier Transform: To address this shortcoming, Dennis Gabor (1946) modified the Fourier transform to evaluate only a small portion of the signal at a time, a technique known as signal windowing known as the Short-Time Fourier Transform (STFT), converts a signal into a two-dimensional frequency and time function.

It gives some details about when and at what frequencies a signal event occurs [81]. Once a time window size is selected, it remains the same for all frequencies is a major disadvantage of short term Fourier transform.

In this signal is split into a series of data points with a fixed window size in the axis of time, and each sub band is then Fourier transformed. Through this transformation one can have the frequency information of the selected window length in the time domain. The STFT of raw signal x(t) in the time domain can be drawn by using equation (1.13).

$$Y(t,\ f) = STFT(x(t)) = \int_{-\infty}^{\infty} x(u)h(u-t)e^{-j2\pi fu}du \qquad (1.13)$$

. Where x (t) is the raw domain signal in time domain h(t) is a STFT window function.

(b) Continuous wavelet Transform: Wavelet offers signal time scale statistics to aid feature extraction for signals that change over time [82]. Wavelet analysis can be used to diagnose transient and non-stationary signals. Whenever, there is any local fault the impulses are formed in the signal, these impulses are high frequency events and can be easily spotted by time-frequency techniques with good time resolution Signal processing techniques such as CWT are effective when dealing with vast amounts of data and providing a timely and reliable analysis of condition monitoring of bearing. Wavelet-based feature extraction technique can be used to obtain or extract features from signal and classify bearing faults is shown in Fig 1.9.

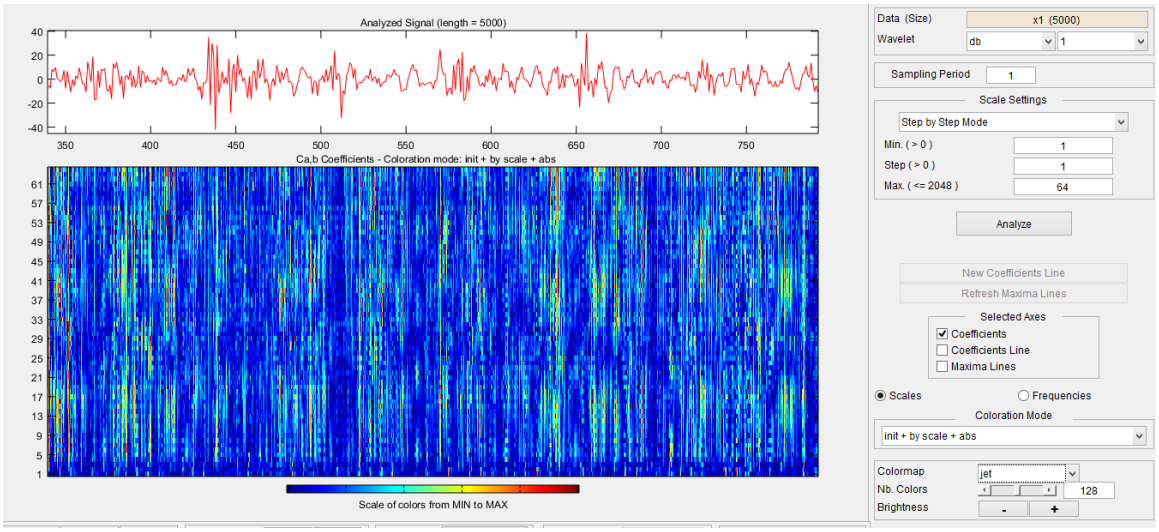

Fig 1. 9 CWT of bearing outer race defect showing burst

The Continuous wavelet transform (CWT) of signal processing technique uses the shifted wavelet function. and given by equation 1.14. The wavelet transform, as compare to STFT, which has a fixed window size allows for different window sizes for analyzing various frequency components present in a signal, when a is chosen in such a way it is compressed it has high frequency and capture all high frequency components and using function b wavelet will be slides along axis. When wavelet is stretched its frequency will reduce and it capture low frequency detail [83-86]. CWT converts a continuous signal f(t) into a wavelet coefficients function comprises of real continuous variables, scale and translation. The wavelet transform is a mathematical method for highlighting the hidden characteristics in a raw signal. These hidden characteristics are having equal significance in time and frequency domain. A wavelet is mathematically defined as a function CWT (a,b) and represented by equation (1.14)

$$CWT(a,b) = \frac{1}{\sqrt{a}} \int_{-\infty}^{\infty} f(t).\phi(\frac{t-b}{a})dt \qquad (1.14)$$

The CWT produces a large number of wavelet coefficients C which are dependent upon scale and position. Multiplying each coefficient by scaled and shifting wavelet provides the component of wavelets of the signal.

Scaling

Wavelet analysis generates a time-scale representation of a signal. Scaling (or compressing) a wavelet is used for stretched or compressed the waveforms.

Shifting

With the help of shifting parameter b wavelet can be shifted along time axis. Examples of scaling and shifting using wavelet is shown in Fig 1.10.

Fig 1. 10 Wavelet function Ψ(t) and shifted wavelet function Ψ(t-k)

The most stretched wavelets correspond to higher scales. If a is compressed it has high frequency and it will capture all high frequency component in signal and with b wavelet will be slide along the axis multiply with signal x(t) and after integrating all coefficients of the wavelet can be capture. When wavelet will be stretch its frequency will be reduce which will capture low frequency detail. Further if wavelet is stretched and slide along the axis it will get all coefficients Fig1.11 shows the compressed and shifted wavelet for capturing high frequency and low frequency

Fig 1. 11 Low scale and high scale wavelet

(c) Mother wavelet: Mother wavelet plays prominent role in time-frequency analysis method that has extensively used in biological, structural machinery applications. [87]. The most significant part in any of the wavelet analysis technique is selecting the mother wavelet. This is because every mother wavelet is having the unique feature and can be used for extracting the unique characteristics of vibration signal. In wavelet theory numbers of wavelets are available and out of which few of them are discussed below.

Haar Wavelet: Haar wavelet is discontinuous, and resembles a step function shown in Fig 1.12. Mathematically Haar wavelet can be written as equation (1.15)

$$\psi_{haar}(t) = \begin{cases} 1 & 0 \le t \le \frac{1}{2} \\ -1 & \frac{1}{2} \le t \le 1 \\ 0 & otherwise \end{cases} \quad (1.15)$$

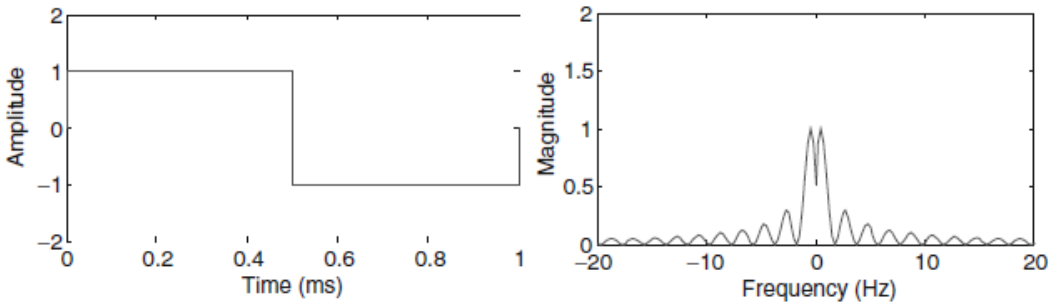

Fig 1. 12 Haar wavelet and its magnitude spectrum

Haar wavelet is symmetrical and orthogonal in nature. It implies that when this base wavelet is used in a wavelet filtering operation on a signal the filtered signal will have no phase distortion. Haar wavelet found application in edge extraction, image coding, fault detection and many more [88].

Daubechies Wavelet: The Daubechies wavelets have been extensively studied for bearing and gear fault diagnostics [89]. This is supported by base wavelet with support width 2n-1, where n is the order of base wavelet. The Daubechies wavelet grows smoother as the support width increases, resulting in greater frequency localization. The expression of Daubechies wavelet is given by the equation (1.16) to equation (1.17).

$$z(y) = \sum_{K=0}^{N-1} X_K^{N-1+K} Y^K X \quad (1.16)$$

Where X_K^{N-1+K} denotes binomial coefficient and Daubechies wavelet upto 10^{th} order can be used for the practical applications . In 10^{th} order, value of n can be taken as 10.

$$\left|mo(\omega)\right|^2 = (\cos^2(\frac{\omega}{2}))^N P(\sin^2(\frac{\omega}{2}))$$

$$where\ mo(\omega) = \frac{1}{\sqrt{2}} \sum_{k=0}^{2n-1} h_k e^{-ik\omega} \qquad (1.17)$$

Morlet Wavelet: The Morlet wavelet has often been used for detecting transient features in signals characteristics and is given by expression (1.18):

$$\psi_m(t) = \frac{1}{\sqrt{\pi f_b}} e^{i2\pi f_c t} e^{\frac{t^2}{f_b}} \qquad (1.19)$$

Where f_b denotes the bandwidth parameter and f_c represents center frequency. Morlet wavelet has been extensively used in bearing, gear and other rotational components defect detection [90-93].

1.11 Signal processing

In vibration analysis signal is being captured from the vibrating machine by transducer and with help of data acquisition system (DAQ). Signal is stored in the computer system. From the raw signal it is difficult to identify the fault at incipient stage because of its weak signature. Signal processing techniques is very useful and can be applied to identify the fault and to extract hidden features. [99-101]. The main working of signal -processing based techniques is shown in Fig1.11 In this firstly raw signal was recorded using transducer which converts physical signal into voltage. Then signal in the form of voltage goes to Data acquisition (DAQ) device and signal gets converted into readable values

format. Then analog signal is converted into digital for the purpose of processing by using analog to digital convertor (ADC). Signal again can be converted from digital to analog form using digital to analog convertor (DAC). Then signal gets analyzed for final results and to extract hidden features. Signal processing techniques is mostly used in detecting the defect of rotating equipments such as shafts, gears, bearings etc. The main advantage of using signal processing for condition monitoring is that one need not to dismantle the rotating equipments for the purpose of inspection. Steps used in vibration analysis for condition monitoring is shown in Fig 1.13.

1.11.1 Transducer

Piezoelectric transducer or accelerometer is used most commonly used to capture the vibration signal from the machineries. It contains piezoelectric crystal and whenever stress is applied it start producing current sensing element detect the change and produces the output. Sensor is used in accelerometer that measures the acceleration of a system as voltage. Accelerometers are the transducers that are usually installed directly on high-frequency components like gearboxes, rolling-element bearings etc. Different methods to mount the accelerometer include probe tips, adhesive magnetic, stud mounts. Different method of attachment directly affects the accelerometer's measured frequency as looser connection will result in different frequency component. High level of stress and temperature can damage it so it is always specified with the temperature and load range by the manufacturer.

1.11.2 Data acquisition

Data acquisition systems, basically interface between machine and computer that record the physical signal from machine by transducer and convert that signal into computer readable language that can be processed in the computer. Data acquisition is an important stage in the condition monitoring of rotating machinery such as gears, bearings in vibration analysis and it mainly depend upon the features such as number of channels, sampling frequency and its resolution.

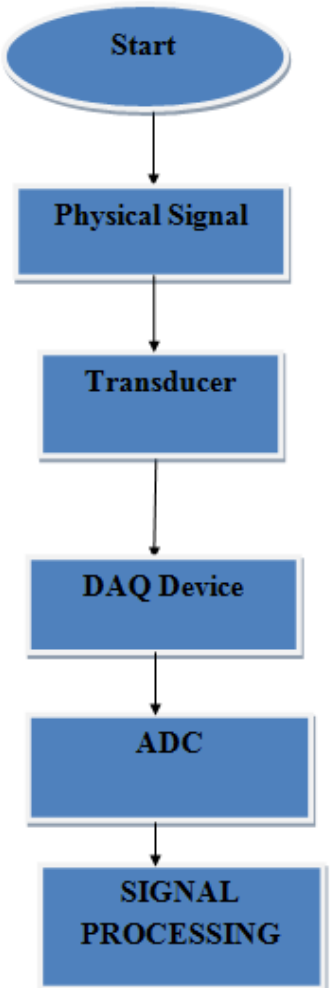

Fig 1. 13 Flow chart Signal Processing

1.11.3 Analog to digital Convertor (ADC)

The computer software that we use for analyze the recorded signal or raw signal cannot understand the electrical signal. Electrical signal is not processed by software so we require changing the electrical signals into digital signal that can be understand by the computer. An analog to digital, or ADC converter, is a device that converts an analogue signal to a digital signal. This converter uses integrated circuit (IC) that converts a signal from one form to another such as continuous to discrete form.

1.11.4 Digital to analog convertor

This type of convertor takes up the data from computer in the binary form to convert it into analog data. This is facilitating the user to read the data easily and in understandable mode.

1.11.5 Signal processor

Vibration signal carries useful information in terms of amplitude, phase, frequency and its shape etc. Signal processor processes the signal which helps in predicting the real state of the component and to abstract the relevant features. Software which are mostly used for signal processing are matlab, lab view etc.

1.12 Motivation: Modern slow-speed rotating machines (such as wind turbines) are fatigue-loaded devices, and operational experience has revealed that their components fail at high rates. Main reason of the failure of this component is the bearing. Components of rotating machinery are repeatedly subjected to bending stresses which may develop cracks and eventually cause the component to fail. Metal fatigue is a well-known problem in industries due to repeated stresses. Hence condition monitoring is important aspect for detecting the fault in mechanical equipments. Reliable and robust monitoring systems can help to plan corrective maintenance before a component fails completely and reducing the damage to other components.

1.13 Objectives of the research

1) To design and manufacture customized Bearing test rig with option of running at different RPM and loading conditions

2) To record the signal after the fix interval of time at constant rpm and different loading conditions for taper roller bearing having seeded defect.

3) To find most appropriate parameter using vibration analysis techniques in relation to defect propagation at different loading conditions

Chapter 2 Literature Survey

2.1 Introduction: Rolling element bearing are basically found application where assembly are subjected to radial or axial load. In few applications rpm of inner race is very slow and the radial load acting on bearing assembly is sufficiently large produces different defects in bearing causes premature fail of the bearing. In this chapter different techniques and methodologies used by different researchers for fault diagnosis and predicting the heath of rolling element bearing using different signal processing techniques were discussed. Further different conventional techniques used for crack propagation analysis such as X-ray residual stress measurements, Strain Measurement, energy-dispersive X-ray spectroscopy, scanning electron microscopy SEM instruments, direct current potential drop method (DCPDM) through previous published research work along with the simulation approach used by different researchers has been discussed. This chapter also focuses on various studies for bearing failure diagnosis such as vibration response analysis, signal processing techniques, feature extraction techniques, and simulation approach using finite element method for rotating equipments such as gears, shafts and bearings etc.

2.2 Effect of loading on different element of bearing: Crucial component in any rotating machineries are shaft, bearing seals and couplings. Main reason of shaft failure are stress concentration due to key way, material impurities from where crack initiation started during its working operation and loose parts resulting in unbalanced force which causes high fatigue loading and can damage shaft. Another major component in any rotating machinery is bearing which is used to support load, constraint motion and to reduce friction between matting part. Within machine tools, rolling element bearings are an essential component for power transmission systems. Rolling element bearings are

employed in the construction of increasingly complex arrangements, such as high speed, high temperature, withstand heavy loads, and operations that must be continuous [102-103]. Bearing are subjected to different loading conditions in actual operation where crack initiation and propagation is directly proportional to load [104-106]. These crack induced excitation causing the bearing to vibrate at high amplitude and produces periodic stresses in machine parts which results in fatigue failure. These excitations at any speed usually depend upon the load acting over the crack and width of the crack. These crack initiation and propagation results in premature failure of bearing. For many decades, bearing fault modeling, simulation, and condition monitoring using vibration signal, acoustic, and thermal characteristics have been topics of constant research, which involves computational approaches. [107-109] Study suggests main reason for failure in any rotating machineries is the rolling element bearing.

2.3 Kinematics of cylindrical roller bearing

Bearing generates different frequency component during its normal working operation. In case of defective bearing when roller/ball pass over the defect then it produce an impulse [110-112] corresponding to its frequency. These impulses will be having its own value of frequency depending upon number of rollers, rpm of the shaft, roller diameter/ball diameter, pitch circle diameter and pressure angle etc. Different bearing defect frequencies are listed below also known as characteristics of bearing frequencies

N_b= Number of balls

W_i = Relative speed difference between inner and outer race (RPM)

V_i= inner race Velocity

V_o= Outer race Velocity

P_d= Pitch diameter = $\{D_i + D_o\}/2$

B_d= Ball diameter

Φ = Contact angle

D_i = Diameter of Inner Race

D_o = Diameter of outer race

F_s= Speed of Shaft Rpm

2.3.1 Fundamental Train Frequency: FTF is also known as cage frequency, and it is the angular velocity of the cage which carries rolling element of bearing. Linear velocity, angular velocity and fundamental train frequency are given by expression 2.1.

$$Vc = \frac{V_I + V_0}{2}$$

$$WC = \frac{V_C}{R} = \frac{(V_I + V_O)/2}{P_D/2}$$

$$FTF = W_C = \frac{[Wt(Pd/2 - BdCOS\phi/2) + Wo(Pd/2 + BdCOS\phi/2)]}{Pd}$$

$$= \frac{1}{2}[Wi(1 - \frac{BdCOS\phi}{Pd}) + Wo(1 + \frac{BdCOS\phi}{Pd})] \quad Where\ Wo = 0$$

$$FTF = \frac{WI}{2}[1 - \frac{Bd}{Pd}COS\phi] \qquad (2.1)$$

2.3.2 Ball pass frequency of outer race (BPFO): The BPFO is defined as the rate at which rolling element travels through a fix point and is given by expression 2.2 where φ is the known as pressure angle.

$$Outer\ race\ \ frequency = Nb.FTF$$

$$Nb\frac{wi}{2}[1 - \frac{Bd}{Pd}\cos\phi]$$

$$= Nb[Wi - \frac{1}{2}[Wi\ (1 - \frac{BdCOS\phi}{Pd}) + Wo(1 + \frac{BdCOS\phi}{Pd})]$$

$$= Nb\ (Wi - Wo)(1 + \frac{Bd\cos\phi}{Pd}) \quad where \quad Wo = 0$$

$$= Nb[\frac{Wi}{2}\{1 + \frac{Bd}{Pd}COS\phi\}] \tag{2.2}$$

2.3.3 Ball spin frequency (BSF): Ball spin frequency (BSF) is the angular velocity of a ball around its own axis. It is calculated by expression given in equation 2.3.

$$BSF = [(\omega i - \omega c)\frac{ri}{rb}] = \omega i - \omega c[\frac{Pd - Bd\ \cos\phi}{\frac{Bd}{2}}]$$

$$BSF = \omega i - \frac{1}{2}[\omega i(1 - \frac{Bd\ \cos\phi}{Pd}) + \omega o(1 + \frac{Bd\ \cos\phi}{Pd})][\frac{Pd - Bd\cos\phi}{Bd}]$$

$$= (\omega i - \frac{\omega i}{2} + \frac{\omega iBd\ \cos\phi}{2Pd} - \frac{\omega o}{2} - \frac{\omega oBd\ \cos\phi}{2Pd})(\frac{Pd - Bd\cos\phi}{Bd})$$

$$= (\frac{\omega i - \omega o)}{2}(1 + \frac{Bd\cos\phi}{Pd})(\frac{Pd - Bd\cos\phi}{Bd})$$

$$= \frac{\omega i - \omega o}{2}(\frac{Pd}{Bd} - \cos\phi + \cos\phi - \frac{Bd\cos^2\phi}{Pd})$$

$$= \frac{\omega i - \omega o}{2}(\frac{Pd}{bd})(1 - \frac{Bd^2\cos^2\phi}{Pd^2})$$

$$= \frac{Pd}{2Bd}(\omega i - \omega o)(1 - \frac{Bd^2\cos^2\phi}{Pd^2})$$

.

Different characteristics of Bearing are BSF, BPFO, BPFI and FTF.

Ball spin frequency (BSF) = $f_s \frac{P_d}{2B_d}\left(1 - \frac{B_D^2}{P_D^2} COS^{\ 2}\phi\right)$ (2.3)

Outer race frequency (BPFO) $= f_s \frac{N_B}{2}\left(1-\frac{B_D}{P_D} COS \quad \phi\right)$ (2.4)

Inner race frequency (BPFI) $= f_s \frac{N_B}{2}\left(1+\frac{B_D}{P_D} COS \quad \phi\right)$ (2.5)

Fundamental train frequency (FTF) $\frac{F_S}{2}\left(1-\frac{B_D}{P_D} COS \quad \phi\right)$ (2.6)

For the last few decades, vibration studies of rolling part bearings have attracted the attention of researchers. Researchers have suggested multiple models with different degrees of freedom to represent the vibration signal. In these experiments, the excitations caused by defects and errors were also treated in different ways. [113-114]

2.4 Conventional techniques for analyzing crack propagation: Contact fatigue is a type of failure that mostly occurs in machine components such as rolling element bearing, gears that have highly stressed due to fatigue cyclic loading. Failure is produced by the loss of material from bearing surfaces due to Initiation and propagation of fatigue cracks [115-116]. Process of crack growth occurs normally in two phases crack initiation and crack propagation. Crack initiation mostly caused by stress raisers on the material's surface such as scratches or by defects introduced during operation debris damage caused by asperity contact. Contact fatigue also results in crack initiation and propagation which occurs due to damage induced by changes in the material microstructure due its fatigue loading. Main parameters which effect the crack initiation includes microstructure of the material, type of applied stress, geometry of the specimen etc all influence the position and mode of fatigue crack propagation which permanently damage the material**.** Further crack initiation can also occur due to dislocations, high stresses at particular regions, plastic deformation around inhomogeneous material, faults or defects in or beneath the contact surface and microstructure of a material.

The number of revolutions performed by the bearing and the intensity of the load define how long it might take for the first sign of crack to appear. Crack is due to shear stresses that develop cyclically below the load carrying surface of the bearing. These stresses eventually result in cracks propagation that spread up to the surface. Crack propagation happens as material fragments break away when the rolling elements move over the defective region. The crack grows worse over time, ultimately making the bearing ineffective and not able to perform its function. This is not to imply that the bearing cannot be used due to crack propagation but will results in increase in noise and vibration level. Initiation and propagation of crack in bearing may lead to failure of bearing in rotating machinery which may result in machine collapse and costly downtime. Further loading can cause a crack in the bearing to spread rapidly and in such cases the bearing should be replaced as it drastically affect the remaining useful life of bearing. During operation crack edges were smoothen out and started new edge formation with passage of time which may be due to healing. The term healing refers to the process in which rolling contact smoothing the sharp edges of a crack or damage zone which further results in reduction in vibration amplitude.

Different conventional techniques available for measuring crack propagation rate includes X-ray residual stress measurements, Strain Measurement, energy-dispersive X-ray spectroscopy, scanning electron microscopy SEM instruments, direct current potential drop method (DCPDM) [117-122]. Major disadvantage of conventional methods is that the bearing needs to be dismantled from bearing casing for inspection and sometimes cannot be used for normal operation again. To overcome this problem vibration analysis can be used an alternative method to analyze bearing condition without disassembling it.

2.5 Significance of vibration analysis in defect identification:

Different techniques used for analyzing crack propagation discussed in previous chapter. Application of these techniques used by different authors is discussed in this section.

Major advantage of vibration analysis is that bearing need not dismantle from bearing casing and it predict the machine failure before breakdown. Sassi et al. (2007) suggested a vibratory model and considered in the analysis to assess the vibration response. The simplistic model ignores the effects of shafts, housing, and other supporting structures focuses on flexural vibration alone [118]. Bearing maximum deflection is depicted in Fig 2.1

Mass of outer race, Inner race and rolling element are represented by M0, Mi and Mr and inner race and outer race stiffness are denoted by Ko , Ki respectively. Stiffness and Damping coefficient between outer race and rolling element are represented with K_{of} and B_{of}. Excitation forces acting on inner race outer race and rolling element are represented with Q_o, Q_i and Q_r resulting in displacements yo, yi and yr of the same elements respectively. Vibratory model of tper roller bearing suggested by Sassi et al is shown in Fig 2.1

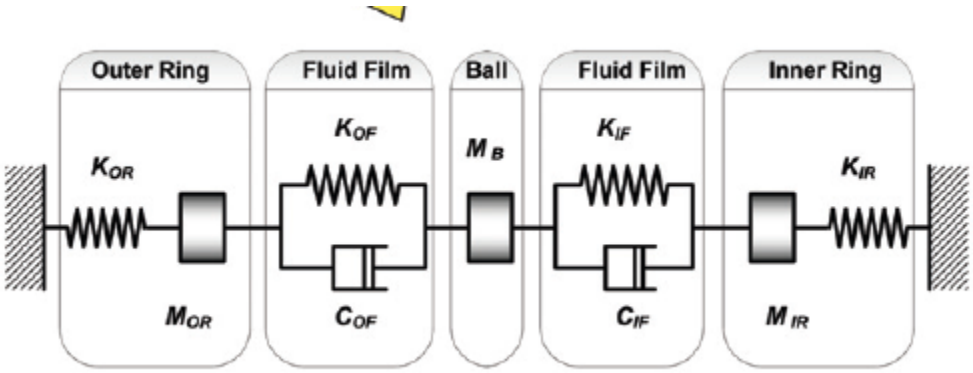

.

Fig 2. 1 Mass, Stiffness and damping model of bearing

The coupled non homogeneous differential equations for the above model for displacements in principal direction can be expressed as shown in

$$[M]\{\ddot{y}\} + [B]\{\dot{Y}\} + [K]\{Y\} = \{Q\}$$

Where [M] is known as mass matrix, [b] is known as damping matrix and [K] is known as stiffness respectively whereas {Q} and {y} are excitation and displacement vectors due to defect.

$$[\mathrm{M}\} = \begin{bmatrix} Mo & 0 & 0 \\ 0 & Mr & 0 \\ 0 & 0 & Mi \end{bmatrix}$$

$$[\mathrm{b}] = \begin{bmatrix} bof & -bof & 0 \\ -bof & bof + bif & -bif \\ 0 & -bif & bif \end{bmatrix}$$

$$[K] = \begin{bmatrix} ko + kof & -kof & 0 \\ -kof & kof + koi & -kif \\ 0 & -kif & kif + ki \end{bmatrix} \{\mathrm{Q}\} = \begin{bmatrix} \mathrm{Qo} \\ \mathrm{Qr} \\ \mathrm{Qi} \end{bmatrix} \text{ and } \{\mathrm{y}\} = \begin{bmatrix} \mathrm{Yo} \\ \mathrm{Yr} \\ \mathrm{Yi} \end{bmatrix} \quad (2.7)$$

a) Impact Force: The steady-state rotation of inner race is needed in most rolling-element bearing applications. As the ball travels through a defect region, the strength of the impact felt by the bearing components is depend upon the relative speeds and the external load applied [123-125]

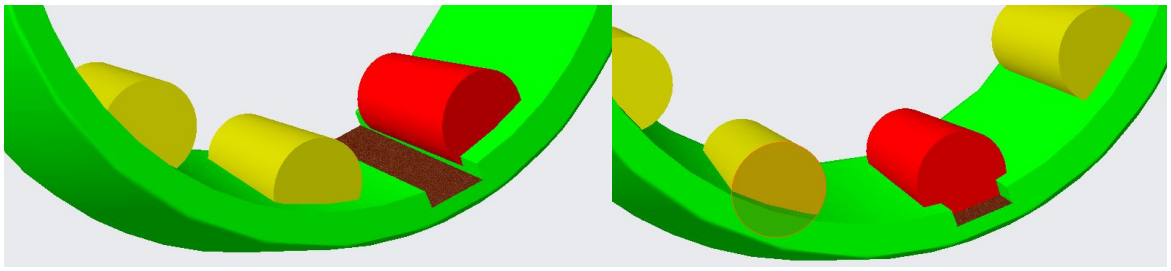

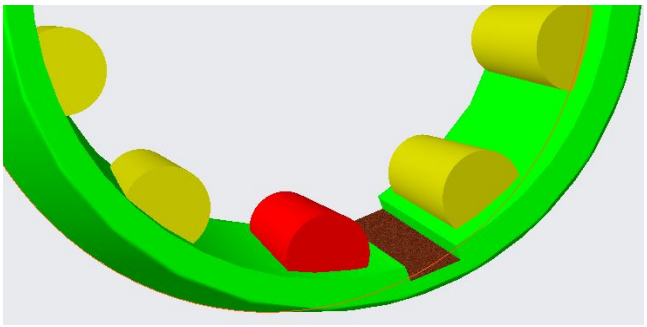

Fig 2. 2 Kinematics of the roller motion around the edge of the defect area: state 1 is before shock, state

b) Shock Pulses

Vibrations caused by impacts are a short-term phenomenon which created high impulses of short duration of time as bearing rotates such impacts recur on a regular basis depending on relative speeds, resulting in repeated shocks. The number of repetitive impacts and the frequency of vibration are therefore determined by the speed and number of rolling bodies [126-127]. Fig 2.2 shows the roller touching the groove defect and passing over the defect creating impact force and shock impulses. These shock impact force produces high stresses in critical region like defect or crack in rolling element bearing.

Review was carried out by Sharma et al. on non linear dynamic analysis on rolling element bearing and discussed different analytical model of rolling element bearing along with its advantages and limitations. The inner radial clearance is significant parameter in the nonlinear investigation of roller element bearing. Smaller clearance values would increase the amount of direct interaction between the ball, metal-to-metal, and races, whereas higher clearance values would result in larger, more unstable systems. Furthermore, the increased clearance resulted in an increase in noise level. On the surface of bearing materials localized and distributed defects grow over time. Some of the

localized defects occur during the handling and installation of the bearings. These defects profiles are unstable, resulting in unwanted defects and unsteady vibrations. [128]

Study was carried out of fatigue loading on spall defect by Hoeprich using vibration signal. It has been observed that raceway spalls in ball bearings are a common failure mode and are caused by sub-surface fatigue cracks that develop after a while even also occur when the bearing is properly lubricated, installed and loaded. Subsurface cracks grow over time and eventually break through to the surface creating a spall or crack. Over time, the spall progresses into more severe damage that affects a larger area of the raceway. [129]

Prabhakar et. al proposed the discrete wavelet transform(DWT) for detection of bearing raceway fault. The discrete wavelet transform (DWT) provides a signal's time-scale information and helps in transient feature extraction that varies with time. Defect on inner race, outer race and combination was analyzed using discrete wavelet transform and further suggested that for analyzing the non stationary signal DWT is an effective tool. [130].

Bearing failure evolution and fault diagnosis were expressed by using statistical parameters by Nistane and Harsha. Work proposes the statistical features for failure evaluation of ball bearing under radial loading conditions. Scalar parameters depict ball bearing damage but do not provide information about the defect's position and location. During experimentation it was proved that loading plays a crucial role in defect initiation and propagation. [131]

Jaiswal et al. proposed different techniques such as wavelet transform and artificial neural network for detecting the defect in roller element bearing. Proposed techniques can be used for identification of defect in outer race, inner race and on roller element bearing. [132]

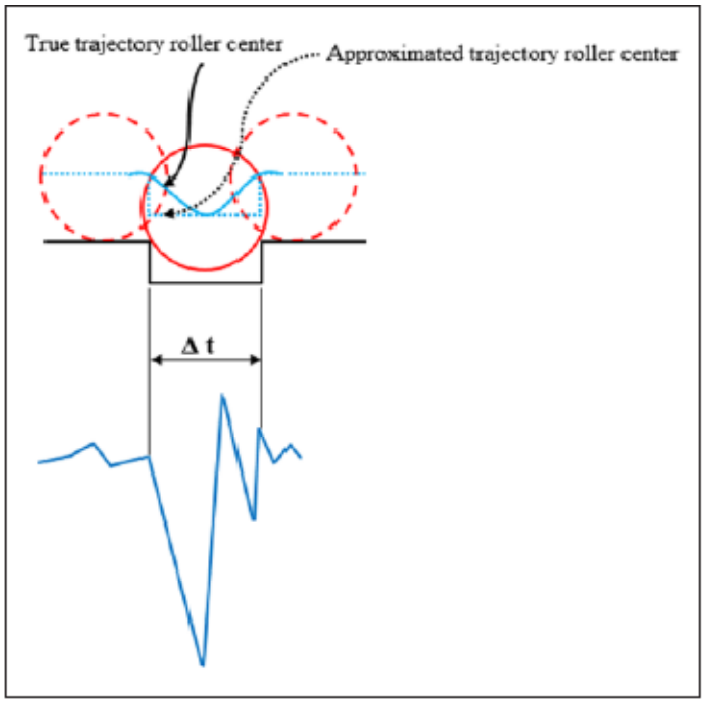

Fig 2. 3 Typical Vibration Impact duration and corresponding to roller duration over an outer race defect.

In another study by Tian et.al author uses a spur gear with crack on one tooth. In this author uses statistical techniques and DWT to study crack propagation . RMS is a better indicator to study crack propagation among all statistical parameters. Crack produced different impulses in defective gearbox and the impulses using the vibration signals can be used to detect the presence of tooth cracks and further helps to estimate crack severity.[133]. A review of vibration and acoustic measurement was carried out by Tandon and Choudhury and was concluded that occurrence of a defect causes vibration levels to increase significantly. The interaction of localized defects with the mating elements of a bearing produces very short-duration pulses. These pulses are specific to a bearing element which are based on kinematic consideration and produced the characteristic such as bearing defect frequency or ball passing frequency [134]. For these frequencies the expressions are given in equation [2.1-2.6]

Li et al. used the Hermitian wavelet as the function for performing CWT for identifying signal singularity. Singularity in the signal was generally caused by localized defect in rolling element. These techniques can be used to extract features for localized defect and hence successfully implemented for diagnosis [135]. Elforjani and Mba used acoustic emission technology to detect natural crack initiation and propagation in rolling element bearing and was one of the few studies on natural degradation of rolling element bearing [136-138]. In almost a similar way controlled experiment was carried out to determine the applicability of AE technology for monitoring fatigue crack initiation and growth and was one of the works attempted to link AE activity to natural defect generation in rolling element bearings [139-141]. To calculate the outer race defect width on taper roller bearing Singh and Kumar used symlet wavelet and image analysis. In their study artificial defect was seeded on outer race of taper roller bearing and proposed a symlet 5th order mother wavelet for detecting the defect width and these techniques successfully implemented for measuring the crack width [142]. Igba et al. used RMS and peak levels of vibration signals and were used to investigate fault detections in wind turbine gearboxes and proposed three new novel techniques (signal correlation, extreme vibration, and RMS intensity) for detecting the fault. The proposed methodologies were validated using a time domain data driven approach and data from wind turbine condition monitoring. Their findings revealed that signal relationship with RMS values were useful for detecting early stages of progressive failure [143].

Coinciding local defect and distributed defect in bearing is results so many different frequencies in spectrum, which is quite difficult to identify the informational frequency. Carrying out this analysis manually has its own limitations. Signal processing technique like wavelet packet transform plays vital role as condition monitoring. The WPT separate detail and approximation coefficients which indicate energy at each node is shown in Fig 2.4 The decomposition mode does not remove or add any information from the original signals. As shown in result, the WPT is well suited as signal processing techniques particularly non-stationary signals from of taper roller bearings. Non stationary signal are

the signal whose frequency content change with respect to time. Equation 2.8 defines the wavelet packet is given below:

$$u_{2n}^{(j)}(t)=\sqrt{2}\sum h(k)u_n^{(j)}(2t-k)$$

with n = 0,1,2 and k =0,1…..m (2.8)

$$u_{2n+1}^{(j)}(t)=\sqrt{2}\sum g(k)u_n^{(j)}(2t-k)$$

Where $U_0^{(0)}(t)$ is scaling function and $U_1^{(0)}(t)$ base wavelet function of $\Psi(t)$.

:

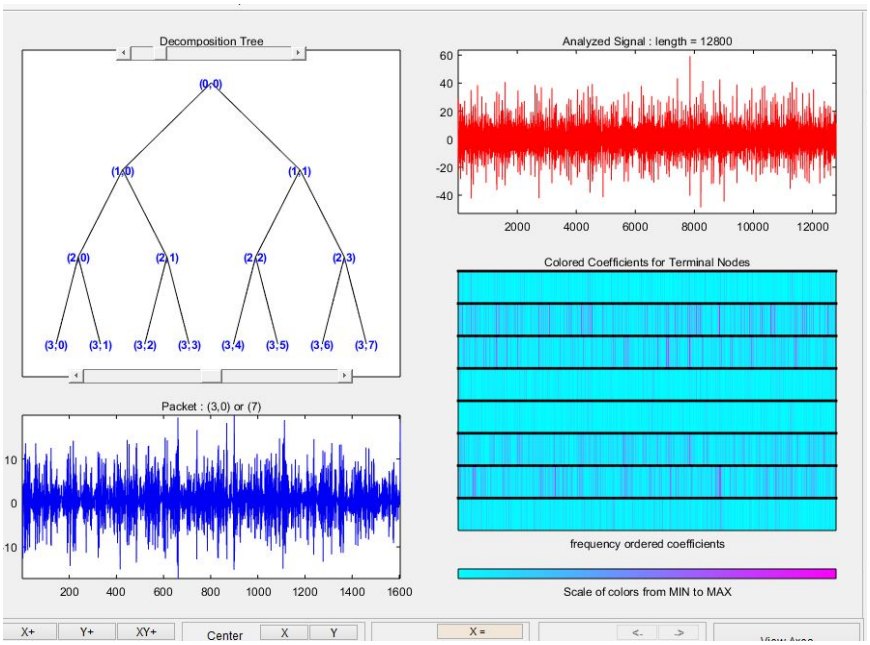

Fig 2. 4 Tree structure for wavelet packet transform

For the identification of Gear box defects Fan et al. used the Hilbert transform to extract features and the wavelet packet transform to analyze the signal. The proposed method is

tested using both simulated and actual vibration signals acquired from a gearbox dynamics simulator. The results of the analysis reveal that the proposed method is effective of extracting features from raw vibration signal and detecting early gear faults [144]. For bearing defect diagnosis Meng et al. computed the statistical parameter kurtosis. Signal was processing using discrete wavelet transform and wavelet packet transform for extracting the features of high frequency band.[145].

Tse et al proposed envelope analysis and wavelet analysis for diagnosing the fault in rolling element bearing. The outer race, inner race, and cage are the main parts of a rolling element bearing that are most likely to fail during its normal working conditions. A sequence of impact vibrations occurs in short time intervals as a result of this causes rolling element bearing failure and they mostly occur at bearing fault frequencies also known as bearing characteristic frequency. As these fault frequencies contain very small energy of short duration of time and are often dominated by high level of noise and larger levels of vibration produced by various sources. These frequencies are difficult to locate in their frequency spectra using the conventional technique such as Fast Fourier Transform (FFT). Envelope detection and wavelet along with the FFT was proposed to identify or diagnosing the fault in rolling element bearing. Series of experiment was performed on motor pump and proposed that envelope analysis and wavelet is useful along with the FFT for detecting fault in rotating equipments such as bearing [146]

In another study by Lin et al. proposed wavelet based de-nosing technique for fault detection in rotating equipments. Periodic impulses produce at regular interval of time in gears form the defective rolling element bearing indicate that the defect is present in the component. However, because the impulses are weak and sometimes hidden by background noise, it is difficult to identify them at the initial phase of a defect. A new approach for denosising the signal was proposed using morlet wavelet as basic wavelet This technique are very useful for low signal to noise ratio. [147]

A Belsak and J Flasker has proposed a technique for path of crack propagation in rotating parts such as gears. Crack is the major reason for failure in gears and produces hindrance in its working operation. Vibration analysis technique plays a vital role for detecting the crack at early stages. Experiment was carried out and time signals were captured for analyzing the broken tooth. A gear unit with a damaged tooth has a different dynamic response as compared to healthy tooth. Proposed a time frequency technique such as Short term Fourier transform for detecting the crack on gears and successfully implemented this technique. Crack initiation mostly occurs in a region where maximum principle stress occurs in a gear tooth [148].

Based on the measurement of local energy density Loutridis suggested a method for monitoring the development of gear defects. Theoretical model was proposed for a pair gear pair with a crack on tooth. Test rig was designed and experiment was conducted on gear with root crack. The continuous wavelet transform and the energy density of the vibration signal related with the meshing of defective gears were used to examine experimental results. The local energy has been found to be a sensitive parameter for determining fault intensity and further empirical law was suggested for relating the energy content to severity of crack. [149]

2.5 Hertz theory of elasticity

A brief description of the Hertz theory was discussed in this section. Contact interaction between the rolling elements and raceways of a rolling element bearing is governed by the conventional Hertz elasticity theory which gives the stress within the rubbing part. Two spheres came into contact creates a point contact and line contact is created when two parallel cylinder came into contact with each other. Increase in pressure cause yielding of two surfaces and creates a very small indentation through yielding. Contact stresses thus created are also called hertzian contact stresses are shown in Fig 2.5. Hertz stresses are also known as stress closest to this area of contact between to spheres or

parts. When two non-planer bodies came into the contact with each other under the effect of force it produces a hertzian contact stresses [150]. Hertzian tells the stress with the rubbing part as found many applications such as taper roller bearing which can be calculated by equation 2.12. Tapered roller bearings used in applications which are typically subjected to harsh loads and environmental conditions. If external variables are neglected, bearing life and failure are primarily determined by surface and sub-surface stresses that develop on the bearing surface.

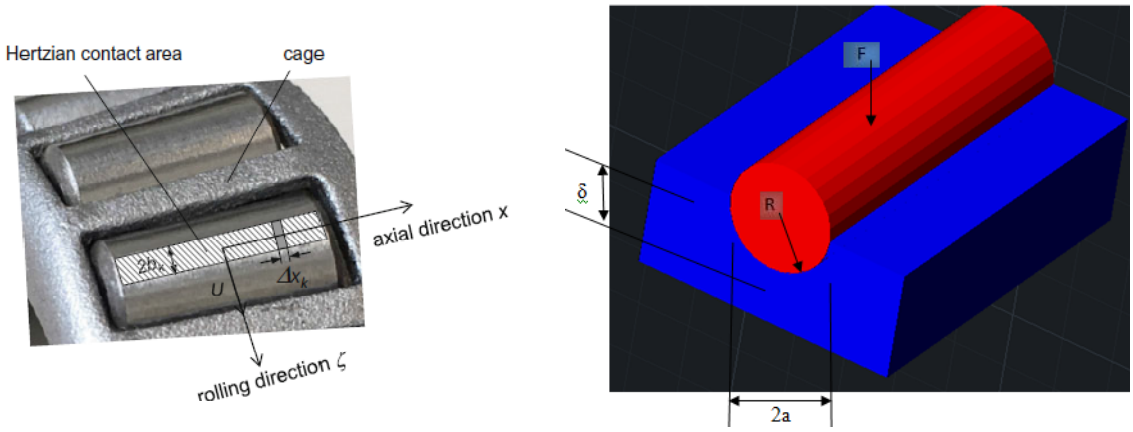

Fig 2. 5 Hertzian Contact Zone and Indentation of a roller on an elastic surface

$$Stiffness \quad k = \frac{df}{du} = \left(E^2\ R\ F\right)^{1/3} \tag{2.9}$$

$$Depth\ of\ indentation\ \mu = \left(\frac{2F^2}{E^2\ R}\right)^{1/3} \tag{2.10}$$

E_1, E_2 are the elastic moduli and v_1, v_2 the Poisson's ratios associated

$$\frac{1}{E} = \frac{1}{2}\left(\frac{1-\mu^2}{E1} + \frac{1-\mu^2}{E2}\right) \tag{2.11}$$

$$Stress\,\sigma_{\max} = \frac{3F}{2\pi a^2} = 0.4\left(\frac{E^2\,F}{R^2}\right)^{1/2} = 0.4\frac{K}{R} \tag{2.12}$$

2.6 Simulation Techniques: The analysis of the forces acting on the various elements of the bearing during action is known as bearing dynamics. The dynamic simulation of a bearing for high-performance applications is difficult and non-linear. Geometrical nonlinearity and kinematic nonlinearity all contribute to the nonlinearity due to material. The performance is periodic and predictable when the system is linear. The performance of a non-linear system is unpredictable it may be periodic, sub-harmonic, or even erratic. When analyzing a physical system, its operation can be modeled mathematically as an equation. A linear equation can be used to express the system if it is supposed to behave linearly. A non-linear differential equation is significantly more difficult to solve than a linear differential equation. Only a few non-linear differential equations have exact or approximate solutions. Most non-linear problems can be solved with less computational effort using modern computational techniques such as finite element method [151-153]. The non-linearity of a system is a factor that can lead to the system's chaotic behavior.

For a long time bearing fault modeling, simulation, and condition monitoring using vibration, acoustic and thermal characteristics have been topics of continuous research, and they are constantly improving with the application of computational approaches. A dynamic loading model of the bearing structure is proposed by Kiral and Karagulle based on bearing kinematics and loading type. The forced vibration analysis of a bearing structure is carried out under the influence of an unbalanced force transfer to the structure by ball bearings. Further for diagnostic rolling element bearing, time and

frequency domain analysis are used. The statistical parameters of vibration signals for bearings with defects and bearings without defects are compared. Sudden Change in value of statistical parameter indicates presence of fault and finite element method can also be used for condition monitoring of rolling element bearing [154].

Singh et al. developed a finite element model to investigate localized outer race defect. An analysis on contact forces among rolling elements and the outer race was presented by the author. LS-DYNA finite element software was used for the analysis of rolling element bearing. To analyze the contact behavior a mathematical model was established and successfully implemented for calculating the noise frequencies. The relative movements of the cage, rollers, outer race and inner race of cylindrical rolling element bearings are critical in understanding their results [155].

In another study commercial program ABAQUS/CAE was used to simulate a three-dimensional finite element model of ball bearing with outer race defect by Nabhan et al. Analytical and numerical method for was used to analyze the contact stress distribution of deep groove ball bearing (SKF6004). Analytical method was based on hertzian contact theory and was developed using MATLAB software. Model developed using finite element method successfully reveal the contact response and hence finite element can be used for analyzing contact stresses in any region which further helps identify critical areas for design optimization.[156]

Commercial package of ANSYS APDL was used to simulate a three dimensional model of ball bearing and further to validate the result hertzian contact theory was used by Zhaoping and Jianping. Proposed model was successfully implemented to get the contact response and will help for strength analysis and designing of rolling element bearing. Contact analysis gives the contact response and contact behavior when one part came in contact with another part such as stress and strain analysis [154]. Xin and Zhu analyze the deep groove ball bearing using ANSYS workbench. Three dimensional model was built to obtain contact stresses and hertz theory was used to validate result. By simulating the

result author concluded that FEM can be used design optimization and failure analysis [155]

Structural analysis was carried out on ball bearing by Sulka et. al and calculate stresses and displacement of rolling element bearing using ANSYS workbench . Simulated result were obtained was compared with hertzian contact theory and results were found closely matched. Lostado et.al. use double row taper roller bearing for the analysis and studied the contact stresses on outer race by experimentally and using FEM analysis. Authors established a method for adjusting the initial mesh by producing successive nonlinear sub-models with decreasing mesh densities. It was proved that experimental values will match closely to FEM value when finer mesh was created by reducing the element size. [156]

Ezaki et al. model taper roller bearing and calculate stress in the retainer experimentally and by using simulation. Author built a three dimensional and analyzed using multi body dynamics software ADAMS and was successfully implemented for simulating the results and contact response. Parameters such as rotational speed and loading play a crucial role in contact response between the retainer and roller [157].

Shaharohit and Kulkarni [158] developed a finite element model using ANSYS with local defect on the bearing inner race and investigated the bearing vibration characteristics under various operating conditions. Author have taking into account the time-varying excitation and the contact force between the rollers and the inner or outer raceway, as well as the influence of sliding, inertia force and other aspects was considered. It has been noticed that variation of speed has high impact on amplitude of vibration signal and simulated vibration pattern has same characteristics as experiment one. Utpat developed a three dimensional finite element model of a deep-groove ball bearing having localized defects on the outer and inner rings. Finite element software ANSYS was used for simulation. Effect of various size of defect was simulated and results were validated with experimental values. Defect on outer race create more amplitude as compare to defect on

inner race under constant speed and amplitude of vibration is less affected by variation in loading. Results using simulation were closely matched with experimental values. [159]

2.7 Scope and research gap: In industries the bearing is subjected to various loading conditions. The defect in the bearing could propagate differently for different loading conditions Vibration analysis techniques were found useful in detecting crack, crack size measurement and crack propagation [160-162]. However, the same crack performing under different loading conditions and its analysis was paid very little attention. The most of literature is for defect detection and defect size measurement is available. However the defect propagation rate was paid very less attention by varying loading conditions. Further interim changes happened during crack propagation such as edge breakage, smoothness was not identified. From the family of wavelet best mother wavelet for edge breakage and crack propagation simultaneously was not identified and presented. Less contribution has been made by authors for finding correlation of crack propagation with simulation parameters. This study presents a controlled experiment to determine the applicability of vibration analysis for monitoring the crack propagation rate on taper roller bearings under different loading conditions**.** Further finite element models was created of taper roller bearing NBC-30205 as per manufacture catalogue to examine and simulate the contact behavior of bearing with outer race defect.

Chapter 3 Experimental methodology and modeling

3.1 Introduction: Finite element models are those that employ a certain commercial finite element software package or code to analyze or solving the complex problems. Finite element software packages that are mostly utilized for simulating contact behavior of rolling element bearing includes ANSYS[163-166], ABAQUS[167], Nastran[168], LS-DYNA[168]. Two methods are normally used in ANSYS for generation of model solid modeling and another is direct generation. Solid modeling is used for complex three dimensional models such as taper roller bearing. If geometry of model is complex then these are imported from Initial Graphics Exchange Specification (IGES) file in ANSYS environment [169-171]. IGES file can be created by using CAD system such as CREO, Solid works, cataia, Proe etc. ANSYS software is the most advanced package used for simulations, offering enhanced tools. ANSYS is basically finite-element simulation software numerically used to solve a wide range of mechanical problems. Static/dynamic, structural analysis, heat transfer, and fluid difficulties, as well as acoustic and electromagnetic problems, are examples of these problems which can be solved using ANSYS software. In this chapter experimental methodology along with the specification of all parts and simulation procedure was discussed..

3.2 Experimental Test Rig: A bearing test rig was designed and prepared for carrying out the experimentation of crack propagation for taper roller bearing with a provision of customized radial load on the bearing. The main shaft of the test rig was driven by an AC current motor having capacity of 1.5 kilowatt (Make: Crompton and speed 1500 rpm). A variable frequency drive (VFD) was provided to vary the shaft speed. Two taper roller bearings (NBC, Model 30205) were placed in bearing casings as shown in Fig 3.1. to support the rotating shaft. An optical tachometer was used to measure shaft

speed during experimentation. A PCB make accelerometer with a sensitivity of 1000mV/g was used to measure vertical acceleration and was positioned at the top of the bearing casing 2. At the top of bearing casing 2 a hole was provided to apply radial load directly on the bearing outer race as shown in Fig 3.2 Complete specification of experimental test rig along with the load cell specification is shown in Table 3.1 A load cell is a type of transducer that transforms force into a measured electrical output. It work on the principal that when a force is applied to the sensor, its resistance changes. During experimentation load cell arrangement was used to measure the applied load is shown in Fig 3.2

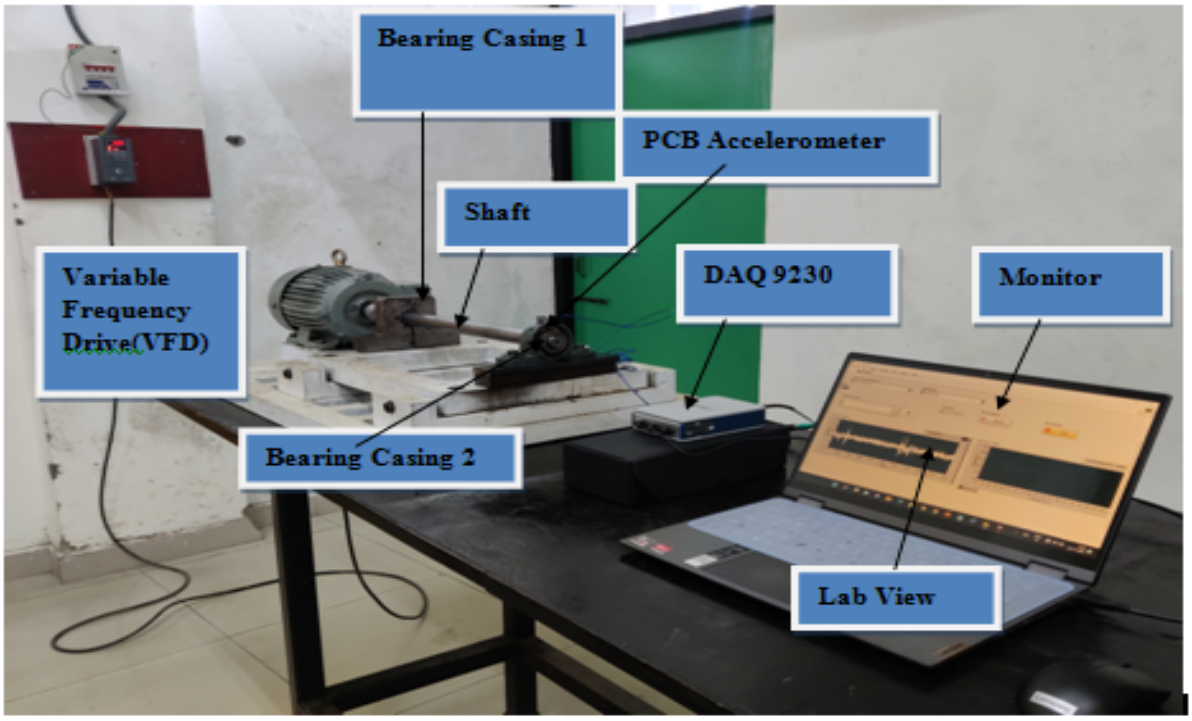

Fig 3. 1 Complete set up bearing test rig

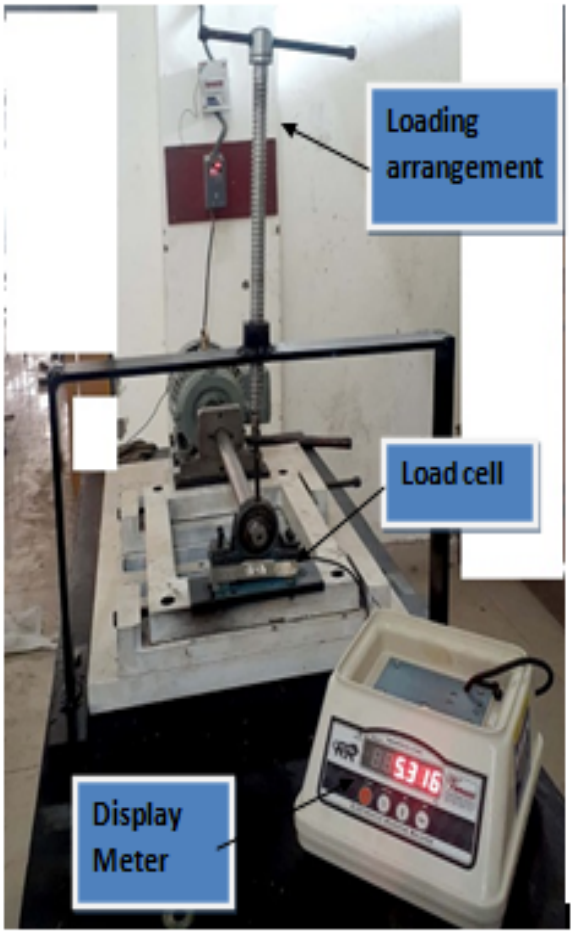

Fig 3. 2 Load Cell arrangement for measuring load

Table3. 1 Specification of test rig

Sr. no.	Component	Specification
1	Supply	A.C
2	RPM	1500

3	Motor	1.5 KW
4	Phase	3
5	Current Rating	2.62 A
6	Variable Frequency Drive(Voltage)	240 to 480 VAC
7	Bearing Specification	NBC 30205(Taper roller bearing)
8	Sensitivity of accelerometer	1000 mV/g
9	Sampling rate of data acquisition	12800 sample/second

3.3 Instrumentation: The analogue to digital conversion and the recording of the signal were done by using DAQ-9230 data acquisition card. It continuously recorded data to a hard drive using lab view. Specification DAQ 9230 used for experimentation is shown in Table 3.2. During operation computer was set up to monitor and record the vibration data from the outer race defective bearing by using accelerometer. Data acquisition software lab view made by national instruments is used for extracting the vibration features from the bearing. Signals from integrated electronic piezoelectric (IEPE) such as accelerometers are measured by the DAQ 9230 and NI software.

Table3. 2 Data Acquisition 9230 configurations

Sr. No	Number of channels	3 analog input channels
1	ADC resolution	24 bits
2	Type of ADC	Delta-Sigma (with analog prefiltering)
3	Sampling mode	Simultaneous

4	Internal master timebase (fM)(Frequency)	13.1072 MHz
5	Internal master timebase (fM)(Accuracy)	±100 ppm

3.3.1 Accelerometer: Microscopic crystal structure in piezoelectric accelerometers provides a voltage output proportional to the acceleration forces applied. Bearing analysis using accelerometer has been used by many authors and provides a satisfactory results[172-173]. The accelerometers used in this study was PCB made PIEZOTRONICS model. The measurement range of these accelerometers was Measurement Range: ±500 g pk (±4905 m/s² pk) with an frequency range Frequency Range: (±5%)1 to 10000 Hz . During experimentation accelerometer mounted on top of bearing casing to capture vibration signal. Sensing element of accelerometer is quartz as per manufacturer catalogue.

Fig 3.3 shows the fundamental design of a piezoelectric accelerometer. Piezoelectric discs are held between a mass and a base to create the transuding element. When vibration occurs in accelerometer the mass applies a dynamic force on the piezoelectric discs resulting in a variable potential produces across the element. Over a specific frequency range the potential will be directly proportional to the acceleration. When a piezoelectric material is stressed it generates an electric charge. The piezoelectric constant, stiffness, dielectric constant, resistance, and curie point are all important properties of a piezoelectric material used in an accelerometer. Ratio of electrical output to mechanical input is known as the sensitivity in accelerometer. Accelerometer is used to collect vibration signal which is further connected to DAQ system. The natural frequency of an accelerometer is not constant and it is influenced by the mass, stiffness of the accelerometer, the mass and stiffness of the bearing casing, and the stiffness of the complete structure.

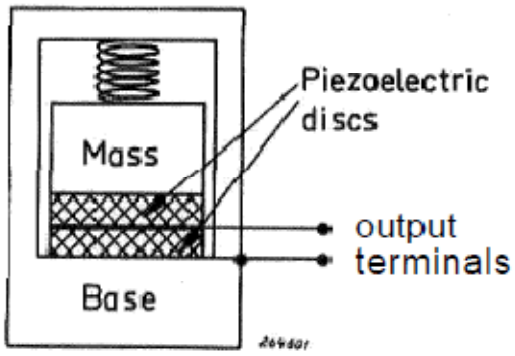

Fig 3. 3 Schematic drawing of a piezo-electronic accelerometer

3.3.2 Lab view: Lab view software was used to capture vibration signal during experimentation. The Lab view software uses language in which icons are created as shown in Fig 3.5: along with the flow chart showing the codes. Icon and code was used to capture vibration signal and generates tdms file which further used for analysis. As compare to another language in which text based instruction are used to execute command but in lab-view icons are used for instruction and capture data. During experimentation both time domain and frequency domain in shown simultaneously is shown in Fig 3.4. In built font panel in lab view having different set of tools in which object is build. Provision of adjusting sampling frequency and duration of time is also provided in lab view. Lab view has processing capabilities for condition monitoring such as frequency analysis. Sampling rate was selected 12800 during experimentation which will give 12800 data point in one second. Lab view also having a provision that it can capture data or different signals simultaneously. Time domain to Frequency domain plotted by in built module in lab view and further having inbuilt functions in which different analysis can performed.

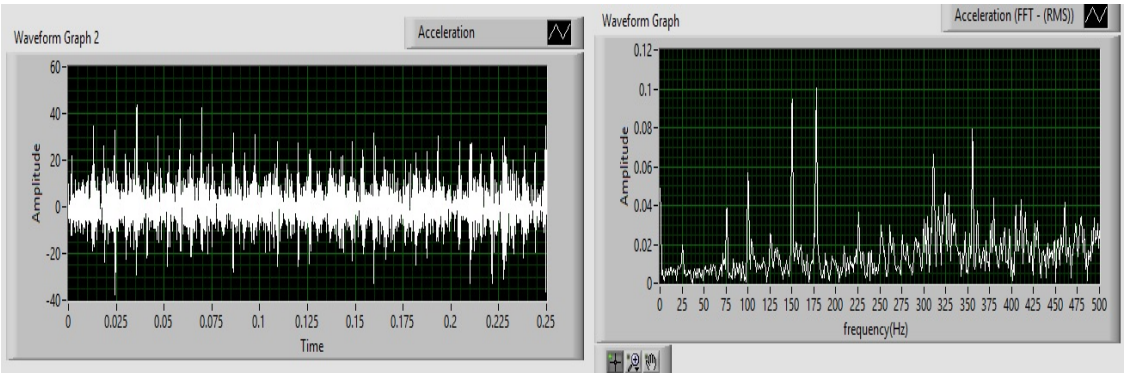

Fig 3. 4 Time domain waveform and FFT generated by lab view

3.4 Experimental Procedure: The vibration data was acquired and stored in personal computer for further processing in Matlab environment. Experimentation was carried out on five different sets of bearings carrying same sized induced defect on the outer race measured as 1.80 mm X 0.5mm (width X depth) under different loading conditions is shown in Fig 3.7 The signals were recorded after a fixed duration of time for the purpose of analyzing the interim changes happening during the crack propagation. Taper roller Bearing NBC30205 was made to run at constant speed of 1500 rpm under five different loading conditions. These loading values were measured using load cell and designated as no load, 5 kg, 10 kg, 15 kg and 20 kg respectively. The study considered a rectangular shaped induced outer race defect which was placed right below the position of applied radial load. The width of defect was taken as 1.80 mm to ensure the contact of roller with the groove bottom and to avoid and abnormal edge breakage while crack propagation. First set of experiment was carried out on without loading conditions by periodically recording the signal and visual inspecting. Signal was recorded after every 2 hours of duration and condition of the crack was checked after every 10 hours for all the loading conditions. The acquired signal was being processed using signal processing technique in Matlab software to find the most appropriate parameter in relation to the interim changes during crack propagation rate under different loading conditions.

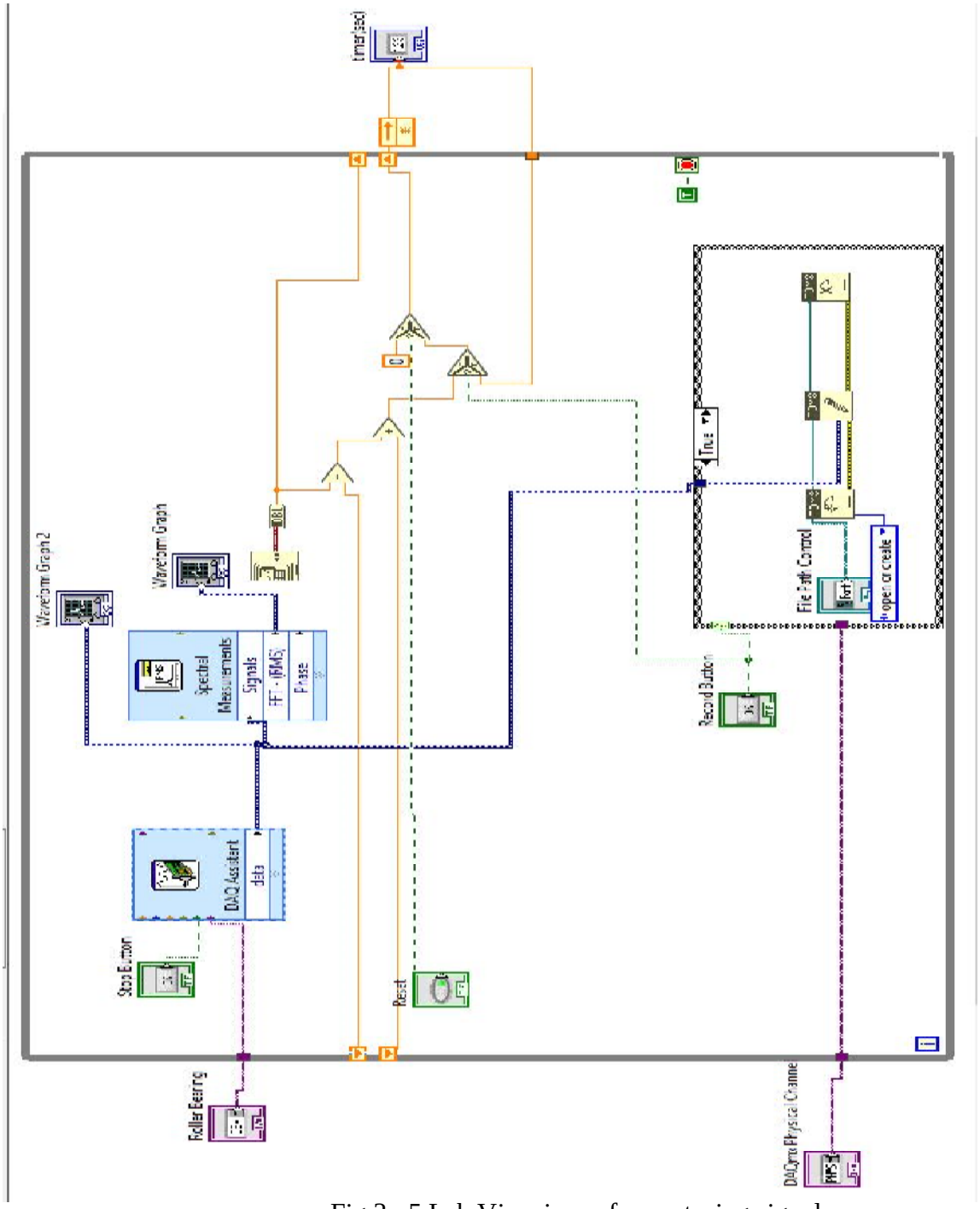

Fig 3. 5 Lab View icons for capturing signal

Table3. 3 Specification of load cell

S.No	**Parameter**	**Value**
1	Type	Single Point Load Cell
2	Total Precision	C3 class
3	Material	Aluminum Alloy
4	Surface	Anodized Treatment
5	Protection	IP65
6	Suggested Platform Size	350 x 350 mm
7	Applications	Weighing Scales, Retail, Bench & Counting Scales
8	Rated Load	40 Kg. Max
9	Rated Output	2.0mV/V+/- 5%
10	Zero Balance	+/- 1% Full Scale
11	Input Resistance	405 +/- 6 Ohm
12	Output Resistance	350 +/- 3 Ohm
13	Excitation Voltage	5-12V DC
14	Nonlinearity	0.017% Full Scale
15	Hysteresis	0.02% Full Scale
16	Repeatability	0.01% Full Scale
17	Creep(30min)	0.015% Full Scale
18	Operating Temperature	-20 ℃ to +65 ℃
19	Temperature Effect on Zero	0.017% Full Scale / 10 ℃

20	Temperature Effect on Span	0.014% Full Scale / 10 ℃
21	Insulation Resistance	5000 Mega Ohm(50V DC)
22	Safe Overload	150% Full Scale
	Ultimate Overload	200% Full Scale
23	Cable	420mm(3mm dia 4 wire shielding cable)

Fig 3. 6 Load cell used for experimentation

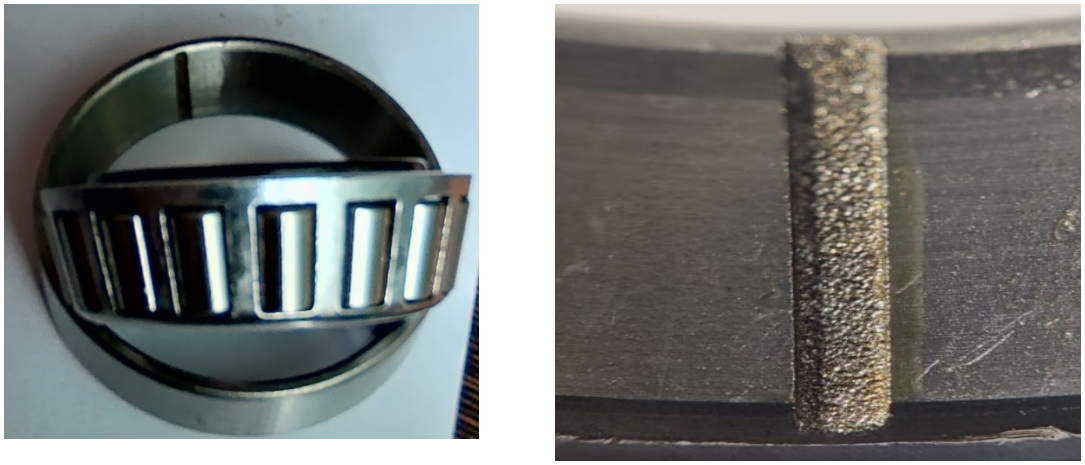

Fig 3. 7 Taper roller Bearing with (a) outer race defect (b) enlarge view of outer race defect

3.5 Test rig design using CREO: Test rig was designed by using Creo is shown in Fig 3.8. Hole of 10 mm was inserted on top of bearing casing 2 for applying the load on taper roller bearing having outer race defect. Shafts in the rotating machinery are misaligned it's becoming very difficult to generate a misalignment condition in the shaft without changing the bearing configuration. In this experiential set up provision for misalignment was also given along with loading. Design will allow producing misalignment without changing the bearing settings. This setup also allows for the application of misalignment in several directions and both parallel and angular misalignment can be provided along with loading conditions. Misalignment can be varied without disturbing the setting of the bearing. Assembled view of taper roller bearing is shown in Fig 3.8. Same model was fabricated for experimentation

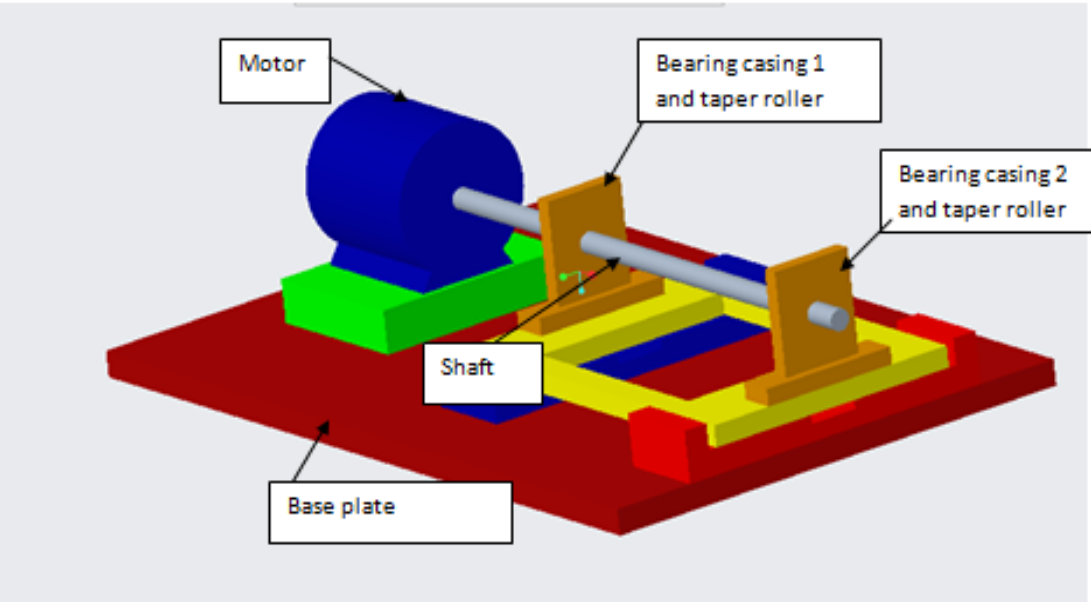

Fig 3. 8 Designing of test rig using Creo

3.6 Simulation Procedure:

The finite element method (FEM) is a numerical method for solving complicated engineering problems such as structural, mechanical components and provides approximate solution. For solving the complex engineering problems such as rolling element bearing assembly large set of differential equations are involved which are not possible to be solved analytically. However, this analysis can be carried out easily by using Ansys software. Taper roller bearing are mechanical devices that are designed to carry radial and axial load. In taper roller bearing outer race is fixed and inner race has rolling motion which produces forces that are transmitted to outer race by roller. Bearing in actual operation subjected to radial, axial and dynamic loads which produce contact stresses and creates a defect like pitting, fatigue, spalling and crack [174-177]. To simulate the contact stresses transient analysis is carried out to analysis stress state of the component subjected to loading condition. Three dimensional model of taper roller

bearing was built by using CREO and defect was created on outer race is shown in Fig 3.9. ANSYS mechanical APDL code was created to carried out nonlinear transient analysis to predict the distribution of contact stresses and its frequency vs amplitude of taper roller bearing. Effect of loading was simulated and changes were shown in terms of stresses and displacement in Cage roller, inner race and defective outer race. Analytical model was constructed which replica of experimental conditions to indentify contact parameters. Simulated result helps in design, optimization and predict the contact stresses and deformation.

Step used in ANSYS are listed below:

1. Creating three dimensional geometry using creo
2. Defining element types
3. Defining and entering properties of material
4. Creating free mesh
5. Selecting analysis type and options
6. Apply force and solve for obtaining results.
7. Analyzing and interpreting the results. (General Post Proc.)

3.6.1 Model Generation: Typical three dimensional model of taper roller bearing was modeled using Creo. Modeling of outer race, Inner race cage and taper roller bearing was carried out as per dimension of [Make: NBC, Model: 30205] taper roller bearing. Taper roller bearing consists of outer race, inner race, cage and rolling element is shown in Fig 3.9. The complete assembled model of taper roller bearing along with the crack of dimension 1.8 mm × 0.5mm (width×depth) on the outer race of taper roller bearing is shown in Fig 3.9. The dimension of the defect was selected to ensure that the roller must come in contact with the base for proper edge brakeage and smoothening. Specification of NBC 30205 is shown in Table 3.4

Table3. 4 Taper roller Bearing(NBC-30205) Specification

S.No	Bearing used	NBC-30205 (Taper roller bearing)
1	Inside diameter of the bearing	25 mm
2	Outside diameter of the bearing	52 mm
3	Pitch circle diameter of the bearing (D)	38.5 mm
4	Mean roller diameter (d)	6.39 mm
5	Material	High carbon hromium Steel
6	Weight	0.16kg

Building a finite element model means generating three dimensional model and specifying all the properties of material. Pre processor is used to define the element types, element real constants, material properties and the model geometry.

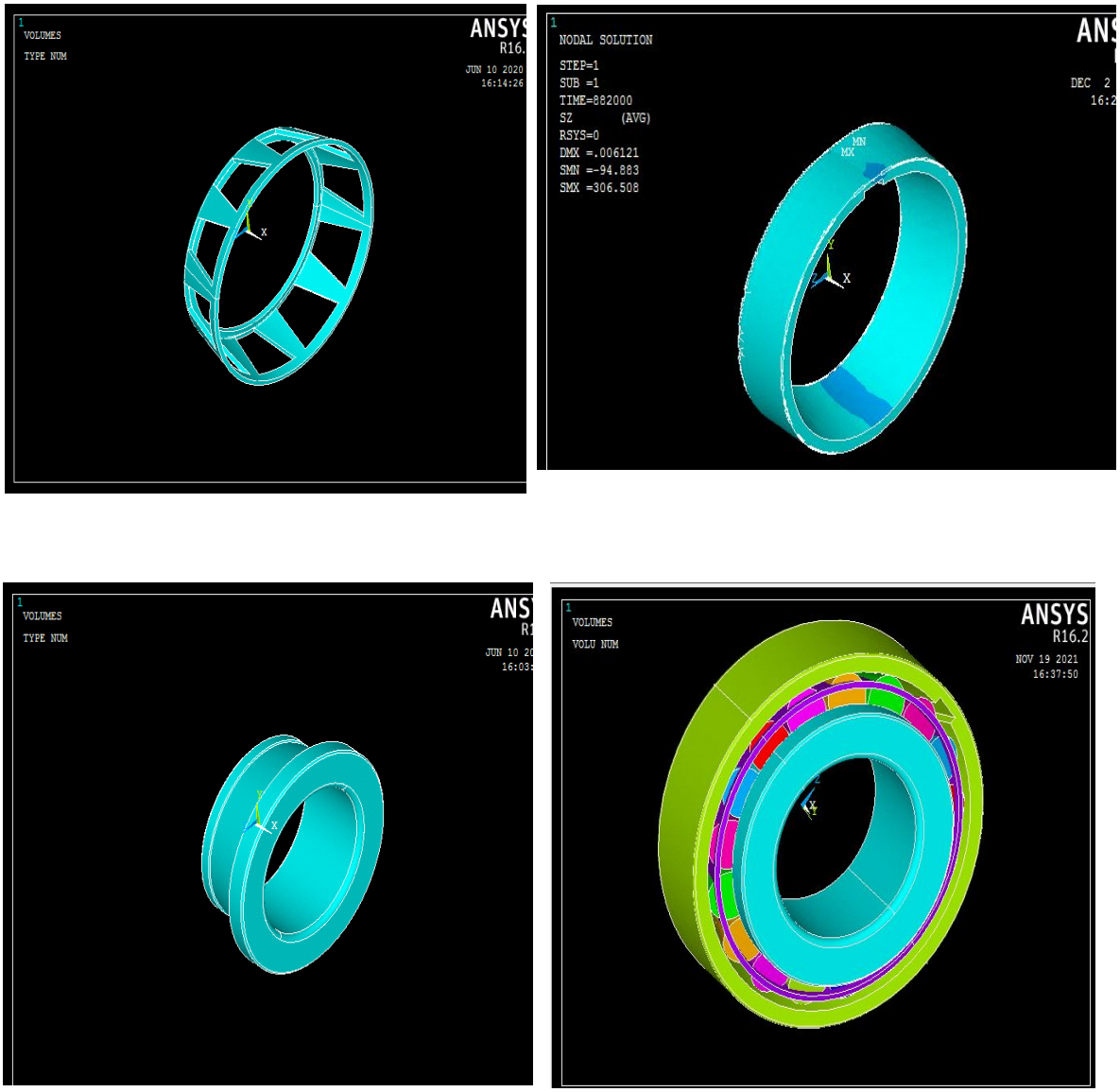

Fig 3. 9 Taper roller bearing parts inner race, defective outer race, cage and assembled model

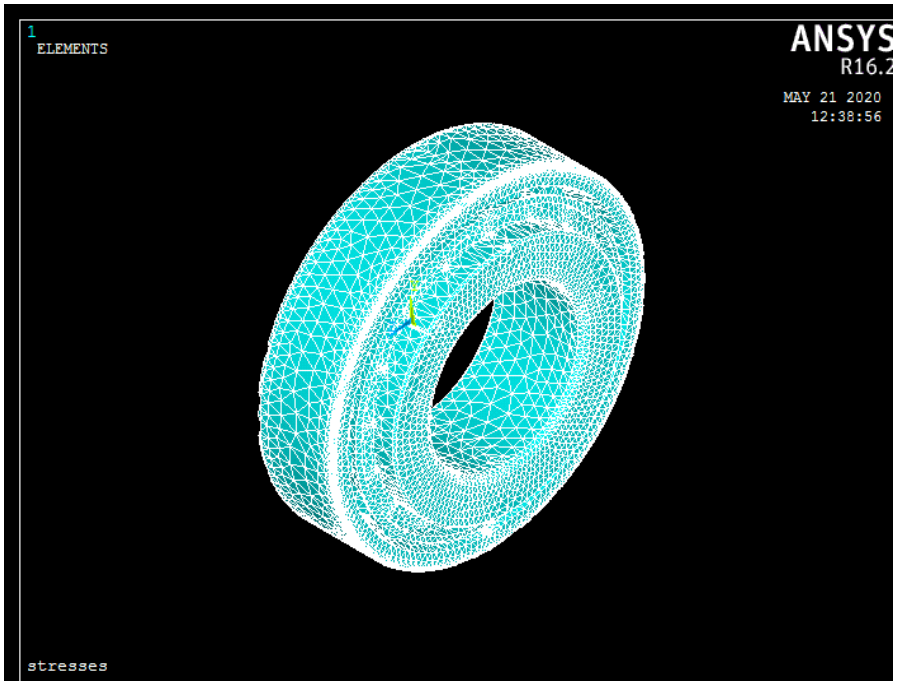

Fig 3. 10 Meshed model of taper roller bearing with outer race defect

3.6.2 Defining Element Types

Different element forms are available in the ANSYS element library. e.g. Shell, Brick8 node, plane 182 etc. These elements are selected according to analysis such as structural, thermal, fluent analysis. The element form also specifies whether the element can be used in two or three dimensional objects. In this analysis Brick 8 node 185 element was selected it's a three dimensional element having 8 nodes in it with capability of three degree of freedom at each node. Few of the three dimensional element is shown in Fig 3.11

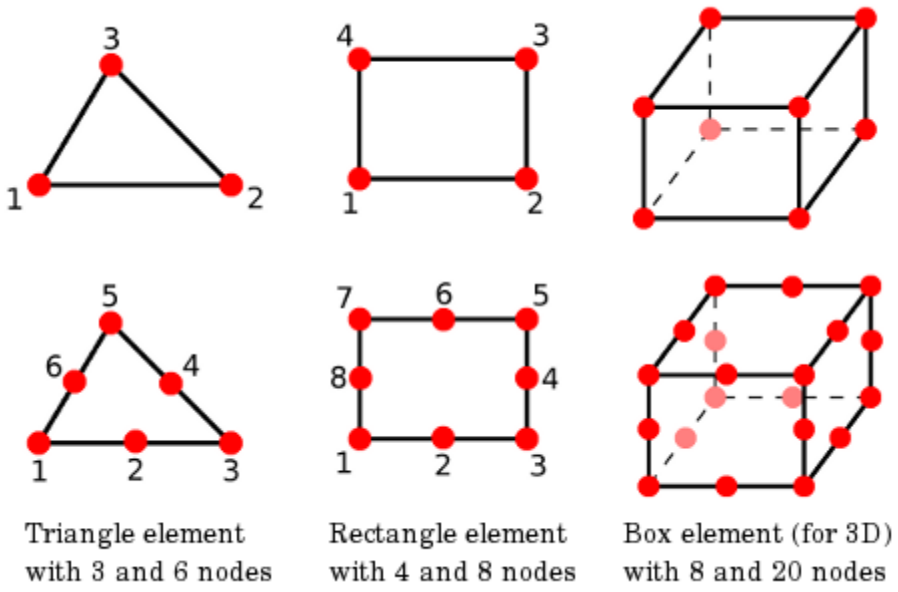

Fig 3. 11 Three dimensional element used in ANSYS

3.6.3 Defining Material Properties: Most element types require material properties following material properties were used for analyzing the contact behavior of taper roller bearing. Density : 7750kg/m^3, Young's modulus : 200000Mpa, Poisson's Ratio : 0.29

3.6.4 Meshing: After specifying the properties of material the next process in an analysis is to create a finite element model, which includes nodes and elements for analysis. Mapped and free mesh are commonly used in FEM analysis. A free mesh has no constraints on the shapes of elements and no pattern particular pattern. In comparison to a free mesh, a mapped mesh has a specific element shape and mesh pattern. Quadrilateral or triangular elements is obtained in mapped two dimensional mesh while in a mapped three dimensional mesh is made up entirely of hexahedron or tetrahedral elements. Furthermore a mapped mesh usually follows a predictable pattern with distinct rows of elements. The discretization is generally carried out which divides the domain into elements and known as meshing. A mesh creates different element that have nodes which

are further used for applying loads and different boundary conditions. Meshing can be classified into two categories mapped and free meshing. Mapped meshing is used for carrying out the analysis for regular areas and volumes such as rectangular plates. On the contrary free mesh it is used for the irregular areas and volumes such as bearing or parts which are complex. Due to this reason free meshing was selected for the analysis of taper roller bearing. Option of element selection is omitted in the free meshing and software creates automatically tetrahedral elements [178]. Meshed model of taper roller bearing is shown in Fig.3.10

3.6.5 Defining Analysis Type and Analysis Options

The ANSYS software may perform the following forms of analysis: static, thermal, harmonic, and nonlinear.etc. once solution is initiated analysis options cant be change is ANSYS.

3.6.6 Define Contact and Check Contact Element

The basic steps for performing a contact analysis are as follows:

1) Identify contact pairs and contact Formulation. The contact pairs are the region where contact can happen in model's deformation. Contact surfaces are created via target and contact elements. There are different contact formulations available in Ansys and these are enlisted below. Penalty method, Augmented Lagrange, Lagrange Method, Multipoint constraint (or MPC) , MPC algorithm , Lagrange and penalty method. In this analysis of taper roller bearing Augmented Lagrange method was used.

2. Select target and contact surfaces. Contact elements are prevented from penetrating the target surface, but target elements are allowed to penetrate through the contact surface. If a convex surface is expected to meet a flat surface the convex surface has to be selected as the contact surface. Smaller surface should be the contact surface as compared

to larger surface. In this analysis contact is created between inner race and roller outer race and taper roller, cage and taper roller for the analysis purpose.

3. Contact Type. The contact was created using target wizard in ANSYS software. Different types of contacts can be produced in ANSYS depending on the nature of the interaction between the target and contact surfaces. These are divided into four categories: bonded, frictionless, rough, and frictional. In this analysis friction coefficient is taken 0.2 between all contact surfaces.

4. Contact surface and closure. Race way of inner ring and outer ring is selected as target surface is shown in Fig 3.12. To make the contact between rolling element and inner and outer race CONTA174 as contact element type was selected and TARGE170 was selected. The contact settings and parameters for the contact between the roller, inner race, and the outer race of the taper roller bearing are listed in the Table 3.5 below.

Table3. 5 Contact setting for creating contact

Contact Type	Frictional
Friction coefficient	.2
Contact opening stiffness	1.0
Contact Formulation	Augmented Lagrange method
Detection method	Automatic
Normal Penalty stiffness	0.1
Maximum Friction stress	1.0 E20
Initial contact closure	.01

5. Contact results analysis and interpreting: Displacements, stresses, strains and contact details, such as contact penetration and pressure can be obtained from contact analysis. Contact has been created between taper roller and outer race, taper roller and inner race, taper roller and cage. In this process contact was created for roller with cage, inner race and outer race. All other elements except roller were selected under non-contact category with one another. The contacts of roller with inner race and outer race are shown in Fig 3.12.

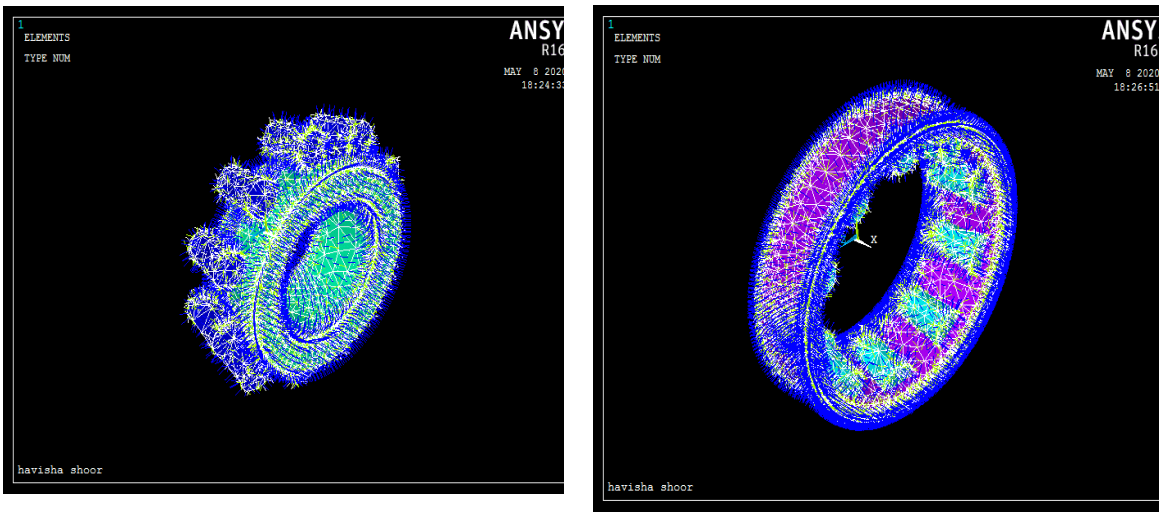

Fig 3. 12 Contact between roller and inner race and roller and outer race

3.6.7 Applying loads and boundary conditions

The Boundary Conditions used while performing the simulations has a substantial impact on the validity of the FE model. Boundary conditions are kinematic constraints required in order to solve a particular problem. Loads/boundary conditions are applied to ANSYS to obtain a solution e.g. degree of freedom is applied to restrict the movement of

body in space which is known as boundary conditions. Load in ANSYS can be classified as:

a. Degree of Freedom (DOF) Constraints

b. Moment/Forces

c. Harmonic load

d. Pressure

e. Temperature

Load can be applied by using following path

Solution - Define Loads - Apply-Structural Displacement on nodes

In this analysis of taper roller bearing all degree of freedom of outer race is constrained as outer race is fixed is shown in Fig 3.13 and radial load was applied on taper roller bearing in y direction (negative) for analysis purpose. Inner race was rotated with uniform rotational speed of 1500 rpm and also same speed was selected for experimentation. Further different analysis was carried out such as, contact analysis, transient analysis for determining the steady-state sinusoidal response.

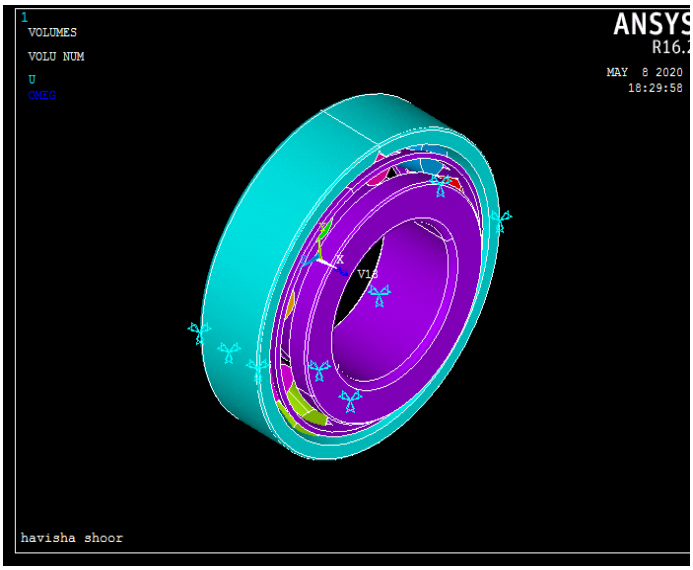

Fig 3. 13 : All degree of freedom constrained outer race

In ANSYS analysis are further classified as Thermal analysis, Fatigue analysis, Linear analysis, Non linear analysis. Non Linear analysis stress vs displacement curve is non linear (polynomial). Non Linearity is further classified as Material Based Non linearity, geometric non linearity. Contact analysis in ANSYS is used to simulate the physical contact between two parts. Element in ANSYS are further classified a h element and P element. In P type of element order is increases to for achieving convergence and was not applicable to all types of elements. H type of element is applicable to all types of element and carried re-meshing in critical area and also element length is reduced for achieving convergence

3.6.8. Initiating the Solution

In ANSYS solve Command is used for initializing the solution. The ANSYS software calculates the result using the model, material properties, load and boundary conditions assigned to it. Results are saved in different files such (Jobname.RST, Jobname.RTH etc) Depending upon the analysis different files are saved in ANSYS software. Path used for initiating the solution are:

Solution -Solve - Current LS

3.6.9 Reviewing the Results (Post Processing)

The ANSYS postprocessors can be used to review the results once the solution has been obtained. Post processing is having different sub parts such as deformed shape, stresses, nodal temperature, nodal acceleration, nodal velocity etc. Reviewing can be done by using following path.

General post processing - Plot Results - Contour Plot - Nodal Solution.

3.7 Taper roller bearing modeling

Taper roller bearing 30205 NBC make is used for analysis effect of loading on outer race fault. Model was created using CREO and IGES file was exported in ANSYS APDL environment. Detail specification and parameter of taper roller bearing used for modeling is shown in Fig 3.14. Components used in taper roller bearing includes outer race, inner race, cage, roller was designed using Creo as per manufactures catalogue. Material of taper roller bearing is high carbon chrome steel is as per manufacture catalogue. The complete assembled model of taper roller bearing along with the crack of dimension 1.8 mm × 0.5mm (width × depth) on the outer race of taper roller bearing along with specificsation is shown in Fig 3.14 and Fig.3.15. Dimensions of outer race defect of taper roller bearing used for experimental analysis and used for simulation are same along with the properties of material. Material Properties of taper roller bearing is mentioned in Table 3.6 and Table 3.7

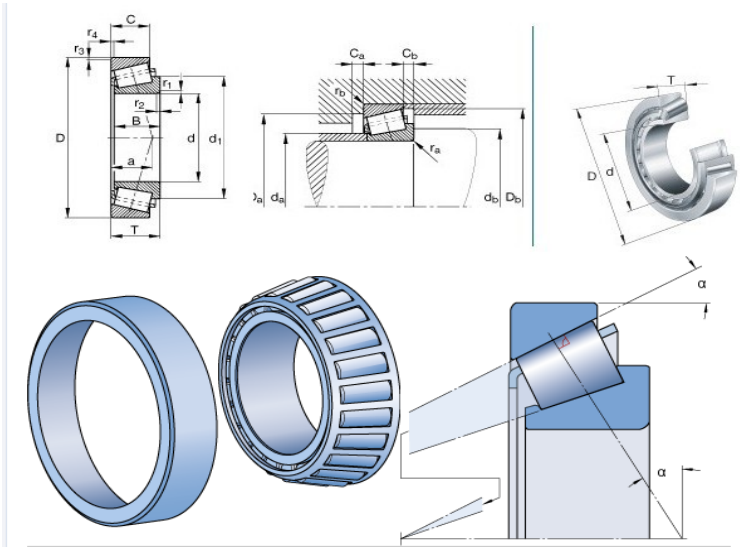

Fig 3. 14 Bearing parameters

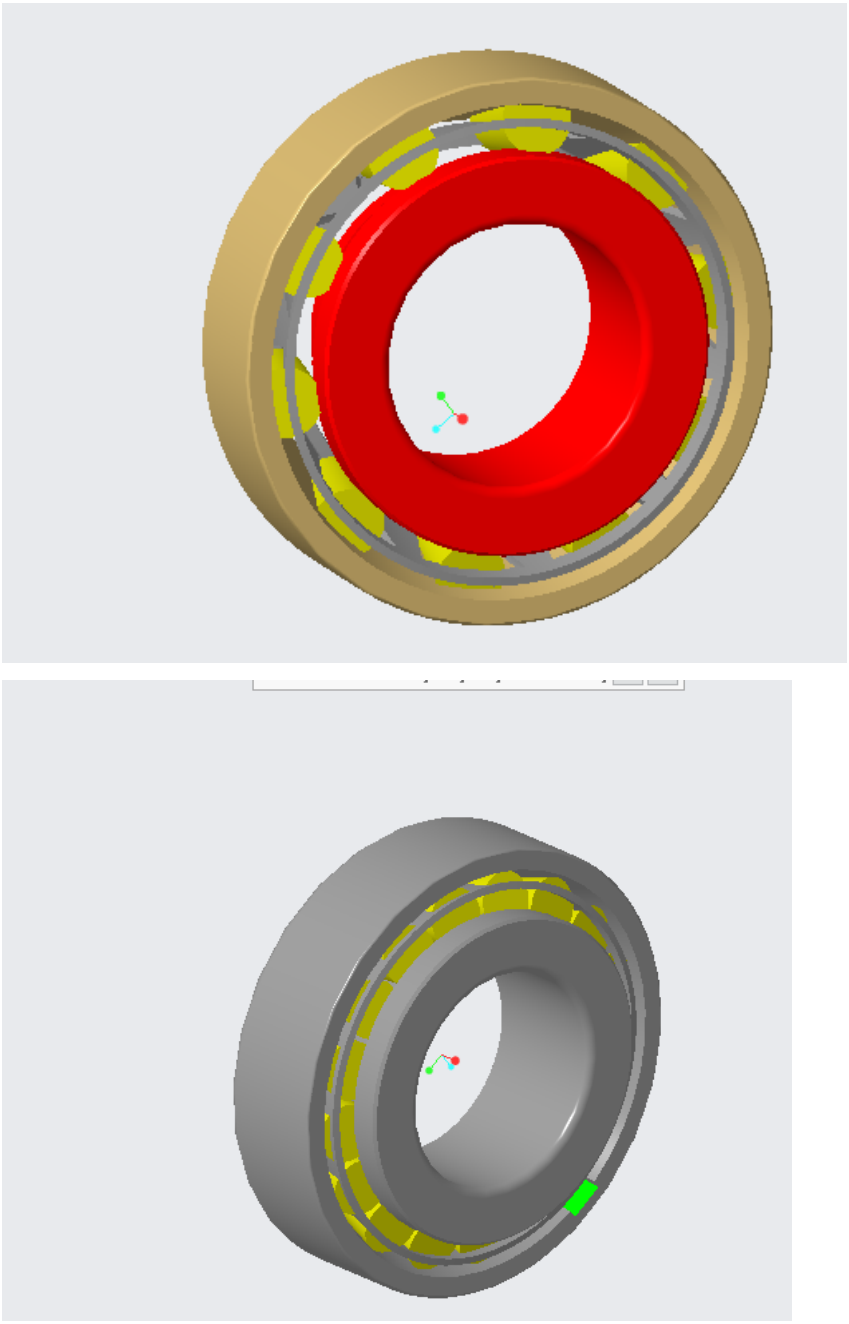

Fig 3. 15 Assembled view of taper roller bearing with outer race defect.(NBC 30205)

Table3. 6 Bearing Specification as per catalogue:

Sr. .No	Dimensions	Size (mm)
1	D	25
2	D	52
3	T	16.25
4	$d1$	38
5	B	15
6	C	13
7	A	12.33
8	$r1,2$	1
9	$r3,4$	1

Table3. 7 Properties of material Taper roller bearing Properties (NBC30205)

Sr.No	Properties	Metric
1	Ultimate strength	530 MPa
2	Yield strength	385 MPa
3	Elastic modulus	190-210 GPa
4	Bulk modulus (typical for steel)	140 GPa
5	Shear modulus (typical for steel)	80 GPa
6	Poisson's ratio	0.27-0.30

7	Izod Impact Hardness, Brinell	115 J 149
8	Thermal expansion co-efficient	11 μm/m°C
9	Thermal conductivity	46.6 W/Mk

3.8 FEM analysis: In field of computer-aided engineering (CAE) FEA code generated by ANSYS is found application in many fields. ANSYS software is widely used to create models of structures, machine components, and to apply operating loads and other design criteria, to analyze physical response including temperature distributions, stress levels and pressure etc[178]. It allows for the analysis of a design without the need of several prototypes to be built and destroyed due to testing. The ANSYS software found application in automobiles, highly sophisticated systems such as aircraft, nuclear reactor containment buildings, bridges, farm machinery, X-ray equipment and orbiting satellites [179-182]. In ANSYS, six-node triangles, four-node quadrilaterals, and eight-node quadrilaterals can be used to simulate two-dimensional problems. Increase in number of number of nodes will result in higher order of polynomial which further improves the accuracy of results describing the displacements, stresses and strains within the element. If the stress is consistent throughout a component can be solved by two dimensional problem such as plane stress and plain strain which further help to depict the stress state of a system. But rotating component such as bearing is subjected to different loading conditions and its design is complicated even not symmetric. These complicated components and can only be solved by creating three dimensional elements such as hexahedron element, tetrahedron element [179-181]. The discretization method divides the domain into elements which is the first step in the finite element solution technique known as meshing

Elements used in Finite element method are classified as one dimensional element also known as line elements and are ideal for the study of one-dimensional problems. Two dimensional elements are commonly used in plane stress and plane strain conditions. Three dimensional elements are used for three dimensional problems which are complex and not symmetric. Most common type of three dimensional element used are Tetrahedral, Hexahedral, Axi-symmetric element. In theoretical analysis in fem shape function, strain displacement matrix, isoparametric elements plays a crucial role.

Shape Function is used to relate field variable at any point within element to field variable at nodal point. N is known as the shape function,. Q is displacement at any point within element. $\{\delta\}_e$ is known as vector of nodal displacement given by equation3.1

$$U = \sum N_i U_i ; V = \sum N_i V_i \; ; \{Q\} = [N]\{\delta\}_e \tag{3.1}$$

Shape function for tetrahedral element is

$$N_1 = \frac{\alpha + \beta_1 X + \gamma_1 Y + \delta_1 Z}{6V} \quad N_2 = \frac{\alpha + \beta_2 X + \gamma_2 Y + \delta_2 Z}{6V}$$
$$N_3 = \frac{\alpha + \beta_3 X + \gamma_3 Y + \delta_3 Z}{6V} \quad N_4 = \frac{\alpha + \beta_4 X + \gamma_4 Y + \delta_4 Z}{6V}$$

Element stiffness matrix is given by equation 3.2

$$K = \iiint_V [B^T][D][B]\, dV$$
$$K = [B^T][D][B]V \tag{3.2}$$

Body forces and surface forces are given by equation 3.3

$$\{F\}_b = \iiint_V [N]^T \{X\}\, dV ; \{F\}_S = \iiint [N]^T \{T\} dS \tag{3.3}$$

$$K^{e} = Element\ Stiffness\ matrix = \iiint_{V(e)} [B]^{T} [D]\ [B] DV$$

Both matrices [B] and [D] are constant for tetrahedral element.

State of bearing can be predicted by contact analysis using FEM which gives information about stresses, displacement and penetration which helps to evaluate bearing performance under different loading conditions [182]. Ansys take contact between surface and friction heat to give state of system. In theoretical analysis using FEM basic step include are listed below.

1) **Creating Finite elements**: The finite element method (FEM) is technique for numerically solving differential equations generated during mathematical modeling. The FEM breaks a complicated system into smaller, simpler sections called finite elements in order to solve a problem. Applications of FEM include electromagnetic potential, heat transfer, fluid flow, structural analysis.

2) Assuming displacement model

$$U(x, y, z, t) = [N(x, y, z)]\, Q(t) \tag{3.4}$$

3) Deriving element stiffness matrices and load vector

Expression for Stress and Strain relations

$$M^{e} = Element\ mass\ matrix = \iiint_{V(e)} \rho [N]^{T} [N]\, DV \tag{3.5}$$

$$P^{s} = vector\ of\ element\ nodal\ forces\ due\ to\ Surface\ Forces = \iiint_{V(e)} [N]^{T} \phi Ds1 \tag{3.6}$$

$$C^e = Element\ Damping\ matrix = \iiint_{V(e)} \mu [N]^T [N]\ DV \tag{3.7}$$

$$P^s = vector\ of\ element\ nodal\ forces\ due\ to\ Body\ Forces = \iiint_{V(e)} [N]^T \phi Dv \tag{3.8}$$

4) Assemble the element matrices and vectors

$$[M]\ddot{Q}(t) + [C]\dot{Q}(t) + [k]Q(t) = P(t) \tag{3.9}$$

Where Q =Vector of nodal acceleration in the global system

5) Solving the equation and applying boundary conditions or initial conditions. Rigid body movement of body is prevented by applying boundary conditions. In bearing analysis outer race is fixed.

3.9 Methods for FEA Solution (h- and p method): Lower order displacement function is assumed in h method of meshing and came in existence in 1970. It automatically increase the number of elements in the region where the displacement is non linear. Increase in number of element in particular region results in reducing error between the exact displacement and finite element. P method came into existence in 1990 and P level increases the polynomial level of finite element shape function. In ANSYS the range of P level can be controlled by key opt settings or by using PRANGE command. Major advantage of P method over h method that more accurate results are obtained without user defined meshing control. P method is mostly used in fracture mechanics and when parts subjected to fatigue loading such as rolling element bearing [183].

3.10 Types of Structural Analysis*:* The most popular application of the FEM is structural analysis. Anything that is built to bear load is referred to as a structure. FEA predict the failure due to unknown stresses. This process of sample making and analyzing after testing is much higher to the costs of manufacturing if each sample was designed and tested. FEA involves stressing and analyzing a replica of the model by assigning material properties. The linear and nonlinear behavior of the structural material was studied in structural analysis. The material is not plastically deformed in linear behavior stressing a material beyond its elastic capabilities is referred to as nonlinear behavior. Different types of analysis which can be performed by using ANSYS software are:

3.10.1 Static analysis. The effects of steady loading conditions on a structure are calculated using a static analysis which ignores inertia and damping effects such as those induced by time-varying loads. Static analysis is used to calculate the displacements, stresses, strains, and forces induced by loads in structures or materials [184]. In a static analysis the following types of loading can be applied such as forces and pressures, inertial forces etc. Both linear and non linear analysis can be performed by using ANSYS. Nonlinearities can be due to creep, contact surfaces, large strain and large deflection etc.

3.10.2 Transient Dynamic Analysis

Transient dynamic analysis is a technique for determining a structure's behavior subjected to time dependent loads. Dynamic analysis is used to evaluate a structure's displacements, strains, stresses subjected to different types of load and to simulate the behavior of component with respect to time. [185]

3.10.3 Modal Analysis. When a structure is being designed modal analysis technique is commonly used to predict the natural frequencies and mode shapes of a system when subjected to force which further helps in formulating the mathematical model. The modal parameters, modal natural frequencies, modal damping characteristics, and mode shapes

were extracted in modal analysis which plays a crucial role in designing of component. [186-191]

3.10.4 Harmonic Analysis. Harmonic response analysis in ANSYS is carried out to obtain steady-state response of a model subjected to a load that changes harmonically (sinusodically) Such load has specific amplitude and frequency at which it acts. This type of loading cause forced vibrations. The calculated response is a function of frequency. In a structural system, cyclic load will produce a cyclic response known as harmonic response. Harmonic response analysis predict the structures dynamic behavior and used to avoid resonance, fatigue and other harmful effects of forced vibrations [192].

3.10.5 Contact Problems. Contact problems are extremely nonlinear problems. It's critical to comprehend the physics of the problem and optimizing or improving the model's efficiency. Few contact problems includes bearings, leaf springs, and gears etc. [193-196]. Finite element of bearing is non linear contact analysis. In rotating equipment such as bearing contact is non linear because part came into contact with each other is unpredictable and depends highly on loading, material, boundary conditions and other factors. Another factor is the friction and all friction models available are non linear.

3.10.6 Fatigue Analysis. When structure is fractured due to repeatedly load then it is known as fatigue. Factors contributing to fatigue failure are number of load cycles, stress occurred in every load cycle and stress concentrations. Loading plays a crucial role in any component as it effect the life of component drastically which further affect the material's natural frequency, causing resonance and subsequent failure. Fatigue analysis shows the impact of cyclic loading on the specimen, which helps the designers calculate the life of a component. This form of study can indicate the area's most prone to crack propagation. [197]

Chapter 4 Experimental result and discussion

4.1 Introduction

In this work, bearing test rig was designed and prepared is shown in Fig 4.1 for analyzing the crack propagation rate of taper roller bearing. (Manufactures NBC, Bearing model 30205). NBC 30205 taper roller bearing is used in front axle of tractors and subjected to different loading conditions. Hence effect of loading on crack propagation was studied. Lab view software is used to and program was devolved to capture the signal is shown in Fig 4.2 and FFT of the raw signal is shown in Fig 4.3. Sampling rate was 12800 samples per second are used for experimentation. For further processing the signal and extracting features Matlab software was used. This study presents a controlled experiment to determine the applicability of vibration analysis and for monitoring the initiation and propagation of cracks on taper roller bearings along with the interim changes. Axial groove defect was seeded on the outer race of taper roller bearing using electrical discharge machining (EDM) for the purpose of initiation of crack propagation. Experimental set up is shown in Fig 4.1.

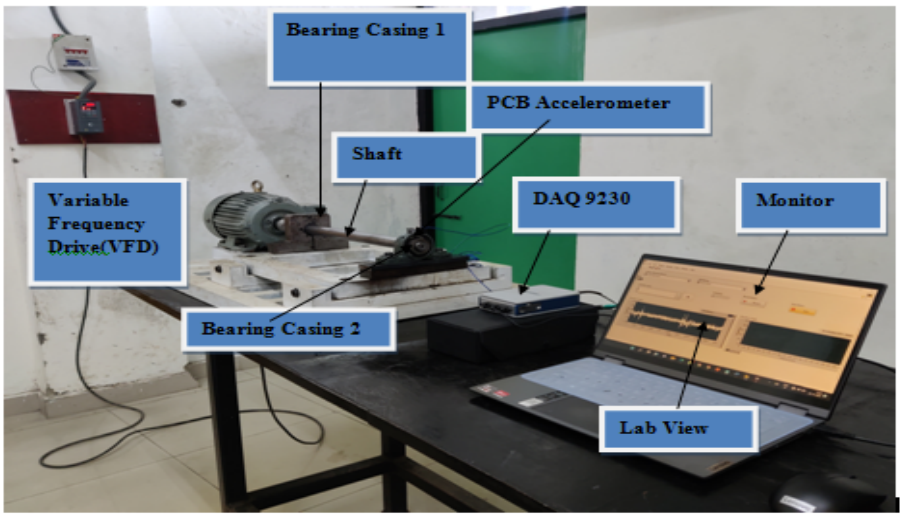

(a)

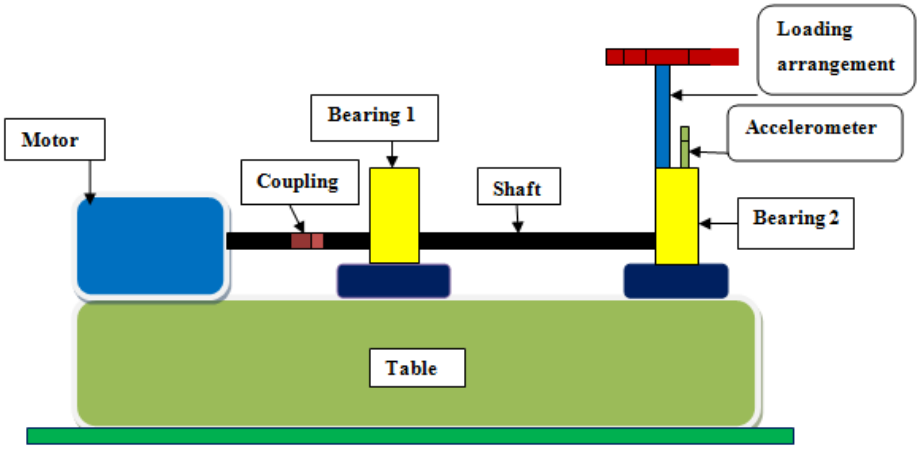

(b)

Fig 4. 1(a) Experimental Test Rig (b) Line diagram of test rig

4.2. Defect identification using FFT

Initially bearing with seeded defect was fixed in bearing casing 2 is shown in Fig 4.2 and bearing is made to run continuously. The vibration signals were recorded using accelerometer after fix time interval for the purpose of analysis. The time domain waveform of signal recorded from a 30205-taper rolling bearing with groove defect on the outer race of approximately 1.8 mm in width and 0.5 mm in depth is shown in Fig 4.2. The raw signal graphs were drawn for acceleration vs time. The raw signal graph has not shown any notable difference over the time but only burst seems to be enlarged after enlargement of the crack size. Further as new crack initiated amplitude was very high but due to smoothening of edges amplitude gets reduced and this trend was noticed with all loading conditions without load, 0 Kg, 5Kg, 10 Kg, 15 Kg, 20 Kg.

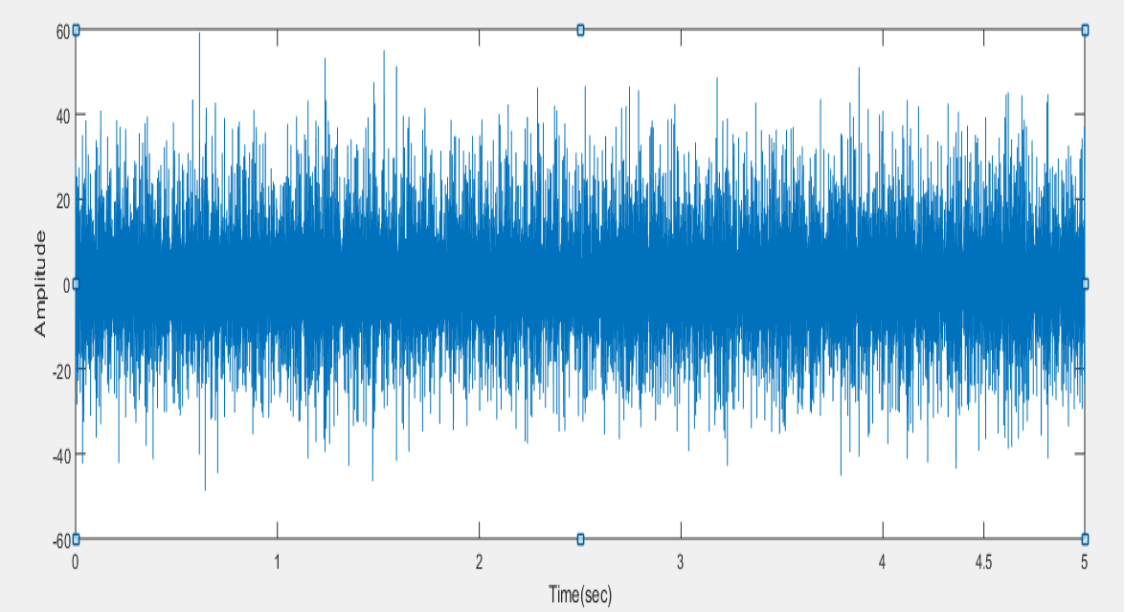

Fig 4. 2 Raw Vibration signal without load for outer race defect

The most prominently used technique for frequency domain is Fast Fourier Transformation (FFT). The FFT of raw signal changes the time domain signal to frequency domain and during this time domain information is completely lost. It generally converts the signal into two parts real and imaginary and in general real part is plotted for the representation. The frequency contents of raw signal are displayed in the graph and one can see the frequency contents strongly present in the signal. In stationary signal frequency content not change over time and in non stationary signal frequency content change over time. Some important characteristics of non stationary signal are trends, abrupt changes, start and end of event. Fourier analysis is not suited to detect these features, which are often the most essential component of the signal. Fourier transform of continuous signal x(t) is shown in Fig 4.3. In this graph prominent frequency 175 Hz are appearing with having energy levels which is corresponding to outer race defect frequency. Both raw signal and FFT indicates presence of defect in the bearing.

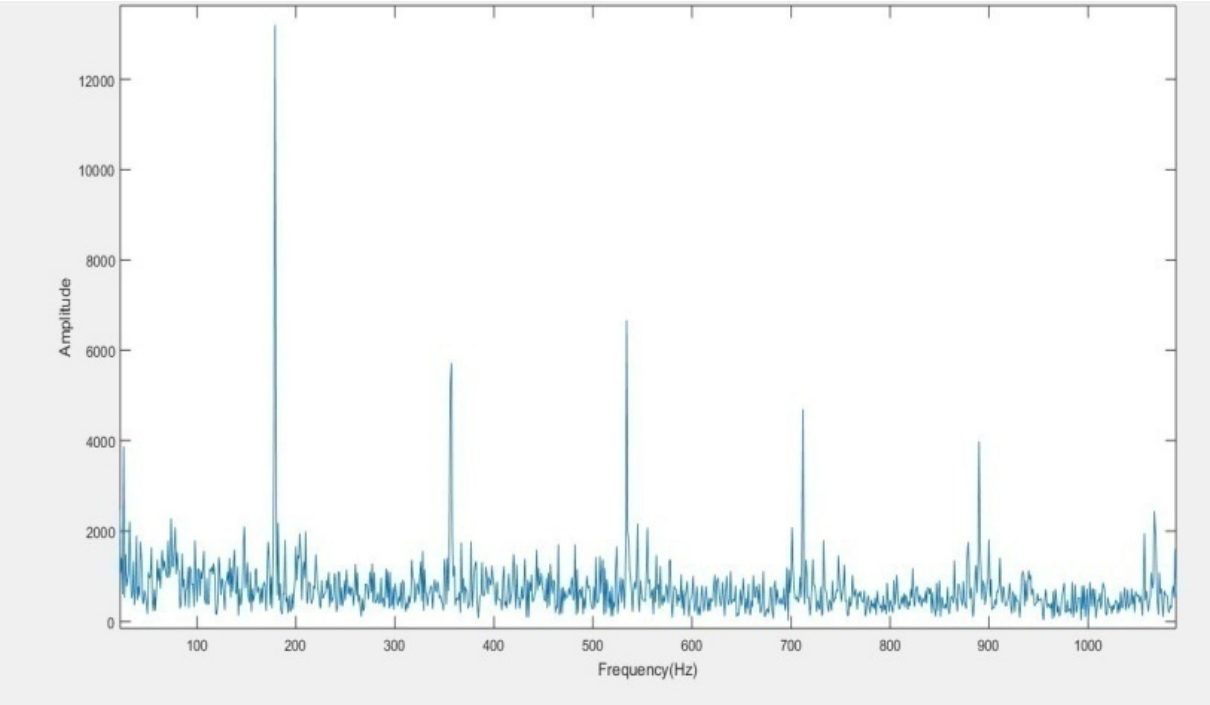

Fig 4. 3 FFT of raw vibration signal

4.3 Statistical analysis

4.3.1 Case 1- without Load: Taper roller Bearing NBC30205 was made to run at constant speed of 1500 rpm under five different loading conditions. These loading values were measured using load cell and designated as no load, 5 kg, 10 kg, 15 kg and 20 kg respectively. The width of defect was taken as 1.8 mm to ensure the contact of roller with the groove bottom and to avoid and abnormal edge breakage while crack propagation. First set of experiment was carried out on without loading conditions by periodically recording the signal and visual inspecting. Signal was recorded after every two hours of duration and condition of the crack was checked after every 10 hours for all the loading conditions. For without load till 180 hours of running no change was observed and condition of crack. The first change in the crack in terms of crack growth was observed at 190 hour and condition of the crack was shown in Fig 4.4. But still it went unnoticed that

when the crack growth actually happened in the duration of 180 hours to 190 hours because the condition of the bearing was not checked in between this period. To elaborate this further, statistical analysis was carried out for all the recorded signals and various parameters such as RMS, Crest factor, SNR, Skewness, Kurtosis and Shannon entropy were calculated and are shown in Table 4.1

It was observed that RMS and Shannon entropy values have shown sudden rise at 184 hours duration and this might have happened due to some changes in crack. Soon after 184 hours duration both the values of RMS and Shannon entropy has shown decrease in the values as time progressed. The experiment was continued after 190 hour and all the statistical parameters were observed for the recorded signals thereafter are shown in Table 4.1.

Both the values showed decreasing trend till 188 hours duration but thereafter, both RMS and Shannon entropy showed no change till 198 hours. The next sudden rise in the values of RMS and Shannon entropy was observed at 200 hours. The bearing was immediately uninstalled and the condition of the crack was checked. The edge of the crack was found to be broken at 200 hours duration.

Table 4. 1 Statistical parameter calculated at various time intervals for without loading condition

Time duration in hours	**RMS**	**Crest factor**	**SNR**	**Skewness**	**Kurtosis**	**Shannon entropy (10^7)**
0	8.347	7.1256	22.98	0.189	5.554	2.42
10	10.22	6.8215	20.77	0.168	6.492	3.59
20	8.087	6.2457	22.33	0.208	5.527	2.02

30	8.472	8.0384	21.7	0.184	5.749	2.27
40	8.485	7.0794	22.46	0.22	5.626	2.27
50	8.448	8.2828	20.71	0.228	5.913	2.26
60	8.456	7.3888	23.4	0.229	5.549	2.26
70	8.449	6.5549	20.99	0.223	5.618	2.25
80	8.365	7.2492	23.45	0.223	5.542	2.19
90	8.308	6.418	22.34	0.221	5.603	2.17
100	8.251	7.0285	21.54	0.216	5.752	2.13
120	8.3	6.4237	22.2	0.218	5.679	2.16
140	8.601	6.7204	21.8	0.225	6.147	2.37
160	9.264	6.8881	20.35	0.168	5.521	2.8
170	8.79	6.0588	20.29	0.18	5.728	2.48
180	7.68	13.357	23.6	0.119	8.537	2.03
184	16.9	11.788	24.1	0.07	7.43	13.9
188	8.1	14.3845	22.1	0.17	9.53	2.07
192	7.97	11.439	22.9	0.04	7.67	1.98
196	8.24	14.1009	24	0.11	11.6	2.19
200	25.02	10.2382	19.67	0.129	7.312	30.7
204	22	9.5045	19.4	0.09	7.53	28

208	25.4	9.4644	22.4	0.11	7.15	20
212	25.7	12.754	19.5	0.16	8.63	26
216	24.9	8.8966	18.18	0.178	8.017	30.5
220	13.8	9.1122	24.3	0.12	7.09	7.27
224	16	10.0815	21.2	0.16	7.63	15.2
229	15.28	11.0412	23.31	0.078	8.1	10.2
232	19.2	11.2517	22.5	0.26	10.2	15.9
239	16.28	7.774	21.91	0.141	6.48	11.7
248	19.21	9.1612	17.67	0.151	6.135	12.2
259	14.86	7.3411	18.42	0.1707	6.824	9.58
267.5	8.723	9.1705	21.7	0.14	4.967	2.66
274.5	9.15	8.3301	19.51	0.041	6.653	3.06
278.5	9.178	9.6329	21.2	0.115	6.682	13.26
284.5	9.603	10.247	19.47	0.014	7.288	3.09
285	9.114	10.4396	19.35	0.009	7.954	2.74

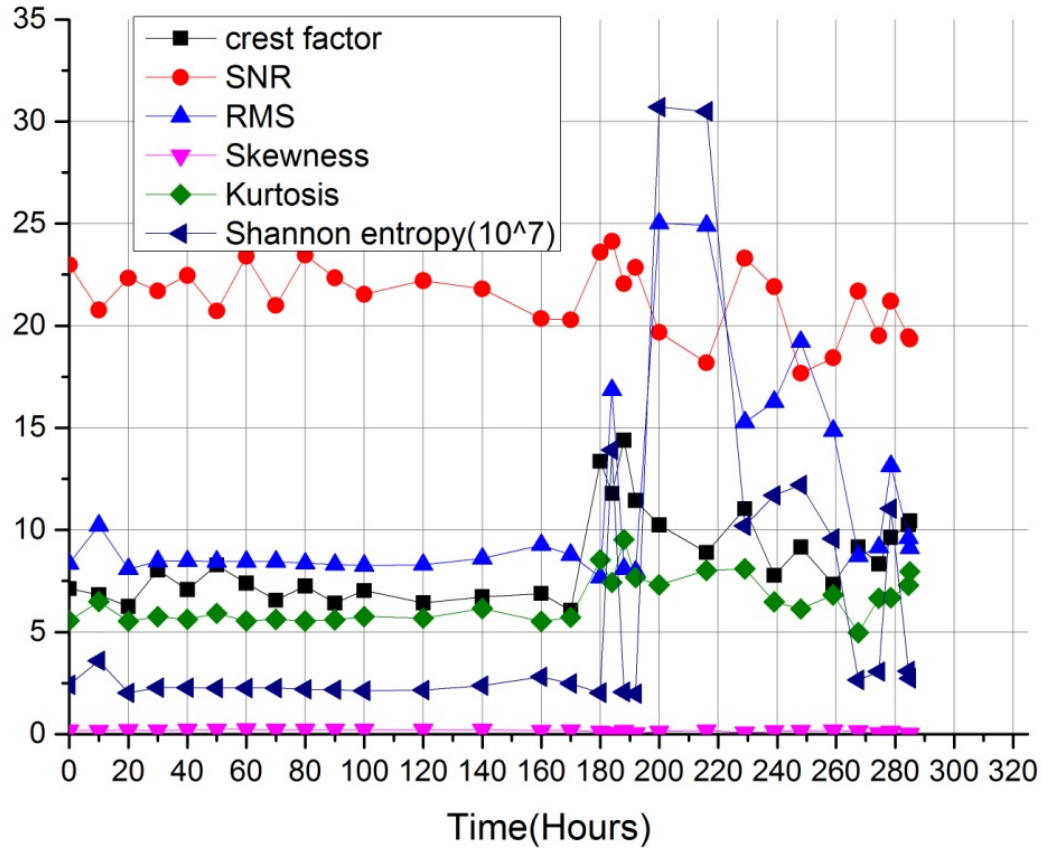

Fig 4. 4 Experimental result of crest factor, SNR, RMS, skewness, Kurtosis, Shannon entropy without load

Thereafter, Shannon entropy values were showing decreasing trend till 208 hours but RMS values have not shown any significant trend in this duration. The crack was observed after 208 hours duration and found that the broken edge was smoothened in the duration of 200 hour to 208 hours. The same observation of the edge breakage was observed with the sudden rise in value of Shannon entropy values at 184 hours, 200 hours, 212 hours, 216 hours, 224 hours, 232 hours and 278.5 hours.

The graph presented in Fig. 4.4 and Fig 4.6 depicts that the RMS values were not significantly changing with the edge breakage during crack propagation however, Shannon entropy values does. The same statistical analysis was carried out for other

loading conditions of 5 kg, 10 kg, 15 kg and 20 kg. Again, similar findings were observed for the relation of sudden rise in Shannon entropy values with the edge breakage. Whenever, the edge breaks out the vibration signal would result into extra high frequency spikes which yielded into increasing the randomness of the signal. This change of randomness in the signal was significantly elaborated with the value of Shannon entropy. Fig. 4.6 shows the RMS and Shannon entropy after first sign of edge breakage till 286 hours. Further SEM analysis were carried out which indicates crack growth rate at 286 hours is shown in Fig. 4.5.

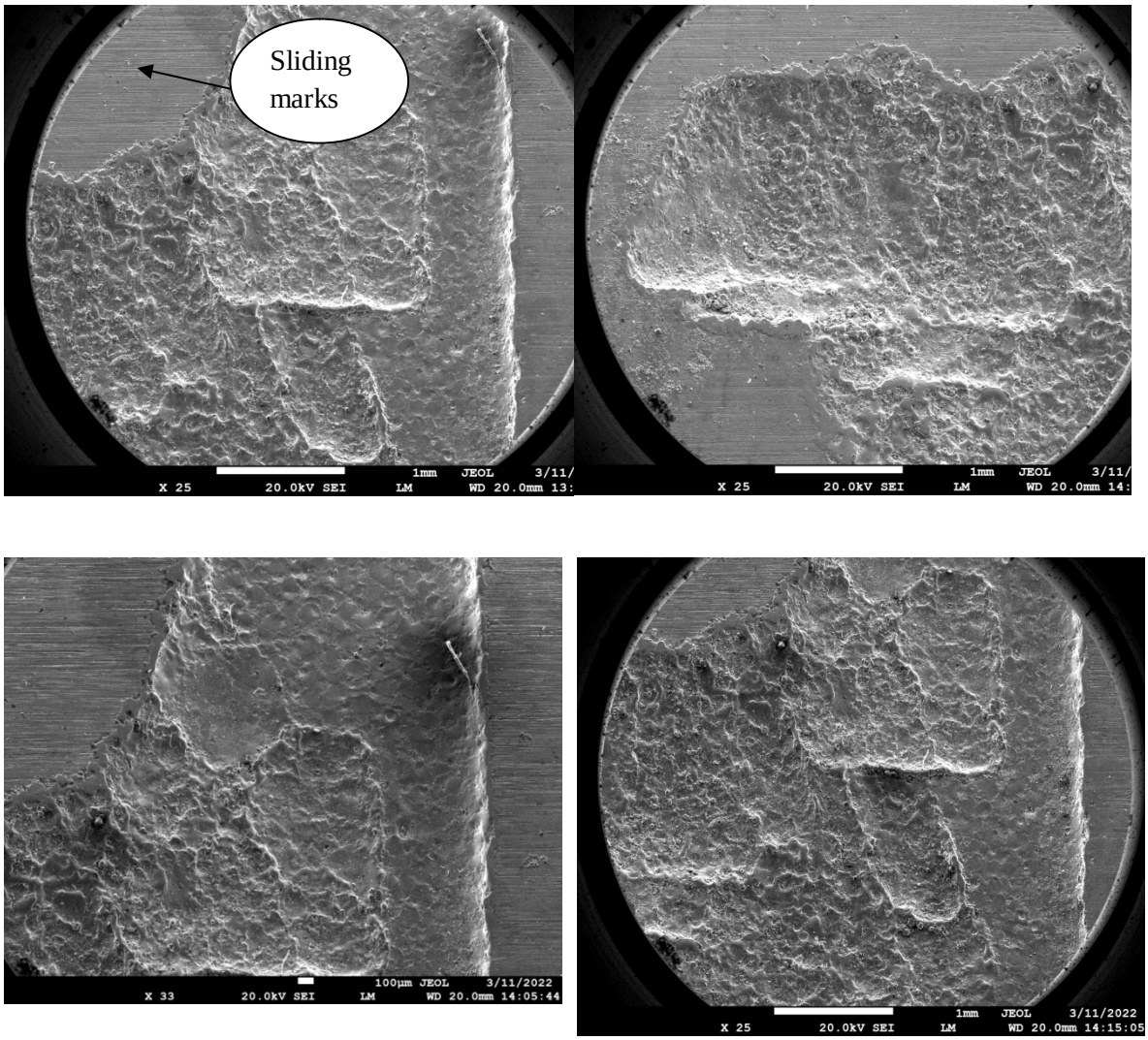

Fig 4. 5 Scanning electron microscope (SEM) without load

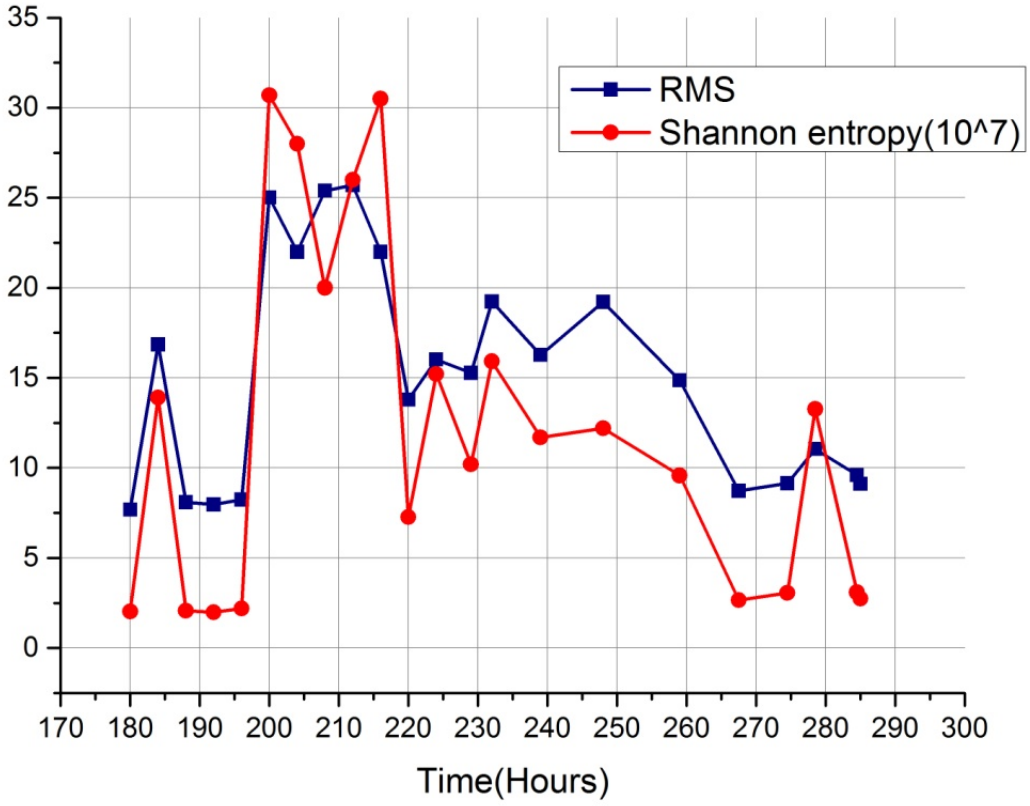

Fig4. 6 RMS and Shannon entropy values from duration 170 hours onward for no load condition.

4.3.2 Case 2-Effect of 5 kg load: For analyzing the effect of loading 5 kg load was applied and measured using load cell. Statistical parameter for 5 Kg load is shown in annexure1. Shannon entropy, RMS, Crest factor, SNR, skewness and kurtosis values were showing no variation till 190 hours is shown in Fig 4.7 The crack was observed after 200 hours duration and found that the broken edge was broken and further was smoothened in the duration of 200 hour to 220 hours. The same observation of the edge breakage was observed with the sudden rise in value of Shannon entropy values at 198 hours, 225 hours, 239 hours and 245.5 hours is shown in Fig 4.8 along with SEM analysis

of the sample. This clearly indicates by comparing no load and 5 kg load that parameter of Shannon entropy responding fairly well to initiation and propagation. It also indicates that loading also plays a crucial role in crack initiation and propagation as less time is required for first sign of crack initiation and propagation.

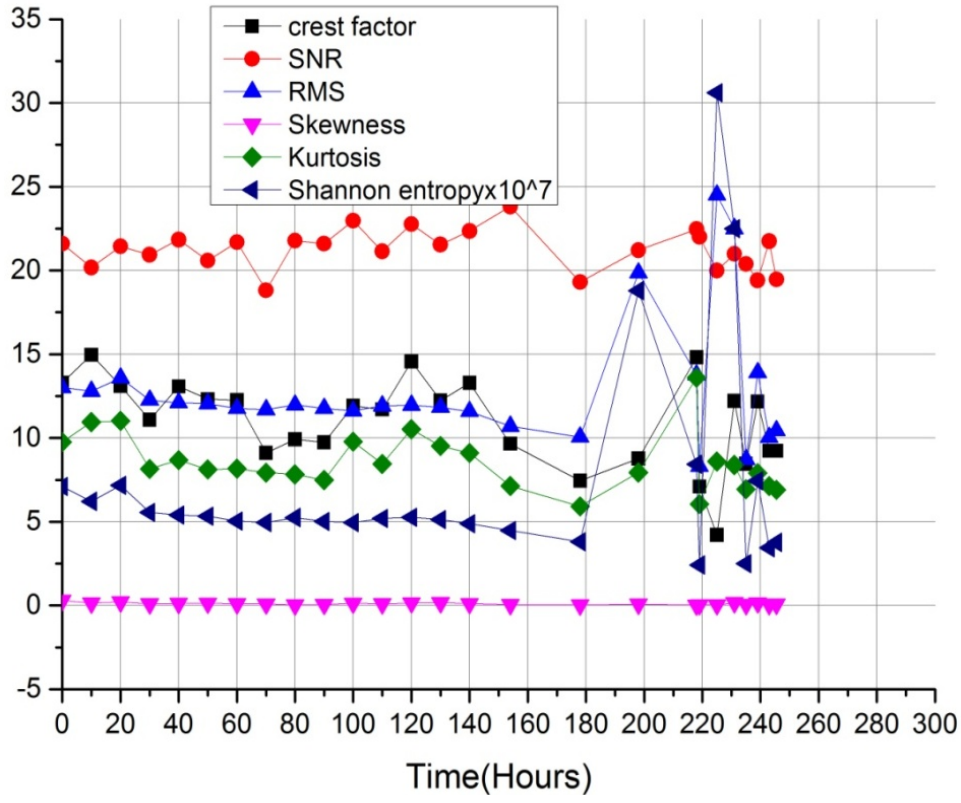

Fig4. 7 Experimental result of crest factor, SNR, RMS, skewness, Kurtosis, Shannon entropy of 5 kg load

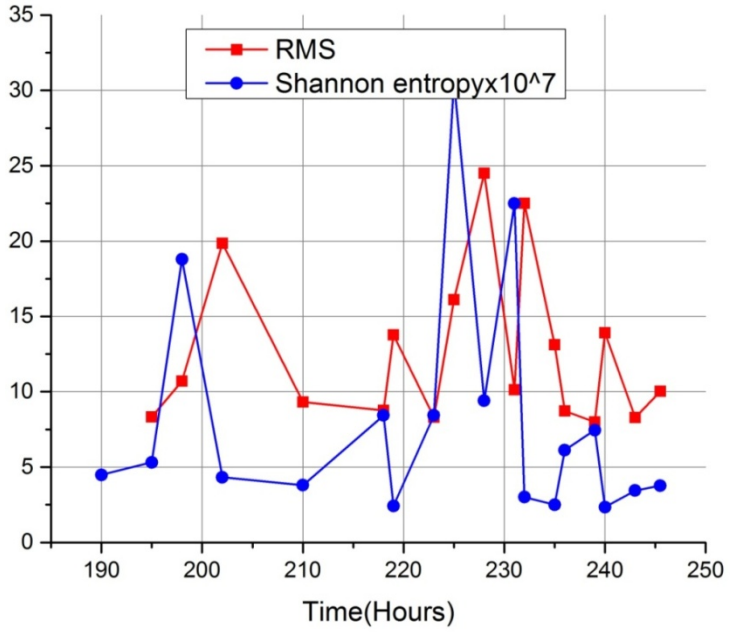

Fig 4. 8 RMS and Shannon entropy values from duration 190 hours onward for 5kg load..

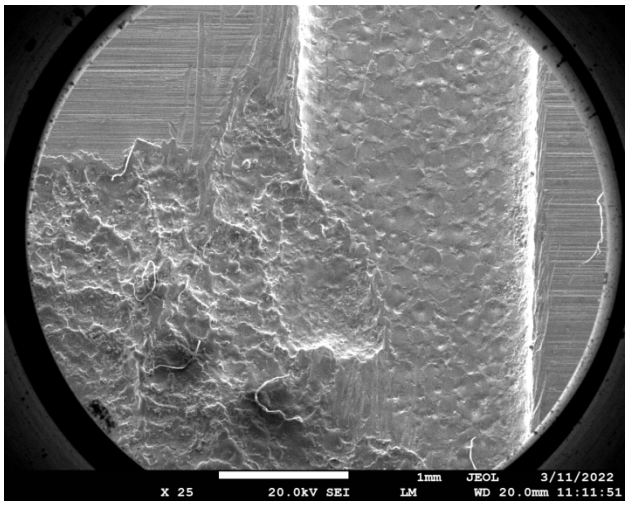

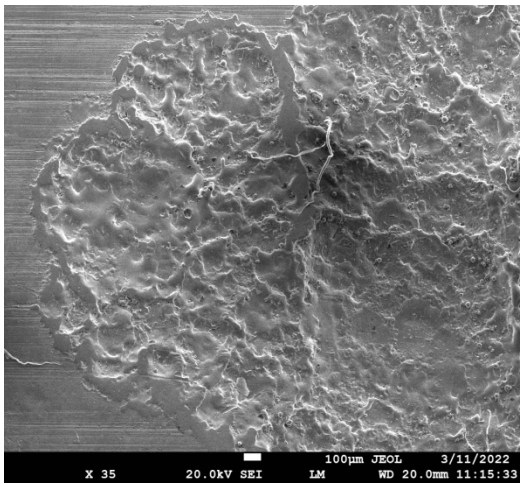

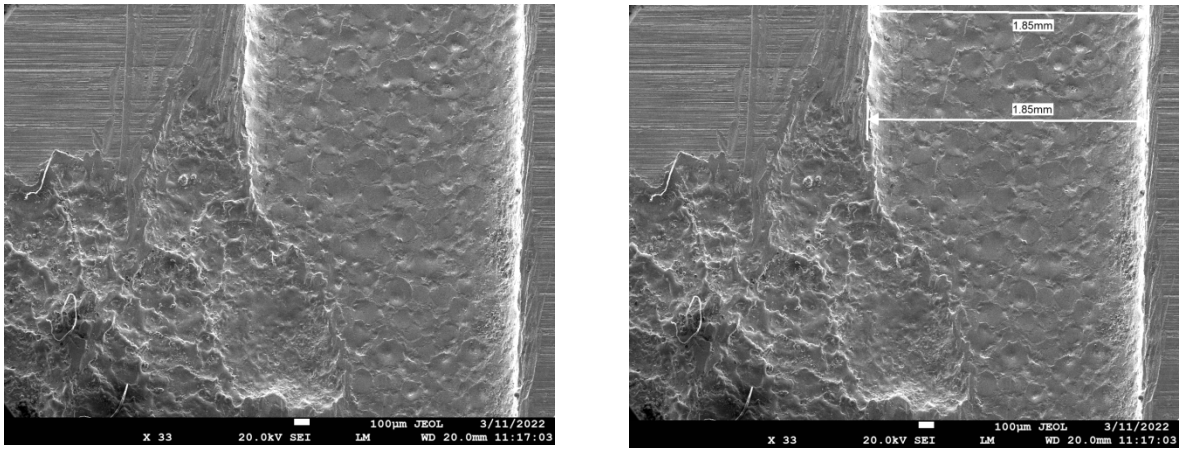

Fig4. 9 Scanning electron microscope (SEM) for 5 Kg

4.3.3 Case 3-10 Kg load: To analyze further the effect of loading on crack propagation of taper roller bearing load intensity was increased to 10 Kg while rpm of 1500 remains same and effect of loading is shown in annexure 1.

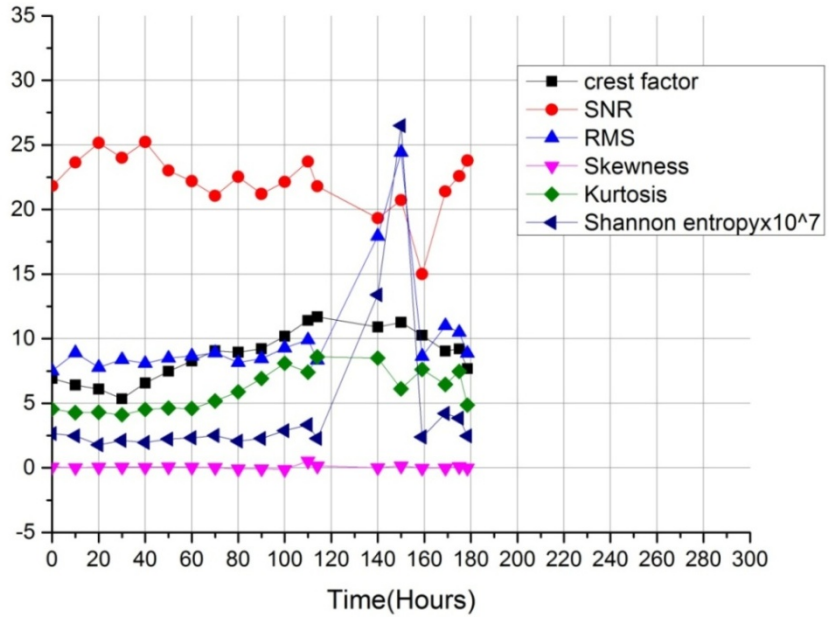

Fig 4. 10 Experimental result of crest factor, SNR, RMS, skewness, Kurtosis, Shannon entropy 10 kg load

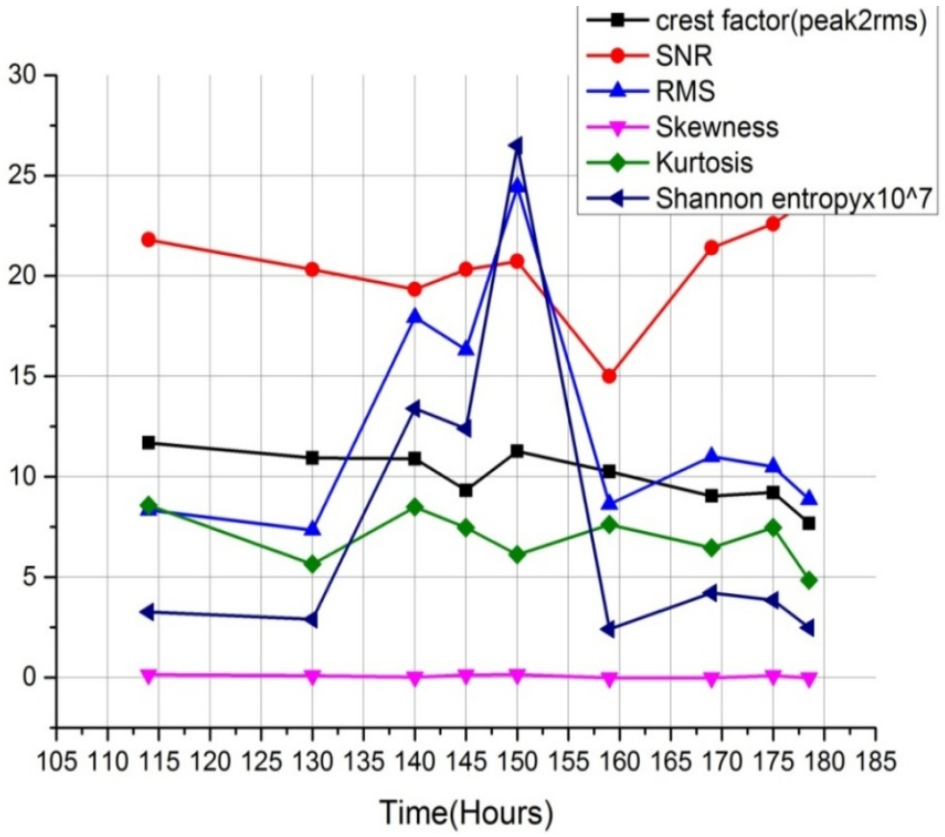

Fig 4. 11RMS and Shannon entropy values from duration 114 hours onward for 10kg load.

It has been found out that whenever edge is broken there is sudden rise of Shannon entropy was noticed. As shown in Fig 4.10 and Fig 4.11 no change was noticed till 138 hours but sudden rise of Shannon entropy due to crack propagation was noticed at 140 hours, 150 hours, 169 hours. High resolution images taken by using scanning electron microscope (SEM) is shown in Fig 4.12. Hence Shannon entropy is a sensitive parameter in case initiation and propagation and responded fairly well with variation of loading.

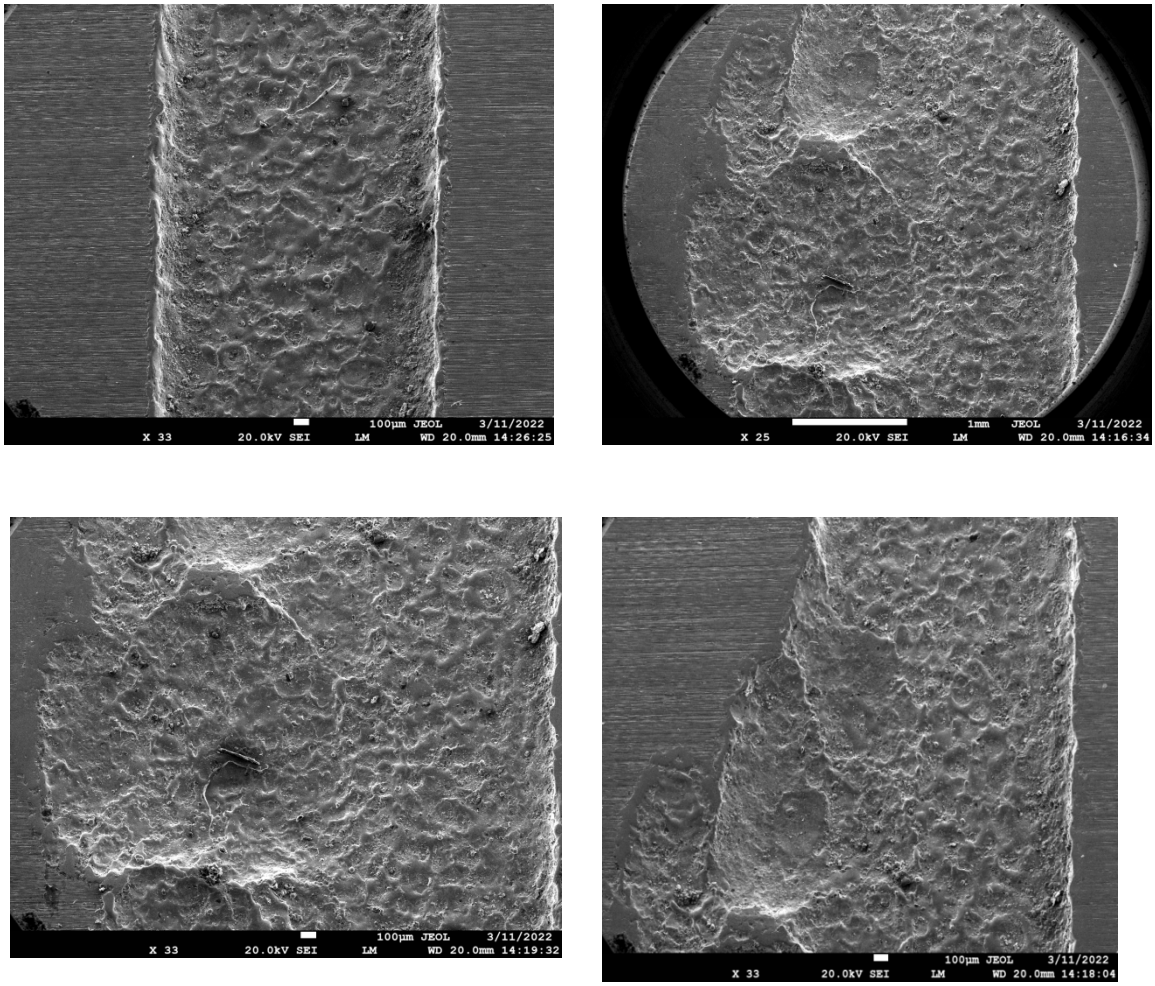

Fig 4. 12 Scanning electron microscope (SEM) for 10 Kg

4.3.4 Case 4- Effect of 15 Kg load. Next set of experiment was conducted by varying the intensity of load to 15 Kg and speed of 1500 rpm is not altered. To analyze the effect of 15 kg load statistical analysis are carried out is shown in annexure 1.

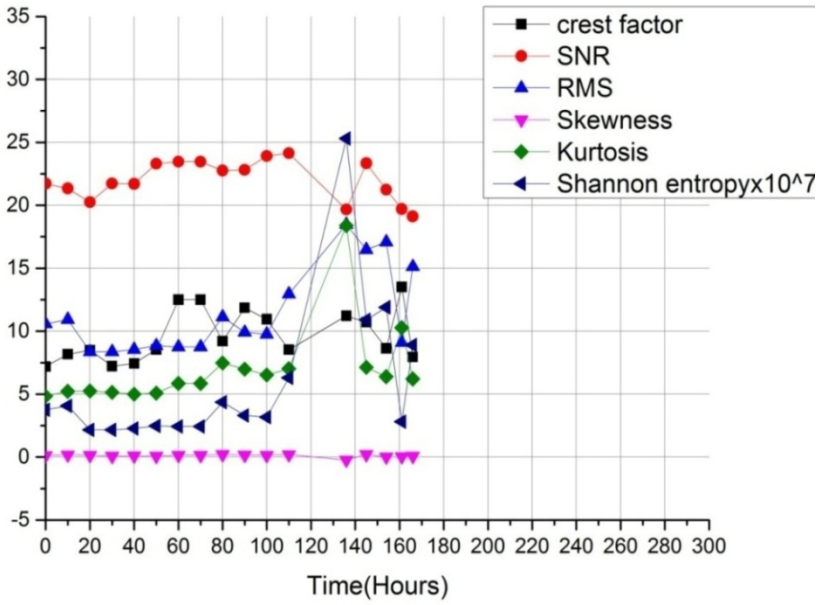

Fig 4. 13 Experimental result of crest factor, SNR, RMS, skewness, Kurtosis, Shannon entropy 15 kg load

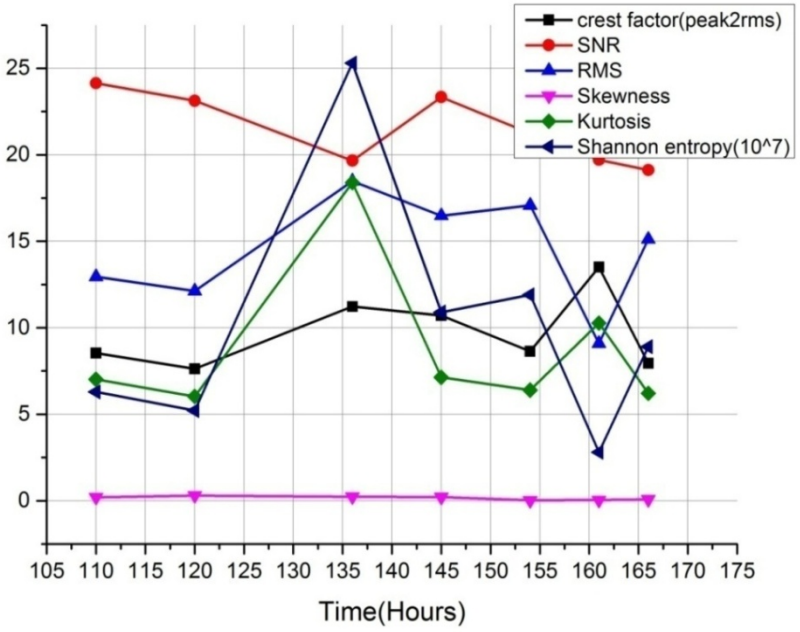

Fig 4.14 RMS and Shannon entropy values from duration 110 hours onward for 15kg load

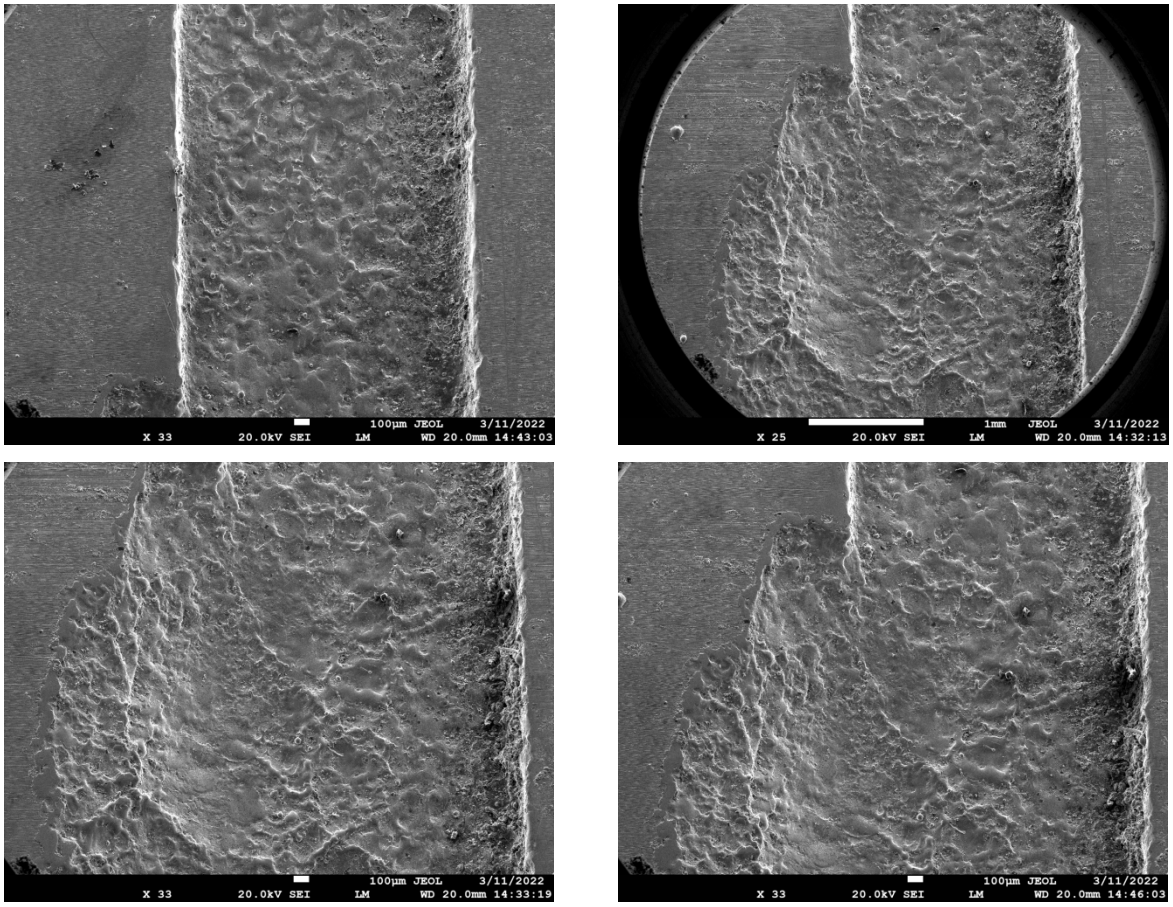

Fig 4. 15 Scanning electron microscope (SEM) for 15 Kg

Bearing having a outer race defect was subjected to a load of 15 kg and no change was observed till 130 hour. Sudden rise in Shannon entropy was observed at 136 hour, 154 hour, 166 hour is shown in Fig 4.13 and Fig 4.14 due to crack initiation. Scanning electron microscope (SEM) taken at 166 Hours of running operation is shown in Fig 4.13 and Fig 4.14.

4.3.5 Case 5 effect of 20 Kg load: Last set of experiment was conducted and load of 20 KG was applied on taper roller bearing. Statistical parameter such as crest factor, SNR,

RMS, Skewness, Shannon entropy etc is shown in annexure1In last set of experiment further load was increased to 20Kg and 15000 rpm was kept constant. In all the parameters, Shannon entropy was showing a steep rise in the values for edge breakage during crack propagation but none of the parameters was showing any relation with the crack propagation. Furthermore, after the completion of experiments it was observed that the loading conditions affect the remaining useful life substantially. In case when loading was set to 20 kg the total time bearing survived in running was 116.5 hours compared to 285 hours when no load was applied. Same trend was observed Shannon entropy shown sudden rise at 103 hour, 114 hour is shown in Fig 4.16 and Fig 4.17 in case of 20 kg load due crack propagation. The test was concluded when the statistical measures indicated sufficient degradation in taper roller bearings and Shannon entropy responded fairly well in case of crack propagation. At constant speed, the values of shannon entropy and RMS exhibit significant variation for crack initiation and propagation with respect to load. For rolling element bearing kurtosis is one of the main parameter in statistical analysis of vibration signal.

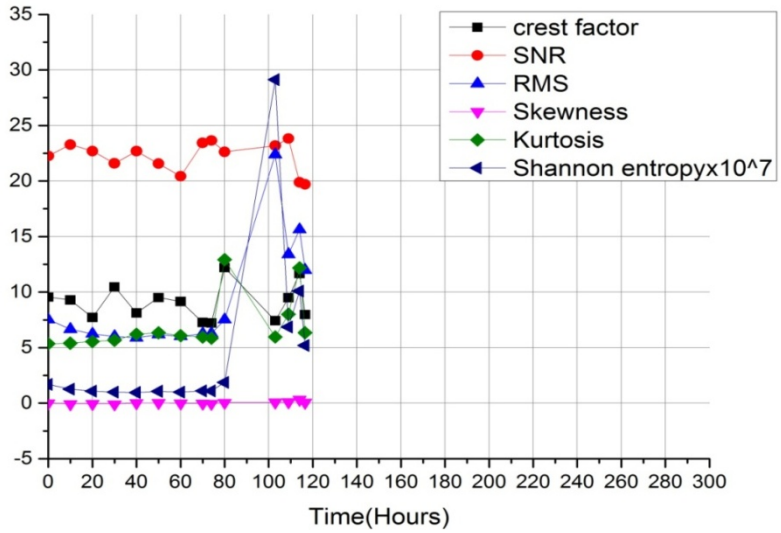

Fig 4. 16 Experimental result of crest factor, SNR, RMS, skewness, Kurtosis, Shannon entropy 20 kg load.

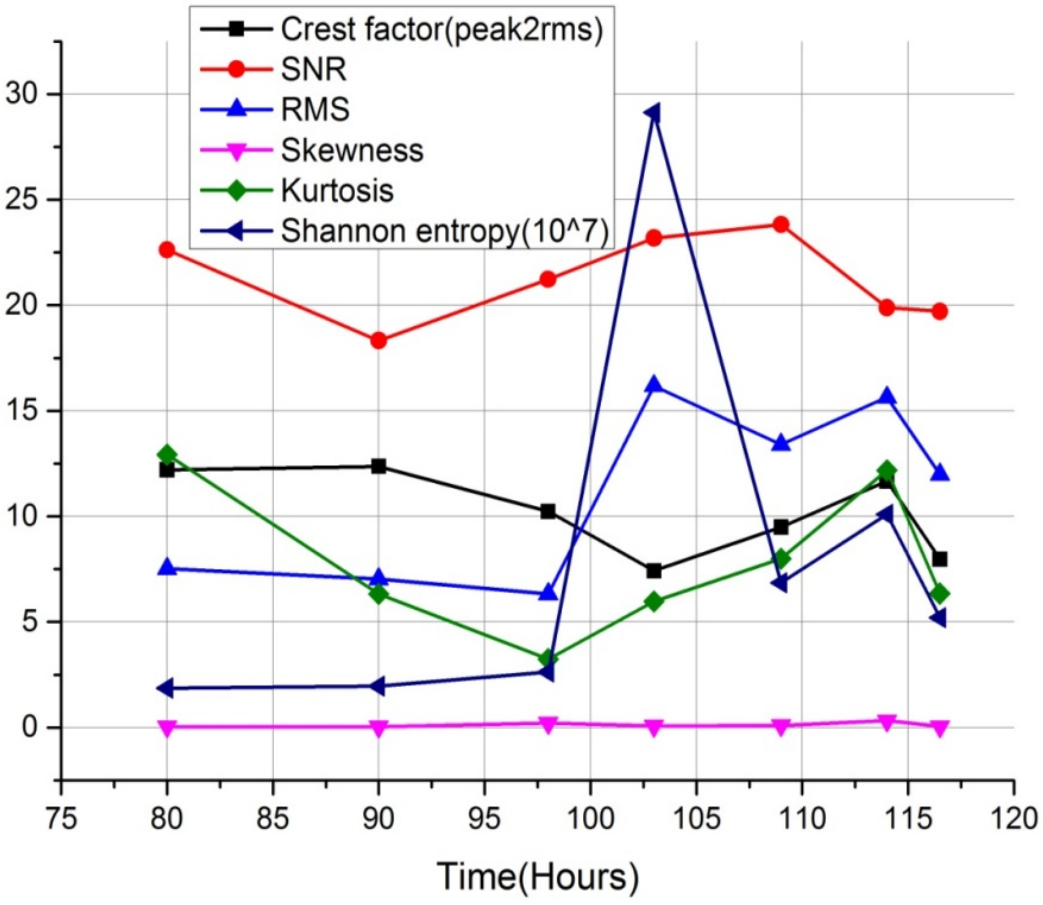

Fig 4. 17 RMS and Shannon entropy values from duration 80 hours onward for 20 kg load condition.

In annexure1 all the statistical parameters under the effect of loading were shown the kurtosis value with increase in radial load. Kurtosis value of defect free bearing is close to 4 and in between 4 to 25 indicates the defect in bearing. Experimental value of kurtosis shown in table is more then 4 which indicates defect is present in bearing. High resolution images taken by Scanning electron microscope (SEM) of 116 hours running of taper roller bearing is shown in Fig 4.18

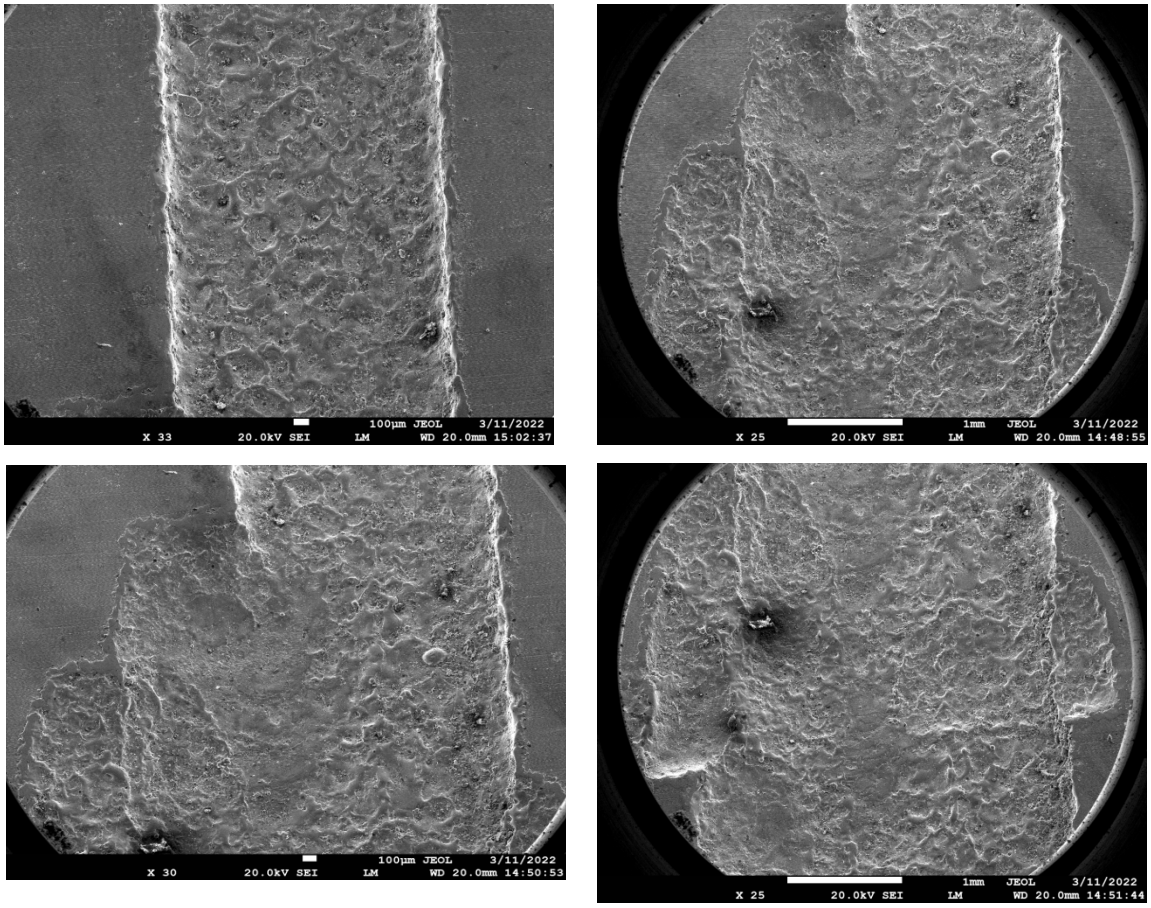

Fig 4. 18 Scanning electron microscope (SEM) for 20 Kg

4.4 Defect width measurement using CWT

Detection of crack initiation and measurement of area plays a crucial role in condition monitoring. Analysis was conducted on the area of the crack patterns created as a result of the load during experimentation. The entire analysis was performed on captured images of the cracked surface of the rolling element bearing during experimentation. Image j software is open source software is found application in many field such as crack width measurement, crack area measurement, Crack detection [198-199]. Complete crack characteristics such as width and area which is not possible to

calculate manually can be obtained using image processing software and CWT. In this experiment was conducted for five different set of loading conditions 0 kg, 5K, 10Kg, 15Kg, and 20 Kg.

	Area	Mean	Min	Max
1	2.118	179.970	134	213

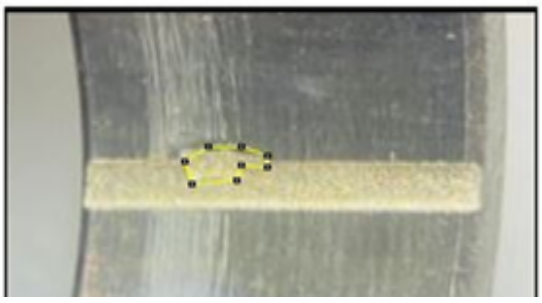

	Area	Mean	Min	Max
1	3.918	130.562	0	255

	Area	Mean	Min	Max
1	4.147	182.482	45	255

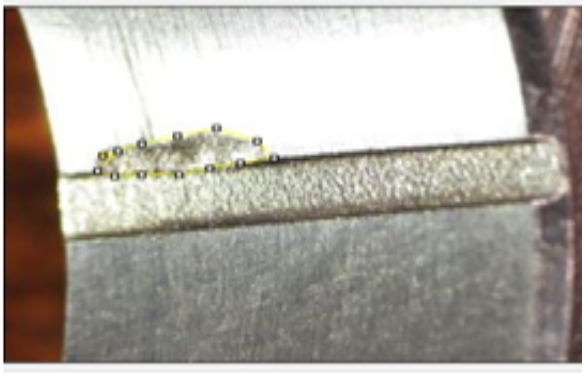

	Area	Mean	Min	Max
1	4.290	179.311	35	255

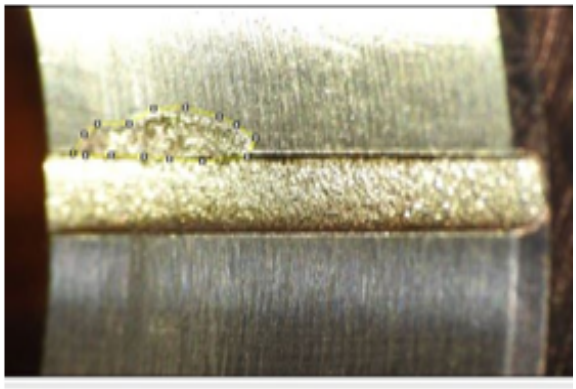

	Area	Mean	Min	Max
1	4.342	103.664	9	247

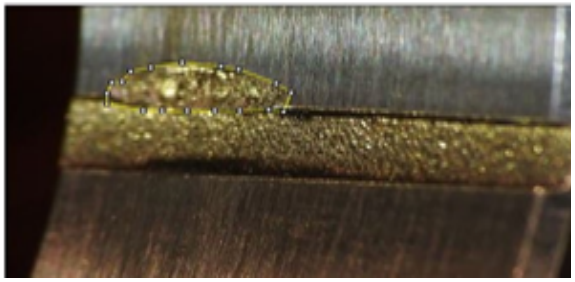

	Area	Mean	Min	Max
1	4.464	144.681	15	252

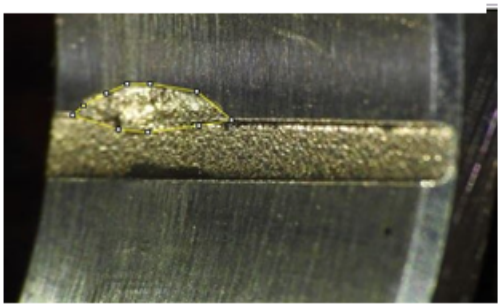

	Area	Mean	Min	Max
1	4.696	56.795	1	242

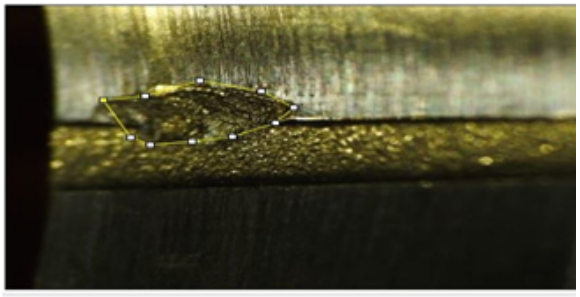

	Area	Mean	Min	Max
1	4.704	163.293	42	255

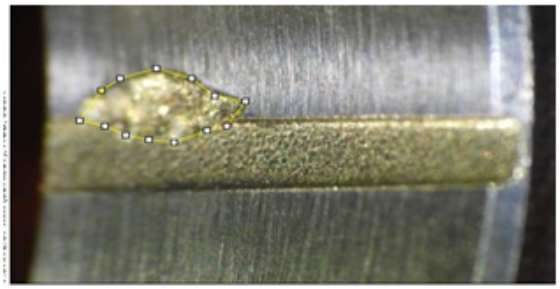

	Area	Mean	Min	Max
1	6.159	127.650	40	235

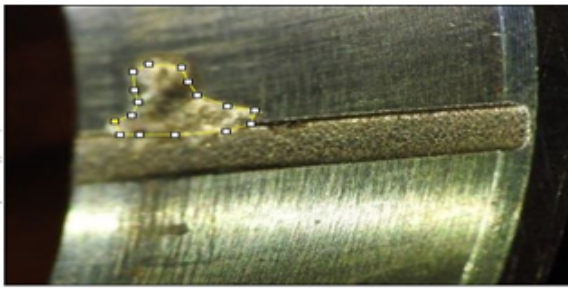

	Area	Mean	Min	Max
1	8.512	101.100	46	229

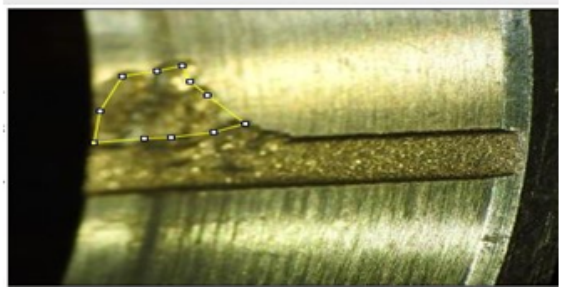

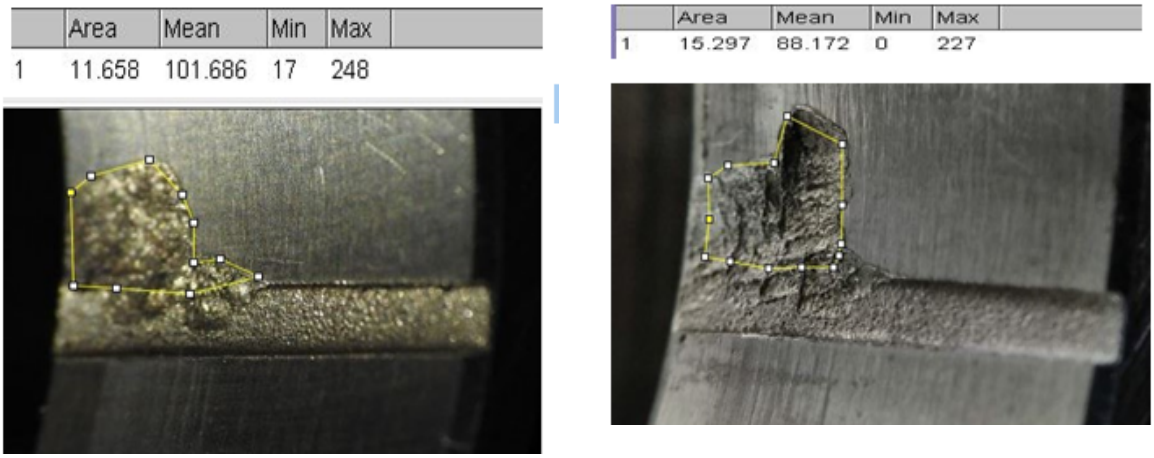

Fig 4. 19 crack propagation without load

For analyzing the status bearings are disassembled from bearing casing to conduct a thorough visual inspection. The bearings are properly cleaned out and a visual inspection is preformed and image was taken using microscope is shown in Fig 4.19. Further image processing software image J is used to calculate the crack propagation rate with respect to time. A series of pictures demonstrating effect of loading on crack propagation rate in terms of area is shown in mm^2. During the test, the signal from the sensor is used to monitor the crack growth rate. The test is interrupted periodically and images of cracks are taken, after which the test is restarted. It has been noticed that loading has distinct effect on crack propagation rate. It has been observed that defect initiates from the edge and grow along the rolling direction and continue to spread with respect to time. Area calculated at different time intervals were shown with respect to time is shown in Fig 4.20 for different loading conditions. The effect of radial loads on crack propagation at different time intervals is shown in Annexure 2. Loading plays a crucial role in crack initiation and propagation. As shown in Fig 4.20 the without load crack area at 285 hour was 15.297 mm^2 when load of 20 kg was applied area is 14.549 mm^2 at 116 hour which clearly indicates increase in loading results in faster rate of crack propagation.

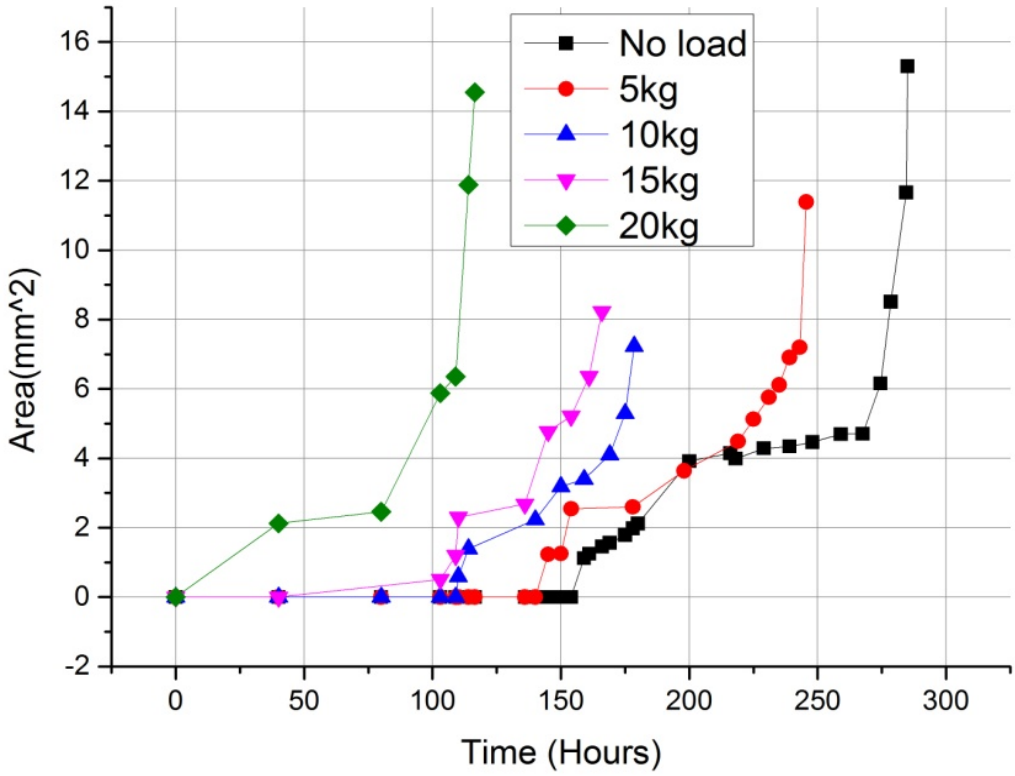

Fig 4. 20 Increase in crack area in (mm^2) for various loading conditions

.

To estimate the crack width CWT graph was drawn for the vibration signal using bi-orthogonal wavelet. Entry and exit point of roller into defect were spotted on the graph. The entry point of the roller was having low/medium frequency characteristics and on the contrary exit point having high frequency. The bi-orthogonal based CWT analysis provided the opportunity to spot both the low and high frequency event in good time resolution. The CWT graphs for the time duration of 178 hours, 235 hours and 246 hours are shown in the Fig. 4.21(a), Fig. 4.21(b) and Fig. 4.21(c) respectively along with the image of the defect.

(a)

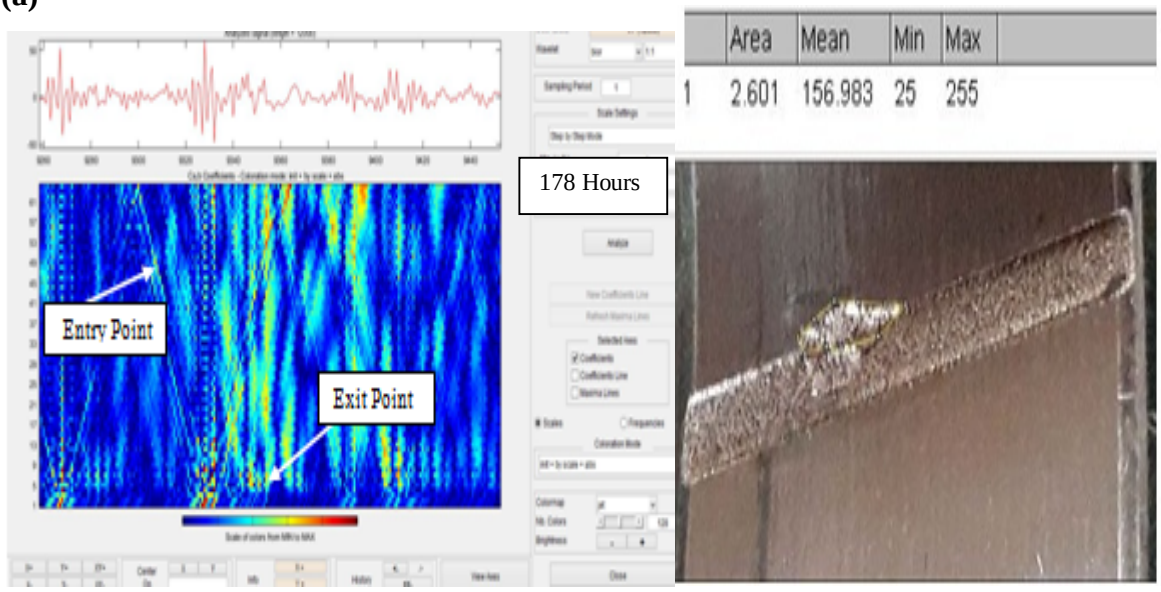
Area Mean Min Max
1 2.601 156.983 25 255
178 Hours
Entry Point
Exit Point

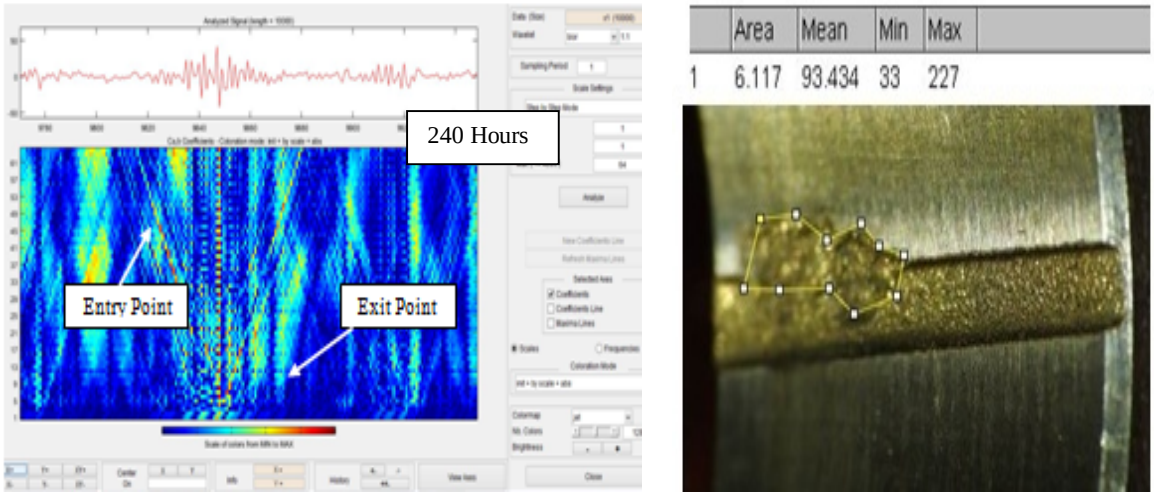
Area Mean Min Max
1 6.117 93.434 33 227
240 Hours
Entry Point
Exit Point

(b)

(c)

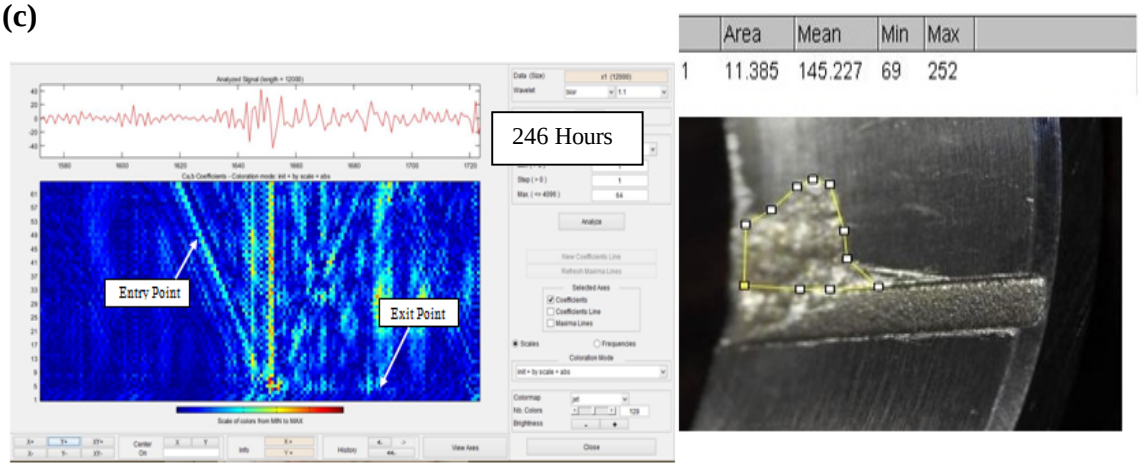

Fig 4. 21 CWT images and experimental images (a)178 Hours (b) 235 hours (c)246 hours

Defect width was calculated by calculating the time roller touches and exit from the corner of the defect. There is no restricting force on the roller until the another roller touches the trailing edge of the defect. Highest amplitude is created at exit point also known as re stressing event. Rolling element at entrance and exit are high frequency events and can easily be spotted using CWT shown in Fig 4.21. The data points were calculated between the entry and exit point from the CWT graph and defect width was calculated using equation (4.1)

Outer race defect width = $\pi . \Delta t . D_{or} . FTF$ (4.1)

The values were calculated for taper roller bearing (NBC 30205) corresponding to 1500 rpm and sampling rate 12800.

Average outer race diameter of taper roller bearing (D_{or}) =44.35 mm

Fundamental train frequency (FTF) = 9.28 Hz

and Δt represents time interval while roller is in contact with the crack and this can be equated as (number of data points between entry and exit point)/12800

Defect width was calculated at different time intervals and results were compared with actual defect width measured using image J software and presented in Table 4. 2.

Table 4. 2 Defect width measured using image J software and CWT graph.\

Running Time (Hours)	**Actual defect width measure by image processing (mm)**	**Difference between entry and exit data points**	**Defect width measured using CWT graph (mm)**	**Error in percentage (%)**
0 hour	2	23	2.322	16.1
178	3.21	35	3.534	10.1
198	3.44	37	3.735	8.57
218	3.61	38	3.836	6.26
230	3.73	38	3.836	2.84
240	3.89	40	4.038	3.80
244	5.13	52	5.250	2.34
246	6.43	63	6.360	1.09

During the crack propagation many interim changes were supposed to happen such as edge brakeage, edge smoothness etc. Even though CWT was found effective in estimating the crack width but it was unable to provide any information about the interim changes happening during crack propagation.

Whenever, rolling element passes over the region of crack then the changes happened in the vibration signal are caused by different stress levels. At entry point roller just falls over the defect and creates the low/medium frequency event but after striking the base impulses of high stress are generated. Furthermore, whenever the roller exits the crack, it put pressure on the trailing edge and creates high amount of stress which sometimes results in damaging or smoothening of the edge.

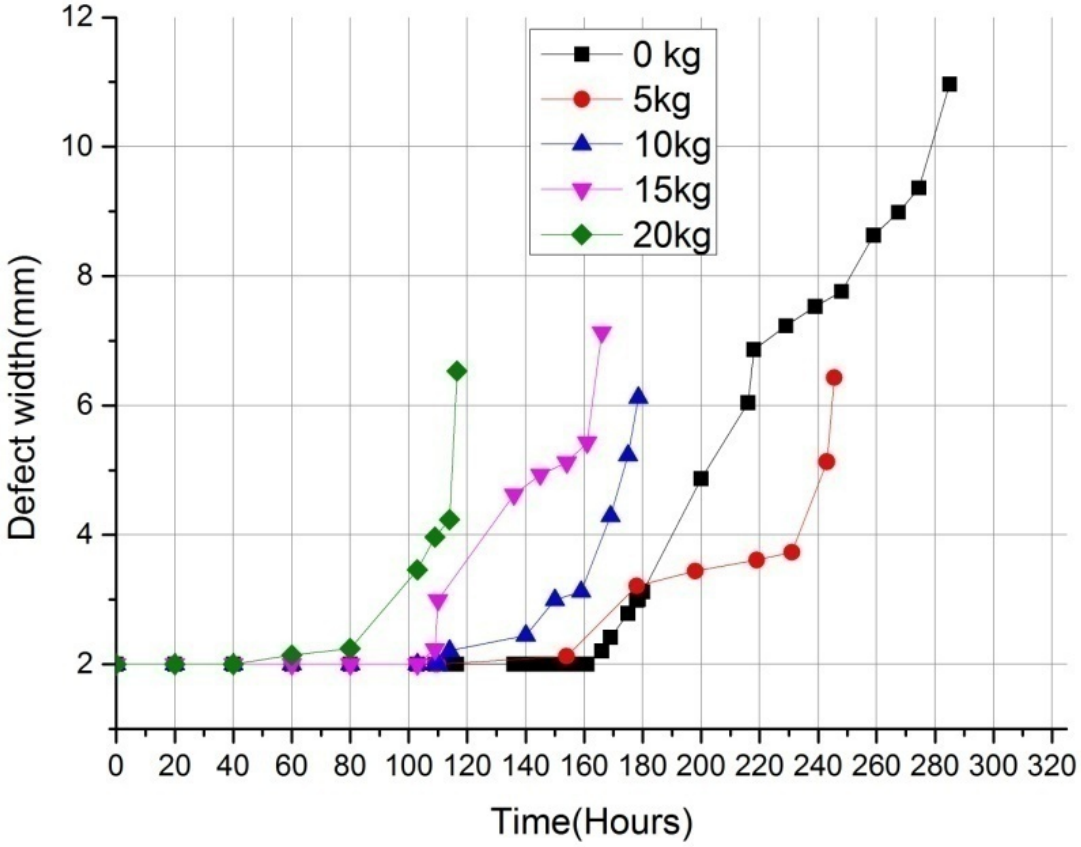

Fig 4. 22 Overall defect width in (mm) for various loading conditions

It can be observed from the graphs that the overall crack width and crack area growth rises rapidly after 267.5 hours, 243 hours, 169 hours, 154 hours and 109 hours for without load. Signal captured during experimentation provides information on roller entry and exit to outer race fault and contains the various band of vibration burst. The nature of the burst is determined by a detailed study of each individual vibration signal which is dependent on the defect width. Scalogram created by Continuous Wavelet Transform (CWT) offers critical information on roller entry and exit to the defect and provide basis for defect width measurement. Both of these area and defect width graphs shown in Fig 4.22 depicts that the loading conditions were significantly affecting the remaining life of the bearing after crack initiation.

4.5 High, medium, low frequency band analysis using CWT:

One of the benefits of using wavelet transform for signal analysis is the number of base wavelets generated and there are 13 wavelet families defined in the library using MATLAB. Such different variety it always creates confusion how to select the appropriate base wavelet for processing a certain signal. Effort has been made for selecting the base wavelet form matlab directory which respond and more sensitive to crack propagation. For analyzing the non stationary signal captured during experimentation of bearing with outer race defect different wavelets such as Haar, Daubechies 2nd order (db2), Morlet (morl) and Daubechies 10th order (db10) were used and best wavelet was selected which responded to crack propagation.

4.5.1 Frequency band analysis without load: CWT based high, medium and low frequency band analysis were carried out using several wavelets. The transient response for longer duration of time was expected in the signal for crack propagation progression. Therefore, in the normal time-frequency analysis the longer duration transient response components were very difficult to quantify except for measuring defect width. Wavelet analysis on the other hand is the decomposition of a signal into shifted and scaled versions of the original known as the mother wavelet. By comparing the wavelets and sine waves signals changes abruptly are better analyzed with a wavelet rather then analyzing a time or frequency domain signal. To carry out this analysis in a simplified way different frequency band were selected from the CWT based analysis and Shannon entropy of these bands was calculated. The calculated Shannon entropy values for four selected wavelets Haar, Daubechies 2nd order (db2), Morlet (morl) and Daubechies 10th order (db10) are shown in Table 4.3

Table 4. 3 Shannon entropy values for high, medium and low frequency bands of CWT using Haar, db2, morl and db10 as mother wavelet

Time duration in hours	**SE high freq. bands Haar (10^7)**	**SE high freq.db2(10^7)**	**SE high Freq.morl (10^7)**	**SE high freq db10 (10^7)**	**SE medium freq. Haar (10^7)**	**SE medium freq. db2 (10^7)**	**SE medium freq morl (10^7)**	**SE medium freq.db10 (10^7)**	**SE low freq. Haar(10^7)**	**SE low freq.db2(10^7)**	**SE low freq.morl(10^7)**	**SE low freq.db10(10^7)**
0	3.73	2.70	2.23	2.46	4.23	4.20	2.11	2.85	0.76	0.23	0.09	0.05
180	3.21	3.20	2.10	2.47	8.10	3.11	9.10	11.75	8.13	1.82	6.63	7.83
184	3.32	2.48	2.16	8.96	8.44	10.00	9.50	12.19	8.80	9.58	7.59	8.77
188	3.71	2.79	2.47	2.89	8.48	10.01	9.77	12.19	8.71	9.46	7.58	8.71
192	3.43	2.56	2.25	2.65	8.84	10.48	10.01	12.77	9.15	9.97	7.83	9.16
196	3.98	2.98	2.66	3.08	8.38	9.82	9.17	11.95	8.82	9.56	7.25	8.78
200	60	47.19	42.9	58	47.	48.	44.	47.9	24.6	23.04	21.67	23.70

	.30		3	.7	01	91	36	0	8			
204	64.27	50.37	45.95	52.0	50.85	53.41	51.31	53.81	25.94	24.20	22.20	24.55
208	62.21	48.63	44.61	40.2	49.52	52.17	50.91	52.83	25.42	23.71	21.96	24.07
212	64.91	50.97	46.51	62.7	49.45	51.93	49.10	52.72	25.82	23.92	21.49	23.75
216	59.81	46.75	42.78	58.2	47.30	49.92	48.84	50.86	23.58	21.69	19.43	21.57
220	**15.07**	10.96	10.30	9.89	10.78	11.46	9.80	12.16	9.22	9.17	8.45	8.85
224	15.67	11.40	10.69	19.3	11.00	11.61	9.90	12.19	9.85	9.91	9.92	9.79
229	18.91	14.90	13.47	15.2	12.00	12.24	10.95	12.24	8.74	8.20	7.80	7.81
239	23.37	18.25	17.41	18.6	9.91	9.80	8.75	9.49	7.14	6.13	5.22	5.72
248	31.90	25.26	22.58	23.4	18.97	19.85	18.70	20.18	13.02	11.47	9.80	10.36
259	19	14.50	14.5	23	7.3	7.6	9.8	7.73	4.70	3.81	3.10	3.15

	.25		8	.3	4	2	0					
267.5	4.72	3.60	3.19	23.6	3.97	4.12	4.67	4.33	1.10	0.70	0.37	0.47
274.5	6.00	4.30	4.26	24.2	2.76	3.01	3.99	3.74	1.74	1.47	1.00	1.18
278.5	5.78	4.17	4.19	25.1	5.19	5.92	7.55	6.73	1.85	1.61	1.07	1.42
282.5	6.47	4.71	4.60	36.6	3.16	3.11	2.84	2.95	1.94	1.82	1.91	2.07
284.5	6.59	4.79	4.76	30.70	4.02	4.15	3.99	3.93	0.89	0.49	0.28	0.37
285	5.81	4.20	4.15	31.1	3.11	3.11	2.79	2.90	1.38	1.19	1.09	1.30

Haar and db2 are lower order wavelets and were initially tested to check the effect of different bands on crack propagation. These wavelet were selected because of its vast use in the field of defect detection and to monitor the defect condition [200-204]. Furthermore, one higher order wavelet db10 was used with the expectation of significantly acknowledge the transient response for longer duration of time. The graphs of calculated Shannon entropy for high, medium and low frequency bands for these four wavelets are shown in Fig 4.23, Fig 4.24 and Fig 4.25 respectively for no load condition.

.

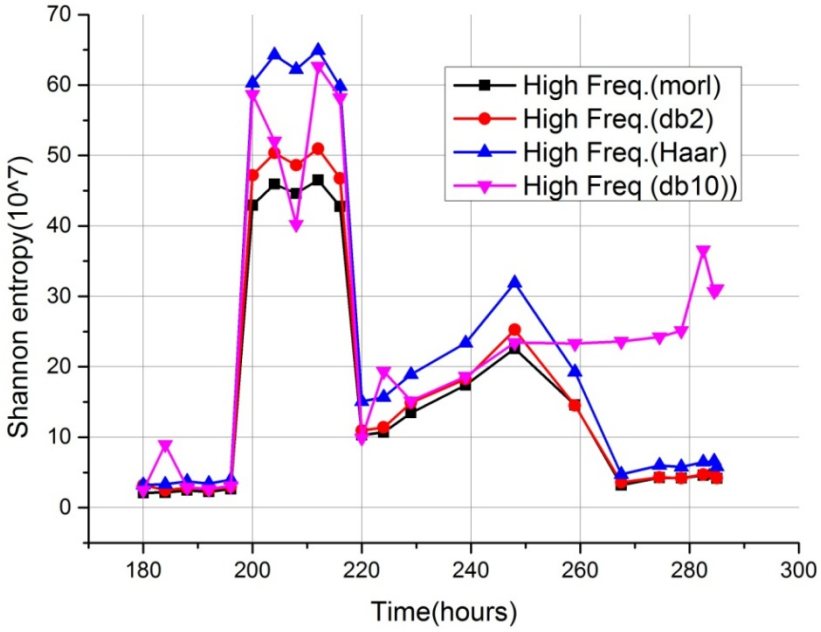

Fig4. 23 Shannon entropy values for high frequency band of CWT using Haar, db2, morl and db10 wavelets

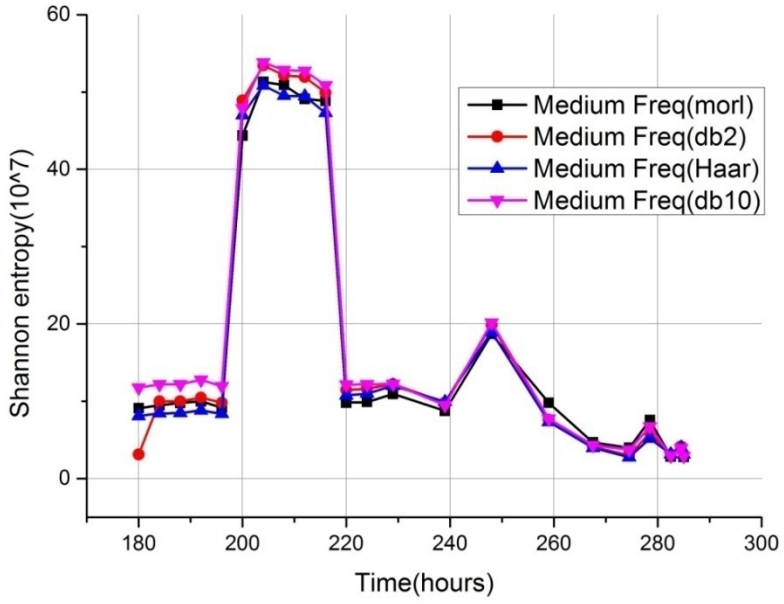

Fig 4. 24 Shannon entropy values for medium frequency band of CWT using Haar, db2, morl and db10 wavelets

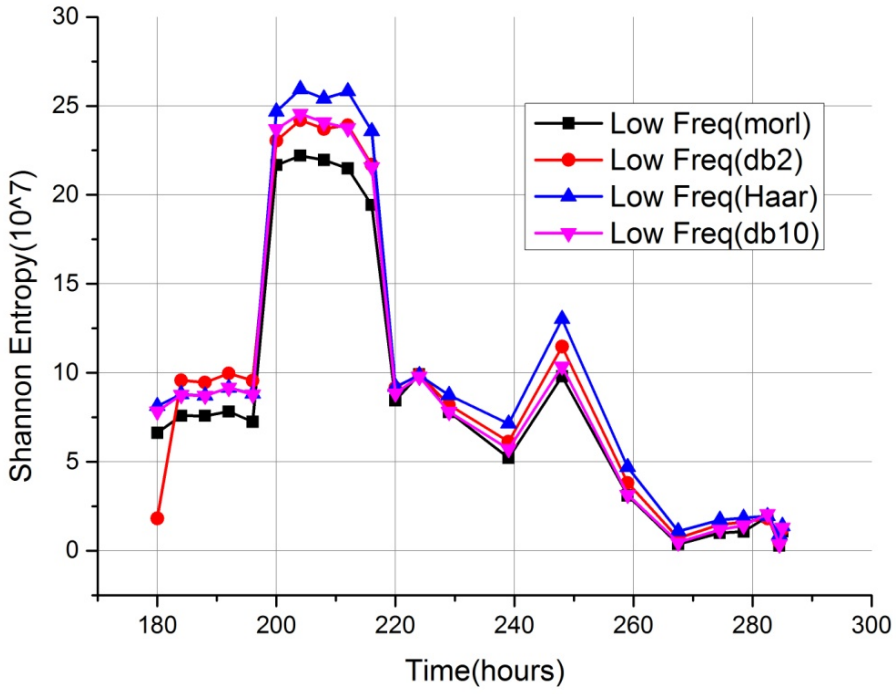

Fig4. 25 Shannon entropy values for low frequency band of CWT using Haar, db2, morl and db10 wavelets

Shannon entropy of high frequency band was observed to be increased for all the wavelets for edge breakage at 200 hours. However, for the edge breakages at 184 hours, 200 hours, 212 hours, 216 hours, 224 hours and 278.5 hours Shannon entropy of db10 was having in better agreement. In the medium and low frequency Shannon entropy showed sharp rise at 200 hours duration only and no other significant rise was observed with the edge breakage. When the roller passes over the defect it generally generates high frequency impulses in the vibration signal therefore, high frequency analysis was better for analyzing the crack propagation.

4.5.2 Frequency band analysis 5 Kg load: For analyzing the effect of loading on outer race defect of tapered roller bearings, a wavelet transform technique by using different

base wavelet were used. Effect of 5 Kg load on the value of high frequency, medium and low frequency is shown in Table 4.4.

Table 4. 4 Shannon entropy values for high, medium and low frequency bands of CWT for 5 kg load using Haar, db2, morl and db10 as mother wavelet

Time (Hours)	**SE high freq. bands Haar(10^7**	**SE high freq. bands db2 (10^7)**	**SE high freq. bands Morlet(10^7)**	**SE high freq. bands db10(10^7)**	**SE med freq. bands Haar(10^7)**	**SE med freq. bands db2 (10^7)**	**SE med freq. bands Morlet(10^7)**	**SE med freq. bands db10(10^7)**	**SE low freq. bands Haar(10^7)**	**SE low freq. bands db2 (10^7)**	**SE low freq. bands Morlet(10^7)**	**SE low freq. bands db10(10^7)**
0	9.5	7.94	4.75	6.37	4.53	3.78	2.59	2.8	3.49	2.12	1.85	1.7
40	6.1	5.2	3.5	6.2	4.5	4.5	3.9	2.7	3.44	2.1	1.9	1.89
80	4.9	6.2	3.7	6.15	5.4	5.4	4.3	2.4	3.3	2.41	1.94	1.64
120	4.3	3.7	3.9	6.14	4.3	5.3	3.7	2.2	3.41	2.8	1.98	1.69
154	8.16	6.17	4.75	6.32	10.1	11.3	4.4	11.9	4.04	3.57	2.77	2.82
178	6.65	4.76	4.56	4.64	7.33	8.61	11.3	10.4	3.98	3.5	2.36	2.53

198	33.7	25.8	24.2	25.4	29.7	27.1	22.7	28	18.1	16.5	12.5	15.1
218	13.2	10.7	9.78	11.4	25.8	27.6	22.6	25.2	11.9	10.8	8.99	9.25
219	4.4	3.55	3.28	3.73	4.83	5.35	6.17	6.34	4.24	4.41	2.64	4.31
225	64.9	49.6	49.5	49.5	9.8	8.63	8.97	8.54	5.71	2.94	2.42	2.13
231	50.4	38.5	37.3	38.8	17.5	16.4	16.4	1.62	5.71	5.89	4.49	4.27
235	5.1	3.66	3.32	3.61	3.72	3.99	5.38	4.71	8.98	0.96	0.519	0.71
239	16.3	12.7	12.2	12.8	9.54	10.6	11	12.8	5.46	4.54	3.3	3.56
243	7.54	5.37	5.4	5.27	3.86	4.03	4.39	4.2	1.04	0.686	0.473	0.567
246	8.91	6.66	6.59	6.64	4.95	5.25	6.21	5.55	1.38	0.839	0.465	0.631

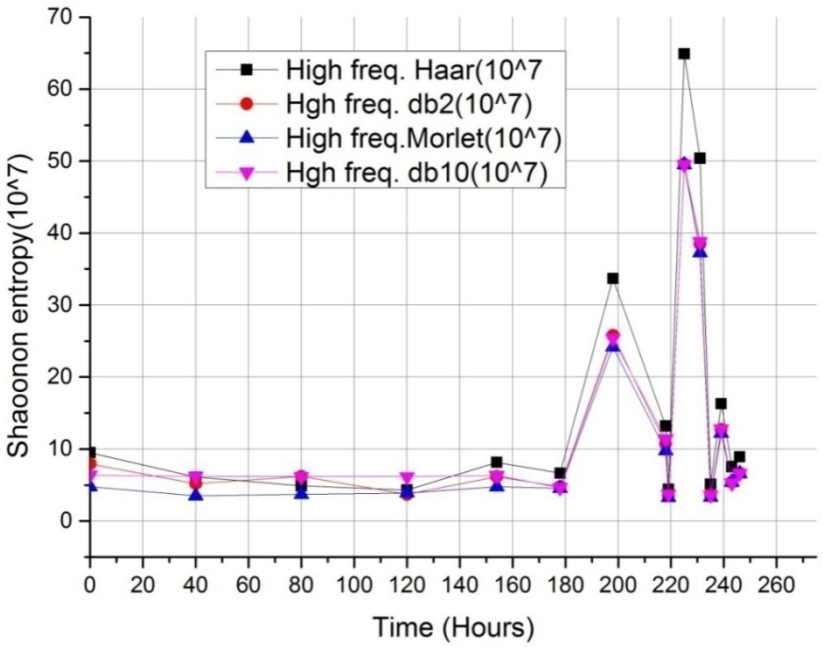

Fig4. 26 Shannon entropy values for high frequency band of CWT using Haar, db2, morl and db10 wavelets

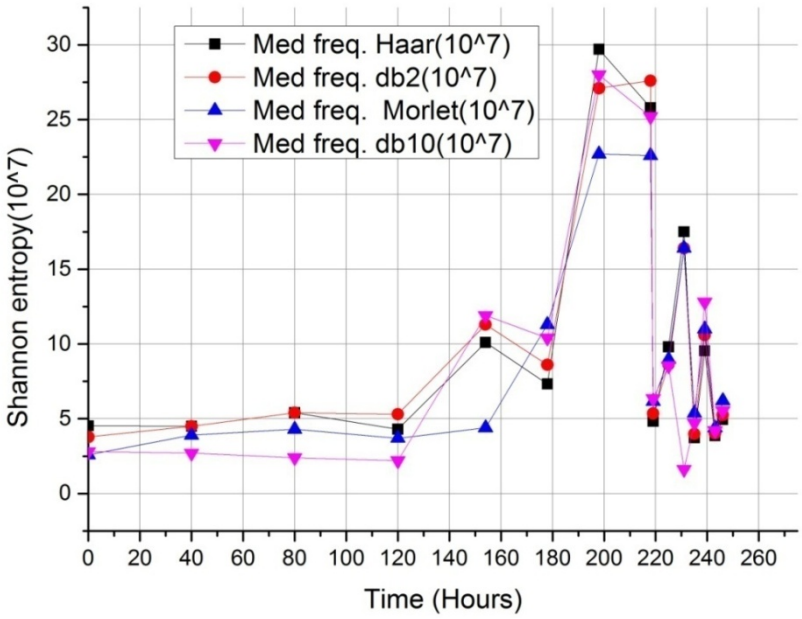

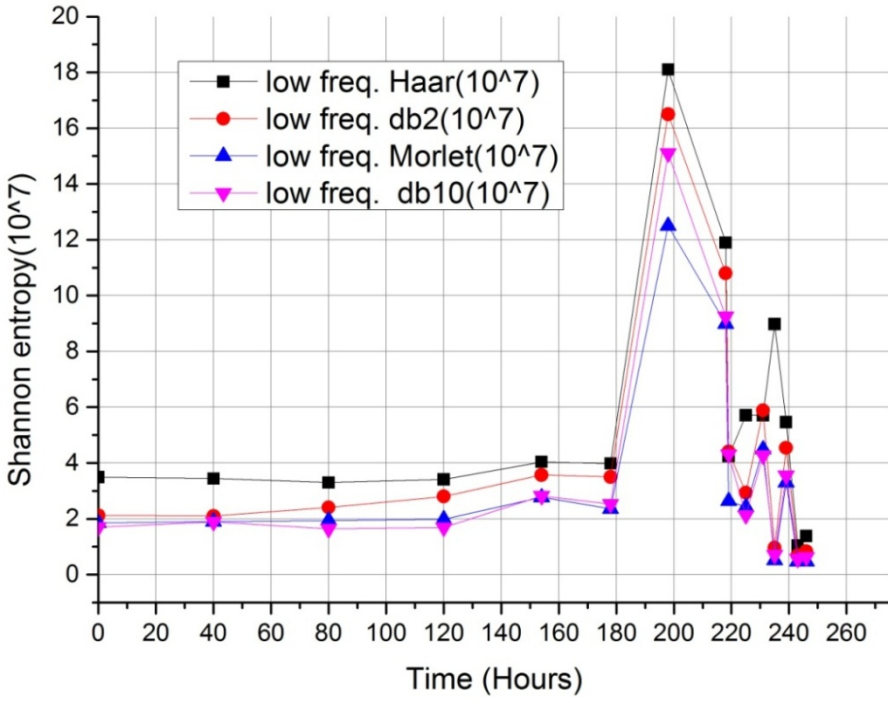

Fig 4. 27 Shannon entropy values for medium and low frequency band of CWT using Haar, db2, morl and db10 wavelets for 5kg load.

Effect of 5 Kg load is shown in Figure in which sudden rise of high frequency component observed at 198 hour, 225 hours, 239 hours and 245.5 hours which is a indication of crack initiation and new edge formation. Results were further compared to statistical analysis same sudden rise was observed at 198 hour, 225 hours, 239 hours and 245.5 hours which is a clear indication of crack initiation. As shown Db10 wavelet is more sensitive among all wavelet which responds to crack propagation with respect to its transient parameters. Further effect of loading was increased from 10 kg,15 Kg, 20 Kg and Fig 4.26, Fig 4.27, depicts the high frequency, and medium frequency, low frequency bands. Similar trend was observed where db10 responded fairly well with respect to loading.

4.5.3 Frequency band analysis 10 Kg load:

Effect of loading was increased and same trend was observed as discussed in case of 5 Kg load. db10 of high frequency component shows the significant rise in edge breakage at 140 hours, 150 hours and 169 hours and is more sensitive among all parameters is shown in Fig 4.28.

Table 4. 4 Shannon entropy values for high, medium and low frequency bands of CWT for 10 kg load using Haar, db2, morl and db10 as mother wavelet.

Time (Hours)	**SE high freq. bands Haar(10^7**	**SE high freq. bands db2 (10^7)**	**SE high freq. bands Morlet(10^7)**	**SE high freq. bands db10(10^7)**	**SE med freq. bands Haar(10^7)**	**SE med freq. bands db2 (10^7)**	**SE med freq. bands Morlet(10^7)**	**SE med freq. bands db10(10^7)**	**SE low freq. bands Haar(10^7)**	**SE low freq. bands db2 (10^7)**	**SE low freq. bands Morlet(10^7)**	**SE low freq. bands db10(10^7)**
0	2.26	1.9	1.29	1.402	2.97	2.59	10.2	0.85	1.84	1.12	1.1	0.6665
40	6.1	3.5	2.29	1.932	5.6	3.9	5.4	0.901	1.9	1.256	1.15	2.32
80	5.4	4.4	3.1	1.423	4.5	4.5	4.3	1.235	1.789	1.36	1.32	1.32
114	2.61	1.9	0.966	1.58	5.6	5.37	1.18	0.921	2.61	1.51	1.18	2.32

130	1.32	1.832	4.32	2.27	4.32	4.52	2.32	0.667	3.75	656	2.32	0.667
140	28.6	2.11	20.1	13.59	27.4	29.8	27.5	11	13.3	12.3	10.7	11
145	12.32	10.23	10.321	2.8779	12.32	10.232	13.632	12.7	10.85	10.23	8.78	12.7
150	12.12	11.389	10.32	16.489	30	30.1	26.4	15.9	20.7	17.7	16.7	15.9
159	2.54	45.1	1.31	2.3989	9.17	8.54	5.5	1.13	5.13	2.98	1.15	1.13
169	9.21	1.85	6.79	14.21	5.25	5.69	6.46	1.14	1.75	1.27	0.834	1.14
175	8.88	6.97	6.42	3.85	1.92	1.64	1.62	0.153	0.789	0.312	0.222	0.153
178.5	4.59	6.557	3.18	2.476	7.48	8.94	10.4	5.19	5.69	5.78	3.85	5.19

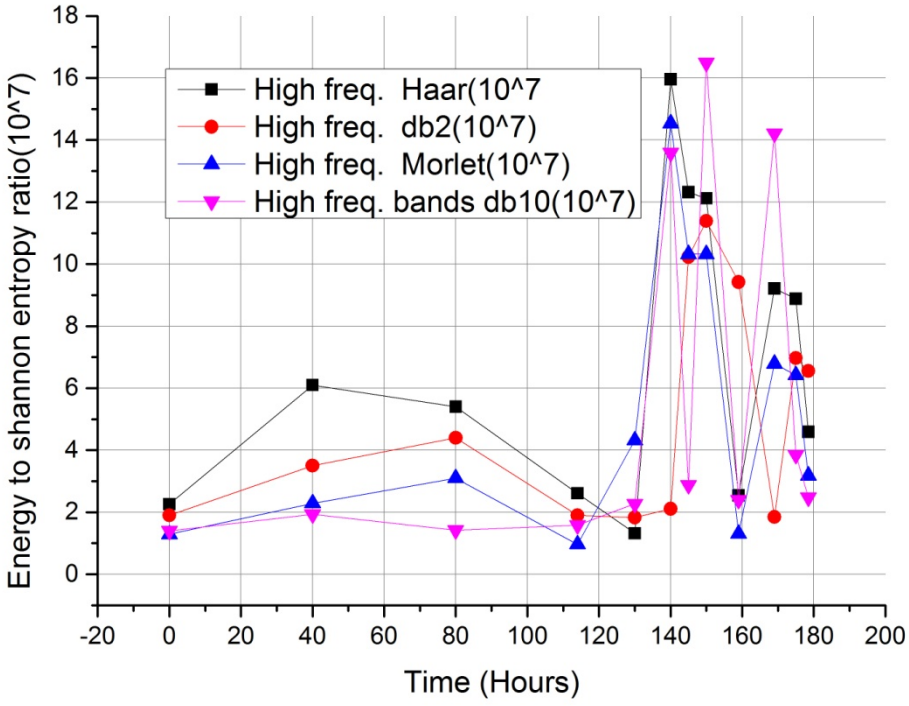
High freq. Haar(10^7
High freq. db2(10^7)
High freq. Morlet(10^7)
High freq. bands db10(10^7)
Energy to shannon entropy ratio(10^7)
Time (Hours)

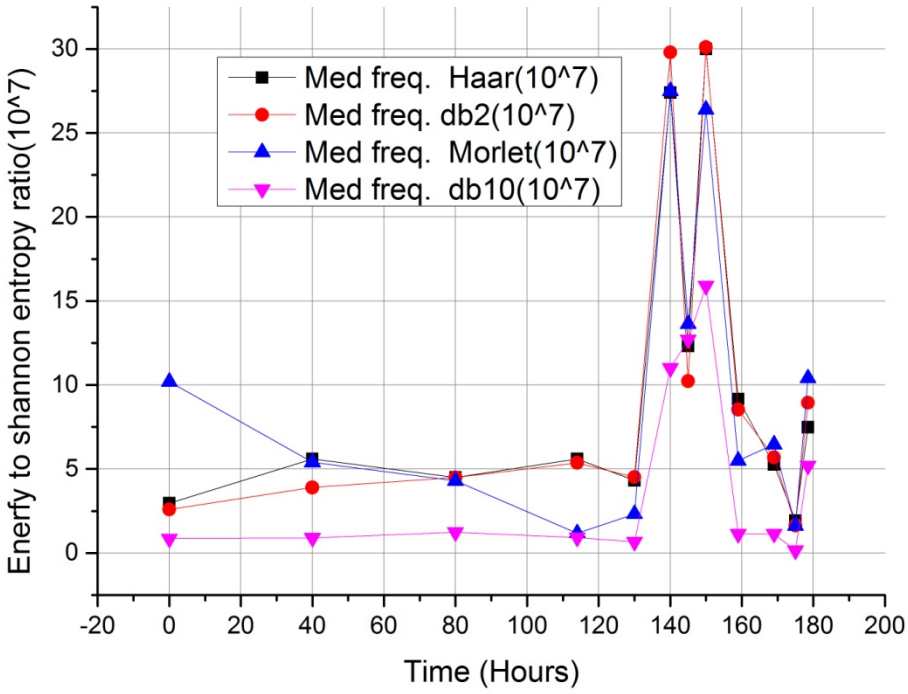
Med freq. Haar(10^7)
Med freq. db2(10^7)
Med freq. Morlet(10^7)
Med freq. db10(10^7)
Enerfy to shannon entropy ratio(10^7)
Time (Hours)

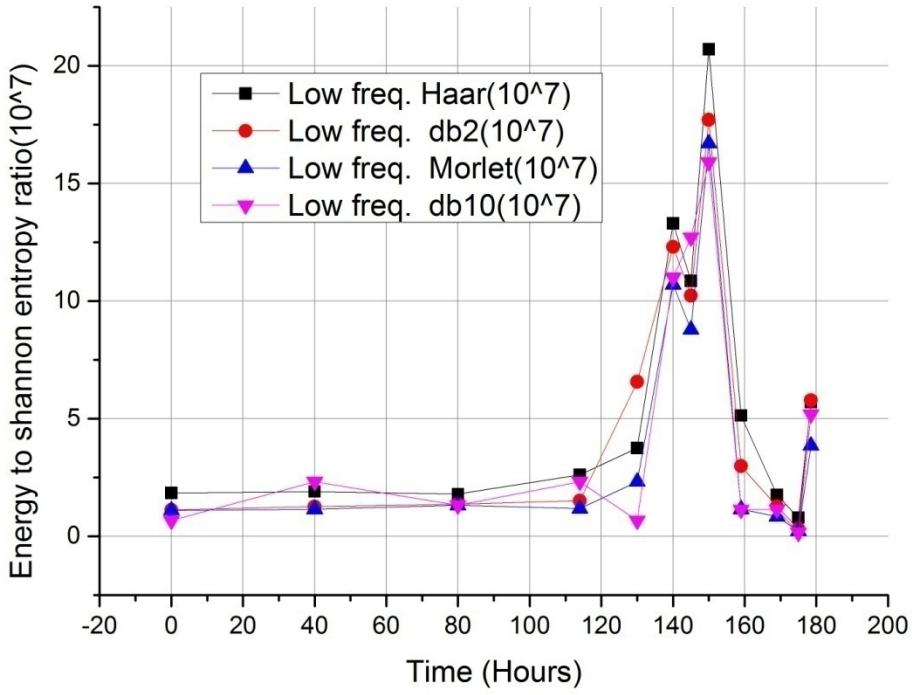

Fig4. 28 Shannon entropy values for high, medium and low frequency band of CWT using Haar, db2, morl and db10 wavelets for 10 Kg load

4.5.4 Frequency band analysis 15 Kg load.

Effect of 15 KG load on crack propagation was analyzed and different bands using mother wavelet is shown in Table 4.5. Further loading was increased for next experiment to 15 Kg and features of high frequency, medium frequency, and low frequency bands were extracted is shown in Fig 4.29. Edge breakage was noticed at 136 hours, 154 hours, 166 hours respectively. As compared to previous experiment it can be pointed out that loading cause faster rate of propagation with lees time and among all mother wavelet db10 is more sensitive in edge breakage. Effect of 15 kg load on crack propagation of taper roller bearing and its High, medium, low frequency bands are shown in Table 4.5

Table 4. 5 Shannon entropy values for high, medium and low frequency bands of CWT for 15 kg load using Haar, db2, morl and db10 as mother wavelet

Time (Hours)	**SE high freq. bands Haar(10^7**	**SE high freq. bands db2 (10^7)**	**SE high freq. bands Morlet(10^7)**	**SE high freq. bands db10(10^7)**	**SE med freq. bands Haar(10^7)**	**SE med freq. bands db2 (10^7)**	**SE med freq. bands Morlet(10^7)**	**SE med freq. bands db10(10^7)**	**SE low freq. bands Haar(10^7)**	**SE low freq. bands db2 (10^7)**	**SE low freq. bands Morlet(10^7)**	**SE low freq. bands db10(10^7)**
0	5.68	4.61	2.66	3.321	4.33	3.86	3.66	2.32	2.53	1.56	1.55	1.96
40	8.1	7.1	4.1	3.96	3.4	5.5	2.9	3.36	3.23	4.1	4.52	3.65
80	7.5	6.4	5.1	4.2	7.5	8.4	6.5	5.32		5.61	5.32	4.12
110	11.2	9.29	8.52	4.76	19.8	22.1	21.9	23.4	11.9	10.9	7.17	8.44
136	16.2	11.7	11.8	21.7	19.5	25.9	21.6	9.34	6.18	5.84	5.66	5.33
145	19.9	15.8	14.5	9.2	26.3	27.3	21.8	24.8	14.1	12.3	10.4	10.4
15	20.2	21	19.5	22	14.5	14.5	12.7	14.1	10.4	9.53	10.3	9.28

4	1											
161	5.9	4.5	4.21	13.21	3.59	3.67	3.28	3.49	1.62	1.31	0.91	1.23
166	19.4	14.4	14.1	36.123	9.37	9.28	7.39	9.31	9.47	9.69	9.02	9.72
170	18.74	13.23	12.21	20.12	8.35	8.32	6.32	8.32	5.31	6.89	7.45	2.23

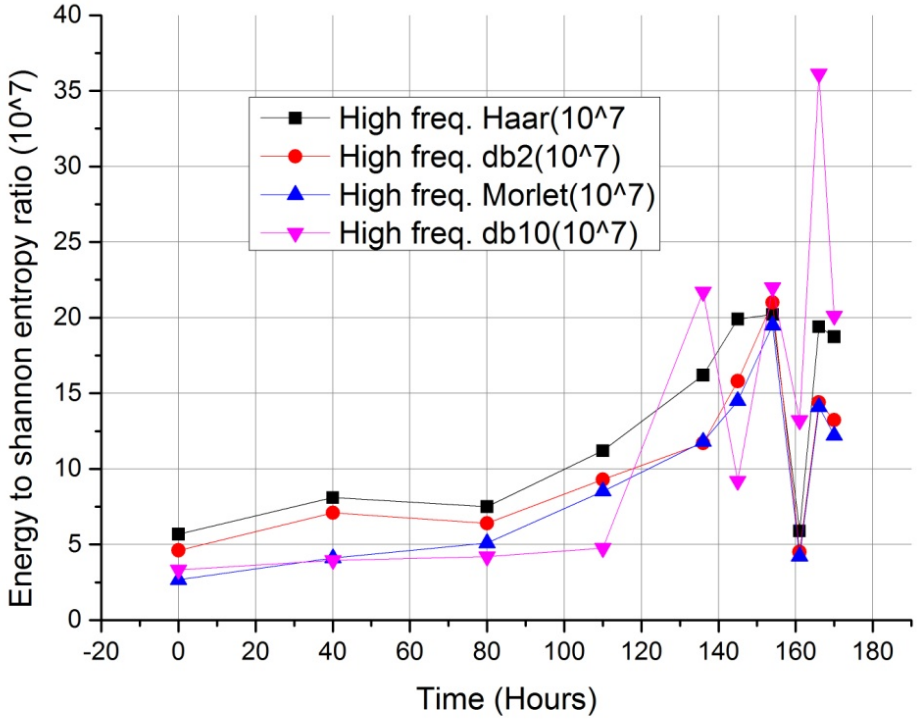

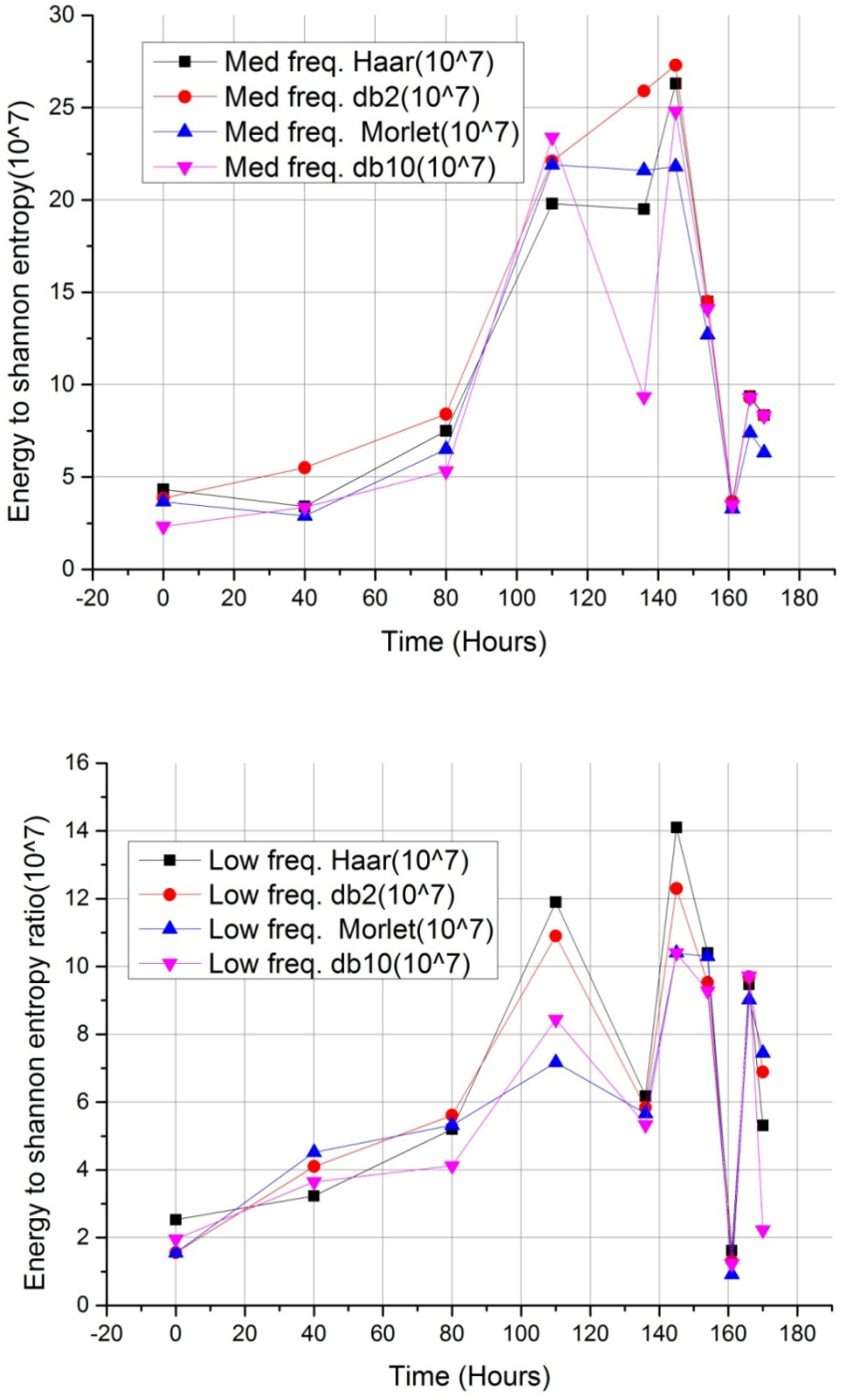

Fig 4. 29Shannon entropy values for high, medium and low frequency band of CWT using Haar, db2, morl and db10 wavelets for 15 Kg load

4.6.5 Frequency band analysis 20 Kg load: Last set of experiment was conducted by applying a load of 20 kg. Edge breakage was noticed at 103 hours and 114 hours which was checked visually also and images were shown in annexure 2. Table 4.6 represents the effect of 20 kg load in high, medium and low frequency bands. Edge breakage and crack propagation noticed at 103 hour and 114 hours is shown in Fig 4.30.

Table 4. 6 Shannon entropy values for high, medium and low frequency bands of CWT for 20 kg load using Haar, db2, morl and db10 as mother wavelet

Time (Hours)	**SE high freq. bands Haar(10^7**	**SE high freq.bands db2 (10^7)**	**SE high freq. bands Morlet(10^7)**	**SE high freq. bands db10(10^7)**	**SE med freq. bands Haar(10^7)**	**SE med freq. bands db2 (10^7)**	**SE med freq. bands Morlet(10^7)**	**SE med freq. bands db10(10^7)**	**SE low freq. bands Haar(10^7)**	**SE low freq. bands db2 (10^7)**	**SE low freq. bands Morlet(10^7)**	**SE low freq. bands db10(10^7)**
0	2.19	1.81	0.928	2.28	3.64	3.7	3.25	2.32	2.71	2.48	3.15	2.1
40	4.9	5.6	3.1	2.46	5.2	6.1	4.4	3.32	2.45	3.34	3.41	2.69
80	3.15	2.61	2.47	2.83	8.44	9.54	7.99	9.72	3.93	3.58	1.38	2.2
90	3.21	3.45	4.12	3.14	7.45	8.56	8.58	10.9	4.125	4.12	4.45	2.5
98	3.25	3.1	3.965	4.14	6.78	7.45	7.64	4.83	5.12	4.56	3.95	1.44

									5			
103	21.5	16.5	15.7	27.1	19.1	20.1	17.2	19.7	9.67	8.73	6.98	7.42
109	11.8	9.19	8.37	9.16	22.4	24.3	20	22.7	12.3	11	8.5	8.61
114	18.69	18.8	15.9	20.3	12.7	12.2	11	11.7	7.38	6.27	5.32	5.66
116.5	11.9	9.3	9.2	14.47	13.5	14.7	12.5	3.17	1.89	1.37	0.867	1.23

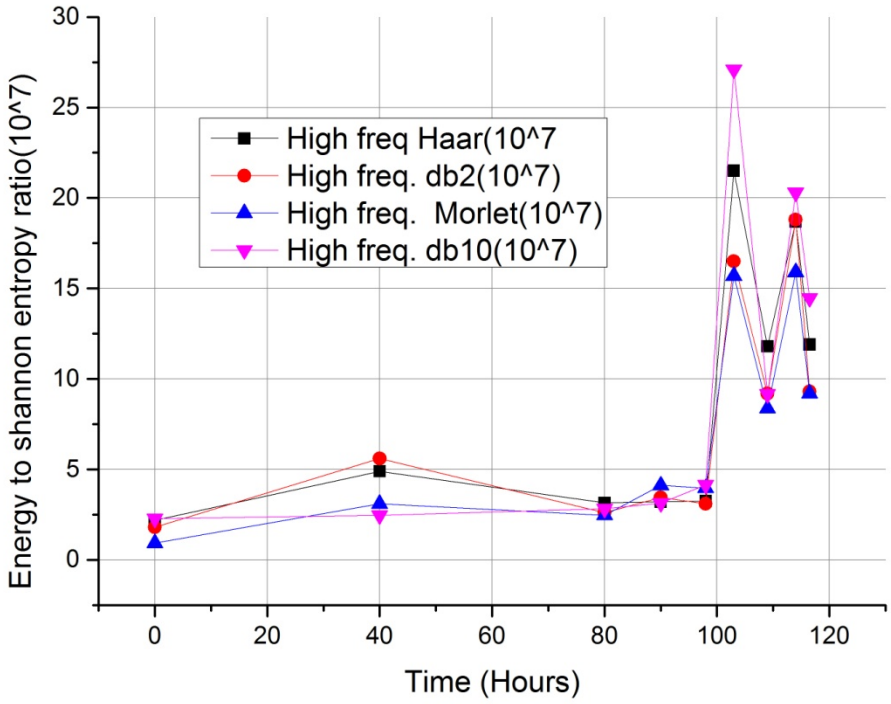

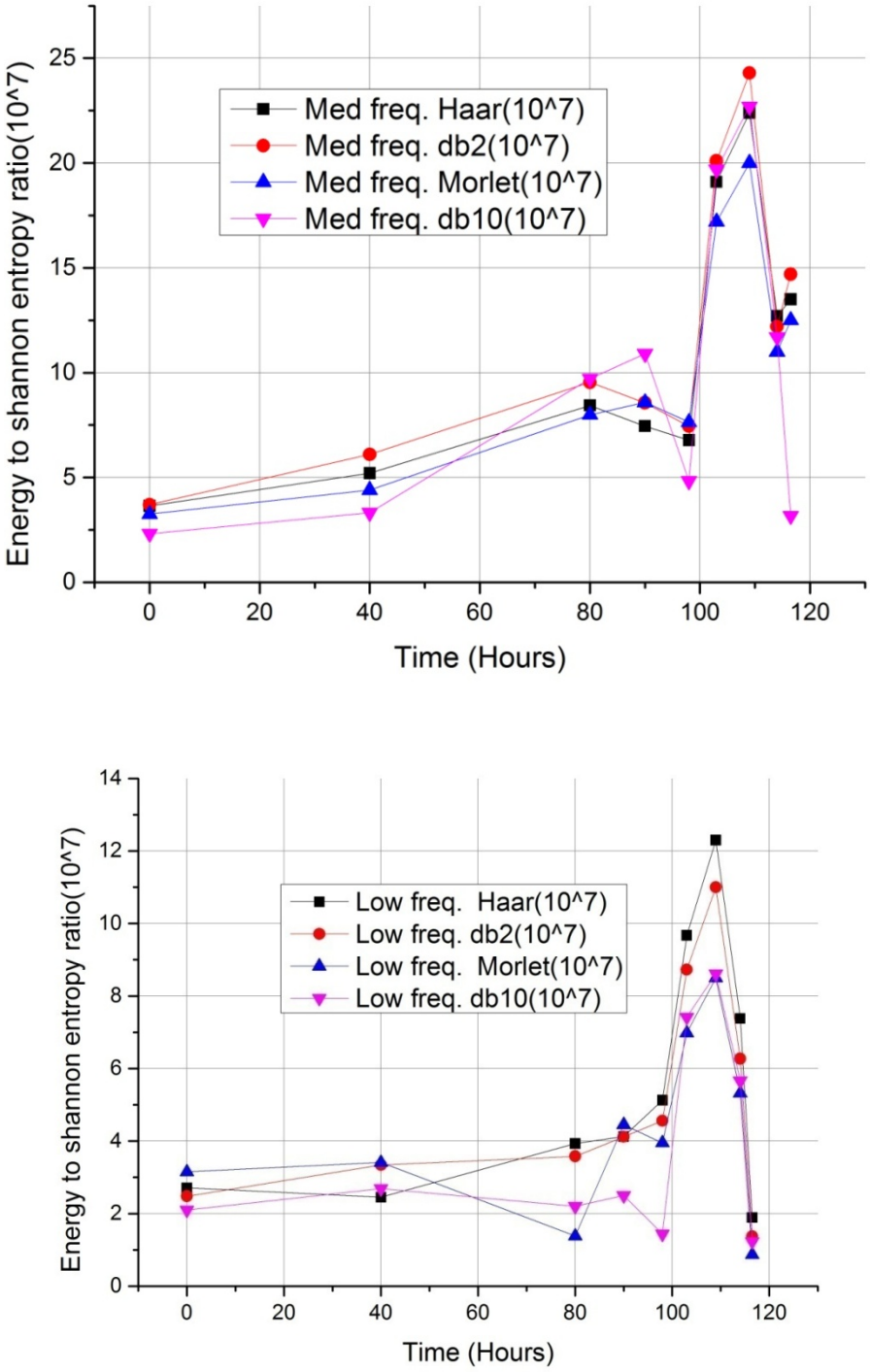

Fig4. 30 Shannon entropy values for high, medium and low frequency band of CWT using Haar, db2, morl and db10 wavelets for 20 Kg load

Shannon entropy values for high frequency band using db10 wavelet showing significant rise in the case of edge breakage for other loading conditions as well and shown in Fig 4.31. Moreover, from the same graph it can be observed that the Shannon entropy of high frequency band using db10 was in overall uptrend with the increase in defect width for all the loading conditions. As defect width increase during the crack propagation generally lead to transient response for longer duration of time in the signal. The db10 wavelet responded well to this transient response for longer duration of time due to its higher order characteristics and also responded fairly well for analyzing the interim changes happened during crack propagation such as edge breakage, edge smoothness, new edge formation etc.

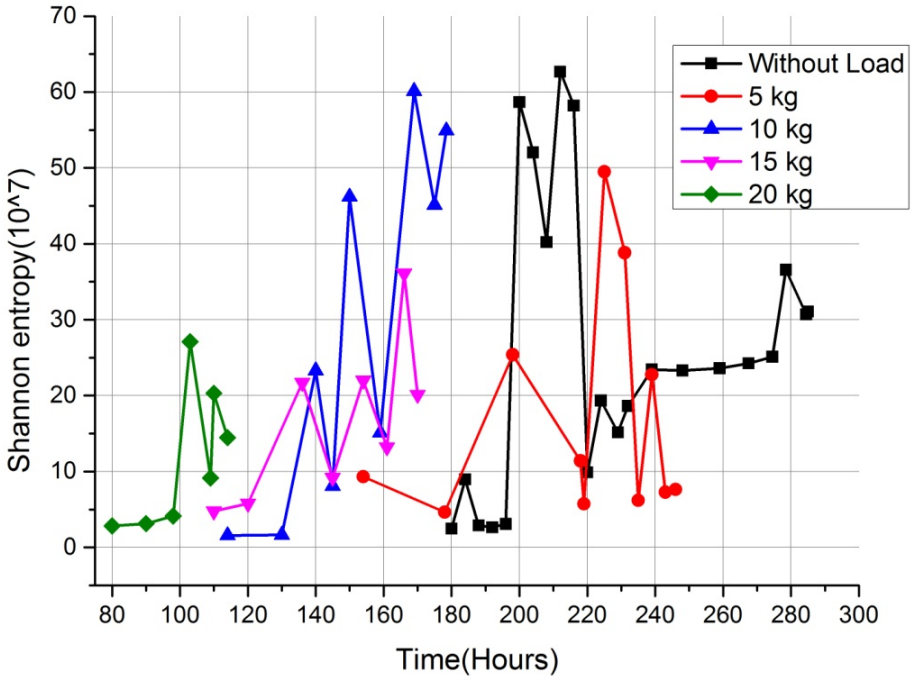

Fig 4. 31 Shannon entropy values for high frequency band of CWT using db10 wavelet for all the loading conditions

4.6 Absolute energy criterion: Rolling contact fatigue is a type of failure that occurs many machine components such as rolling element bearing that have highly stressed due to loading under cyclic loading, failure is produced by the loss of material from bearing surfaces due to initiation and propagation of fatigue cracks. Process of crack growth occurs normally in two phases crack initiation and crack propagation. Crack initiation mostly caused by stress raisers on the material's surface, such as scratches or by defects introduced during operation, such as debris damage caused by asperity contact. Contact fatigue is described as a type of damage induced by changes in the material microstructure that leads in crack initiation and propagation due to time dependent upon the loading.

a) Cracks Initiation are mostly occurred due to dislocations, high stresses at particular regions, plastic deformation around inhomogeneous material, faults or defects in or beneath the contact surface and also depend upon the microstructure of a material[205-206] b) The propagation of a crack that results in permanent damage to a mechanical component[207]. The microstructure of the material, the type of applied stress, geometry of the specimen all influence the position and mode of fatigue fracture propagation.

a)

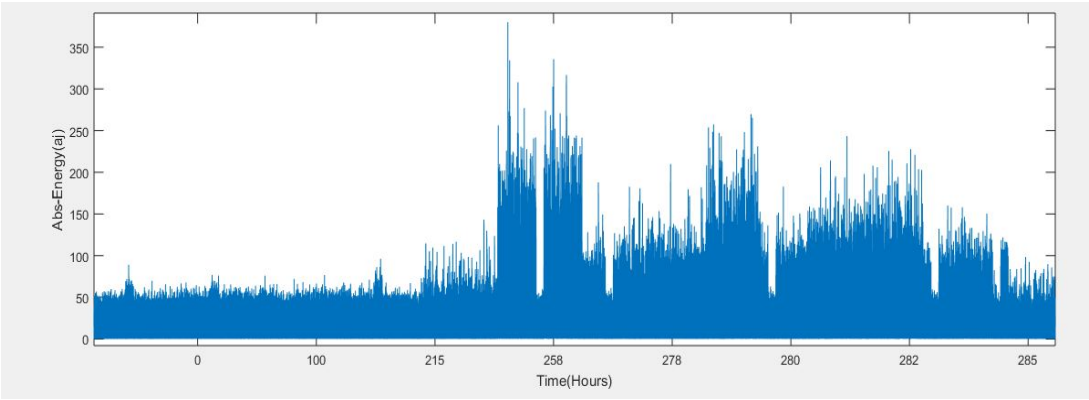

b)

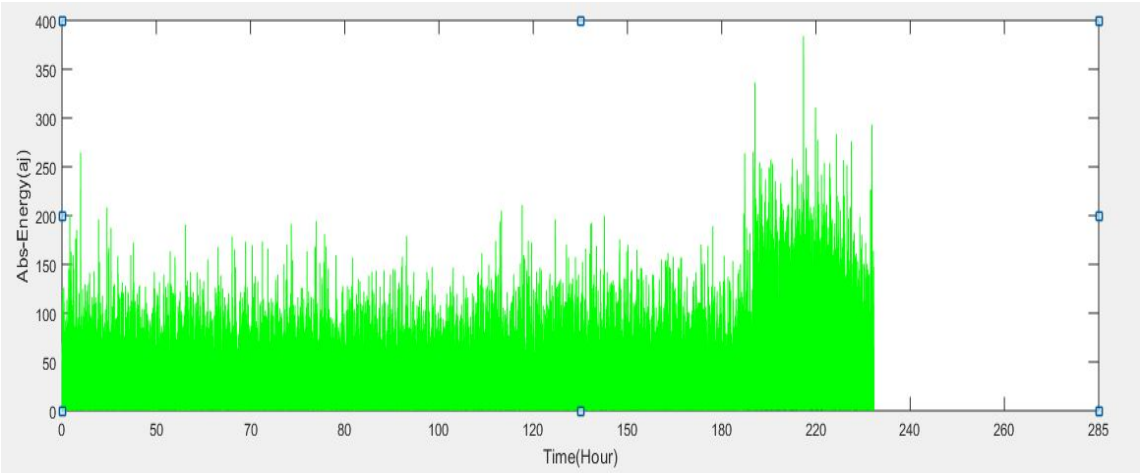
Abs-Energy(aj)
Time(Hour)

c)

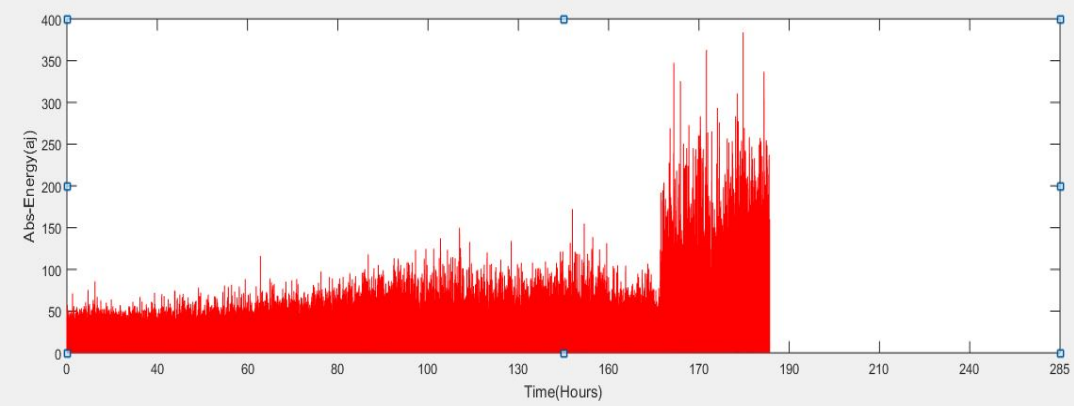
Abs-Energy(aj)
Time(Hours)

d)

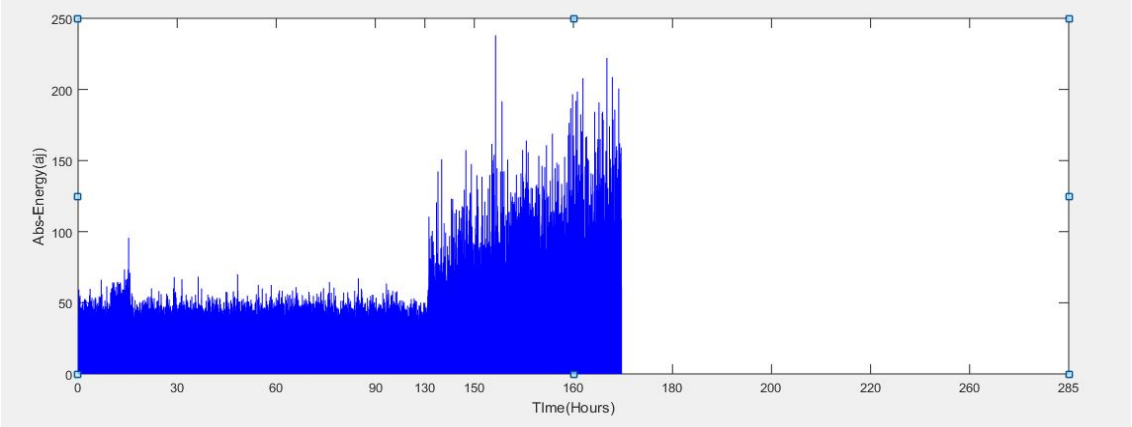
Abs-Energy(aj)
TIme(Hours)

e)

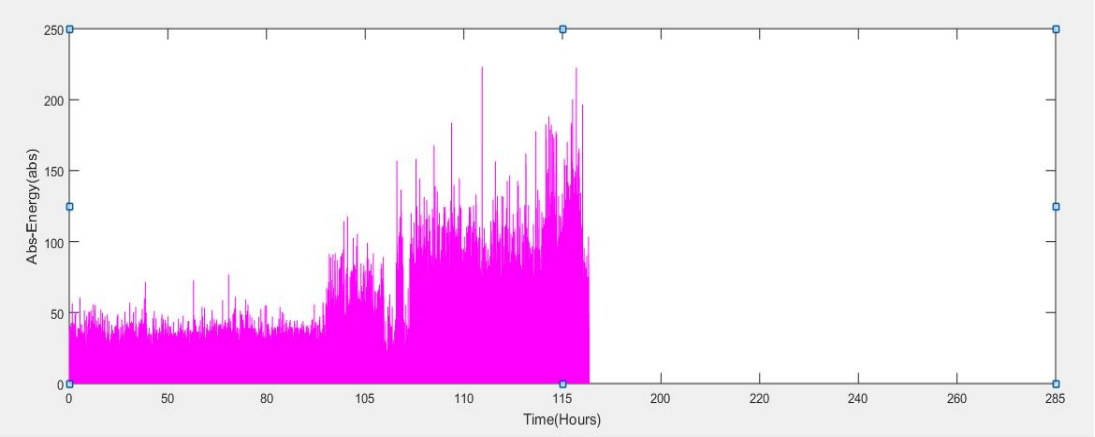

Fig4. 32 Absolute energy graph for 0, 5, 10, 15, 20 Kg load

Fig.4.32 presents observations absolute energy of continuous monitoring of the vibration levels under different loading conditions. First set of experiment was conducted without load is shown in Fig 4.32(a). The overall energy levels are increasing for no load at 184-h operation and significant large transient rises were clearly noted during the period from 200 hour to 285 hour. Further effect of loading was analyzed when load of 5 Kg was applied the vibration levels start increasing due to crack propagation at 190 hours and large transient waves are seen due to crack propagation between 198 to 230 hours is shown in Fig. 4.32 (b). In third set of experimentation load was increased from 5 kg to 10 Kg and high transient waves start at 140 hours shown in Fig 4.32 (c). and high transient rises observed between 140 to 179 hours. As to analyze further effect of loading experimentation was carried out by taking 15 Kg load large transient rises was observed at 136 hour and sudden increase in energy levels was observed between 136 to 166 hour is shown if Fig 4.32(d). Same set of observations were noticed fort 20 kg load. Fig 4.32(e) represents the effect of 20 Kg load where propagation starts at 103 hour and high energy level observed between 103 to 117 hours which is due to crack initiation and propagation.. Hence it can be concluded that loading plays a crucial role in crack propagation. Increase in loading cause fast propagation with respect to time and drastically affect the life of bearing. As surface defects, such as cracks are continually developing it is postulated that a newly formed crack will contribute

relatively higher absolute energy as the edges of this newly formed defect will be rougher in comparison to an already existing crack which becomes smoothened with the passage of time. As such crack propagates at different passage of time operation one of the crack developed was relatively less mature than the other and resulted in high levels of absolute energy. The measures given above indicated that the conditions of the bearings were getting worse and loading plays a crucial role for crack initiation and propagation.

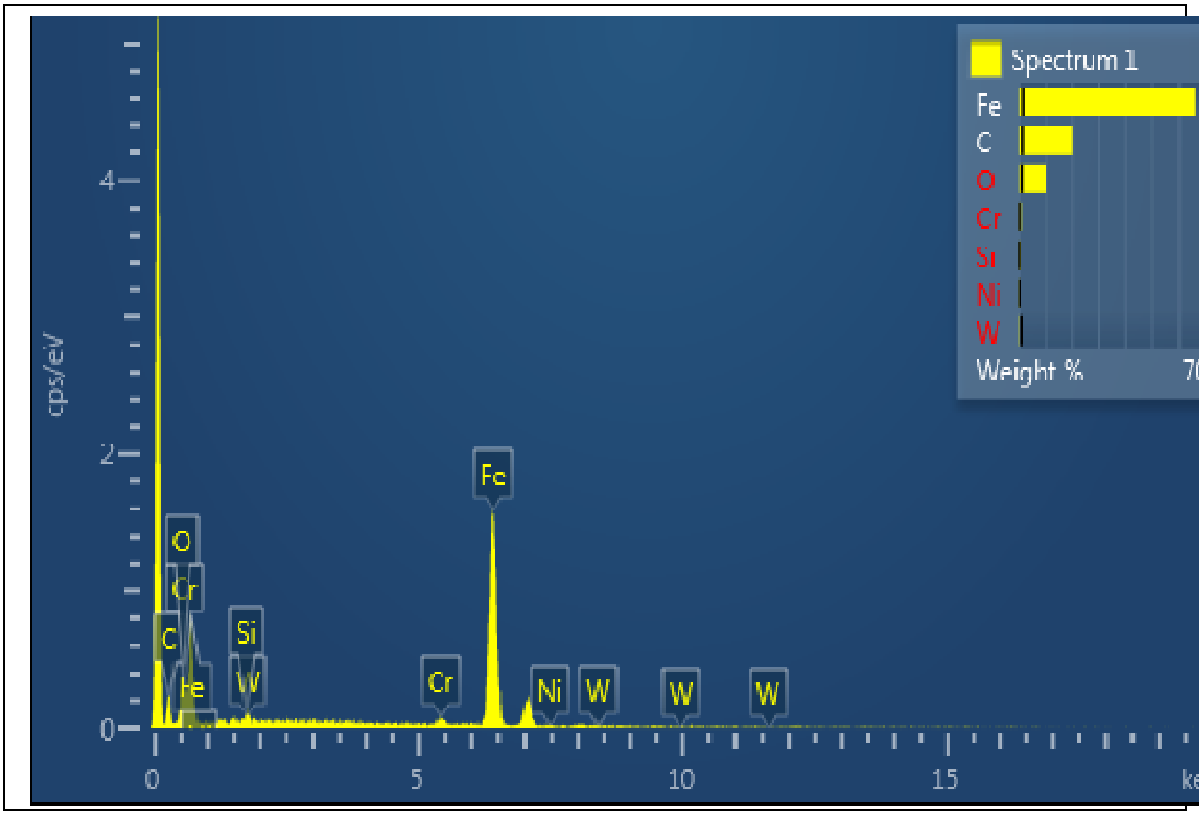

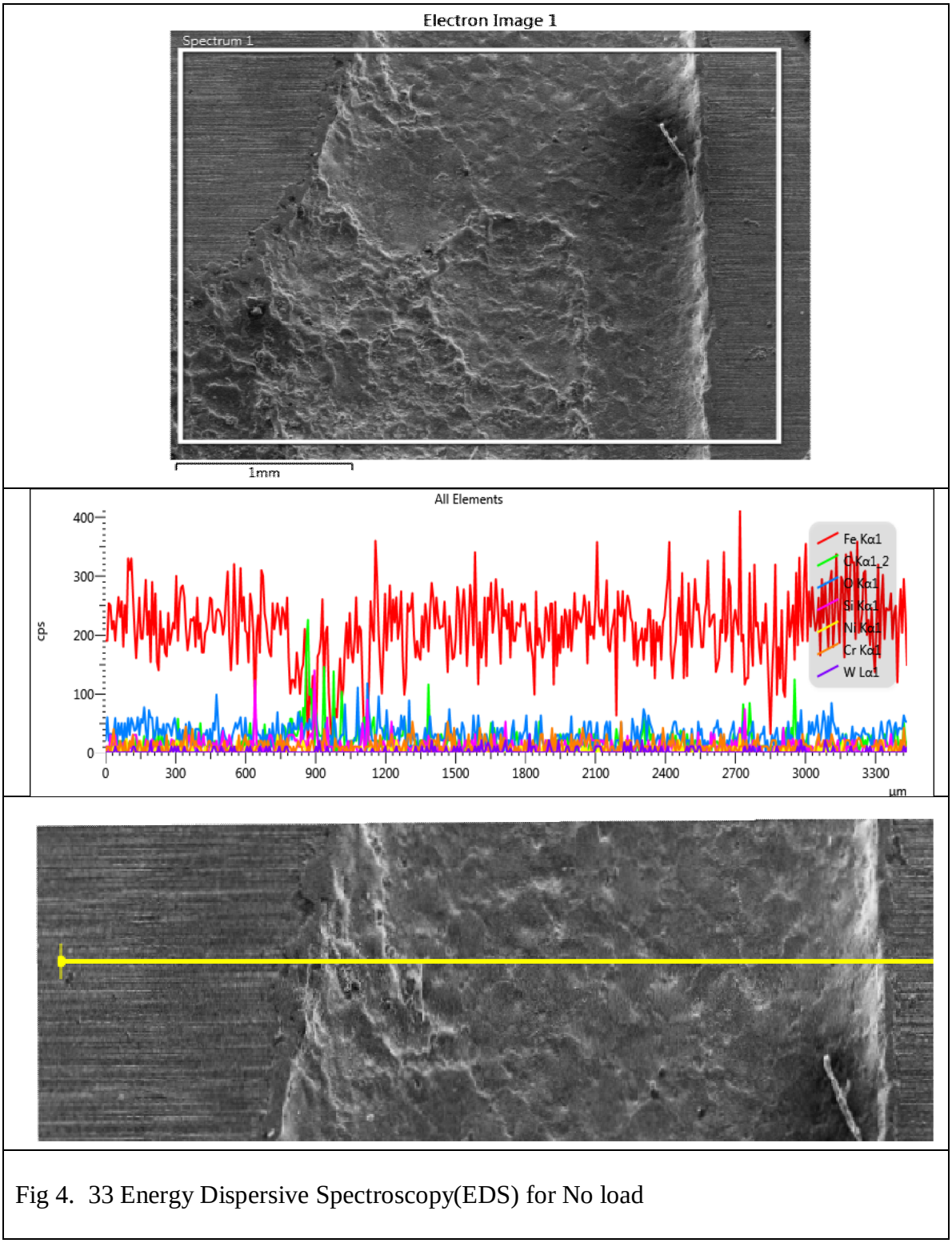

Fig 4. 33 Energy Dispersive Spectroscopy(EDS) for No load

4.7 SEM Analysis: The outer race of bearing surface was cleaned with acetone and analyzed under a scanning electron microscope (SEM), with the investigation's findings was shown in Fig 4.5, Fig.4.9, 4.12, 4.15, 4.18. During the examination the bearing components' surfaces were not prepared and no coating was applied. The outer race surface of the tested bearings is examined after the accelerated lifetime tests are completed by using scanning electron microscope (SEM). High resolution microscopic images reveal the effect of static loading on the crack propagation. Metallurgical investigations showed that cracks have initiated from the end of seeded defect and propagates in the direction of roller. The markings are generated by solid particles of rolling element embedded in the surfaces and which slide axially along the rolling direction. As slide markings are evident and clearly visible on the raceway surfaces they are less useful for evaluating surface damage as compared to the region where crack initiation has been started.

Sliding markings cover the raceway surfaces of the bearing tested under high static loading and were seen along with the deep grooves which was propagating towards the rolling direction from an artificial seeded defect on outer race of taper roller bearing. Deep grooves occur due to the uneven distribution of load which produces irregular rubbing action of roller. Such deep grooves act as stress raisers and were responsible for causing the crack initiation and propagation which further lead that lead to the fatigue failure of rolling element bearing and is effected by the intensity of load bear by the bearing during its working. Fatigue flacks visible in all loading conditions on outer race of taper roller bearing all are along the direction of rolling. There are various spots identified along the crack path in all loading conditions from where the crack propagation direction changes. From Energy Dispersive X ray Spectroscopy EDS analysis shown in Fig 4.33 it was noticed that chemical composition of bearing was according to the composition of NBC30205 taper roller bearing. For without load percentage of Fe was found 66.63 which was reduced to maximum of 27.73 % at 20 kg load which occurred due to more wear rate in surface if rolling element bearing. Whereas oxygen increases from 10.39 % to 30.99 % and carbon percentage increases from 20.39 % to 39.30 % happened due to the formation of oxides. As value of

carbon increases value of hardness also increases and was noticed by using hardness test shown in Fig.4.34. Value of silicon from without load, 5kg load, 10 kg load, 15 kg load , 20 kg was found to be 0.88, 0.90, 1.12, 1.39, 1.49 as silicon value increases it indicates more wear rate which indicates increase in loading results in more wear rate in taper roller bearing. Hardness experiment was performed to check the effect of loading and time duration of continuous running of taper roller bearing. Hardness experiment was performed using hardness testing machine under load of 150 kgf holding it for 10 sec. Four different test positions were taken shown in Fig 4.34. along the axial direction hardness was measured. When an external load is applied to the outer race of taper roller bearing the strain field created by normal and tangential pressures produces plastic deformation of the contact surface layer which increases value of hardness. It has been found out that value of C scale hardness increases at the region where plastic deformation occurs due to crack propagation and further decreases. Further it was analyzed from the experiment that as running time increases value of hardness decreases.

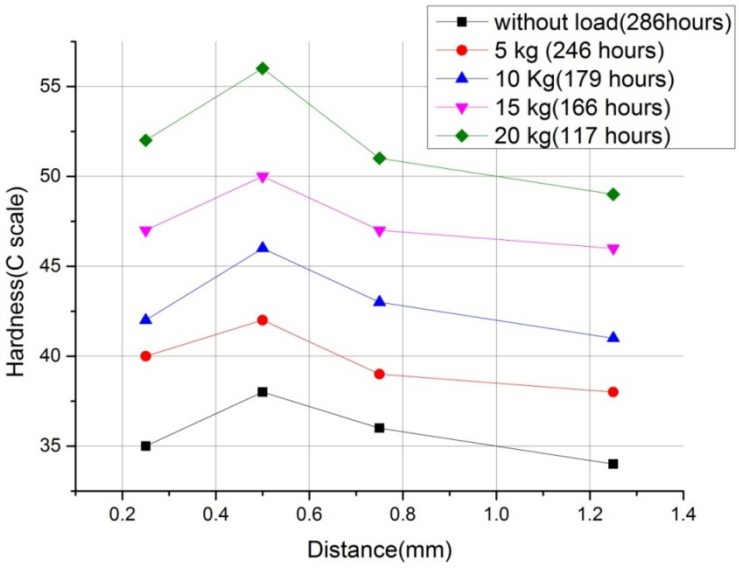

Fig 4. 34 Effect of loading on hardness value

Chapter 5: Simulation result and validation

5.1 Introduction: ANSYS is finite element software used to simulate model of machine components structures and is used for analyzing strength, temperature distribution, fluid flow and other related parameters. In FEM domain or body is spitted into finite number of sub domains known as elements are shown in Fig 5.1 for which approximate solution is constructed. Finite element method using ANSYS software is used to solve complex engineering problems such as rolling element bearing. In this study taper roller bearing(NBC30205) was analyzed using the ANSYS software and transient analysis, Contact analysis was simulated by commercial software package of ANSYS APDL. Basic features studied in simulation are deformation, contact stresses, FFT, raw vibration signal. Mathematical representation of practical engineering problem is obtained by dividing domain into elements known as sub domains. The common nodes connect these elements to each other is shown in Fig 5.1.

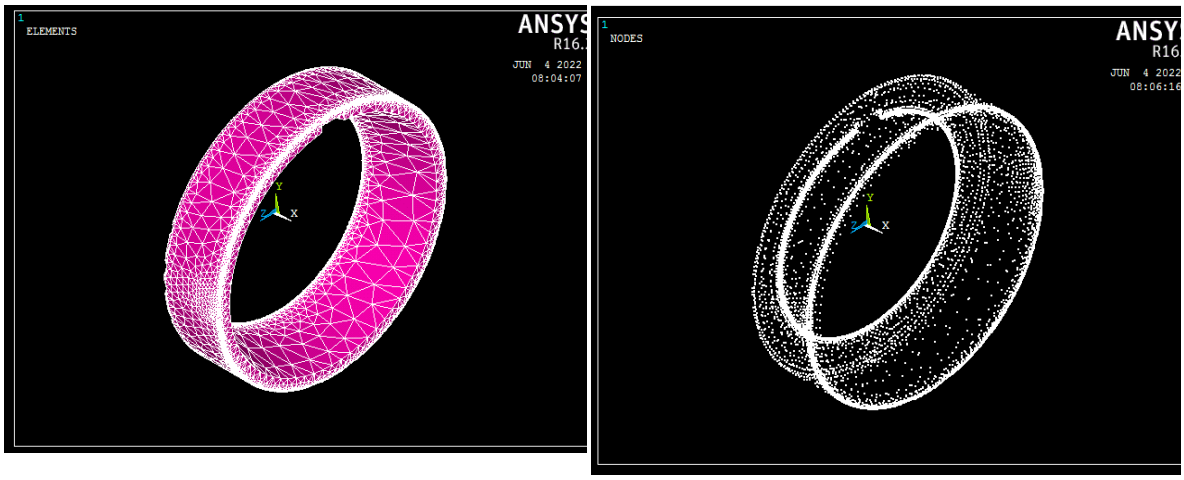

Fig 5. 1Discretization process showing nodes and elements

According to geometry and problem the domain can be discretized into line, area, volume. State of bearing can be predicted by contact analysis using FEM which gives information about stresses, displacement and penetration which helps to evaluate bearing performance under different loading conditions. Ansys take contact between surface and friction heat to give state of system and mathematical models of physical situations are used to solve engineering problems. In circumstances when the system is reasonably simple some of the standard approaches such as ordinary and partial differential equations may be used to analyze the problem and to obtain exact solution but there are many practical and complex problem where exact solution is not possible to obtain such as rotating machineries, bearings, gears etc. To deal or solve such problems numerical solution are used and these numerical solution provides solution at points known as nodes and give approximate solution to complex engineering problem.

5.3 Model Validation: In actual operation bearing was subjected to different types of loading which produces contact stresses. Contact stresses reduce the service life of a rolling bearing and results in premature failure of rolling element bearing. In roller bearings, the outer ring is usually fixed and the inner ring has the rolling motion. Concerning TRB (tapered roller bearings) this motion generates forces that are transmitted to the outer ring by the tapered rollers. Thus, contact stresses occur and the number of rollers plays a major role with respect to the load distribution. Contact analysis using finite element gives the state of running condition such as stresses displacement, penetration etc and further helps in designing and analyzing the critical part of any component in machinery.

5.3.1 Contact penetration: When two elastic bodies came into contact with each other and subjected to loading conditions and exceeds the yield pint results in permanent deformation also results in one surface to be penetrated to the another surface. Contact

penetration was simulated uses ANSYS and results are compared using experiential is shown in Fig 5.5 Value of Contact penetration using ANSYS matches fairly well with experimental values obtained is shown in Table 5.1

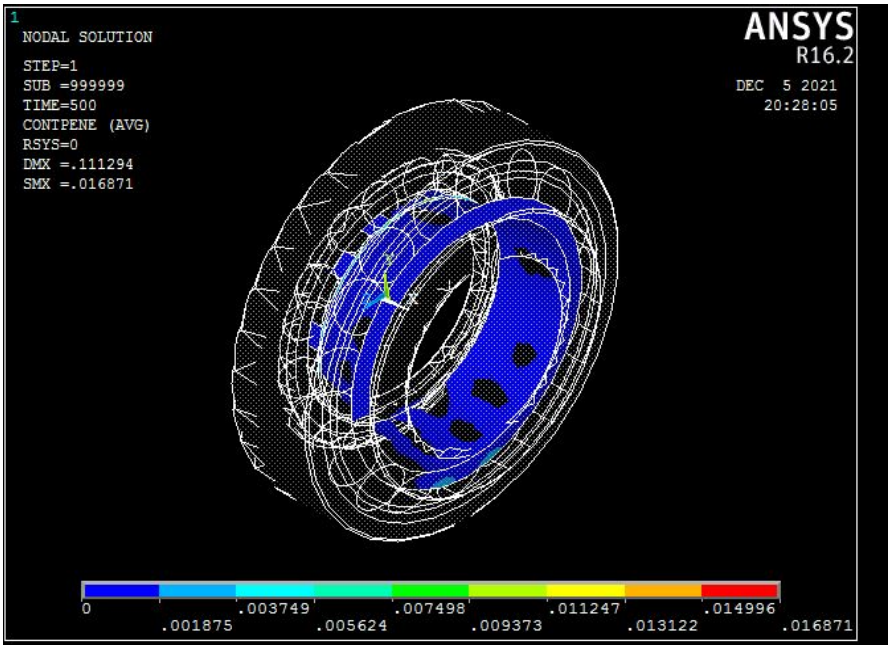

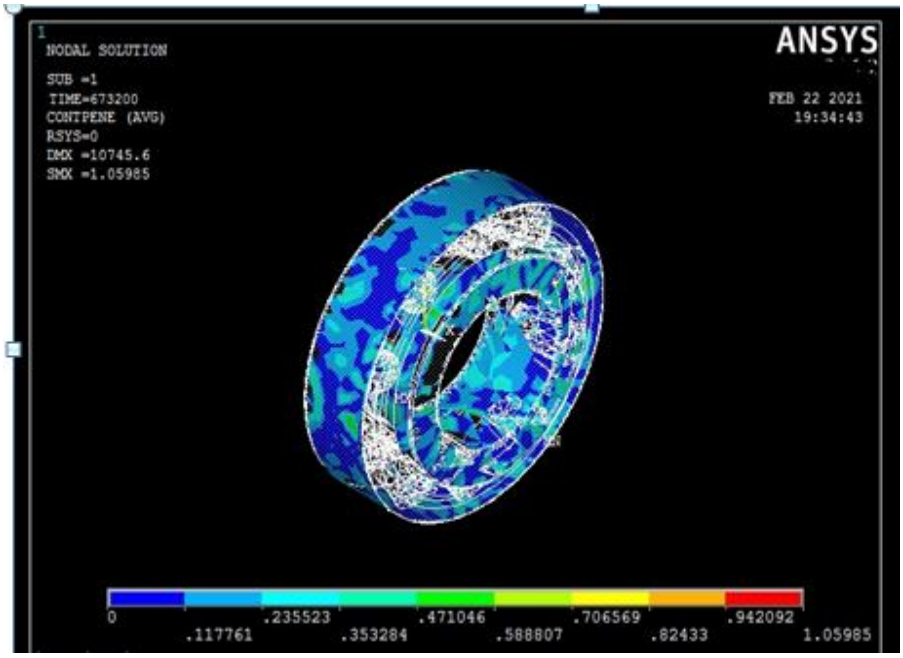

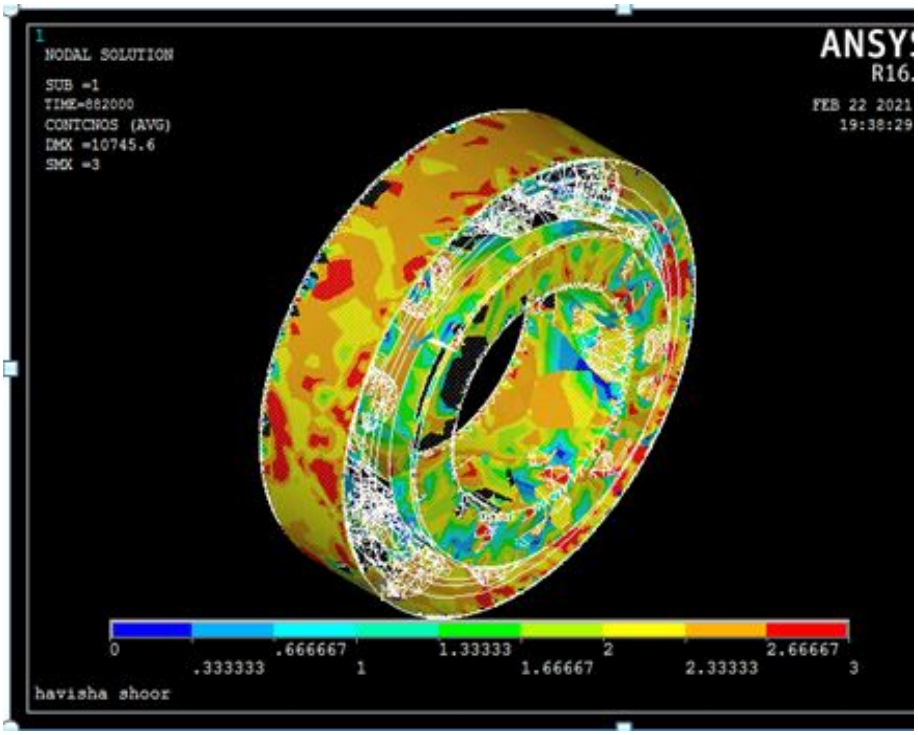

Fig 5. 2 Contact penetration using ANSYS and experiment

Table 5. 1Contact penetration in mm experimental and simulation

Time(Hours)	ANSYS(mm)	Experiment(mm)	Δ Percentage variation
0.13 hour	0.01	0.013	26.087%
187 hour	1.05	0.95	10%
245 hour	3	2.6	14.28%

5.4 Defect identification: Structural impacts induced by a localized defect often excite one or more resonance modes of the structure and generate impulsive vibrations in a repetitive and periodic way. Frequencies related to such resonance modes are often located in higher frequency regions than those caused by machine borne vibrations and are characterized by an energy concentration. Generally vibration signals from a bearing may include the following constituent components:

a) Vibration caused by bearing imbalance with a characteristic frequency equal to the bearing rotational speed which occurs when the gravitational center of the bearing does not coincide with its rotational center

b) Vibration caused by bearing misalignment at frequency equal to twice the shaft speed which occurs when the two raceways of the bearing (inner and outer) fall out of the same plane resulting in a raceway axis that is no longer parallel to the axis of the rotating shaft

c) Vibration due to rolling elements periodically passing over a fixed reference position on the outer raceway or defect at the frequency Ball pass frequency outer race (BPFO)

d) Structure-borne vibration attributed by other components. When a localized structural defect occurs on the surface of the bearing raceways (inner or outer) a series of impacts will be generated every time the rolling elements interact with the defects subsequently exciting the bearing system. Such forced vibration is represented by high-frequency resonances that are amplitude modulated at the repetition frequency of the impacts. The analysis of taper roller bearing having seeded outer race defect and its structural born vibrations due to crack propagation are carried out in this study.

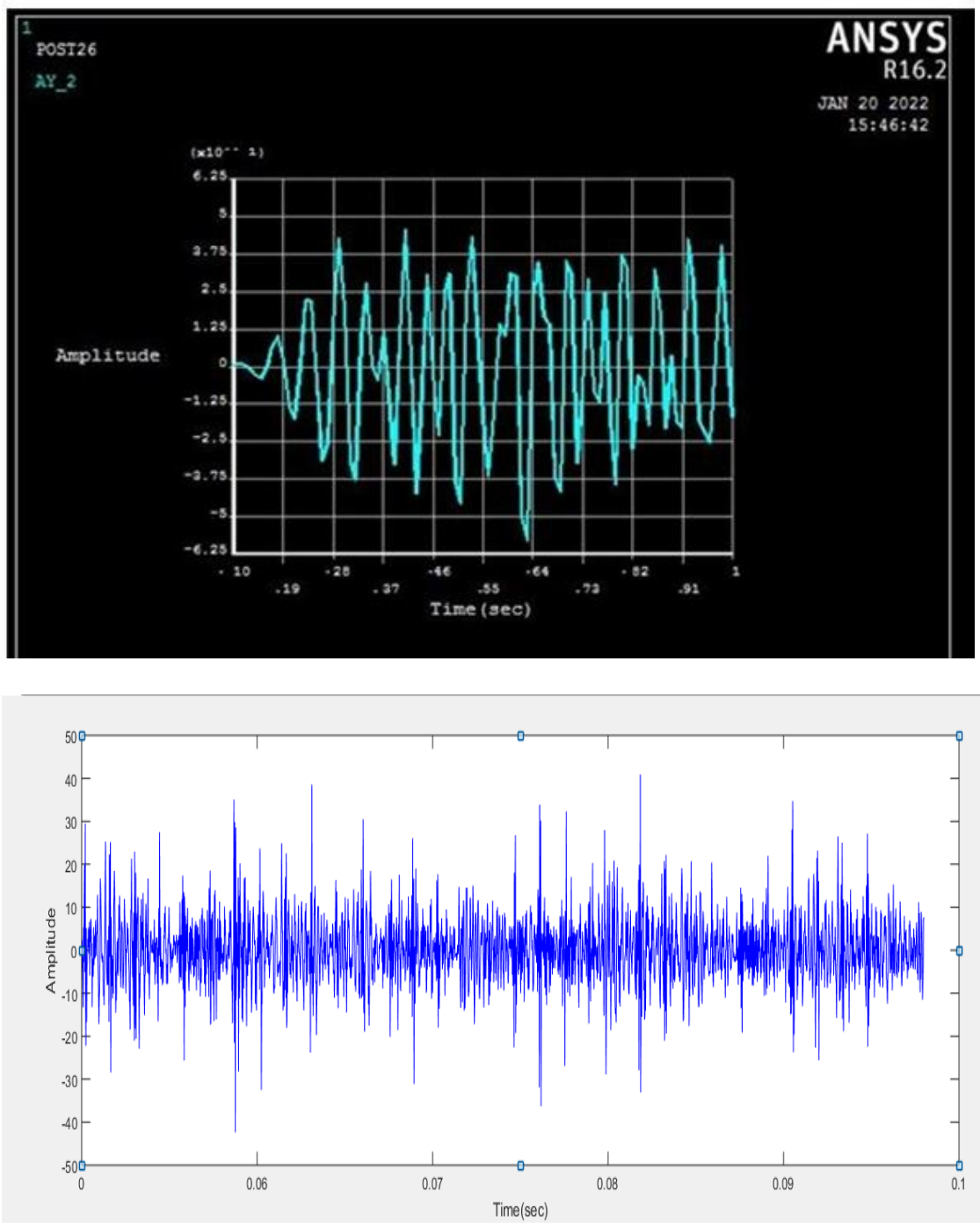

Fig 5. 3 Raw Vibration signal using ANSYS and experiment

Raw signal graphs were drawn for acceleration vs time using ANSYS and experiment for 1 sec is shown in Fig 5.3. In actual experiment there are different sources of vibration such as motors, couplings, shaft misalignment, defective bearing etc. But during experiment all these sources are ignored and both raw vibration signal and signal plotted using ANSYS indicates presence of defect.

The most prominently used technique for frequency domain is Fast Fourier Transformation (FFT). The FFT of raw signal changes the time domain signal to frequency domain and during this time domain information is completely lost. It generally converts the signal into two parts real and imaginary and in general real part is plotted for the representation. The frequency contents of raw signal are displayed in the graph and one can see the frequency contents strongly present in the signal. Fourier analysis is the process of splitting a signal into sine waves of different frequencies. Fast Fourier transform of raw vibration signal is shown along with the simulated result is shown in Fig 5.4. Simulated and experimental results of FFT are showing the same prominent frequency which is nearly 178 Hz and matching closely with the outer race defect frequency of 175 Hz. This signifies that the FFT of both raw signal and simulated signal were effective in detecting the local defect but not giving any information regarding the crack width and any other information related to crack propagation.

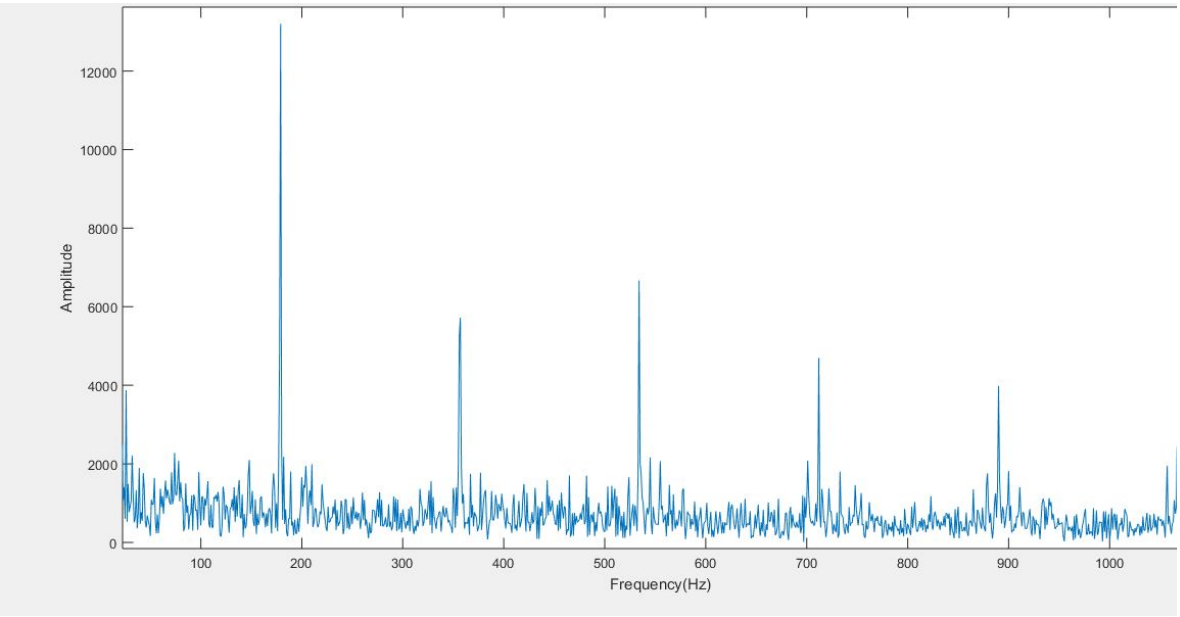

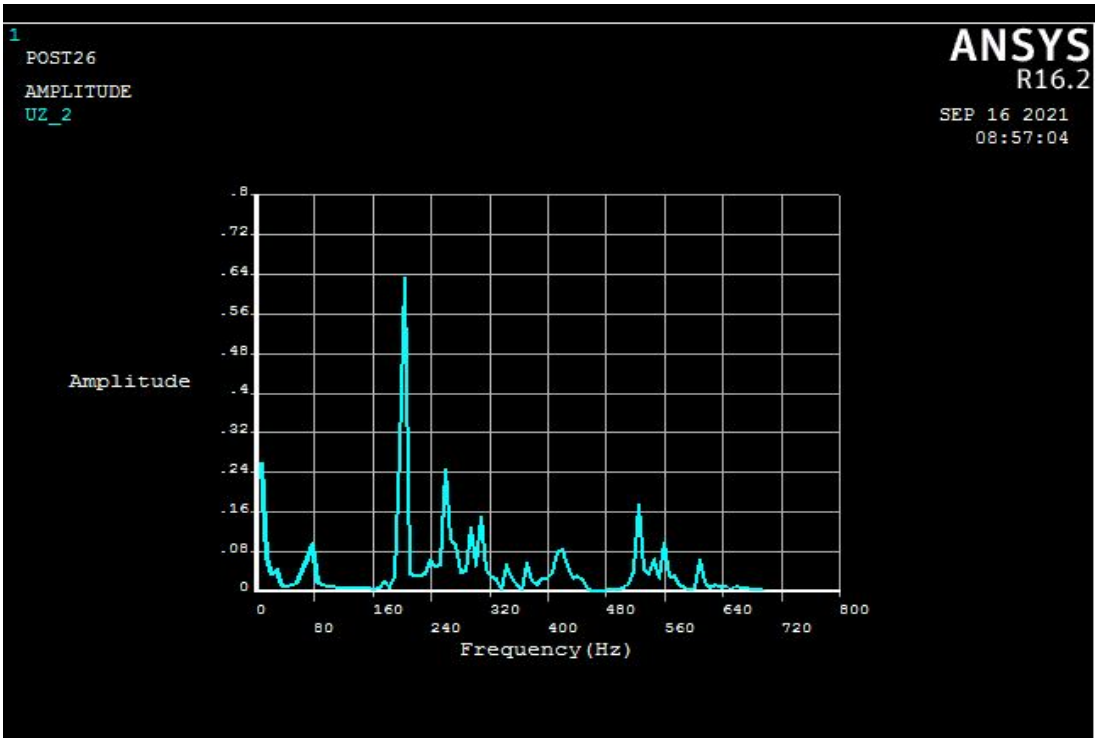

Fig 5. 4 FFT of raw signal and simulated signal

It was noticed that as crack propagates amplitude of signal also increases and different frequency component were seen by using simulation and experiment is shown in Fig 5.5.

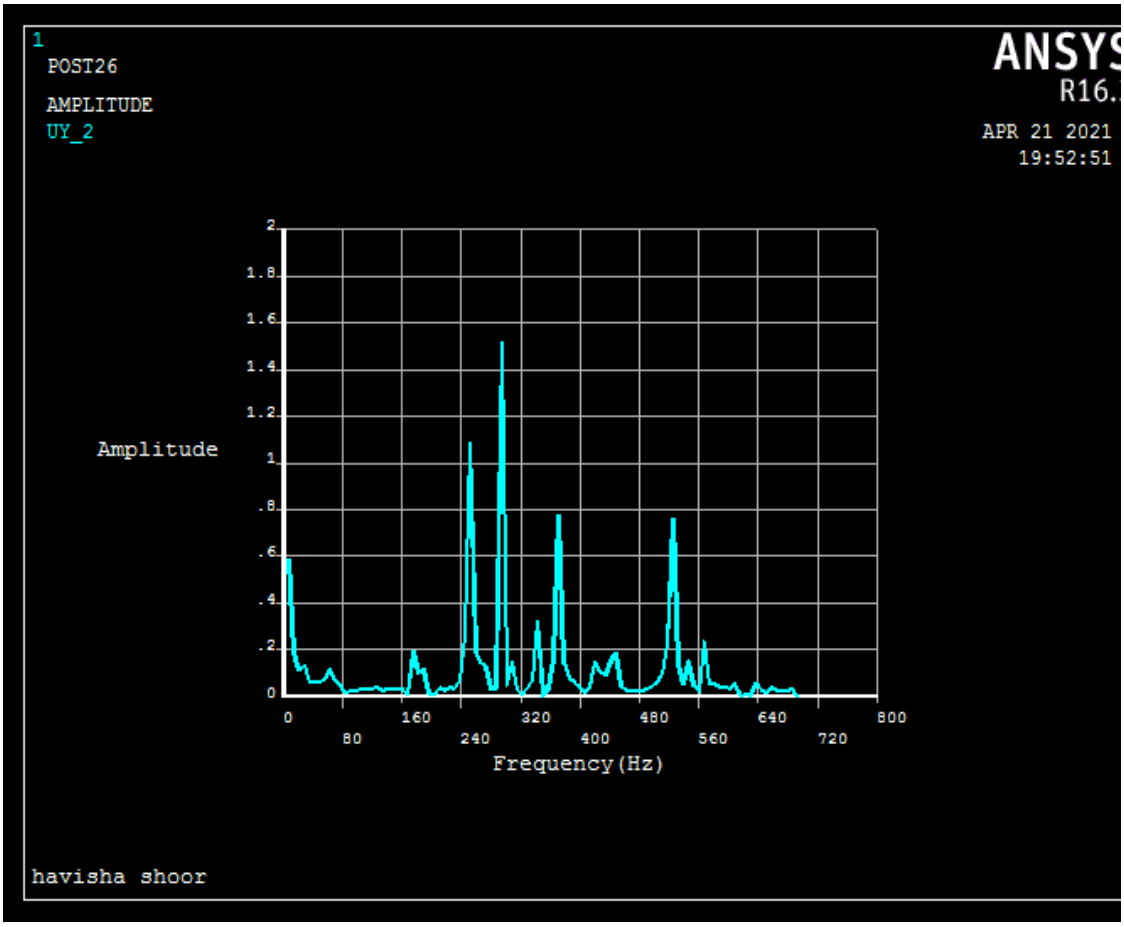

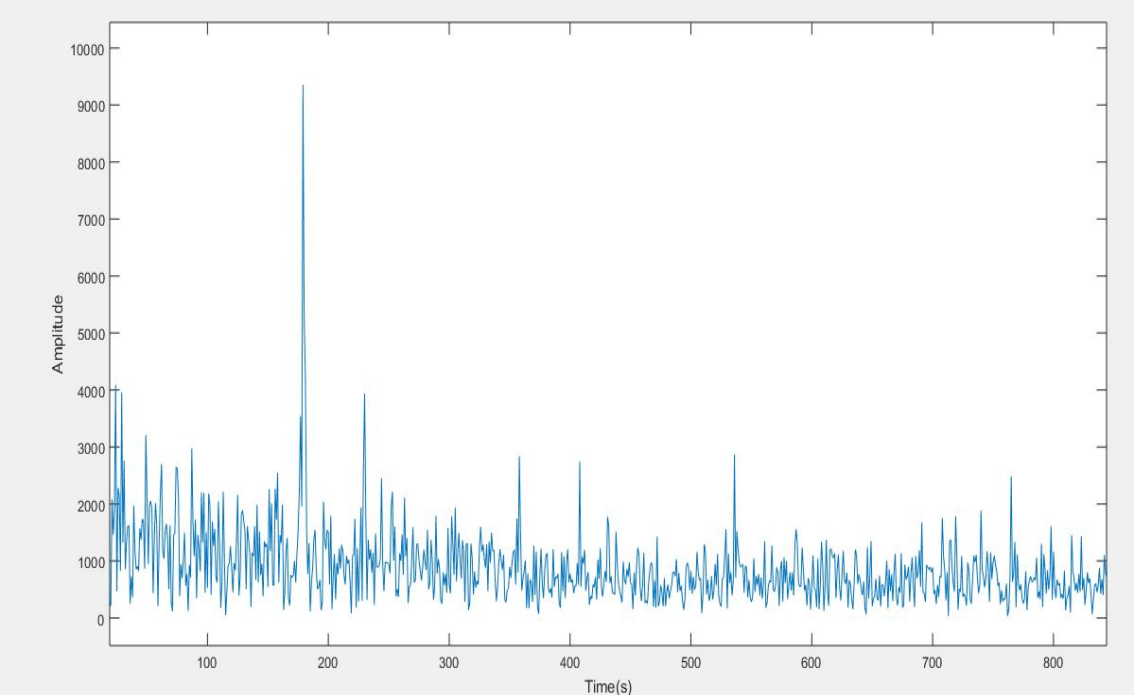

Fig 5. 5 FFT of signal after crack propagation

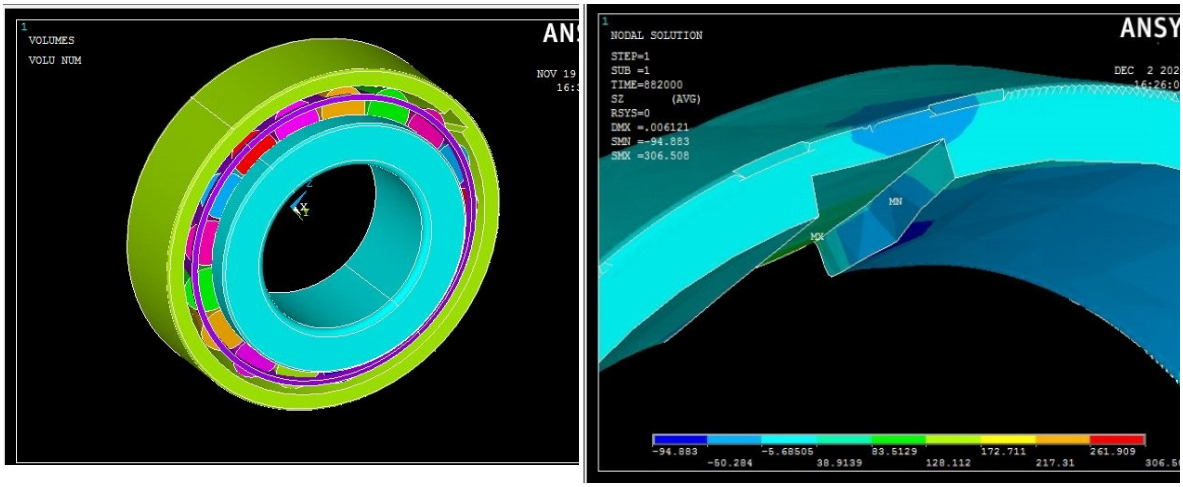

Fig 5. 6 Assembled view of taper roller bearing with enlarged view of outer race defect

5.2 Transient analysis for taper roller bearing using Ansys: Finite element models are those that employ a certain sort of commercial finite element software code to analyze the stress strain behavior or load distribution within rolling element bearings. Transient dynamic analysis is a technique for determining the dynamic response of a structure to general time-dependent loads. The purpose of transient analysis is to estimate the time-varying displacements, strains, stresses, and forces in a structure subjected to static transient and harmonic loading. [208]

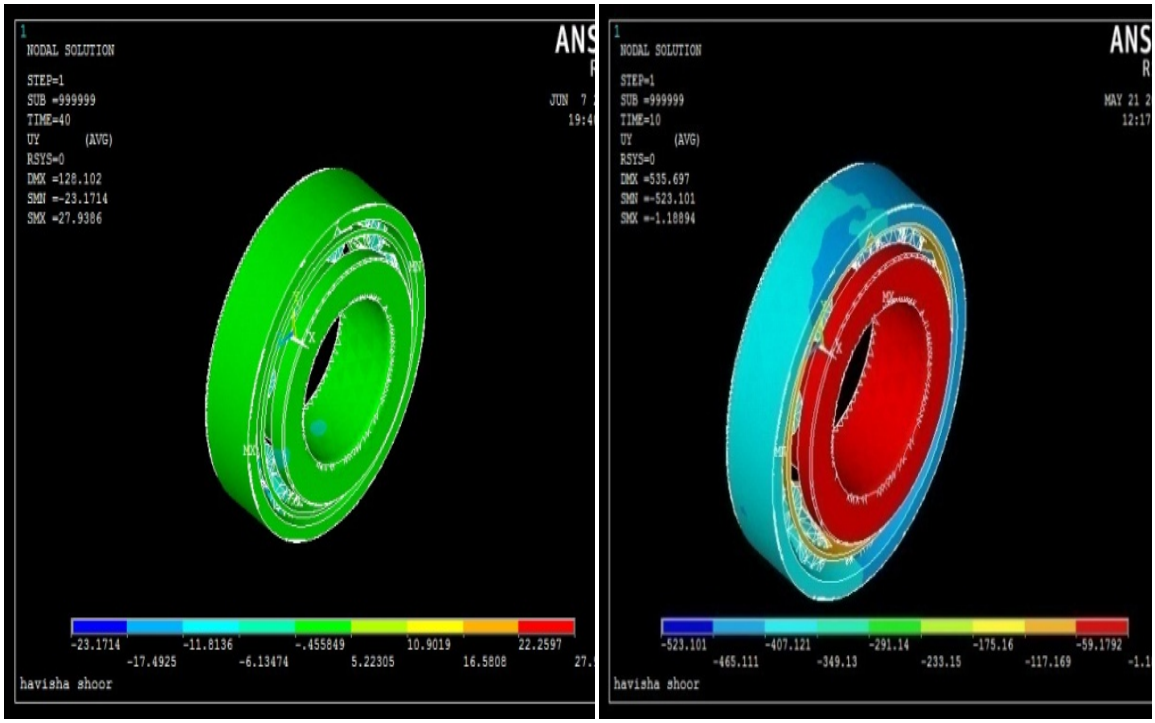

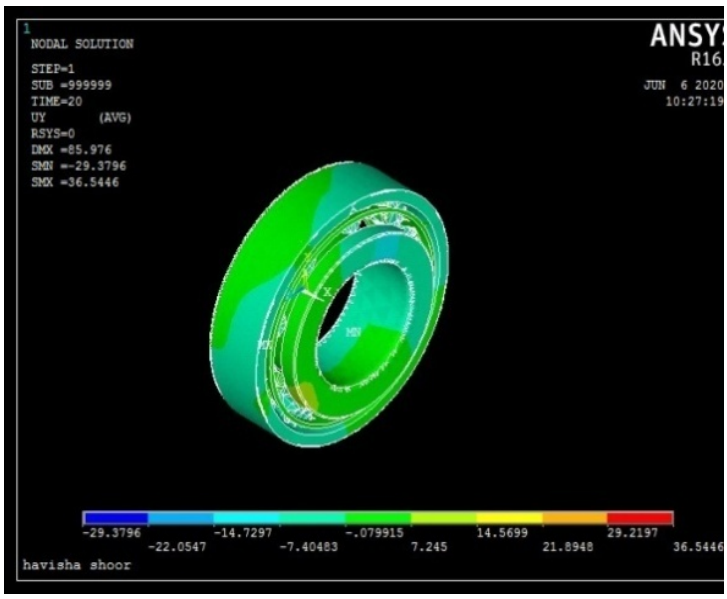

Fig 5. 7 Transient analysis of displacement

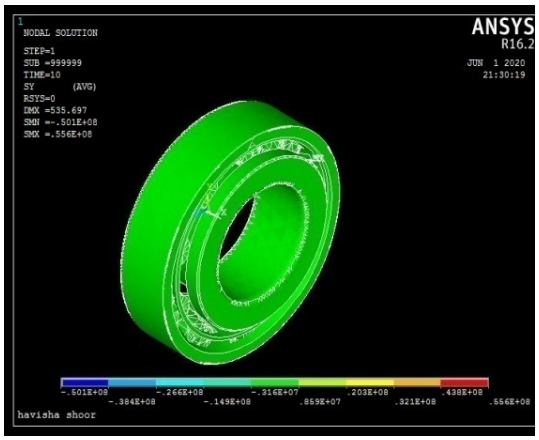

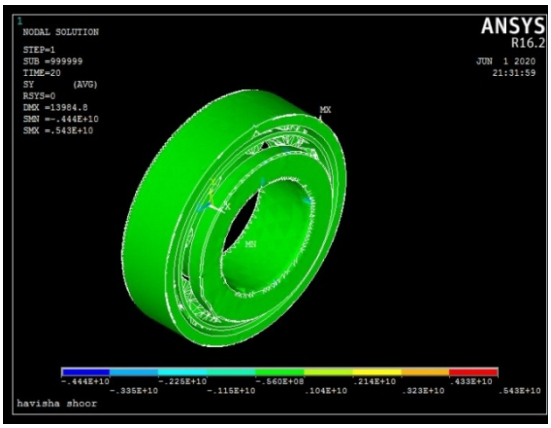

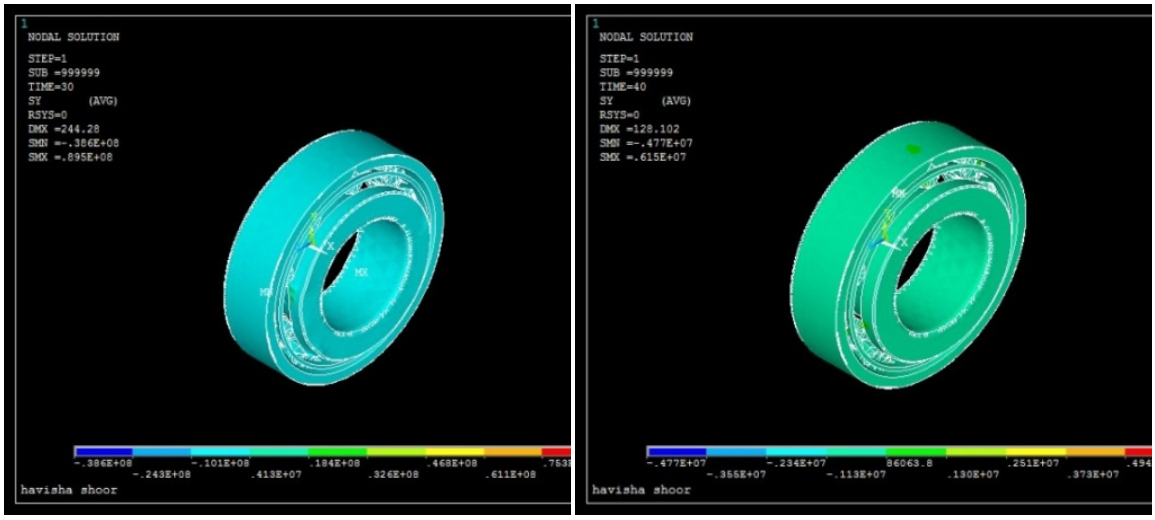

Fig 5. 8 Transient analysis of contact stresses

For analyzing the transient behavior of taper roller bearing radial load was applied along with 1500 rpm. As shown from simulated results maximum displacement is 36.5 mm at 50 sec. shown in Fig 5.3. Displacement at 10sec was found 1.1 mm which is further increased to 36.5mm at 20 sec due to contact between taper roller and defect on outer race region further value of displacement decreases to 27.9mm at 40 sec. Simulated result revealed the maximum stress generated at outer race of taper roller bearing was shown in Fig 5.6. At 10 sec stress noted was 55 MPa and value increased to 85.68 MPa at 40 sec is shown in Fig 5.7. Maximum variation of contact stress found from 10 sec to 40 sec 35.80 % is may be due to the roller pass the defective region of outer race. Fig 5.9 shows the graph in the vicinity of maximum stress region nodes are selected in region where maximum stress is generated and graph is plotted. Maximum stress noted was 85.68 MPa in the defective region of outer race and also shows the graph of maximum displacement of 36.5 mm. As per simulated results fluctuating stresses were obtained which vary with respect to time. Stresses are fluctuating may be smoothening of edges. Graph was plotted using ANSYS software in the vicinity of maximum stress and displacement by selecting nodes is shown in Fig 5.9.

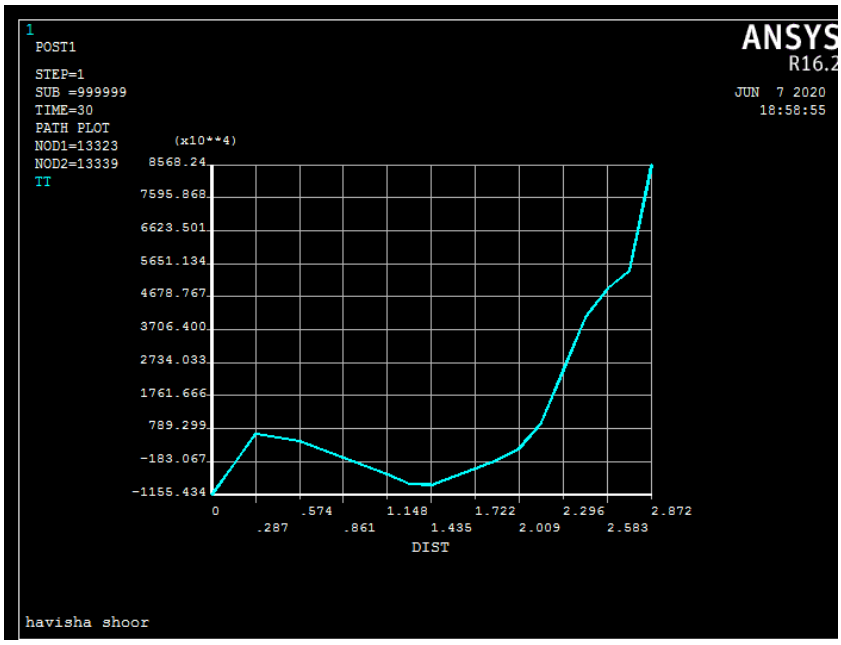

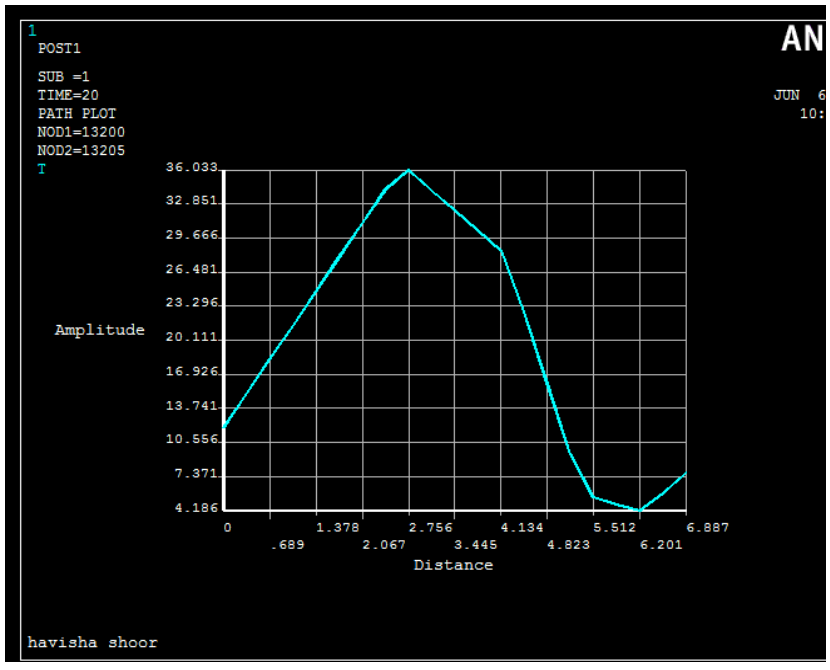

Fig 5. 9 Graph showing maximum amplitude and stresses

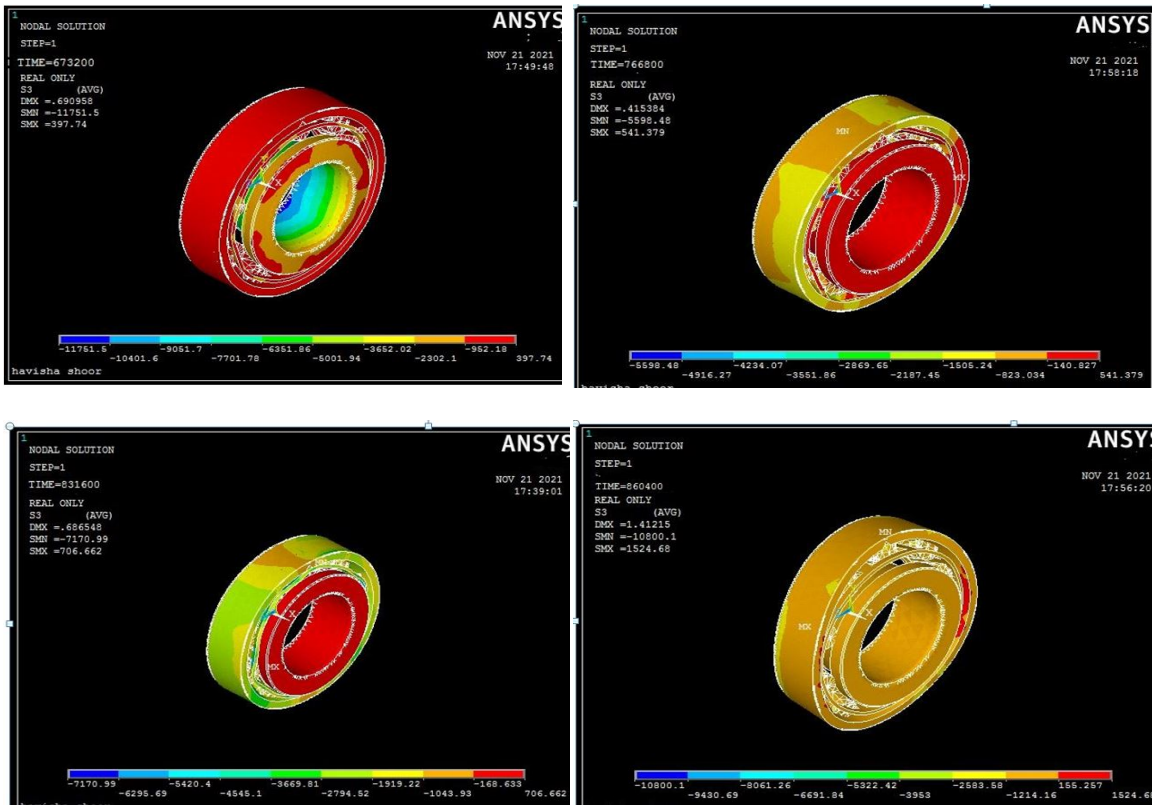

Fig 5. 10Transient response of contact stresses

5.6 Comparison of stress with high frequency db10: FEM analysis was further carried out for the taper roller bearing assembly with respect to time and contact behavior of simulated result is shown in Fig. 5.6 to 5.10. Contact stress values from simulated model were taken at different intervals of time and presented in Fig 5.11. It can be observed from the graph that the contact stresses showed sudden rise at 196 and 240 hours respectively. It is estimated that edge breakage also leads to sudden increase in stress value and can also taken into consideration while studying the interim changes it has also noticed that as at particular time when stress was increased suddenly at same time db10 value was also increased. Numerical approach using ANSYS detect two times edge breakage but db10 detected three times. Hence finite element provide the

approximate solution to given problem and can be used for design optimization as not only predicts the maximum stress value but also locate the region where maximum stress occurs.

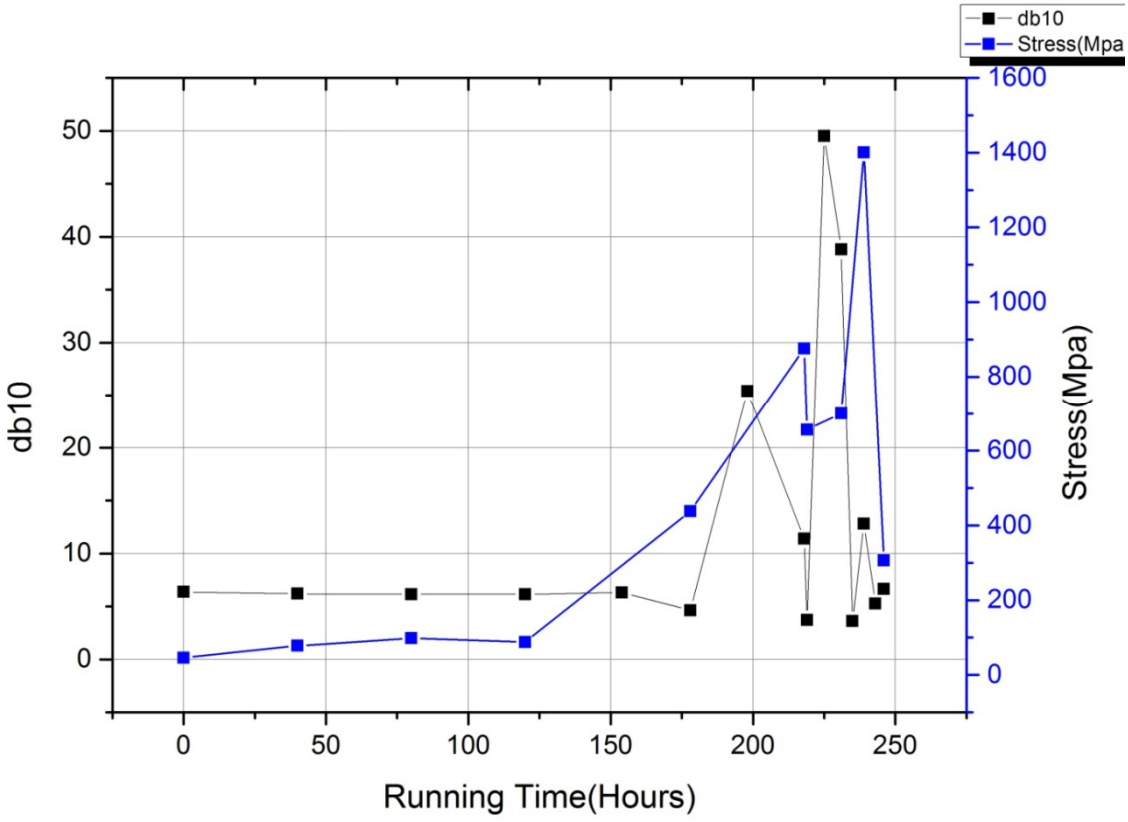

Fig 5. 11 High Frequency Component (db10) and Stress analysis

Chapter 6 Conclusion and Future Scope

Condition monitoring using vibration analysis is mostly used in diagnosis and monitoring the rotating machinery components such as bearing. To analyze the crack propagation rate test rig was designed and taper roller bearing was run continuously at different loading conditions(without load, 5Kg, 10Kg, 15Kg, 20Kg) and rpm was kept constant(1500rpm) and signal were recorded at different intervals of time and condition of bearing was checked regularly by dismantling the bearing. Vibration analysis' ability to detect the crack propagation rate and interim changes of having outer race defect in taper roller bearing has been investigated using a different signal processing techniques and following conclusions were drawn:

1) The various signal processing techniques for detecting bearing defects were analyzed and compared. Techniques based on time-frequency such as wavelet analysis and frequency band analysis were shown to be the most appropriate techniques for measuring the defect width and detecting the detect.

2) Statistical analysis was used to obtain transient features from raw vibration signal. Statistical analysis was carried out by calculating RMS, crest factor, Signal to noise ratio (SNR), skewness, kurtosis and Shannon entropy values for the recorded signals at different intervals of time. In all the parameters, Shannon entropy was showing a steep rise in the values for edge breakage during crack propagation but none of the parameters was showing any relation with the crack propagation. Kurtosis has showed great sensitivity in the detection of bearing faults but it does not responded to crack initiation and propagation.

3) It was observed that the loading conditions affect the remaining useful life substantially. Increase in loading results in faster rate of crack propagation and less time is required for crack initiation and propagation. In case when loading was set to 20 kg the total time bearing survived in running was 116.5 hours compared to 285 hours when no load was applied.

4) To analyze the interim changes during crack propagation, high frequency, medium frequency and low frequency band analysis was carried out on using CWT based different mother wavelet. Calculated value of Shannon entropy for high frequency band of CWT using db10 mother

wavelet has shown good correlation with edge breakage during crack propagation and crack growth simultaneously. This is because the Shannon entropy has capability to detect small change in transient response and db10 having ability to address transient response duration changes. Shannon entropy values of high frequency band of CWT using higher order mother wavelet was found to be successfully addressing the edge breakage during crack propagation and crack growth at the same time and is more sensitive among all mother wavelet.

5) Further findings revealed that choosing the right signal processing technique can have a major impact on defect detection and interim changes of crack propagation which further helps in increasing the reliability of bearing condition monitoring.

6) Images taken at different intervals of time during experiment was analyzed using open source image processing software image J and crack area and width was measured using image J and CWT are results are fairly matched.

Dynamic characteristics play a crucial role in design of machine system. To implement the design tool CAD software was used for analysis the crack propagation of taper roller bearing and further ANSYS software was used for simulating contact behavior. Using finite element analysis following conclusions was extracted.

1) FEM analysis was carried out for the taper roller bearing assembly with respect to time and contact penetration was simulated. It has been observed that the simulation results of contact stresses were showing the significant rise in terms for crack edge breakage

2) FEA can clearly predict the changes in behavior caused by crack propagation and it can be utilized to investigate the source and effect of crack propagation which further helps in design optimization.

3) It can be concluded from studies on bearing vibration monitoring that the FFT spectrum indicates the location of the fault. FFT and Raw signal plotted using ANSYS matches fairly well with the experiment.

4) Contact analysis using finite element gives the state of running condition such as stresses displacement, penetration etc. Finite element method helps choose optimal parameter, which

reduce stresses and displacement, as it will be time saving, reduce cost as replica of the model need not to be constructed which further helps to reduce stresses, distortion and prevent the sudden failure of bearing.

Future Scope

In this thesis work has been carried out on crack propagation of taper roller bearing and optimal mother wavelet was selected which responded to crack propagation and further helps in analyze the interim changes. The proposed method for analyzing the crack propagation in rolling element bearing components has been successfully implemented.

1) Run to failure test can be conducted to for remaining useful life of bearing.

2) Crack propagation of other rotating equipment such as gears can investigated using statistical parameter and other mother wavelets.

3) Effect of altering the rotational speed along with different loading conditions can be analyzed.

4) Modeling and analysis can be carried out to predict to predict fatigue life or fatigue failure of rolling element bearing.

5) Better prediction of Remaining useful life (RUL) can be carried out under different loading conditions.

6) Better simulation model can be developed and more parameters can be studied in relation to interim changes happening during crack propagation.

References

[1] D. Koulocheris, A. Stathis, T. Costopoulos, and A. Atsas, “Wear and multiple fault diagnosis on rolling bearings using vibration signal analysis,” vol. 3, no. 4, pp. 11–19, 2014.

[2] S. Shanbr, F. Elasha, M. Elforjani, and J. Teixeira, “Detection of natural crack in wind turbine gearbox,” *Renew. Energy*, vol. 118, pp. 172–179, 2018.

[3] A. M. Umbrajkaar, A. Krishnamoorthy, and R. B. Dhumale, “Vibration Analysis of Shaft Misalignment Using Machine Learning Approach under Variable Load Conditions,” *Shock Vib.*, vol. 2020, 2020.

[4] N. Vikram and R. Kumar, “Review on Fatigue-Crack Growth and Finite Element Method,” *Int. J. Sci. Eng. Res.*, vol. 4, no. 4, pp. 833–843, 2013.

[5] H. Wang, W. Zhang, J. Zhang, W. Dai, and Y. Zhao, “Investigative method for fatigue crack propagation based on a small time scale,” *Materials (Basel).*, vol. 11, no. 5, 2018.

. [6] G. Fajdiga and M. Sraml, “Fatigue crack initiation and propagation under cyclic contact loading,” *Eng. Fract. Mech.*, vol. 76, no. 9, pp. 1320–1335, 2009.

[7] H. Shi, Z. Liu, X. Bai, Y. Li, and Y. Wu, “A theoretical model with the effect of cracks in the local spalling of full ceramic ball bearings,” *Appl. Sci.*, vol. 9, no. 19, 2019.

[8] G. Singh, R. Kumar, M. Singh, and J. Singh, “Detection of crack initiation in the ball bearing using FFT analysis,” *Int. J. Mech. Eng. Technol.*, vol. 8, no. 7, pp. 1376–1382, 2017.

[9] Z. Yuan, B. Wang, C. Liu, Z. Wang, X. Zhang, and Y. Zhang, “The Crack Propagation Trend Analysis in Ceramic Rolling Element Bearing considering Initial Crack Angle and Contact Load Effect,” *Shock Vib.*, vol. 2021, 2021.

[10] S. Okazaki, K. Wada, H. Matsunaga, and M. Endo, “The influence of static crack-opening stress on the threshold level for shear-mode fatigue crack growth in bearing steels,” *Eng. Fract. Mech.*, vol. 174, pp. 127–138, 2017.

[11] M. Cerullo, “Sub-surface fatigue crack growth at alumina inclusions in AISI 52100 roller bearings,” *Procedia Eng.*, vol. 74, pp. 333–338, 2014.

[12] C.Longching, C.Qing, and S.Eryu, “Study on initiation and propagation angles of subsurface cracks in GCr15 bearing steel under rolling contact,” Wear, vol. 133, no. 2, pp. 205–218, 1989.

[13] . S.A.kumar, D.Ramchandra, K.S.kumar , “Theoretical and Experimental Studies on Vibrations Produced By Defects in Double Row Ball Bearing Using Response Surface Method,” Int. J. Res. Eng. Technol., vol. 03, no. 07, pp. 140–145, 2014.

[14] B. Fang, J. Zhang, K. Yan, J. Hong, and M. Yu Wang, “A comprehensive study on the speed-varying stiffness of ball bearing under different load conditions,” *Mech. Mach. Theory*, vol. 136, pp. 1–13, 2019.

[15] F. Gougam, C. Rahmoune, D. Benazzouz, A. Afia, and M. Zair, “Bearing faults classification under various operation modes using time domain features, singular value decomposition, and fuzzy logic system,” *Adv. Mech. Eng.*, vol. 12, no. 10, pp. 1–17, 2020.

[16] T. Govardhan, A. Choudhury, and D. Paliwal, “Load distribution in a rolling element bearing under dynamic radial load,” *Appl. Mech. Mater.*, vol. 592–594, pp. 1099–1103, 2014.

[17] F. Larizza, A. Moazen-Ahmadi, C. Q. Howard, and S. Grainger, “The importance of bearing stiffness and load when estimating the size of a defect in a rolling element bearing,” *Struct. Heal. Monit.*, vol. 18, no. 5–6, pp. 1527–1542, 2019.

[18] H. Saruhan, S. Saridemir, A. Çiçek, and I. Uygur, “Vibration analysis of rolling element bearings defects,” *J. Appl. Res. Technol.*, vol. 12, no. 3, pp. 384–395, 2014.

[19] R. K. Upadhyay, L. A. Kumaraswamidhas, and M. S. Azam, “Rolling element bearing failure analysis: A case study,” Case Stud. Eng. Fail. Anal., vol. 1, no. 1, pp. 15–17, 2013.

[20] A. Hu, L. Xiang, S. Xu, and J. Lin, “Frequency Loss and Recovery in Rolling Bearing Fault Detection,” *Chinese J. Mech. Eng. (English Ed.*, vol. 32, no. 1, 2019.

[21] T. Nagatomo, K. Takahashi, Y. Okamura, T. Kigawa, and S. Noguchi, “Effects of load distribution on life of radial roller bearings,” *J. Tribol.*, vol. 134, no. 2, pp. 1–7, 2012.

[22] V. M. Nistane and S. P. Harsha, “Failure Evaluation of Ball Bearing for Prognostics,” Procedia Technol., vol. 23, pp. 179–186, 2016.

[23] D. Petersen, C. Howard, and Z. Prime, “Varying stiffness and load distributions in defective ball bearings: Analytical formulation and application to defect size estimation,” J. Sound Vib., vol. 337, pp. 284–300, 2015.

[24] A. Rezaei, A. Dadouche, V. Wickramasinghe, and W. Dmochowski, “A comparison study between acoustic sensors for bearing fault detection under different speed and load using a variety of signal processing techniques,” Tribol. Trans., vol. 54, no. 2, pp. 179–186, 2011.

[24] Y. Fan, C. Zhang, Y. Xue, J. Wang, and F. Gu, “A Bearing Fault Diagnosis Using a Support Vector Machine Optimised by the Self-Regulating Particle Swarm,” vol. 2020, 2020.

[25] R. Huang, L. Xi, X. Li, C. Richard Liu, H. Qiu, and J. Lee, “Residual life predictions for ball bearings based on self-organizing map and back propagation neural network methods,” Mech. Syst. Signal Process., vol. 21, no. 1, pp. 193–207, 2007

[26] L. Eren, “Bearing fault detection by one-dimensional convolutional neural networks,” Math. Probl. Eng., vol. 2017, 2017.

[27] B. Samanta, “Networks and Genetic Algorithm,” EURASIP J. Appl. Signal Processing, pp. 366–377, 2004.

[28] J. ZHANG, Y. SUN, L. GUO, H. GAO, X. HONG, and H. SONG, “A new bearing fault diagnosis method based on modified convolutional neural networks,” Chinese J. Aeronaut., vol. 33, no. 2, pp. 439–447, 2020.

[29] M. Elforjani and D. Mba, “Detecting natural crack initiation and growth in slow speed shafts with the Acoustic Emission technology,” Eng. Fail. Anal., vol. 16, no. 7, pp. 2121–2129, 2009.

[30] M. Elforjani and D. Mba, “Monitoring the onset and propagation of natural degradation process in a slow speed rolling element bearing with acoustic emission,” J. Vib. Acoust. Trans. ASME, vol. 130, no. 4, pp. 1–14, 2008.

[31] M. Elforjani and D. Mba, “Natural mechanical degradation measurements in slow speed bearings,” Eng. Fail. Anal., vol. 16, no. 1, pp. 521–532, 2009.

[32] X. Li, K. Chen, Y. Huangfu, and H. Ma, “Vibration characteristic analysis of spur gear systems under tooth crack or fracture,” 2021.

[33] N. Sawalhi, W. Wang, and A. Becker, “Vibration signal processing using cepstrum editing technique to enhance spall-related vibration features in rolling element bearings,” Int. J. Mech. Eng. Robot. Res., vol. 8, no. 1, pp. 65–68, 2019.

[34] N. Sawalhi, W. Wang, and A. Becker, “Vibration signal processing for spall size estimation in rolling element bearings using autoregressive inverse filtration combined with bearing signal synchronous averaging,” Adv. Mech. Eng., vol. 9, no. 5, pp. 1–20, 2017.

[35] D. Liu and D. J. Pons, “Crack Propagation Mechanisms for Creep Fatigue : A Consolidated Explanation of Fundamental Behaviours from Initiation to Failure,”metals, vol. 8, 2018.

[36] P. Rycerz, A. Olver, and A. Kadiric, “Propagation of surface initiated rolling contact fatigue cracks in bearing steel,” International Journal of Fatigue, vol. 97, pp. 29–38, 2017.

[37] S. Shoor and M. Singh, “Detecting Crack Propagation Rate in Taper Roller Bearing Using FEA Analysis and Signal Processing Techniques,” *Iran. J. Sci. Technol. Trans. Mech. Eng.*, no. 0123456789, 2022.

[38] M. Singh, R. Kumar, P. Gulati, J. Singh, and S. Shoor, “A review on various signal processing techniques used in bearing fault detection,” vol. 5, no. 12, pp. 659–668, 2018.

[39] N. Fang, P. S. Pai, and N. Edwards, “Tool-edge wear and wavelet packet transform analysis in high-speed machining of inconel 718,” *Stroj. Vestnik/Journal Mech. Eng.*, vol. 58, no. 3, pp. 191–202, 2012.

[40] H. Feng, R. Chen, and Y. Wang, “Feature extraction for fault diagnosis based on wavelet packet decomposition: An application on linear rolling guide,” *Adv. Mech. Eng.*, vol. 10, no. 8, pp. 1–12, 2018.

[41] R. X. Gao and R. Yan, “Wavelets: Theory and applications for manufacturing,” *Wavelets Theory Appl. Manuf.*, no. Wickerhauser 1991, pp. 1–224, 2011.

[42] J. Guo, X. Liu, S. Li, and Z. Wang, “Bearing Intelligent Fault Diagnosis Based on Wavelet Transform and Convolutional Neural Network,” *Shock Vib.*, vol. 2020, 2020.

[43] Y. Imaouchen, R. Alkama, and M. Thomas, “Bearing fault detection using motor current signal analysis based on wavelet packet decomposition and Hilbert envelope,” *MATEC Web Conf.*, vol. 20, pp. 1–5, 2015.

[44] N. G. Nikolaou and I. A. Antoniadis, “Application of Wavelet Packets in Bearing Fault Diagnosis,” *Proc. 5th WSES Int. Conf. Circuits, Syst. Commun. Comput. (CSCC 2001), Rethymno, Greece,* , pp. 12–19, 2001.

[45] D. H. Pandya, S. H. Upadhyay, and S. P. Harsha, “Fault diagnosis of high-speed rolling element bearings using wavelet packet transform,” Int. J. Signal Imaging Syst. Eng., vol. 8, no. 6, pp. 390–401, 2015.

[46] S. Kumar, D. Goyal, and S. S. Dhami, “Statistical and frequency analysis of acoustic signals for condition monitoring of ball bearing,” Mater. Today Proc., vol. 5, no. 2, pp. 5186–5194, 2018.

[47] J. Antoni, “Cyclic spectral analysis of rolling-element bearing signals: Facts and fictions,” J. Sound Vib., vol. 304, no. 3–5, pp. 497–529, 2007.

[48] C. Rajeswari, B. Sathiyabhama, S. Devendiran, and K. Manivannan, “Bearing fault diagnosis using wavelet packet transform, hybrid PSO and support vector machine,” *Procedia Eng.*, vol. 97, pp. 1772–1783, 2014.

[49] D. Strömbergsson, P. Marklund, K. Berglund, and P. E. Larsson, “Bearing monitoring in the wind turbine drivetrain: A comparative study of the FFT and wavelet transforms,” *Wind Energy*, vol. 23, no. 6, pp. 1381–1393, 2020.

[50] Q. Sun and Y. Tang, “Singularity analysis using continuous wavelet transform for bearing fault diagnosis,” *Mech. Syst. Signal Process.*, vol. 16, no. 6, pp. 1025–1041, 2002.

[51] D. Y. Wang, W. Z. Zhang, W. P. Lu, and J. W. Du, “Application of wavelet packet transform for detection of ball bearing race fault,” Mater. Sci. Forum, vol. 626 627, pp. 511–516, 2009.

[52] B. Chen, Y. P. Kang, P. Y. Li, and W. P. Xie, “Detection on structural sudden damage using continuous wavelet transform and lipschitz exponent,” *Shock Vib.*, vol. 2015, 2015.

[53] N. G. Nikolaou and I. A. Antoniadis, “Rolling element bearing fault diagnosis using wavelet packets,” NDT E Int., vol. 35, no. 3, pp. 197–205, 2002.

[54] N. Lu, G. Zhang, Z. Xiao, and O. P. Malik, “Feature Extraction Based on Adaptive Multiwavelets and LTSA for Rotating Machinery Fault Diagnosis,” *Shock Vib.*, vol. 2019, 2019.

[55] J. Rafiee, M. A. Rafiee, and P. W. Tse, “Application of mother wavelet functions for automatic gear and bearing fault diagnosis,” Expert Syst. Appl., vol. 37, no. 6, pp. 4568–4579, 2010.

[57] N. Minhas, N. Nikhil, and S. S. Banwait, “Vibration analysis and fault identifications of rolling element bearings-a review,” Int. J. Mech. Prod. Eng. Res. Dev., vol. 9, no. 4, pp. 1133–1142, 2019.

[58] A. Rafsanjani, S. Abbasion, A. Farshidianfar, and H. Moeenfard, “Nonlinear dynamic modeling of surface defects in rolling element bearing systems,” Journal of Sound and Vibration, vol. 319, pp. 1150–1174, 2009.

[59] P. W. Tse, W. Yang, and H. Y. Tam, “ Machine fault diagnosis through an effective exact wavelet analysis,” Journal of Sound and Vibration vol. 277, pp. 1005–1024, 2004.

[60] N. Raje, F. Sadeghi, and R. G. Rateick, “A statistical damage mechanics model for subsurface initiated spalling in rolling contacts,” J. Tribol., vol. 130, no. 4, pp. 1–11, 2008.

[61] A. Glowacz, W. Glowacz, Z. Glowacz, and J. Kozik, “Early fault diagnosis of bearing and stator faults of the single-phase induction motor using acoustic signals,” *Meas. J. Int. Meas. Confed.*, vol. 113, pp. 1–9, 2018.

[62] D. H. Pandya, S. H. Upadhyay, and S. P. Harsha, “Fault diagnosis of rolling element bearing with intrinsic mode function of acoustic emission data using APF-KNN,” Expert Syst. Appl., vol. 40, no. 10, pp. 4137–4145, 2013.

[63] J. Chebil, M. Hrairi, and N. Abushikhah, “Signal analysis of vibration measurements for condition monitoring of bearings,” *Aust. J. Basic Appl. Sci.*, vol. 5, no. 1, pp. 70–78, 2011.

[64] X. W. Deng, P. Yang, J. S. Ren, and Y. W. Yang, “Rolling bearings time and frequency domain fault diagnosis method based on Kurtosis analysis,” *Asia-Pacific Power Energy Eng. Conf. APPEEC*, vol. 2015-March, no. March, pp. 3–8, 2014.

[65] S. Fu, K. Liu, Y. Xu, and Y. Liu, “Rolling bearing diagnosing method based on time domain analysis and adaptive fuzzy C -means clustering,” *Shock Vib.*, vol. 2016, 2016.

[66] Y. H. Kim, A. C. C. Tan, J. Mathew, and B. S. Yang, “Condition monitoring of low speed bearings: A comparative study of the ultrasound technique versus vibration measurements,” *Proc. 1st World Congr. Eng. Asset Manag. WCEAM 2006*, pp. 182–191, 2006.

[67] S. Priya, M. R. Ramesh, and V. Naidu, “Bearing Health Condition Monitoring: Frequency Domain Analysis Multi-sensor Data Fusion,” Int. J. Adv. Res. Electr. Electron. Instrum. Eng. vol. 3, no. 5, pp. 260–268, 2014.

[68] D. Dyer and R. M. Stewart, “Detection of Rolling Element Bearing Damage By Statistical Vibration Analysis.,” *Am. Soc. Mech. Eng.*, vol. 100, no. 77-DET-83, pp. 229–235, 1977.

[69] S. Kumar, D. Goyal, and S. S. Dhami, “Statistical and frequency analysis of acoustic signals for condition monitoring of ball bearing,” *Mater. Today Proc.*, vol. 5, no. 2, pp. 5186–5194, 2018.

[70] B. S and K. T, “Life Prediction of a Spindle CNC Machining Centre Using Natural Frequency Method of Vibration,” *Ind. Eng. Manag.*, vol. 04, no. 05, 2015.

[71] D. S. Shah and V. N. Patel, “A Review of Dynamic Modeling and Fault Identifications Methods for Rolling Element Bearing,” *Procedia Technol.*, vol. 14, pp. 447–456, 2014.

[72] V. Sharma and A. Parey, “Gearbox fault diagnosis using RMS based probability density function and entropy measures for fluctuating speed conditions,” *Struct.* Heal. Monit., vol. 16, no. 6, pp. 682–695, 2017.

[73] P. Singh and S. P. Harsha, “Statistical and frequency analysis of vibrations signals of roller bearings using empirical mode decomposition,” Proc. Inst. Mech. Eng. Part K J. Multi-body Dyn., vol. 233, no. 4, pp. 856–870, 2019.

[74] S. A. Aye, “Statistical approach for tapered bearing fault detection using different methods,” *Proc. World Congr. Eng. 2011, WCE 2011*, vol. 3, pp. 2112–2115, 2011.

[75] Y. Wu, Y. Zhou, G. Saveriades, S. Agaian, J. P. Noonan, and P. Natarajan, “Local Shannon entropy measure with statistical tests for image randomness,” Inf. Sci. (Ny)., vol. 222, pp. 323–342, 2013

[76] M. Vishwakarma, R. Purohit, V. Harshlata, and P. Rajput, “Vibration Analysis & Condition Monitoring for Rotating Machines: A Review,” Mater. Today Proc., vol. 4, no. 2, pp. 2659–2664, 2017.

[77] Y. Wu, Y. Zhou, G. Saveriades, S. Agaian, J. P. Noonan, and P. Natarajan, “Local Shannon entropy measure with statistical tests for image randomness,” Inf. Sci. (Ny)., vol. 222, pp. 323–342, 2013.

[78] T. K. Lin and J. C. Liang, “Application of multi-scale (cross-) sample entropy for structural health monitoring,” Smart Mater. Struct., vol. 24, no. 8, p. 85003, 2015.

[79] D. Camarena-Martinez, M. Valtierra-Rodriguez, J. P. Amezquita-Sanchez, D. Granados-Lieberman, R. J. Romero-Troncoso, and A. Garcia-Perez, “Shannon Entropy and K - Means Method for Automatic Diagnosis of Broken Rotor Bars in Induction Motors Using Vibration Signals,” Shock Vib., vol. 2016, 2016.

[80] X. Shuiqing, Z. Ke, C. Yi, H. Yigang, and F. Li, “Gear Fault Diagnosis in Variable Speed Condition Based on Multiscale Chirplet Path Pursuit and Linear Canonical Transform,” Complexity, vol. 2018, 2018.

[81] H. Liu, L. Li, and J. Ma, “Rolling Bearing Fault Diagnosis Based on STFT-Deep Learning and Sound Signals,” Shock Vib., vol. 2016, 2016.

[82] S. S. Kulkarni, A. K. Bewoor, and R. B. Ingle, “Vibration signature analysis of distributed defects in ball bearing using wavelet decomposition technique,” Noise Vib. Worldw., vol. 48, no. 1–2, pp. 7–18, 2017.

[83] N. Minhas, N. Nikhil, and S. S. Banwait, “Vibration analysis and fault identifications of rolling element bearings-a review,” Int. J. Mech. Prod. Eng. Res. Dev., vol. 9, no. 4, pp. 1133–1142, 2019.

[84] P. G. Kulkarni and A. D. Sahasrabudhe, “Application Of Wavelet Transform For Fault Diagnosisof Rolling Element Bearings,” *Int. J. Sci. Technol. Res.*, vol. 2, no. 4, pp. 138–148, 2013.

[85] R. Hao and F. Chu, “Morphological undecimated wavelet decomposition for fault diagnostics of rolling element bearings,” Journal of Sound and Vibration, vol. 320, pp. 1164–1177, 2009.

[86] C. Mishra, A. K. Samantaray, and G. Chakraborty, “Rolling element bearing defect diagnosis under variable speed operation through angle synchronous averaging of wavelet de-noised estimate,” Mech. Syst. Signal Process., pp. 1–17, 2015.

[87] D. Strömbergsson, P. Marklund, K. Berglund, and P. E. Larsson, “Bearing monitoring in the wind turbine drivetrain: A comparative study of the FFT and wavelet transforms,” Wind Energy, vol. 23, no. 6, pp. 1381–1393, 2020.

[88] J. S. Kim, J. H. Lee, J. H. Kim, J. G. Baek, and S. S. Kim, “Fault detection of cycle-based signals using wavelet transform in FAB processes,” Int. J. Precis. Eng. Manuf., vol. 11, no. 2, pp. 237–246, 2010.

[89] K. F. Al-raheem and A. Roy, “Rolling element bearing faults diagnosis based on autocorrelation of optimized : wavelet de-noising technique,” Int J Adv Manuf Technol, pp. 393–402, 2009.

[90] Y. Jiang, B. Tang, Y. Qin, and W. Liu, “Feature extraction method of wind turbine based on adaptive Morlet wavelet and SVD,” Renew. Energy, vol. 36, no. 8, pp. 2146–2153, 2011.

[91] C. Malla, A. Rai, V. Kaul, and I. Panigrahi, “Rolling element bearing fault detection based on the complex Morlet wavelet transform and performance evaluation using artificial neural network and support vector machine,” *Noise Vib. Worldw.*, vol. 50, no. 9–11, pp. 313–327, 2019.

[92] J. Lin and L. Qu, “Feature extraction based on morlet wavelet and its application for mechanical fault diagnosis,” *J. Sound Vib.*, vol. 234, no. 1, pp. 135–148, 2000.

[93] K. Belaid, A. Miloudi, and H. Bournine, “The processing of resonances excited by gear faults using continuous wavelet transform with adaptive complex Morlet wavelet and sparsity measurement,” Meas. J. Int. Meas. Confed., vol. 180, no. May, p. 109576, 2021.

[94] J. Igba, K. Alemzadeh, C. Durugbo, and E. T. Eiriksson, “Analysing RMS and peak values of vibration signals for condition monitoring of wind turbine gearboxes,” Renew. Energy, vol. 91, pp. 90–106, 2016.

[95] A. Glowacz, W. Glowacz, Z. Glowacz, and J. Kozik, “Early fault diagnosis of bearing and stator faults of the single-phase induction motor using acoustic signals,” *Meas. J. Int. Meas. Confed.*, vol. 113, pp. 1–9, 2018.

[96] S. Ebersbach, Z. Peng, and N. J. Kessissoglou, “The investigation of the condition and faults of a spur gearbox using vibration and wear debris analysis techniques,” *Wear*, vol. 260, no. 1–2, pp. 16–24, 2006.

[97] A. Choudhury and N. Tandon, “Application of acoustic emission technique for the detection of defects in rolling element bearings,” *Tribol. Int.*, vol. 33, no. 1, pp. 39–45, 2000.

[98] S. Al-dossary, R. I. R. Hamzah, and D. Mba, “Observations of changes in acoustic emission waveform for varying seeded defect sizes in a rolling element bearing,” Appl. Acoust., vol. 70, no. 1, pp. 58–81, 2009.

[99] J. P. Patel and S. H. Upadhyay, “Comparison between Artificial Neural Network and Support Vector Method for a Fault Diagnostics in Rolling Element Bearings,” *Procedia Eng.*, vol. 144, pp. 390–397, 2016.

[100] S. Singh, A. Kumar, and N. Kumar, “Motor Current Signature Analysis for Bearing Fault Detection in Mechanical Systems,” *Procedia Mater. Sci.*, vol. 6, no. Icmpc, pp. 171–177, 2014.

[101] S. Singh and N. Kumar, “Rotor faults diagnosis using artificial neural networks and support vector machines,” Int. J. Acoust. Vib., vol. 20, no. 4, pp. 153–159, 2015.

[102] M. Vishwakarma, R. Purohit, V. Harshlata, and P. Rajput, “Vibration Analysis & Condition Monitoring for Rotating Machines: A Review,” Mater. Today Proc., vol. 4, no. 2, pp. 2659–2664, 2017.

[103] Y. Xing, H. Xu, S. Pei, X. Zhang, and W. Chang, “Mechanical analysis of spherical roller bearings due to misalignments between inner and outer rings,” Proc. Inst. Mech. Eng. Part C J. Mech. Eng. Sci., vol. 231, no. 17, pp. 3250–3262, 2017.

[104] J. A. F. O. Correia, A. M. P. De Jesus, P. M. G. P. Moreira, and P. J. S. Tavares, “Crack Closure Effects on Fatigue Crack Propagation Rates: Application of a Proposed Theoretical Model,” *Adv. Mater. Sci. Eng.*, vol. 2016, 2016.

[105] G. Fajdiga and M. Sraml, “Fatigue crack initiation and propagation under cyclic contact loading,” Eng. Fract. Mech., vol. 76, no. 9, pp. 1320–1335, 2009.

[106] Z. Yuan, B. Wang, C. Liu, Z. Wang, X. Zhang, and Y. Zhang, “The Crack Propagation Trend Analysis in Ceramic Rolling Element Bearing considering Initial Crack Angle and Contact Load Effect,” Shock Vib., vol. 2021, 2021.

[107] T. Akagaki, M. Nakamura, T. Monzen, and M. Kawabata, “Analysis of the behaviour of rolling bearings in contaminated oil using some condition monitoring techniques,” *Proc. Inst. Mech. Eng. Part J J. Eng. Tribol.*, vol. 220, no. 5, pp. 447–453, 2006.

[108] S. Kulkarni and S. B. Wadkar, “Experimental Investigation for Distributed Defects in Ball Bearing Using Vibration Signature Analysis,” Procedia Eng., vol. 144, pp. 781–789, 2016.

[109] R. Lostado, R. F. Martinez, and B. J. Mac Donald, “Determination of the contact stresses in double-row tapered roller bearings using the finite element method, experimental analysis and analytical models,” J. Mech. Sci. Technol., vol. 29, no. 11, pp. 4645–4656, 2015.

[110] J. J. Jayakanth and M. Chandrasekaran, “Recent approaches and measurement techniques for the bearing fault analysis – A review,” *Int. J. Mech. Eng. Technol.*, vol. 9, no. 13, pp. 134–146, 2018.

[111] Z. Liu and L. Zhang, “A review of failure modes, condition monitoring and fault diagnosis methods for large-scale wind turbine bearings,” *Meas. J. Int. Meas. Confed.*, vol. 149, p. 107002, 2020.

[112] A. Sharma, N. Upadhyay, P. K. Kankar, and M. Amarnath, “Nonlinear dynamic investigations on rolling element bearings: A review,” *Adv. Mech. Eng.*, vol. 10, no. 3, pp. 1–15, 2018.

[113] T. Makino, Y.Neishi, D. Shiozawa, S. Kikuchi, S. Okada, K. Kajiwara , “Effect of defect shape on rolling contact fatigue crack initiation and propagation in high strength steel,” *Int. J. Fatigue*, vol. 92, pp. 507–516, 2016.

[114] V. N. Patel, N. Tandon, and R. K. Pandey, “Experimental study for vibration behaviors of locally defective deep groove ball bearings under dynamic radial load,” *Adv. Acoust. Vib.*, vol. 2014, 2014.

[115] T. H. Kim, A. V Olver, and P. K. Pearson, “Fatigue and Fracture Mechanisms in Large Rolling Element Bearings Fatigue and Fracture Mechanisms in Large Rolling Element ,” Tribology Transactions , vol. 2004, no. June, 2016.

[116] H. Shi, Z. Liu, X. Bai, Y. Li, and Y. Wu, “A theoretical model with the effect of cracks in the local spalling of full ceramic ball bearings,” *Appl. Sci.*, vol. 9, no. 19, 2019.

[117] M. H. Nazir, Z. A. Khan, and A. Saeed, “Experimental Analysis and Modelling of C-crack Propagation in Silicon Nitride Ball Bearing Element under Rolling Contact Fatigue,” Tribol. Int., 2018.

[118] T. Tokiyoshi, F. Kawashima, T. Igari, and H. Kino, “Crack propagation life prediction of a perforated plate under thermal fatigue,” *Int. J. Press. Vessel. Pip.*, vol. 78, no. 11–12, pp. 837–845, 2001.

[119] U. Zerbst, M. Vormwald, R. Pippan, H. Gänser, C. Sarrazin-baudoux, and M. Madia, “About the fatigue crack propagation threshold of metals as a design criterion – A review q,” *Eng. Fract. Mech.*, vol. 153, no. November 2014, pp. 190–243, 2016.

[120] J. Guan, L.wang, C. Zhang , “Effects of non-metallic inclusions on the crack propagation in bearing steel,” Tribiology Int., 2016.

[121] S. Mobasher Moghaddam, F.Sadegi, K.Paulson, M.Correns, V.Bakalos., “Effect of non-metallic inclusions on butterfly wing initiation, crack formation, and spall geometry in bearing steels,” *Int. J. Fatigue*, vol. 80, pp. 203–215, 2015.

[122] Y. You, Y. Zhang, Z. Moumni, G. Anlas, and W. Zhang, “Effect of the thermomechanical coupling on fatigue crack propagation in NiTi shape memory alloys,” *Mater. Sci. Eng. A*, vol. 685, pp. 50–56, 2017.

[123] H. Cheng, Y. Zhang, W. Lu, and Z. Yang, “Research on ball bearing model based on local defects,” *SN Appl. Sci.*, no. September, 2019.

[124] M. Kale and P. J. Sawant, “Review of Vibration Studies of Deep Groove Ball Bearing Considering Single and Multiple Defects in Races .,” *Int. J. Adv. Res. Sci. Eng. Technol.*, vol. 3, no. 1, pp. 1169–1173, 2016.

[125] A. Nabhan, N. M. Ghazaly, A. Samy, and M. M.O, “Bearing fault detection techniques - a review,” *Turkish J. Eng. Sci. Technol.*, vol. 3, no. May 2016, pp. 1–18, 2015.

[126] X. Li and W. Chen, “Rolling bearing fault diagnosis based on physical model and one-class support vector machine,” *ISRN Mech. Eng.*, vol. 2014, 2014.

[127] D. S. Shah and V. N. Patel, “A Review of Dynamic Modeling and Fault Identifications Methods for Rolling Element Bearing,” Procedia Technol., vol. 14, pp. 447–456, 2014.

[128] M. El, L. Wang, T. J. Harvey, B. Vierneusel, M. Correns, and T. Blass, “Tribology International Further understanding of rolling contact fatigue in rolling element bearings - A review,” Tribiology Int., vol. 140, no. June, p. 105849, 2019.

[129] M. R. Hoeprich, “Rolling Element Bearing Fatigue Damage Propagation,”Journal of tribology, vol. 114, no. April, 1992.

[130] S. Prabhakar, A. R. Mohanty, and A. S. Sekhar, “Application of discrete wavelet transform for detection of ball bearing race faults,” *Tribol. Int.*, vol. 35, no. 12, pp. 793–800, 2002.

[131] V. M. Nistane and S. P. Harsha, “Failure Evaluation of Ball Bearing for Prognostics,” *Procedia Technol.*, vol. 23, pp. 179–186, 2016.

[132] P. Jayaswal, S. N. Verma, and A. K. Wadhwani, “Development of EBP-Artificial neural network expert system for rolling element bearing fault diagnosis,” *JVC/Journal Vib. Control*, vol. 17, no. 8, pp. 1131–1148, 2011.

[133] Z. Tian, M. J. Zuo, and S. Wu, “Crack propagation assessment for spur gears using model-based analysis and simulation,” *J. Intell. Manuf.*, vol. 23, no. 2, pp. 239–253, 2012.

[134] N. Tandon and A. Choudhury, “Review of vibration and acoustic measurement methods for the detection of defects in rolling element bearings,” *Tribol. Int.*, vol. 32, no. 8, pp. 469–480, 1999.

[135] H. Li, Y. Zhang, and H. Zheng, “Application of Hermitian wavelet to crack fault detection in gearbox,” Mech. Syst. Signal Process., vol. 25, no. 4, pp. 1353–1363, 2011.

[136] M. Elforjani and S. Shanbr, “Prognosis of Bearing Acoustic Emission Signals Using Supervised Machine Learning,” *IEEE Trans. Ind. Electron.*, vol. 65, no. 7, pp. 5864–5871, 2018.

[137] M. Elforjani and E. Bechhoefer, “Analysis of extremely modulated faulty wind turbine data using spectral kurtosis and signal intensity estimator,” *Renew. Energy*, vol. 127, pp. 258–268, 2018.

[138] M. Elforjani, “Estimation of Remaining Useful Life of Slow Speed Bearings Using Acoustic Emission Signals,” *J. Nondestruct. Eval.*, vol. 35, no. 4, pp. 1–16, 2016.

[139] M. Elforjani, D. Mba, A. Muhammad, and A. Sire, “Condition monitoring of worm gears,” *Appl. Acoust.*, vol. 73, no. 8, pp. 859–863, 2012.

[140] M. Elforjani and D. Mba, “Detecting natural crack initiation and growth in slow speed shafts with the Acoustic Emission technology,” *Eng. Fail. Anal.*, vol. 16, no. 7, pp. 2121–2129, 2009.

[141] M. Elforjani and D. Mba, “Accelerated natural fault diagnosis in slow speed bearings with Acoustic Emission,” *Eng. Fract. Mech.*, vol. 77, no. 1, pp. 112–127, 2010.

[142] R. Kumar and M. Singh, “Outer race defect width measurement in taper roller bearing using discrete wavelet transform of vibration signal,” Meas. J. Int. Meas. Confed., vol. 46, no. 1, pp. 537–545, 2013.

[143] J. Igba, K. Alemzadeh, C. Durugbo, and E. T. Eiriksson, “Analysing RMS and peak values of vibration signals for condition monitoring of wind turbine gearboxes,” *Renew. Energy*, vol. 91, pp. 90–106, 2016.

[144] X. Fan and M. J. Zuo, “Gearbox fault detection using Hilbert and wavelet packet transform,” Mech. Syst. Signal Process., vol. 20, no. 4, pp. 966–982, 2006.

[145] F.G Meng., L. Ye, P. Chen, ‘Wavelet Transform-based Higher-order Statistics for Fault Diagnosis in Rolling Element Bearings”, Journal of Vibration and Control, 14(11), 2008, pp. 1691–1709.

[146] P. W. Tse, Y. H. Peng, and R. Yam, “Wavelet analysis and envelope detection for rolling element bearing fault diagnosis—their effectiveness and flexibilities,” J. Vib. Acoust. Trans. ASME, vol. 123, no. 3, pp. 303–310, 2001.

[147] J. Lin, M. J. Zuo, and K. R. Fyfe, “Mechanical fault detection based on the wavelet de-noising technique,” J. Vib. Acoust. Trans. ASME, vol. 126, no. 1, pp. 9–16, 2004.

[148] A. Belsak and J. Flasker, “Detecting cracks in the tooth root of gears,” Eng. Fail. Anal., vol. 14, no. 8 SPEC. ISS., pp. 1466–1475, 2007..

[149] S. Loutridis, “A local energy density methodology for monitoring the evolution of gear faults,” *NDT E Int.*, vol. 37, no. 6, pp. 447–453, 2004.

[150] R. Pandiyarajan, M. S. Starvin, and K. C. Ganesh, “Contact stress distribution of large diameter ball bearing using Hertzian Elliptical contact theory,” Procedia Eng., vol. 38, pp. 264–269, 2012.

[151] A. Daidie, “3D Simplified Finite Elements Analysis of Load and Contact Angle in a Slewing Ball Bearing,” vol. 130, no. August 2008, Journal of Mechanical Design, pp. 1–8, 2013.

[152] Z. Tang and J. Sun, “The contact analysis for deep groove ball bearing based on ANSYS,” *Procedia Eng.*, vol. 23, pp. 423–428, 2011.

[153] Z. Yongqi, T. Qingchang, Z. Kuo, and L. Jiangang, “Analysis of Stress and Strain of the Rolling Bearing by FEA method,” *Phys. Procedia*, vol. 24, no. 2011, pp. 19–24, 2012.

[154] Z. Kiral and H. Karagülle, “Simulation and analysis of vibration signals generated by rolling element bearing with defects,” *Tribol. Int.*, vol. 36, no. 9, pp. 667–678, 2003.

[155] S. Singh, U. G. Ko, C. Q. Howard, and D. Petersen, “Analyses of contact forces and vibration response for a defective rolling element bearing using an explicit dynamics finite element model,” Journal of Sound and Vibration, 2014.

[156] R. Lostado, R. F. Martinez, and B. J. Mac Donald, “Determination of the contact stresses in double-row tapered roller bearings using the finite element method , experimental analysis and analytical models ,” *Journal of Mechanical Science and Technology*, vol. 29, no. 11, pp. 4645–4656, 2015.

[157] Yuya EZAKI, Hideo TERASAWA and Takuma WADA, “Vibration Analysis for Tapered Roller Bearing Fatigue Prevention Vibration Analysis for Tapered Roller Bearing Fatigue Prevention ,” Journal of System Design and Dynamics. January 2012, 2015.

[158] S. R. D and P. S. S. Kulkarni, “Vibration Analysis of deep groove ball bearing using Finite Element Analysis,” Int. Journal of Engineering Research and Applications, vol. 5, no. 5, pp. 44–50, 2015.

[159] A. Utpat, “Vibration Signature analysis of defective deep groove ball bearings by Numerical and Experimental approach,” International Journal of Scientific & Engineering Research. November, 2020.

[160] B. Alfredsson, I. Linares Arregui, and S. Hazar, “Numerical analysis of plasticity effects on fatigue growth of a short crack in a bainitic high strength bearing steel,” Int. J. Fatigue, vol. 92, pp. 36–51, 2016.

[161] I. El-thalji and E. Jantunen, “Fault analysis of the wear fault development in rolling bearings,” Engineering Failure Analysis, vol. 57, pp. 470–482, 2015.

[162] S. Mobasher Moghaddam et al., “Effect of non-metallic inclusions on butterfly wing initiation, crack formation, and spall geometry in bearing steels,” Int. J. Fatigue, vol.80, pp. 203–215, 2015.

[163] S. J. Lorenz, F. Sadeghi, H. K. Trivedi, L. Rosado, M. S. Kirsch, and C. Wang, “A continuum damage mechanics finite element model for investigating effects of surface roughness on rolling contact fatigue,” Int. J. Fatigue, vol. 143, no. October 2020, p. 105986, 2021.

[164] P. Singh and S. P. Harsha, “MODAL ANALYSIS OF BEARING USING,” vol. 6, no. 6, pp. 75–79, 2019.

[165] H. R. Xin and L. Zhu, “Contact stress FEM analysis of deep groove ball bearing based on ANSYS workbench,” Appl. Mech. Mater., vol. 574, pp. 21–26, 2014.

[166] Z. Yongqi, T. Qingchang, Z. Kuo, and L. Jiangang, “Analysis of Stress and Strain of the Rolling Bearing by FEA method,” Phys. Procedia, vol. 24, no. 2011, pp. 19–24,2012.

[167] A.D. Scari and P.A. Magalhães , “Influence of the Number of Rollers on a Tapered Roller Bearing,” J. Mech. Eng. Autom., vol. 4, no. 7, pp. 560–564, 2014.

[168] B. Wen, H. Ren, X. Zhou, L. Qiao, and Q. Han, “Dynamic Analysis for Cage in a Ball Bearing Using LS-DYNA,” Innovative Application Research and Education vol. 6, no. 1, pp. 4–6, 2016.

[169] S. Murer, F. Bogard, and L. Rasolofondraibe, “Determination of loads transmitted by rolling elements in a roller bearing using capacitive probes : Finite element validation,” Mech. Syst. Signal Process., pp. 1–8, 2014.

[170] T. Zhaoping, “Procedia Engineering The Contact Analysis for Deep Groove Ball Bearing Based on,” Procedia engineering, 2011.

[171] S. G. Kumbhar and E. S. P, “An overview of dynamic modeling of rolling- element bearings,” Noise & Vibration Worldwide 2020 https://doi.org/10.1177/0957456520948279

[172] Y. LI, S. Billington, C. Zhang, T. Kurfess, S. Danyluk, and S. Liang., “Dynamic Prognostic Prediction of Defect Propagation on Rolling Element Bearings Dynamic Prognostic Prediction of Defect Propagation on Rolling Element,” vol no. September 2014, pp. 37–41.

[173] R. S. Gunerkar, A. K. Jalan, and S. U. Belgamwar, “Fault diagnosis of rolling element bearing based on artificial neural network †,” Journal of Mechanical Science and Technology vol. 33, no. 2, pp. 505–511, 2019.

[174] P. Gupta and M. K. Pradhan, “Fault detection analysis in rolling element bearing: A review,” Mater. Today Proc., vol. 4, no. 2, pp. 2085–2094, 2017.

[175] M. Tiboni, C. Remino, R. Bussola, and C. Amici, “A Review on Vibration-Based Condition Monitoring of Rotating Machinery,” Appl. Sci., vol. 12, no. 3, p. 972, 2022.

[176] Z. Tang and J. Sun, “The contact analysis for deep groove ball bearing based on ANSYS,” Procedia Eng., vol. 23, pp. 423–428, 2011.

[177] F. Ebert, “Fundamentals of Design and Technology of Rolling Element Bearings,” Chinese J. Aeronaut., vol. 23, no. 1, pp. 123–136, 2010.

[178] A. O. Ayhan, “Three-dimensional fracture analysis using tetrahedral enriched elements and fully unstructured mesh,” Int. J. Solids Struct., vol. 48, no. 3–4, pp. 492–505, 2011.

[179] A. Nabhan and A. Rashed, “Experimental and numerical investigation of defect- size estimation in taper roller bearing,” Noise Vib. Worldw., vol. 49, no. 11, pp. 345–354, 2018.

[180] S. Rehman, N. M. S. Kumar, and S. Abrar, “Structural and Thermal Analysis on the Tapered-Roller Bearing,” Int. J. Mech. Eng., vol. 3, no. 7, pp. 5–12, 2016.

[181] Y. Yin, Y. X. Chen, and L. Liu, “Lifetime prediction for the subsurface crack propagation using three-dimensional dynamic FEA model,” Mech. Syst. Signal Process., vol. 87, no. June 2016, pp. 54–70, 2017.

[182] A. Bhalerao and S. Mujumdar, “Analysis of Deep Groove Ball Bearingbased on Static, Dynamic and Frequency Analysis Using Ansys R3,” Int. J. Adv. Res., vol. 8, no. 1, pp. 1065–1072, 2020.

[183] S. Shoor and M. Singh, “Detecting Crack Propagation Rate in Taper Roller Bearing Using FEA Analysis and Signal Processing Techniques,” Iran. J. Sci Technol. Trans. Mech. Eng., no. 0123456789, 2022.

[184] P. Šulka, A. Sapietová, V. Dekýš, and M. Sapieta, “Static structural analysis of rolling ball bearing,” MATEC Web Conf., vol. 244, 2018.

[185] S. Creţu, N. Mitu, and I. Bercea, “A dynamic analysis of tapered roller bearings under fully flooded conditions part 2: results,” Wear, vol. 188, no. 1–2, pp. 11– 18, 1995.

[186] M. L. Chandravanshi and A. K. Mukhopadhyay, “Modal analysis of structural vibration,” *ASME Int. Mech. Eng. Congr. Expo. Proc.*, vol. 14, no. November, 2013.

[187] S. P. Chaphalkar, S. N. Khetre, and A. M. Meshram, “Modal Analysis of Cantilever Beam with T-Section using Finite Element Method,” *Am. J. Eng. Res.*, vol. 4, no. 10, pp. 178–185, 2015.

[188] D. C. Chen, M. F. Chen, J. H. Kang, and C. C. Lai, “Vibration characteristics and modal analysis of a grinding machine,” *J. Vibroengineering*, vol. 19, no. 8, pp. 6288–6300, 2017.

[189] O. Ikechukwu, I. Aniekan, S. Pau, and E. Ikpe, “Experimental Modal Analysis of a Flat Plate Subjected To Vibration,” *Am. J. Eng. Res.*, no. 5, pp. 30–37, 2016.

[190] M. A. B. Marzuki, M. H. A. Halim, and A. R. N. Mohamed, “Determination of natural frequencies through modal and harmonic analysis of space frame race car chassis based on ANSYS,” *Am. J. Eng. Appl. Sci.*, vol. 8, no. 4, pp. 538–548, 2015.

[191] A. R. Sonawane, P. S. Talmale, and L. G. N. Sapkal, “Modal Analysis of Single Rectangular Cantilever Plate by Mathematically, FEA and Experimental,” *Int. Res. J.* Eng. Technol., vol. 4, no. 8, pp. 264–269, 2017.

[192] S. Shoor and M. Singh, “Contact analysis for taper roller bearing by using fea simulation,” Int. J. Mech. Prod. Eng. Res. Dev., vol. 10, no. 4, pp. 11–20, 2020.

[193] M. J. Hartnett, “The Analysis of Contact Stresses in Rolling Element Bearings,” Journal of tribology. vol. 101, no. 78, pp. 105–109, 1979.

[194] M. V. Puneethkumar and S. Sunil, “Analysis Of Contact Pressure Distribution Of The Straight And Crowning Profiles Of Tapered Roller,” *Int. J. Mech. Eng. Robot. Res.*, vol. 3, no. 4, pp. 483–492, 2014.

[195] Z. Tang and J. Sun, “The contact analysis for deep groove ball bearing based on ANSYS,” *Procedia Eng.*, vol. 23, pp. 423–428, 2011.

[196] Z. Yongqi, T. Qingchang, Z. Kuo, and L. Jiangang, “Analysis of Stress and Strain of the Rolling Bearing by FEA method,” *Phys. Procedia*, vol. 24, no. 2011, pp. 19–24, 2012.

[197] M. P. Kumar and C. J. Rao, “Structural and Thermal Analysis on a Tapered Roller Bearing,” *International Journal of Innovative Science, Engineering & Technology* vol. 2, no. 1, pp. 502–511, 2015.

[198] M. M. Rahman, I. Saifullah, and S. K. Ghosh, “Detection and Measurements of Cracks in Axially Loaded Tension RC Members by Image Processing Technique,” *Am. J. Civ. Eng. Archit.*, vol. 7, no. 2, pp. 115–120, 2019.

[199] M. Szeląg, "Application of an automated digital image-processing method for quantitative assessment of cracking patterns in a lime cement matrix," Sensors (Switzerland), vol. 20, no. 14, pp. 1–24, 2020.

[200] J. S. Kim, J. H. Lee, J. H. Kim, J. G. Baek, and S. S. Kim, "Fault detection of cycle-based signals using wavelet transform in FAB processes," Int. J. Precis. Eng. Manuf., vol. 11, no. 2, pp. 237–246, 2010.

[201] X. Lou and K. A. Loparo, "Bearing fault diagnosis based on wavelet transform and fuzzy inference," Mechanical Systems and Signal Processing ,18 vol. 18, pp. 1077–1095, 2004.

[202] N. G. Nikolaou and I. A. Antoniadis, "Demodulation of vibration signals generated by defects in rolling element bearings using complex shifted Morlet wavelets," Mech. Syst. Signal Process., vol. 16, no. 4, pp. 677–694, 2002.

[203] J. Rafiee, M. A. Rafiee, and P. W. Tse, "Application of mother wavelet functions for automatic gear and bearing fault diagnosis," Expert Syst. Appl., vol. 37, no. 6, pp. 4568–4579, 2010.

[204] R. Yan and R. X. Gao, "An efficient approach to machine health diagnosis based on harmonic wavelet packet transform," Robot. Comput. Integr. Manuf., vol. 21, no. 4–5, pp. 291–301, 2005.

[205] B. Alfredsson, M. Öberg, and J. Lai, "Propagation of physically short cracks in a bainitic high strength bearing steel due to fatigue load," *Int. J. Fatigue*, vol. 90, pp. 166–180, 2016.

[206] M. H. Nazir, Z. A. Khan, and A. Saeed, "Experimental analysis and modelling of c-crack propagation in silicon nitride ball bearing element under rolling contact fatigue," *Tribol. Int.*, vol. 126, no. March, pp. 386–401, 2018.

[207] R. Huang, L. Xi, X. Li, C. Richard Liu, H. Qiu, and J. Lee, “Residual life predictions for ball bearings based on self-organizing map and back propagation neural network methods,” Mech. Syst. Signal Process., vol. 21, no. 1, pp. 193–207, 2007.

[208]S. M. Rehman, M. S. Babu, Y. Siva, S. Rao, and T. M. Rao, “Fatigue , Modal and Transient Analysis on the Tapered-Roller Bearing,” International Journal of Innovative Research in Science, Engineering and Technology, pp. 19108–19117, 2

Annexure 1

a) Statistical parameters at various time intervals for 5 kg load

Time	Crest factor	SNR	RMS	Skewness	Kurtosis	Shannon entropyx10^7
0	13.2945	21.6	13.01	0.295	9.757	7.11
10	14.9651	20.18	12.8	0.139	10.95	6.22
20	13.0969	21.45	13.59	0.208	11.02	7.18
30	11.0833	20.93	12.26	0.096	8.158	5.55
40	13.0745	21.84	12.11	0.116	8.674	5.39
50	12.3122	20.59	12.05	0.132	8.126	5.33
60	12.2518	21.69	11.77	0.101	8.174	5.04
70	9.1122	18.81	11.69	0.086	7.93	4.96
80	9.9202	21.78	11.97	0.028	7.827	5.25
90	9.7328	21.6	11.77	0.063	7.487	5.02
100	11.9185	22.97	11.62	0.132	9.788	4.94
110	11.6994	21.14	11.92	0.103	8.448	5.2
120	14.5678	22.76	11.96	0.15	10.53	5.27
130	12.2272	21.54	11.84	0.166	9.522	5.12
140	13.2876	22.36	11.59	0.114	9.11	4.88
154	9.6573	23.82	10.7	0.058	7.139	4.48

178	7.4401	19.31	10.06	0.033	5.909	3.8
190	6.4123	19.2136	8.3213	0.176	9.5725	4.48
195	9.6573	23.8152	10.7043	0.0576	7.1386	5.31
198	8.7758	21.21	19.86	0.077	7.942	18.8
202	5.2136	21.0231	9.3212	0.03216	6.3215	4.32
210	7.4401	19.3076	8.767	0.0334	5.9086	3.8
218	14.8149	22.46	13.77	0.024	13.61	8.43
219	7.0945	22.01	8.305	0.045	6.06	2.42
223	14.8149	22.4647	16.123	0.0243	13.6121	8.43
225	4.214	19.99	24.51	0.037	8.602	30.6
228	7.0945	22.0069	10.1236	0.0446	6.0601	9.412
231	12.2114	20.99	22.5	0.16	8.388	22.5
232	6.421	20.0116	13.123	0.0979	6.1125	3.01
235	8.4599	20.39	8.719	0.053	6.942	2.5
236	8.2145	21.6326	7.9834	0.0769	6.0404	6.123
239	12.1766	19.41	13.9	0.158	7.908	7.45
240	10.215	23.696	8.2832	0.0622	6.1276	2.35
243	9.2289	21.74	10.04	0.047	7.137	3.44
245.5	9.2281	19.46	10.44	0.08	6.903	3.77

b) Statistical parameters at various time intervals for 10 kg load condition						
Time	**Crest factor**	**SNR**	**RMS**	**Skewness**	**Kurtosis**	**Shannon entropyx10^7**
0	6.9198	21.8205	7.5086	0.0651	4.5574	2.65
10	6.4147	23.6474	8.907	0.0158	4.2769	2.48
20	6.0941	25.1572	7.7797	0.0503	4.2954	1.79
30	5.3443	24.0097	8.3811	0.0624	4.1082	2.13
40	6.5692	25.2295	8.0885	0.0454	4.5228	1.97
50	7.4775	23.0172	8.4948	0.0804	4.6271	2.23
60	8.2776	22.1902	8.6607	0.0543	4.6011	2.33
70	9.0621	21.0592	8.9075	0.0248	5.1775	2.51
80	8.9535	22.5281	8.1578	-0.0835	5.8839	2.07
90	9.2178	21.2083	8.4519	-0.0735	6.914	2.27
100	10.1828	22.1399	9.2889	-0.1239	8.0933	2.88
110	11.4127	23.7162	9.9097	0.5263	7.4101	3.34
114	11.6908	21.8052	8.3408	0.1377	8.5879	2.27
140	10.9013	19.3333	17.9378	0.0189	8.4938	13.4
150	11.2693	20.7239	24.4335	0.1454	6.1217	26.5
159	10.2613	15.0051	8.6323	-0.0221	7.6176	2.4
169	9.0444	21.4007	11.0011	-0.016	6.453	4.22
175	9.2103	22.594	10.4926	0.0946	7.4736	3.85

178.5	7.6767	23.7939	8.8695	-0.02	4.85	2.48

c) Statistical parameters at various time intervals for 15 kg load condition

Time	**Crest factor**	**SNR**	**RMS**	**Skewness**	**Kurtosis**	**Shannon entropyx10^7**
0	7.1876	21.7196	10.5756	0.1182	4.8422	3.76
10	8.1742	21.3403	10.9222	0.1785	5.2229	4.07
20	8.4913	20.2498	8.3576	0.1401	5.2539	2.16
30	7.2174	21.7334	8.3706	0.0782	5.1458	2.17
40	7.4392	21.7028	8.5427	0.0954	4.9941	2.27
50	8.5493	23.3058	8.8529	0.0765	5.0783	2.48
60	12.4989	23.4657	8.7525	0.1412	5.8454	2.43
70	12.4989	23.4657	8.7525	0.1412	5.8454	2.43
80	9.2098	22.7529	11.1275	0.2048	7.4734	4.37
90	11.8551	22.8101	9.9101	0.1704	6.989	3.3
100	10.9537	23.9128	9.7542	0.1477	6.5224	3.17
110	8.5324	24.1415	12.9533	0.2021	7.0174	6.29
136	11.2243	19.6642	18.4772	-0.2334	18.39	25.3
145	10.7111	23.3374	16.4772	0.2093	7.1368	10.9
154	8.639	21.2379	17.0798	0.0173	6.3924	11.9

161	13.5067	19.7062	9.0926	0.0366	10.2749	2.81
166	7.9492	19.1153	15.1188	0.0798	6.2093	8.91

d) Statistical parameters at various time intervals for 20 kg load condition

Time	**crest factor(peak2rms)**	**SNR**	**RMS**	**Skewness**	**Kurtosis**	**Shannon entropyx10^7**
0	9.5488	22.2513	7.5281	-0.0058	5.3458	1.69
10	9.2913	23.2789	6.6546	-0.0775	5.3986	1.26
20	7.7141	22.692	6.2379	-0.0615	5.5511	1.08
30	10.4701	21.5835	6.0014	-0.0918	5.669	0.986
40	8.116	22.6892	5.8941	0.0102	6.2163	0.958
50	9.5027	21.5655	6.1733	0.0254	6.3378	1.07
60	9.1552	20.4288	6.0131	-0.0148	6.0804	1
70	7.266	23.4279	6.2566	-0.0283	5.9512	1.1
74	7.2244	23.6471	6.2804	-0.0536	5.8426	1.11
80	12.2019	22.6227	7.5225	0.0417	12.921	1.87
103	7.4202	23.1817	22.391	0.0759	5.9674	29.13
109	9.4937	23.8267	13.4037	0.099	7.9975	6.85
114	11.6679	19.8841	15.6363	0.3223	12.1749	10.1

116.5	7.9711	19.7038	11.9823	0.0479	6.347	5.2

Annexure 2

a) Effect of 5kg Load on crack propagation

	Area	Mean	Min	Max
1	2.546	169.805	124	215

	Area	Mean	Min	Max
1	2.601	156.983	25	255

	Area	Mean	Min	Max
1	3.640	114.923	24	248

	Area	Mean	Min	Max
1	3.990	163.569	65	246

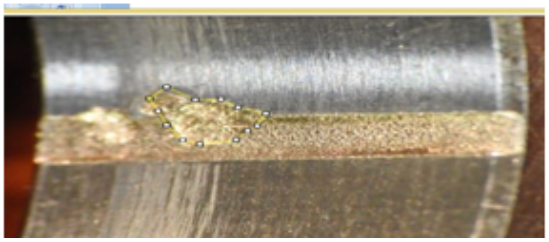

	Area	Mean	Min	Max
1	4.489	124.041	17	247

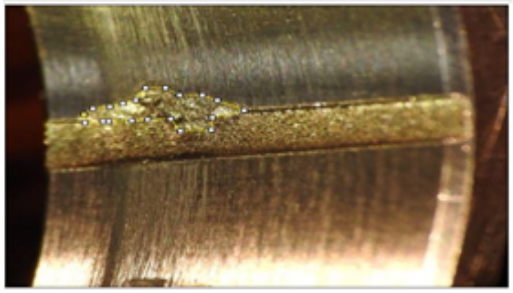

	Area	Mean	Min	Max
1	5.128	124.656	13	254

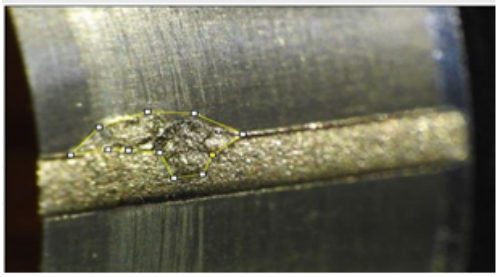

	Area	Mean	Min	Max
1	5.758	132.300	55	246

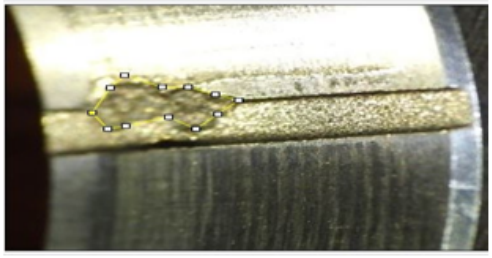

	Area	Mean	Min	Max
1	6.117	93.434	33	227

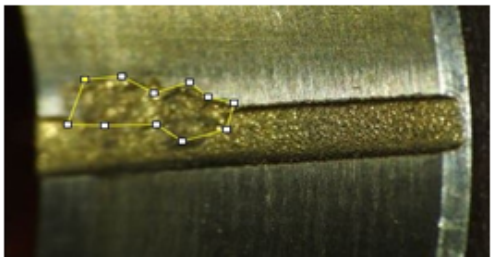

	Area	Mean	Min	Max
1	6.907	150.894	60	255

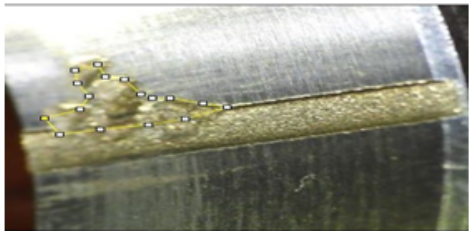

	Area	Mean	Min	Max
1	7.198	131.991	48	244

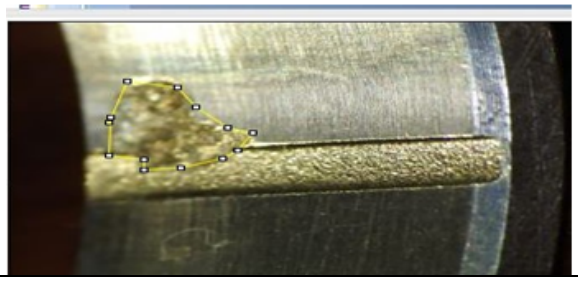

	Area	Mean	Min	Max
1	11.385	145.227	69	252

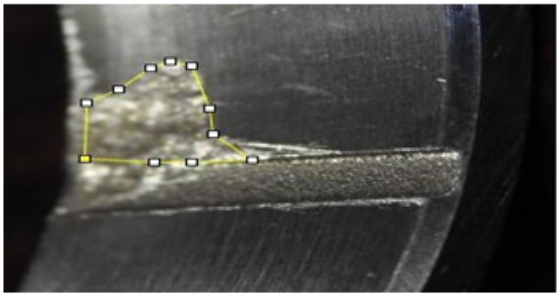

b) Effect of 10 Kg load on crack propagation

Area	Mean	Min	Max
1.394	168.584	125	216

Area	Mean	Min	Max
2.323	165.726	41	251

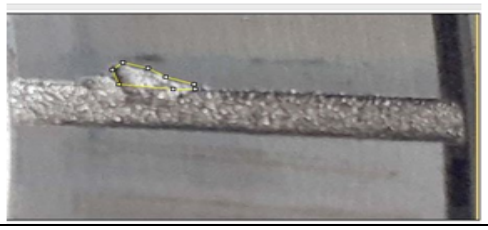

Area	Mean	Min	Max
3.184	114.189	21	253

Area	Mean	Min	Max
3.394	67.982	16	238

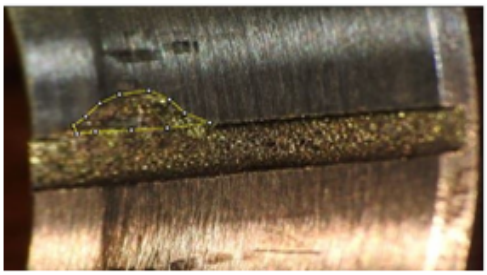

Area	Mean	Min	Max
4.104	108.430	22	243

	Area	Mean	Min	Max
1	5.296	168.208	47	255

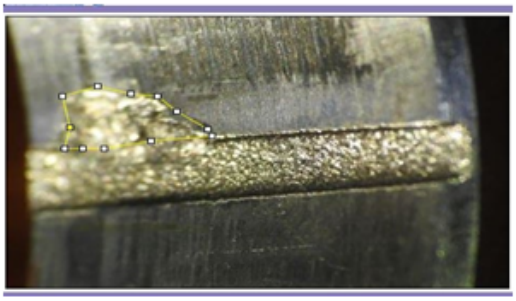

	Area	Mean	Min	Max
1	5.731	65.033	3	238

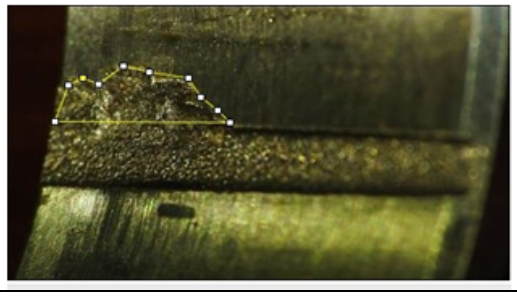

c) Effect of 15 Kg load on crack propagation

	Area	Mean	Min	Max
1	2.301	207.471	144	243

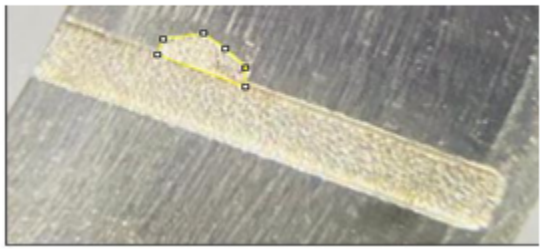

	Area	Mean	Min	Max
	2.679	84.479	11	249

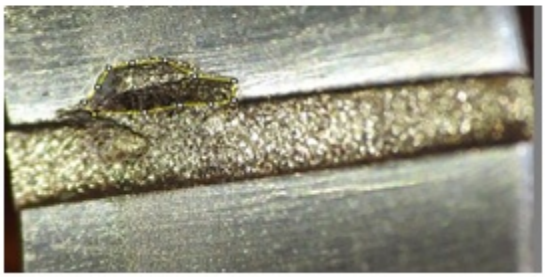

	Area	Mean	Min	Max
	4.773	42.637	1	240

	Area	Mean	Min	Max
	5.216	131.093	25	247

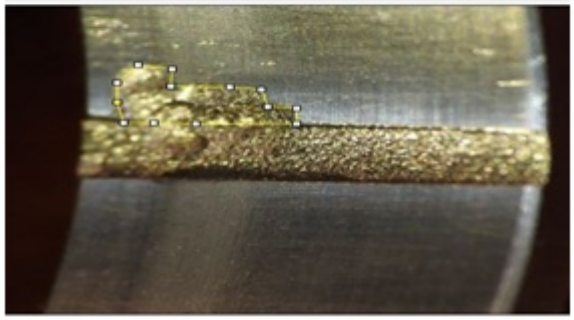

	Area	Mean	Min	Max
1	6.357	137.861	22	253

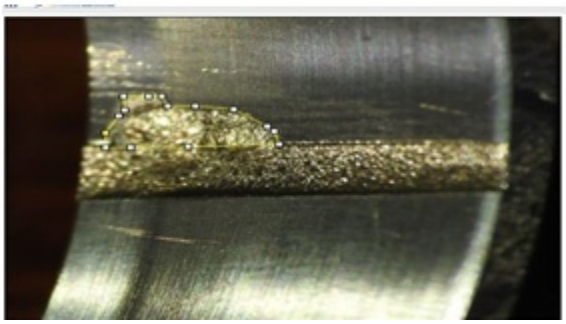

	Area	Mean	Min	Max
1	6.755	103.406	16	238

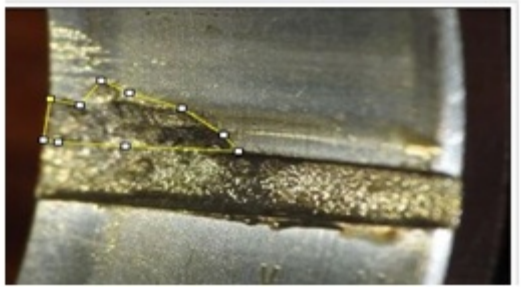

d) Effect of 20 Kg load on crack propagation

Area	Mean	Min	Max
2.461	111.846	36	228

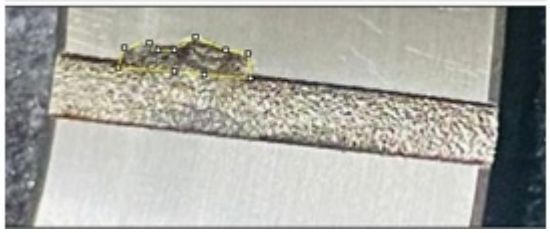

	Area	Mean	Min	Max
1	5.878	104.349	0	254

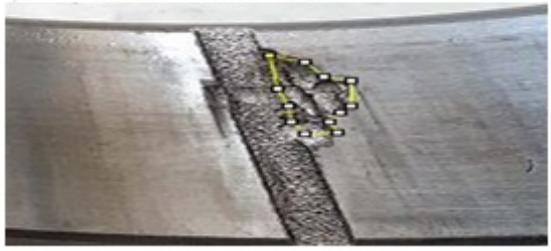

	Area	Mean	Min	Max
1	6.354	143.347	30	254

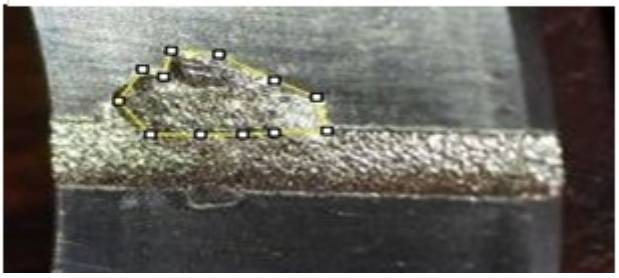

	Area	Mean	Min	Max
1	11.879	113.173	20	255

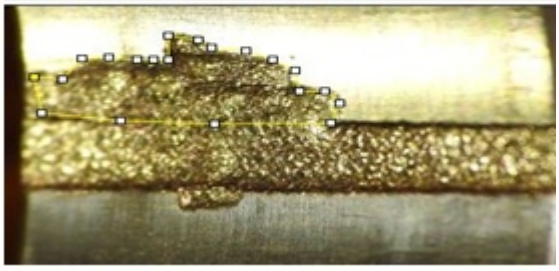

	Area	Mean	Min	Max
1	14.549	180.521	50	255

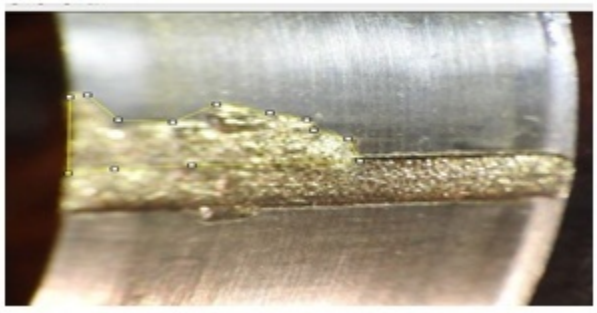

Annexure 3

Energy Dispersive Spectroscopy(EDS) analysis

a) Initial sample of Energy Dispersive Spectroscopy(EDS)

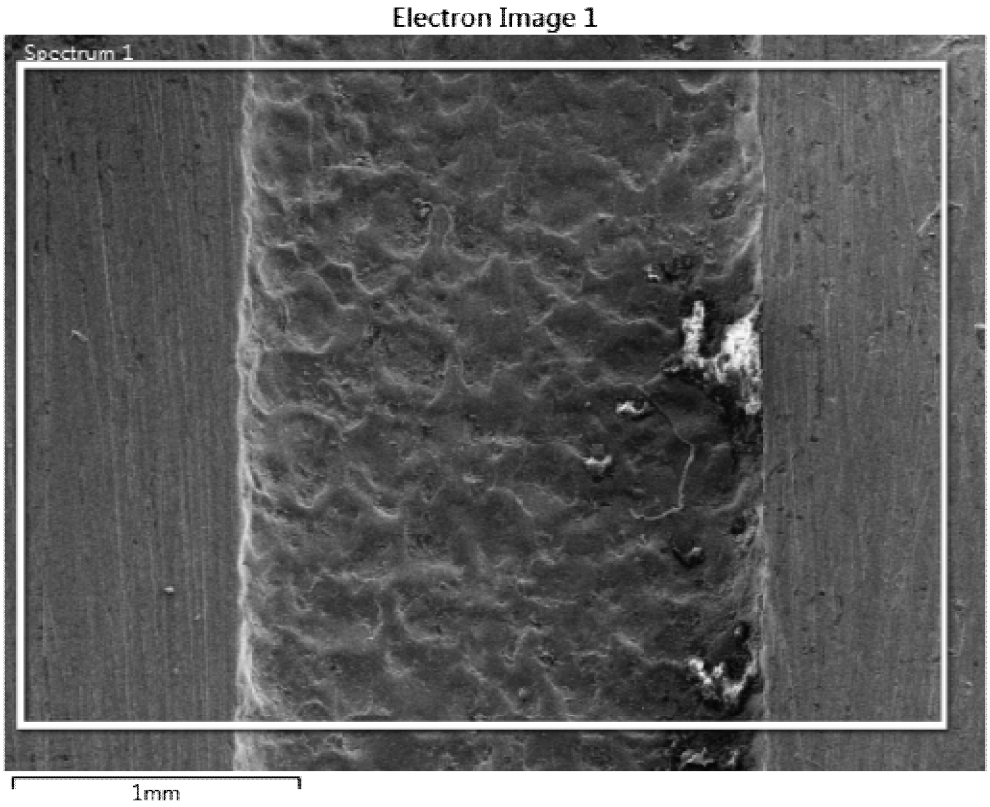

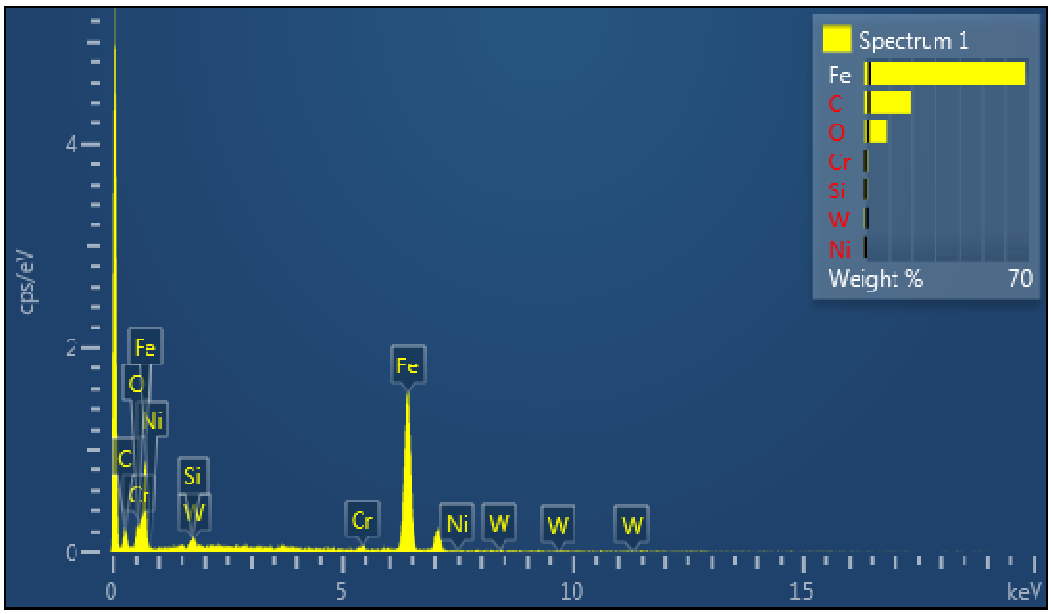

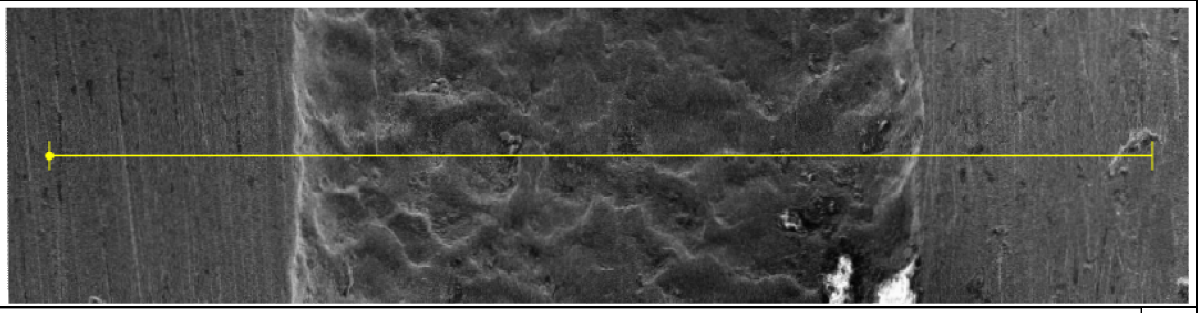

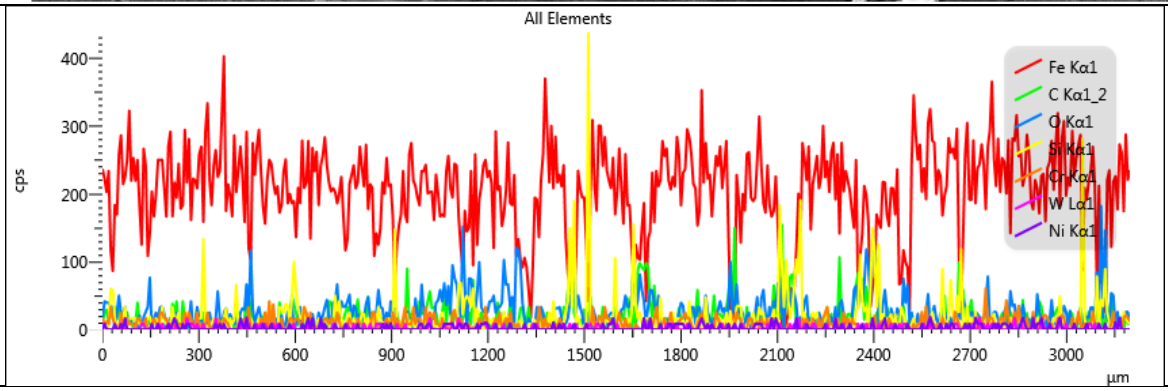

b) Energy Dispersive Spectroscopy(EDS) for No load

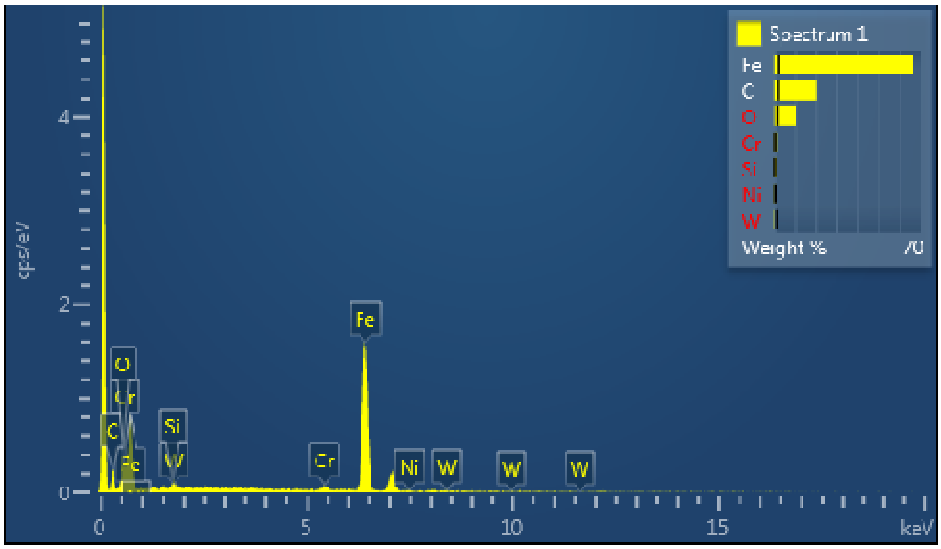

Electron Image 1

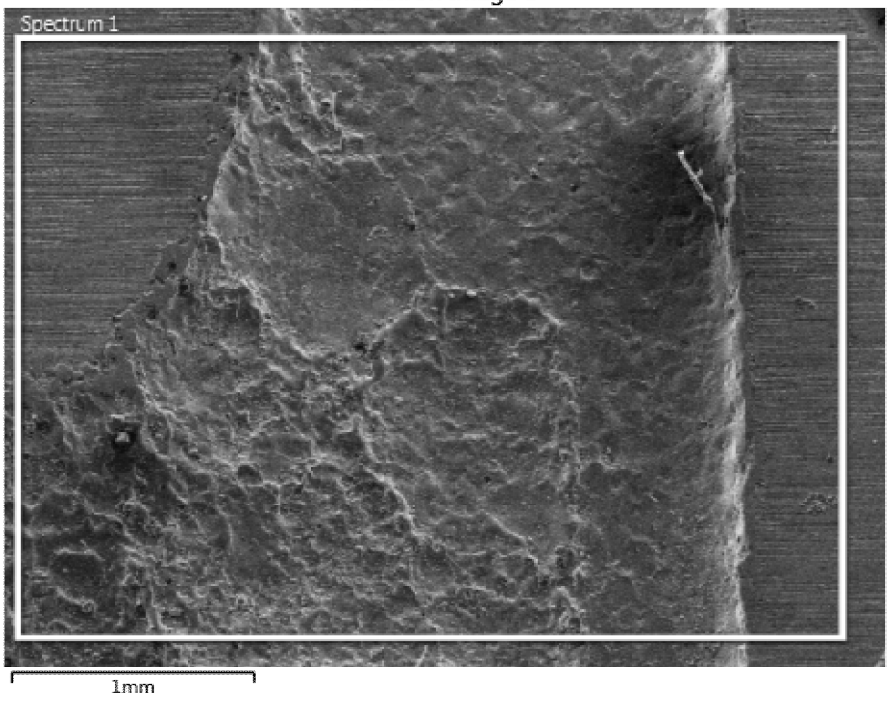

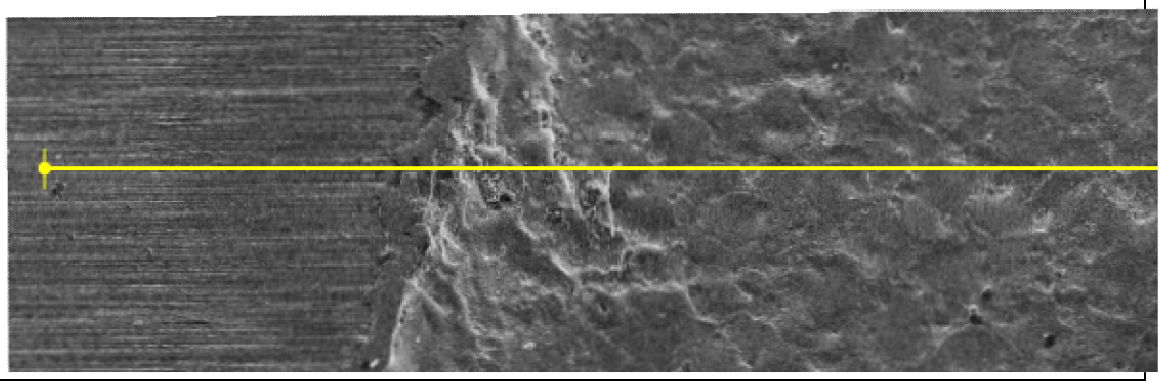

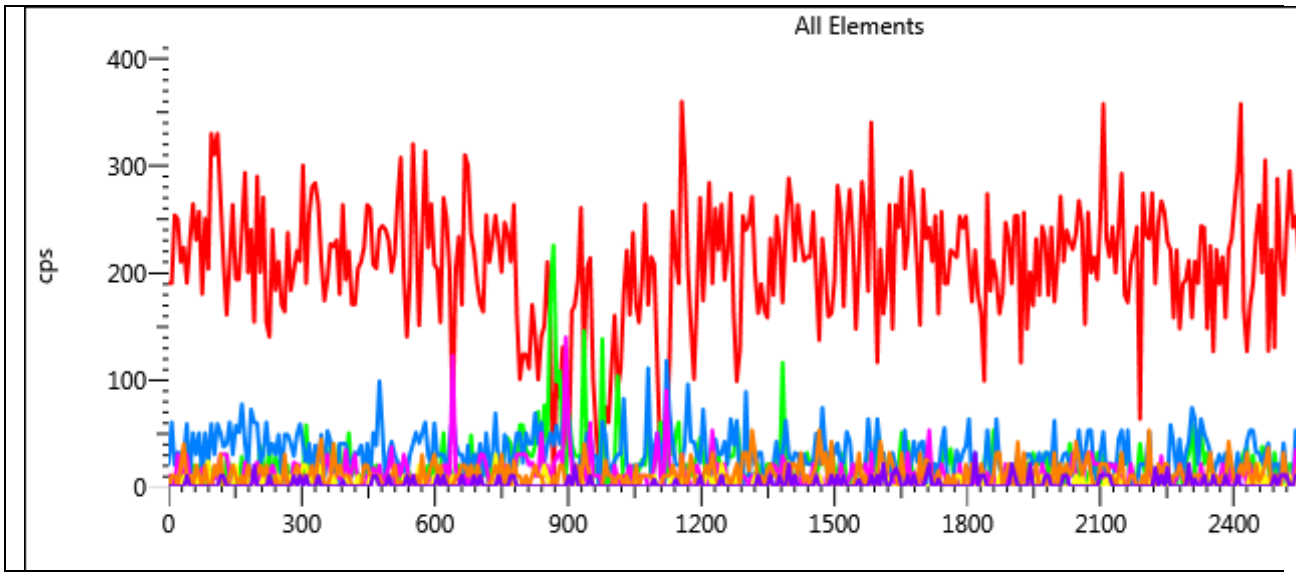

Spectrum 1	Wt%	Wt% Sigma
C	20.39	1.67
O	10.39	1.30
Si	0.88	0.21
Cr	1.14	0.22
Fe	66.63	1.87
Ni	0.42	0.33
W	0.15	1.11
Total	100.00	

Spectrum 1	Atomic %
C	47.14
O	18.03
Si	0.87
Cr	0.61
Fe	33.13
Ni	0.20
W	0.02
Total	100.00

c) Energy Dispersive Spectroscopy(EDS) for 5 kg load

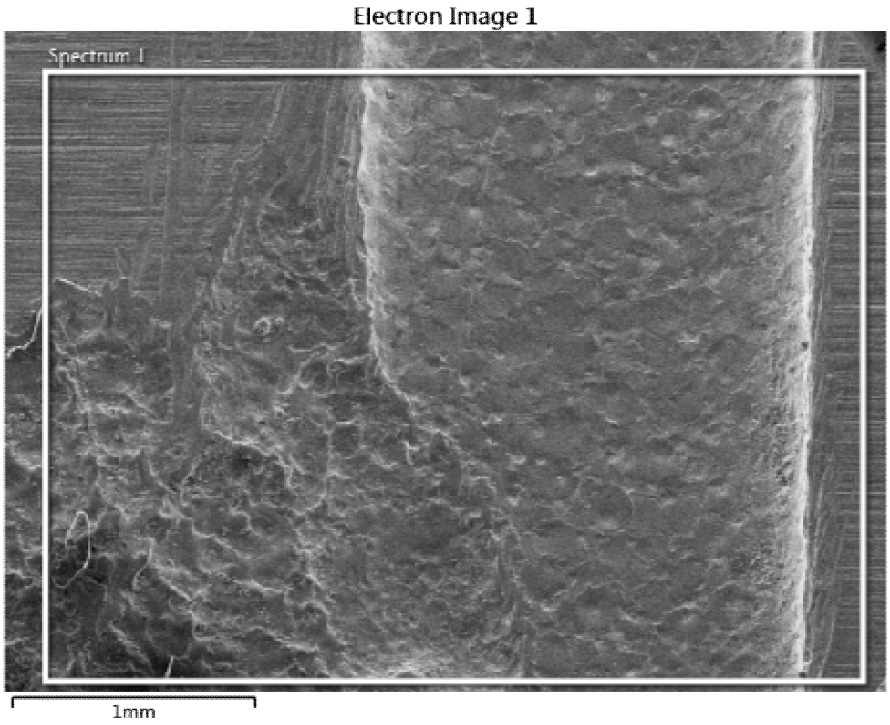

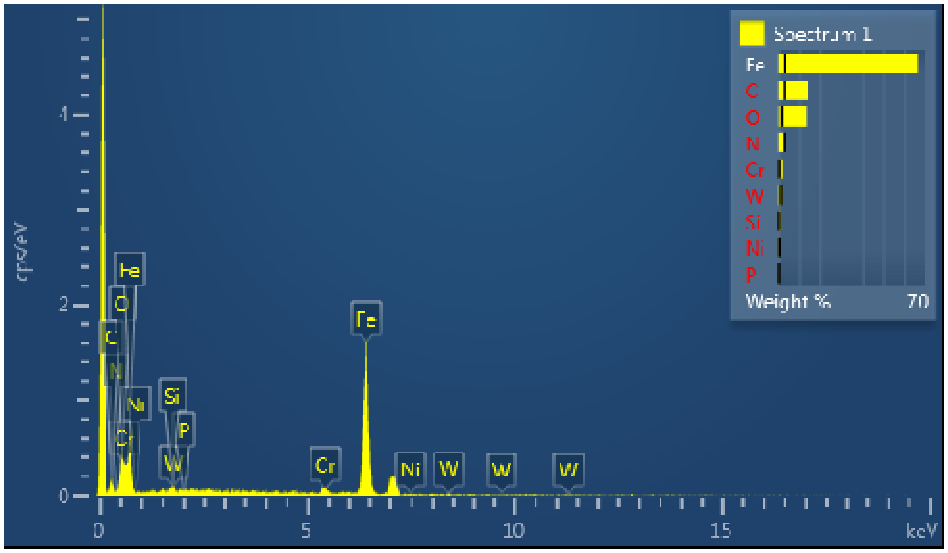

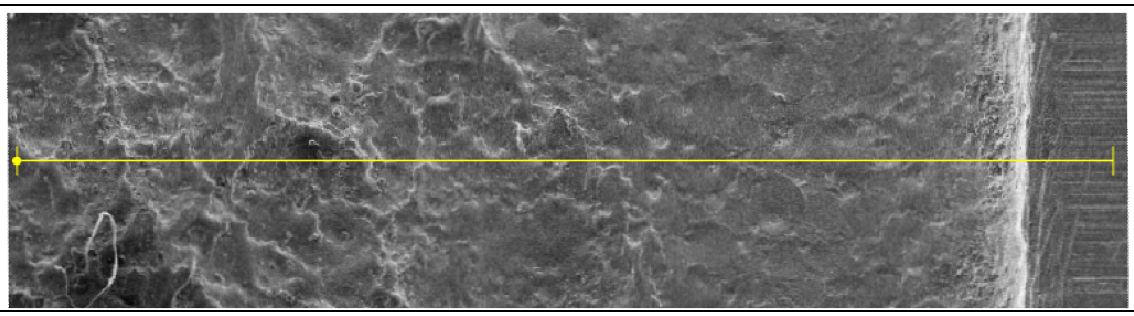

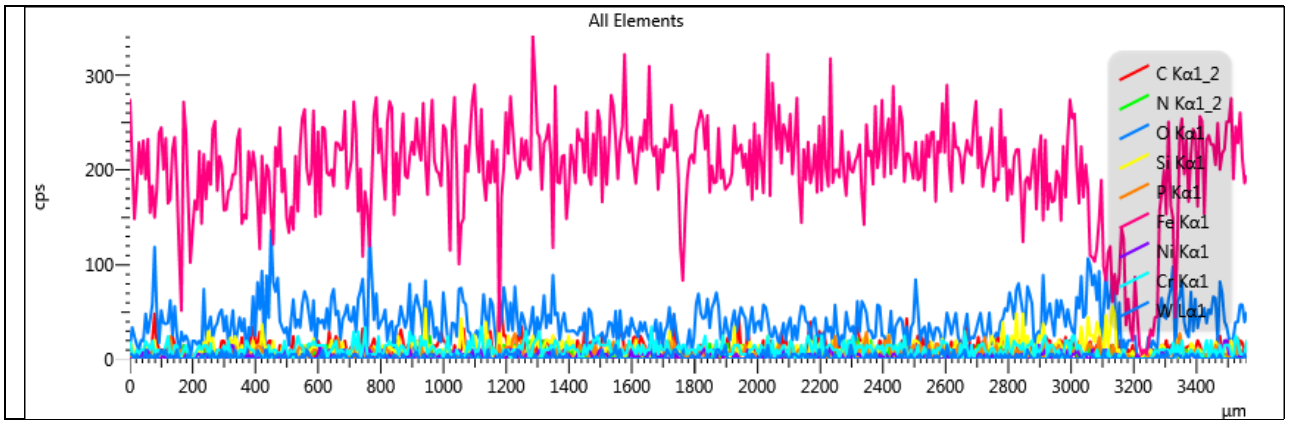

Spectrum 1	Wt%	Wt% Sigma
C	14.33	2.57
N	2.33	2.60
O	13.01	1.38
Si	0.90	0.21
P	0.12	0.16
Cr	1.51	0.23
Fe	66.32	2.92
Ni	0.17	0.32
W	1.31	0.97
Total	100.00	

Spectrum 1	Atomic %
C	34.73
N	4.84
O	23.67
Si	0.93
P	0.12
Cr	0.85
Fe	34.57
Ni	0.09
W	0.21
Total	100.00

d) Energy Dispersive Spectroscopy(EDS) for10 kg load

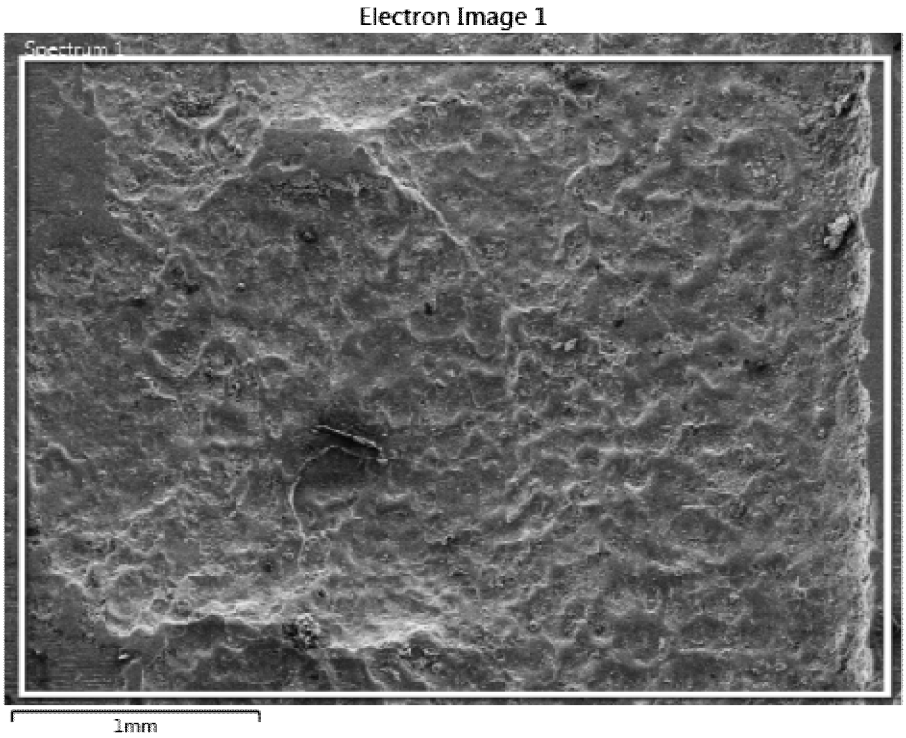

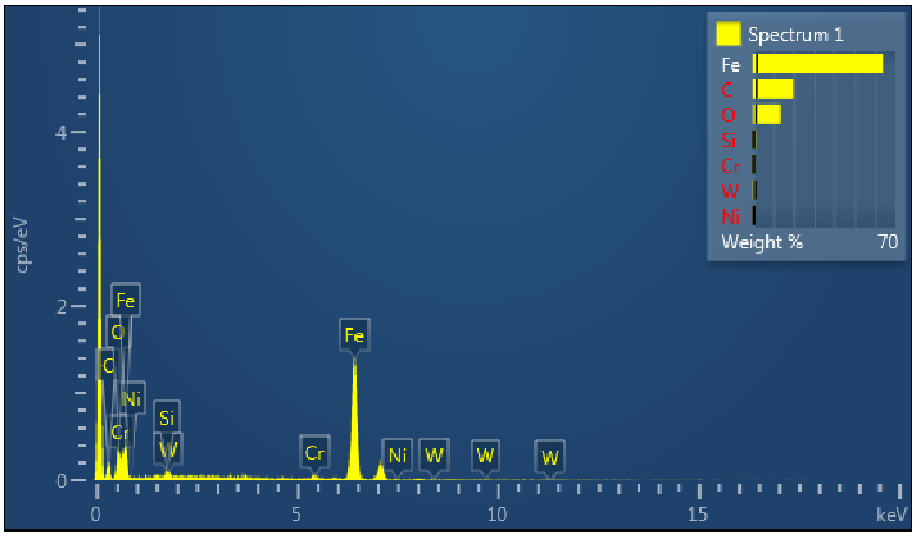

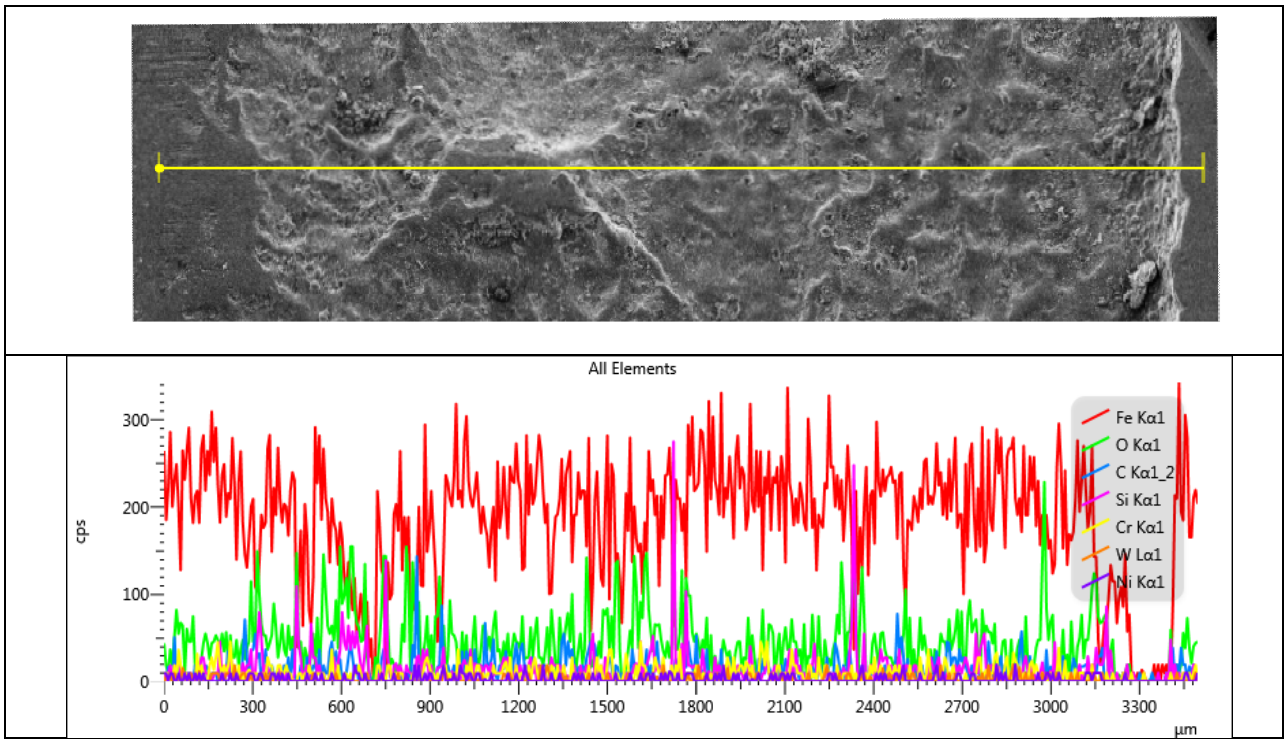

Spectrum 1	Atomic %
C	44.85
O	22.40
Si	1.12
Cr	0.50
Fe	30.91
Ni	0.14
W	0.08
Total	100.00

Spectrum 1	Wt%	Wt% Sigma
C	19.92	1.67
O	13.25	1.35
Si	1.16	0.22
Cr	0.95	0.22
Fe	63.85	1.81
Ni	0.31	0.33
W	0.55	1.01
Total	100.00	

e) Energy Dispersive Spectroscopy(EDS) for 15 kg load

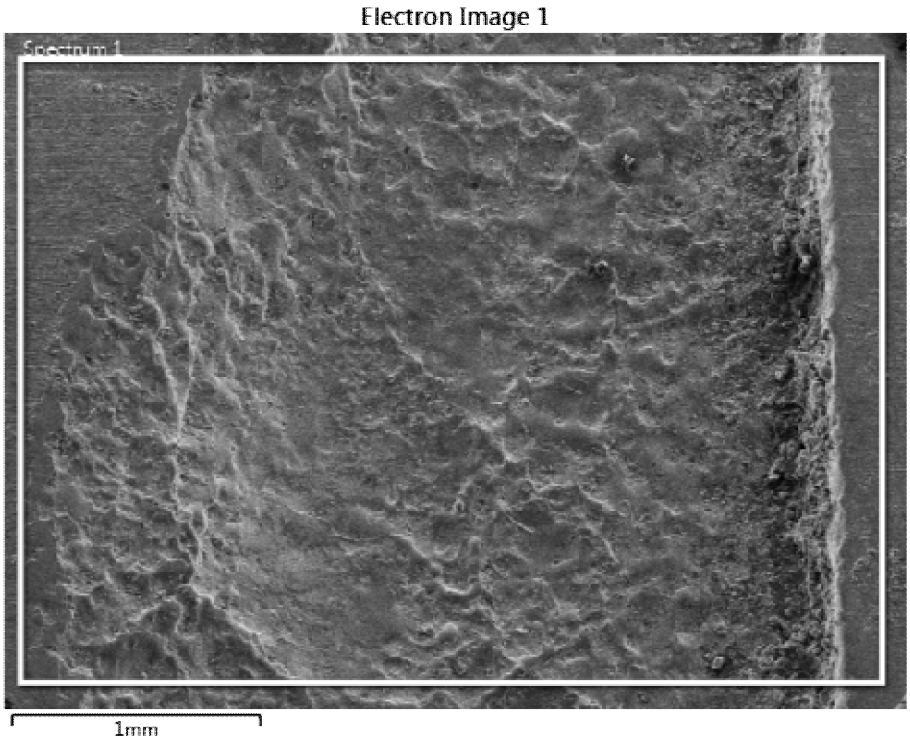

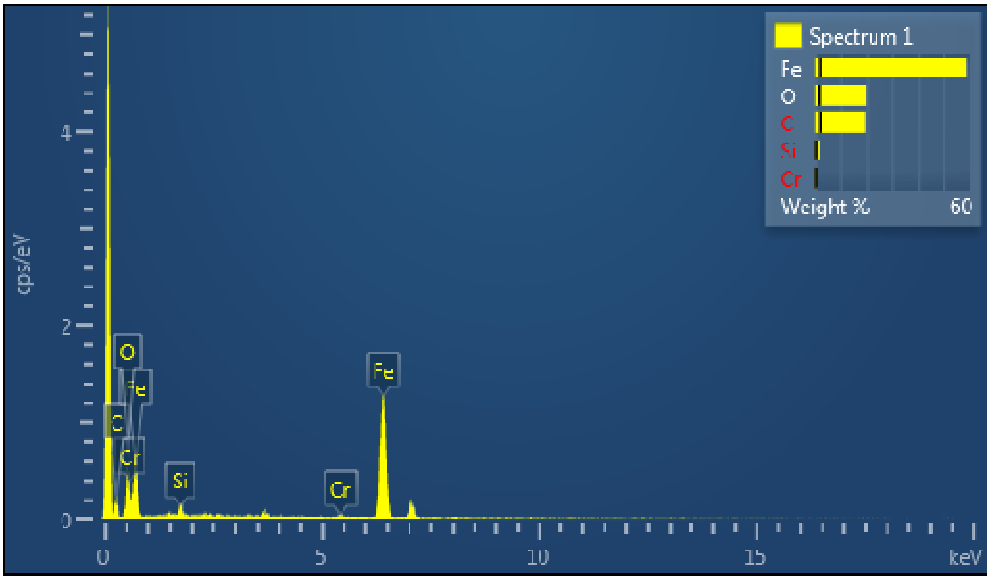

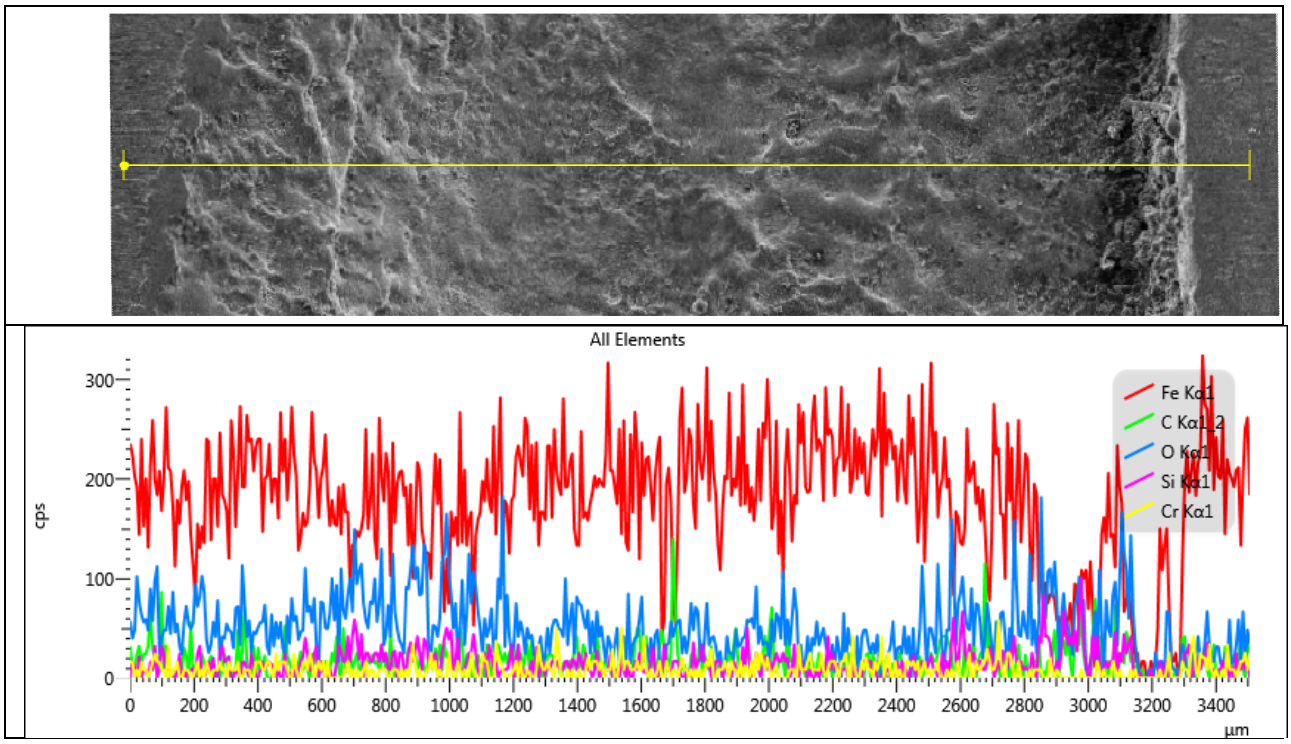

Spectrum 1	Wt%	Wt% Sigma
C	19.44	1.62
O	19.70	1.32
Si	1.39	0.21
Cr	0.69	0.21
Fe	58.78	1.55
Total	100.00	

Spectrum 1	Atomic %
C	40.83
O	31.05
Si	1.25
Cr	0.34
Fe	26.54
Total	100.00

f) Energy Dispersive Spectroscopy(EDS) for 20 kg load

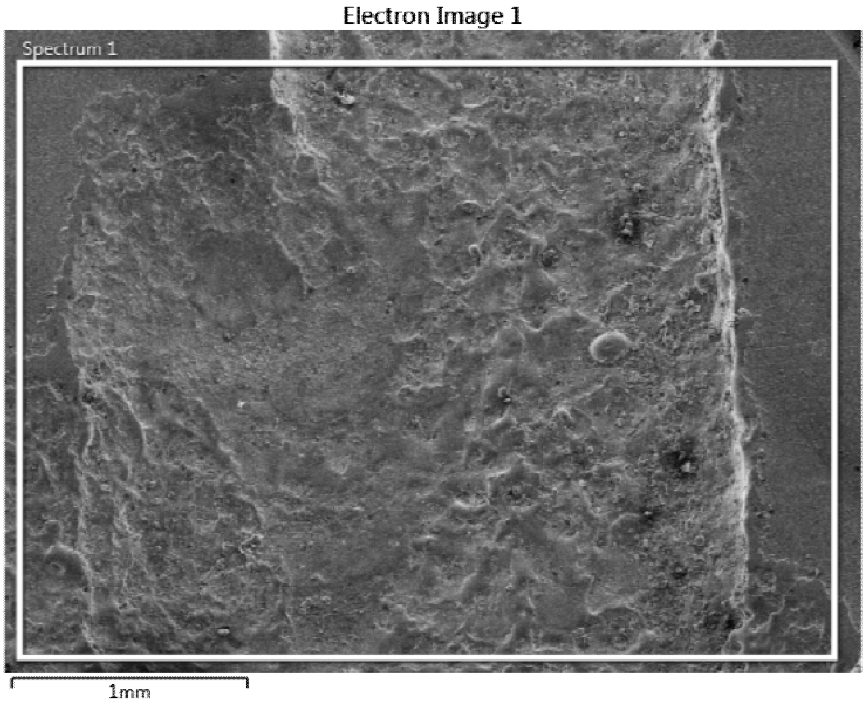

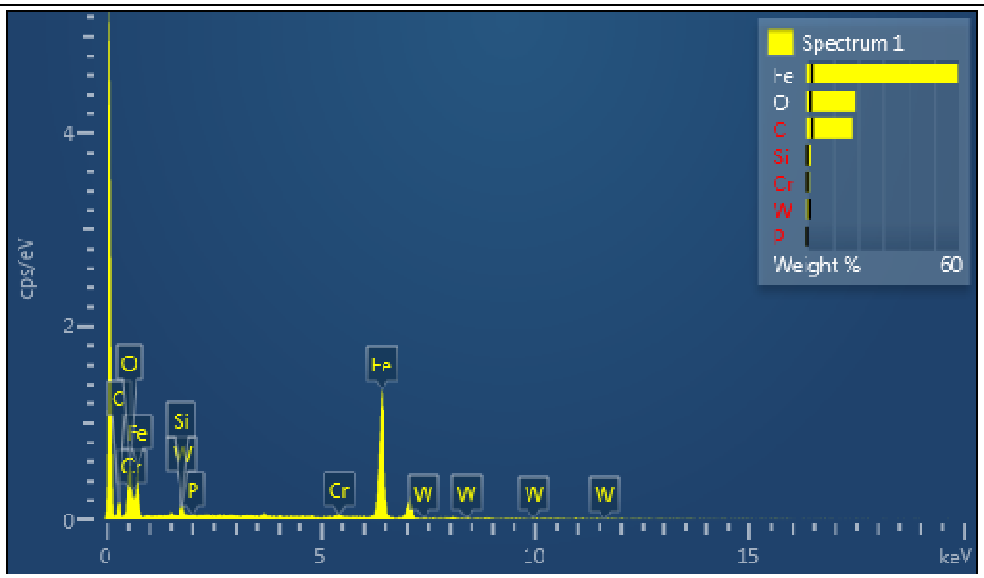

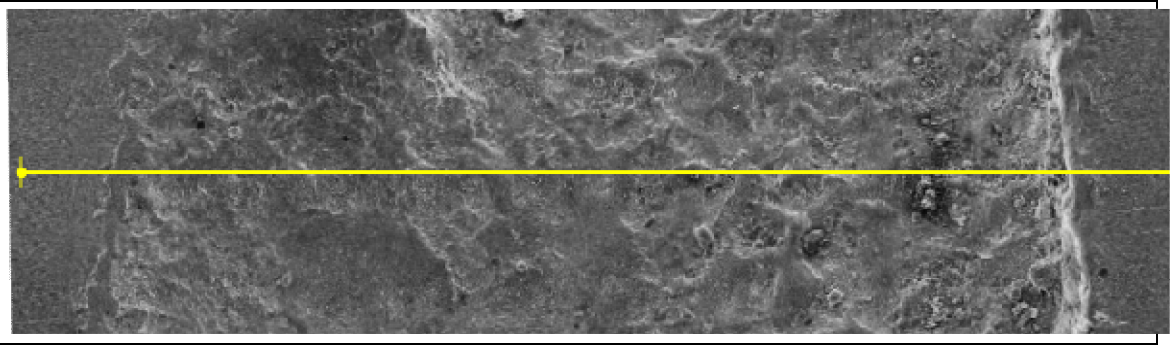

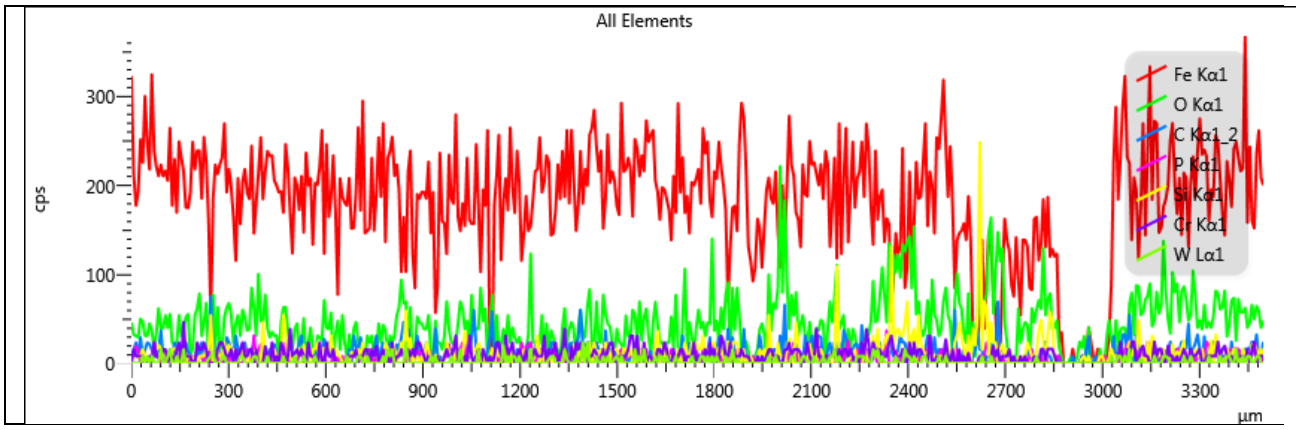

Spectrum 1	Atomic %
C	39.30
O	30.99
Si	1.29
P	0.10
Cr	0.50
Fe	27.73
W	0.10
Total	100.00

Spectrum 1	Wt%	Wt% Sigma
C	18.16	1.89
O	19.07	1.30
Si	1.40	0.23
P	0.12	0.16
Cr	0.99	0.22
Fe	59.58	1.79
W	0.68	1.01
Total	100.00	

Annexure 4

Patents

a) Bearing casing with multiple loading arrangement

1. Bearing casing, 2 Nut arrangement fixed with load cells (4 no.s), 3 Lock nut, 4 Bearing Frame, 5 Nut bolt (2 no.s)

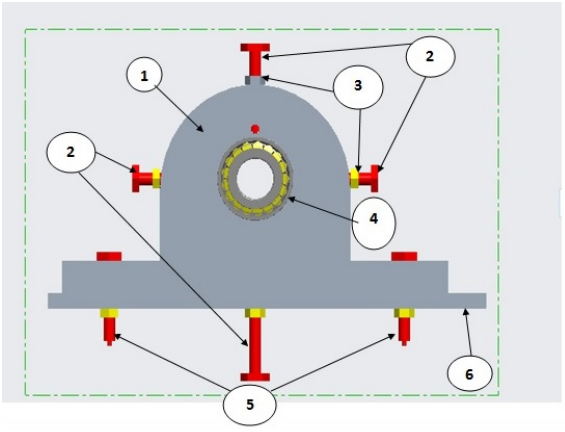

Front View

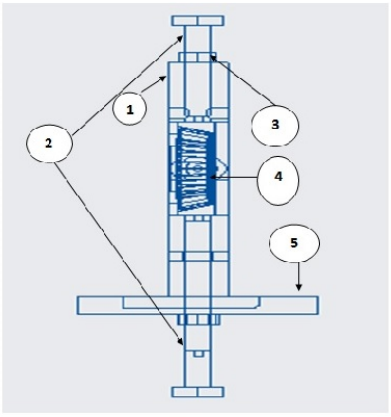

Side view wire frame model

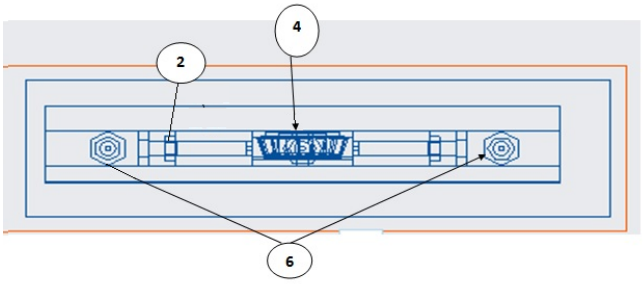

Top view wire frame model

1. Bearing casing
2. Nut arrangement fixed with load cell
3. Lock nut
4. Bearing
5. Frame
6. Nut and bolt

b) Parallel and Angular Misalignment of shaft

1. Bearing casing and roller Bearing, 2. Shaft, 3. Coupling, 4. Motor, 5. Threaded Bolt 1, 6. Base plate, 7. Threaded Bolt 2, 8. Threaded nut 1, 9. Threaded nut 2, 10.Dial Indicator 1, 11.Dial indicator 2

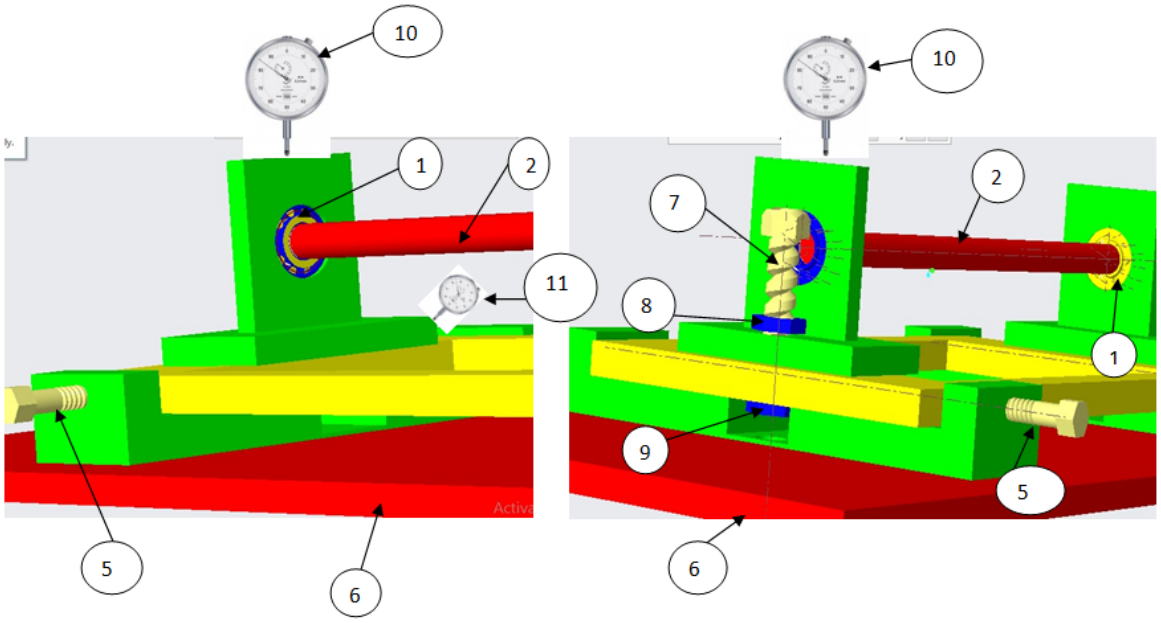
10
1
2
11
5
6
10
2
7
8
1
9
5
6

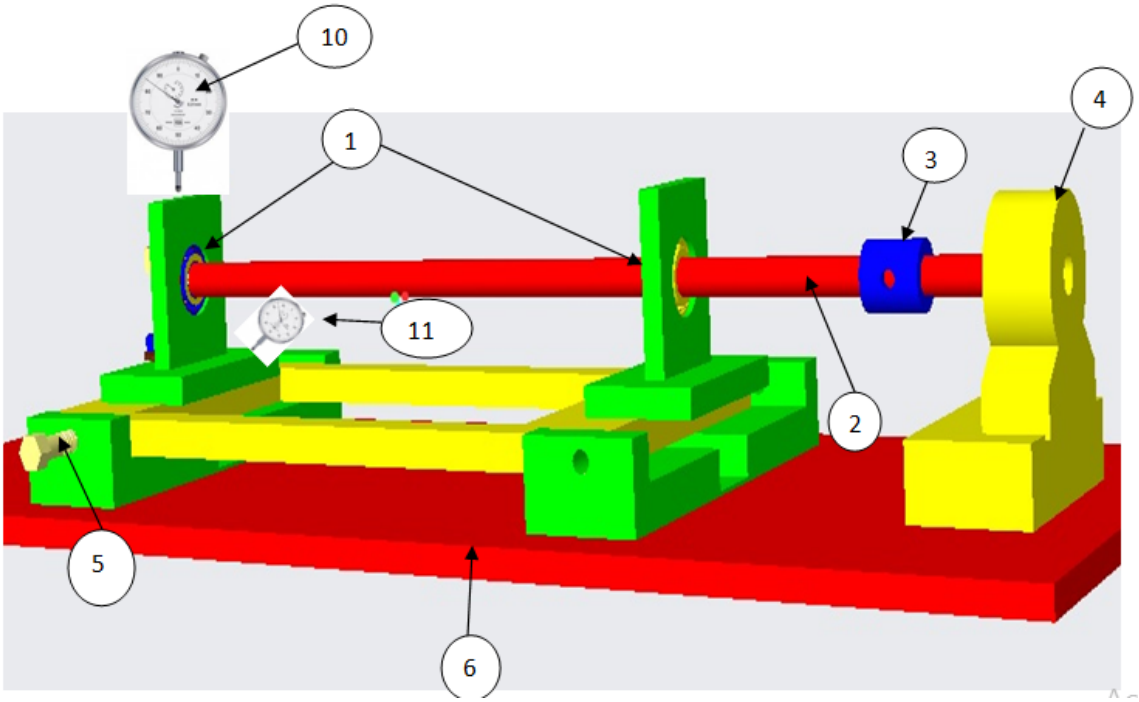
10
1
4
3
11
2
5
6

c) Bearing casing with Fatigue Harmonic loading arrangement

1. Gear, 2. Motor, 3. Cam, 4. Follower, 5. Bearing casing and Bearing, 6. CAM Shaft , 7. Shaft 8.Base plate1, 9.Base plate

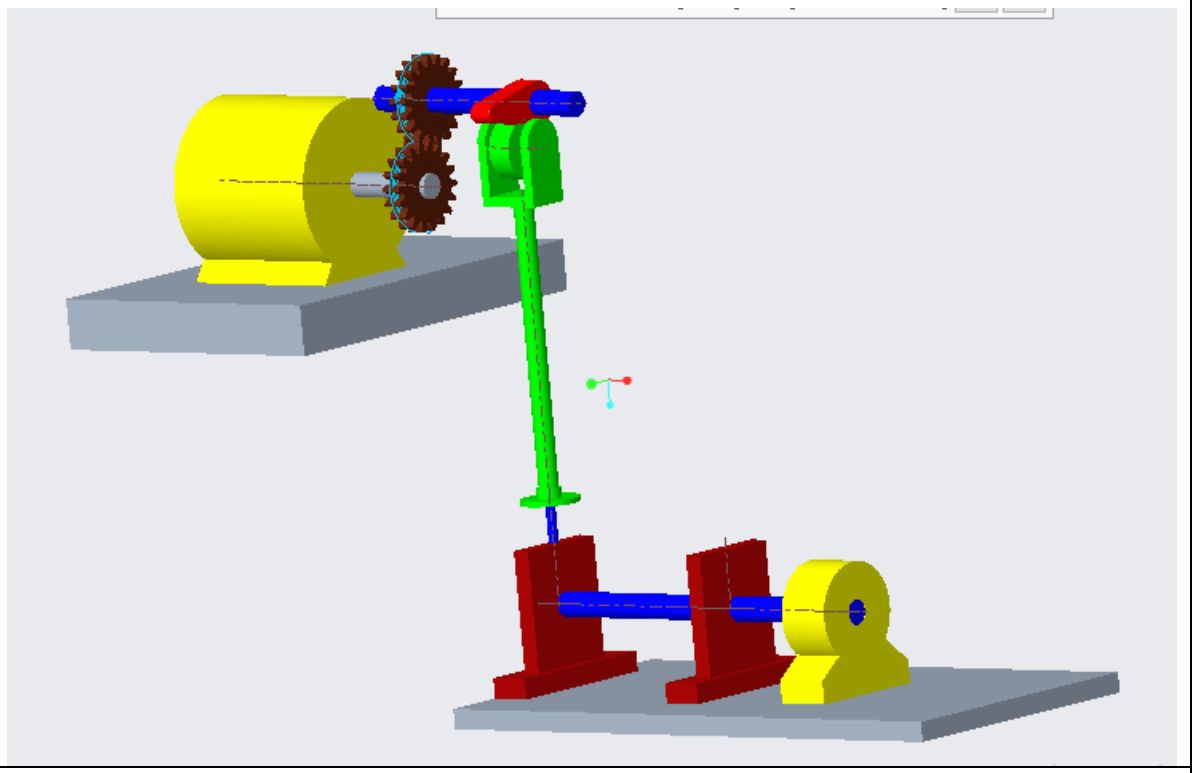

d) Arrangement for Creating Bending Moment on shaft using Hydraulic Loading 1. Plumber Block and Bearing, 2. Motor, 3. Coupling, 4. Base Plate, 5. Cylinder, 6. Piston , 7. Spring, 8. Lever Operated controlled, 3/2 DCV, 9. Pressure Gauge, 10. Shut Off valve, 11. Pump, 12. Filter, 13. Reservoir, 14. Motor, 15. Pressure Relief Valve

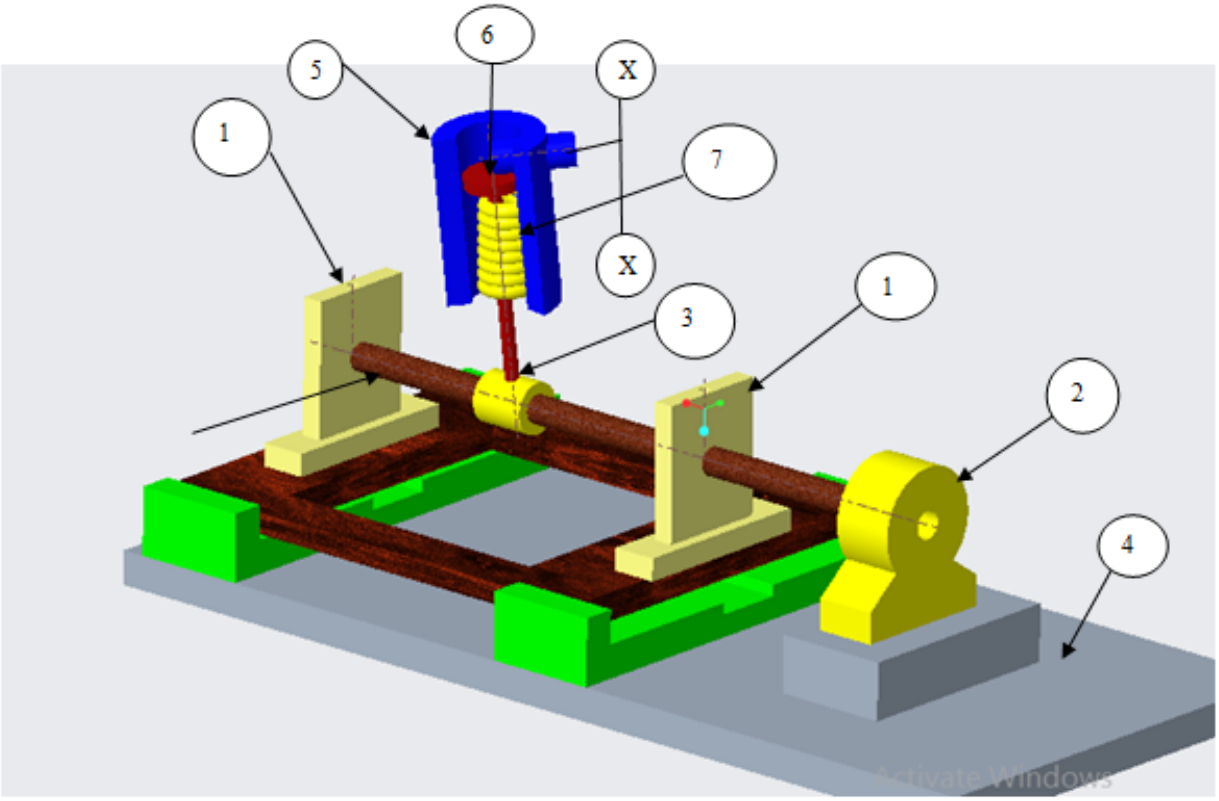

e) Defect detection of Bearing Using MEMS Magnetic Field Sensor

1. Motor and driving shaft , 2. Bearing Casing and Bearing, 3. Magnetic Field Sensor (MEMS)

4. Data acquisition systems (DAQ), 5. PCB, 6. Computer, 7. Coupling, 8. Shaft

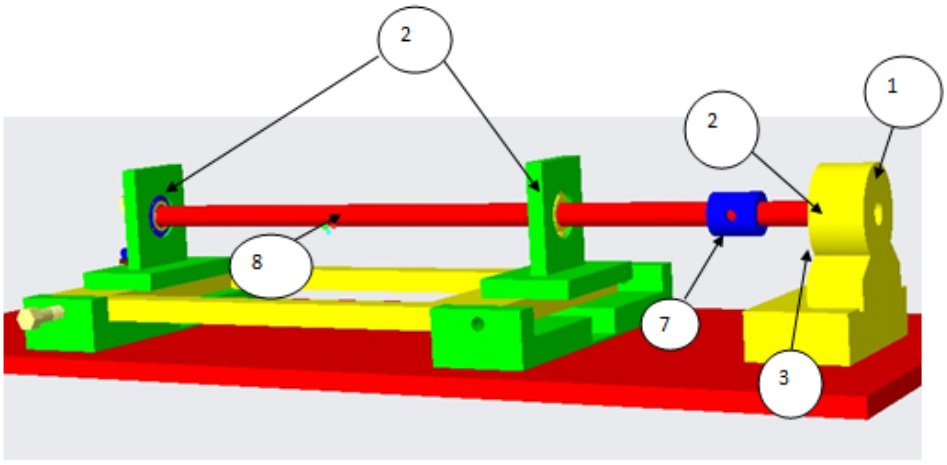

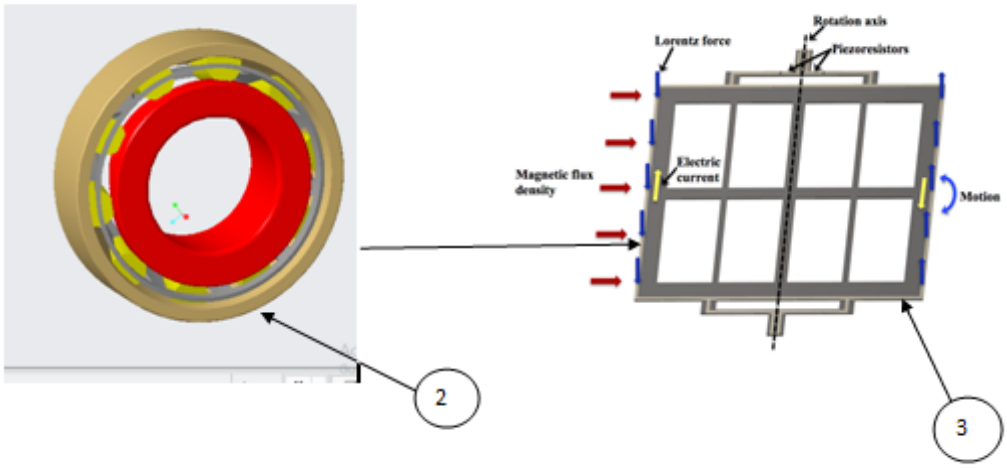
Rotation axis
Lorentz force
Piezoresistors
Magnetic flux density
Electric current
Motion
2
3

List of publication

In journals

[1] S. Shoor and M. Singh, “Detecting Crack Propagation Rate in Taper Roller Bearing Using FEA Analysis and Signal Processing Techniques,” *Iran. J. Sci. Technol. Trans. Mech. Eng.*, no. 0123456789, 2022.

[2] M. Singh, S. Shoor, and H. Singh, “Shannon entropy a better indices for local defect detection and to study the effect of variable loading conditions for taper roller bearing,” *Int. J. Mech. Eng. Technol.*, vol. 9, no. 7, pp. 198–208, 2018.

[3] S. Shoor and M. Singh, “Contact analysis for taper roller bearing by using fea simulation,” *Int. J. Mech. Prod. Eng. Res. Dev.*, vol. 10, no. 4, pp. 11–20, 2020.

Conferences

[4] S. Shoor and M. Singh, “Modal and Static Analysis for Analyzing the Effect of Loading on Crack Propagation Rate Using FEM,” Recent Trends in Industrial and Production Engineering., 978-981-16-3135-1.

[5] S. Shoor and M. Singh, “Three-Dimensional Non-linear Transient Analysis for Predicting the Defect Propagation Rate of Taper Roller Bearing Using Finite Element Method,” Recent Trends in Engineering Design., 978-981-16-1079-0.

[6] S. Shoor and M. Singh, “Comparison of Line Contact and Point Contact Behavior in Rolling Element Bearing Using Statistical Analysis of Vibration Signal,” Recent Trends in Engineering Design., 978-981-16-1079-0.

[7] Application of wavelet packet transform for monitoring crack propagation rate of taper roller bearing

UGC journals

[8]S. Shoor and M. Singh “A review on taper roller bearing defects using vibration signature,” vol. 5, no. 10, pp. 42–47, 2018.

[9] M. Singh, R. Kumar, S. Shoor, P. Gulati, and J. Singh, “Detection of outer race defect in bearing using signal processing techniques,” vol. 5, no. 12, pp. 543–552, 2018.

[10] M. Singh, R. Kumar, P. Gulati, J. Singh, and S. Shoor, “A review on various signal processing techniques used in bearing fault detection,” vol. 5, no. 12, pp. 659–668, 2018.

Communicated

[11] S. Shoor and M. Singh, “Crack propagation analysis on taper roller bearing under different loading conditions using vibration signal. ,” Journal of Nondestructive Evaluation

[12] S. Shoor and M. Singh, “Microstructure and vibration analysis of crack propagation rate for taper roller bearing at different loading conditions,” Sadhna .

Patents

Name	**DESCRIPTION**	Application Number
Bearing casing with multiple loading arrangement	The bearing casing with multiple loading arrangements is an invention to help the researchers working in the field of condition monitoring of bearing. In this arrangement bolts attached with load cells are inserted from all the four direction in the bearing casing. Each bolt can be tightened to apply the load on bearing with the help tooling by making contact with the surface of the bearing in all the four directions independently. The load cells are attached with wire to display the value of load acting in each of the four direction on the bearing surface. The	202011003934

	load cells are hard coated at the bottom to avoid the wearing due to loading action. The researchers can use this arrangement and can apply loads in all the four directions independently for carrying experiments.	
A NOVEL LOADING ARRANGEMENT FOR BEARING CASING	The bearing casing with harmonic loading arrangement is an invention to help the researchers working in the field of condition monitoring of bearing. There are many working under the harmonic loading and its very difficult for researchers to work in the similar kind of environment. This invention will help them to work with the bearing under the influence of harmonic load. There is a provision given to the setup for varying the frequency of Harmonic load by just changing the gear size.	202111049209
A METHOD FOR PROVIDING ANGULAR AND PARALLEL MISALIGNMENT OF SHAFT	Arrangement of misalignment in different direction is an invention to help the researchers working in the field of condition monitoring of shaft misalignment. In this arrangement provision is given for parallel and angular misalignment	202111049213

Arrangement for Creating Bending Moment on shaft using Hydraulic Loading	The bearing casing with Bending moment arrangement is an invention to help the researchers working in the field of condition monitoring. Bending Load can be varied by varying hydraulic pressure. The advantages of a hydraulic system include the ease and accuracy by which they can be controlled, and the large amounts of power they can generate. In general, hydraulic systems use fewer moving parts than some mechanical and electrical systems. Hydraulic pump Provide power to cylinder which further results in elimination of mechanical, train, gears, belt, cam and linkages etc	In process
Defect detection of Bearing Using MEMS Magnetic Field Sensor	The bearing casing with defect detection using MEMS Magnetic Field Sensor an arrangement is an invention to help the researchers working in the field of condition monitoring. Machines mainly driven by motor and produces rotating magnetic field and driving shaft of motor is supported by bearing . Bearing in any machinery subjected to different dynamic loads which further produces defect in bearing. This arrangement helps to detect the defect using MEMS Magnetic Field sensor	202011051365